Physics of Polymer Gels

Physics of Polymer Gels

Edited by

Takamasa Sakai

WILEY-VCH

Editor

Prof. Takamasa Sakai
The University of Tokyo
Graduate School of Engineering
Department of Bioengineering
7-3-1 Hongo, Bunkyo-ku
113-8656 Tokyo
Japan

Cover Images:
Polymer gel, @Kozlova/Shutterstock;
Graph: courtesy of Prof. Takamasa Sakai, The University of Tokyo, Japan

Library of Congress Card No.:
applied for

British Library Cataloguing-in-Publication Data
A catalogue record for this book is available from the British Library.

Bibliographic information published by the Deutsche Nationalbibliothek
The Deutsche Nationalbibliothek lists this publication in the Deutsche Nationalbibliografie; detailed bibliographic data are available on the Internet at <http://dnb.d-nb.de>.

Print ISBN: 978-3-527-34641-7
ePDF ISBN: 978-3-527-34653-0
ePub ISBN: 978-3-527-34655-4
oBook ISBN: 978-3-527-34654-7

Typesetting SPi Global, Chennai, India
Printing and Binding

Printed on acid-free paper

10 9 8 7 6 5 4 3 2 1

Contents

Preface

Polymer gels are defined as a three-dimensional polymer network swollen with a solvent. If properly designed, polymer gel can hold 1000 times as much solvent as polymer weight, have deformability more than 10 times, and can retain/release macromolecular substances like protein. Such high swellability, deformability, and permeability of polymer gel are unique characteristics not found in other materials. Due to these characteristics, hydrogels are used for many applications such as absorbent materials for paper diapers, soft contact lenses, drug reservoir, etc. Recently, considerable attention has been paid as a material for future medical care such as tissue-replacement material and scaffold for regenerative medicine. This book explains the correlation between the physical properties and structure of polymer gels and is prepared for university students learning polymer gels for the first time.

Unique properties of polymer gels stem from their unique structure; though the significant component is solvent, a polymer gel is solid due to the 3D polymer network with a few percent by weight. Notably, the polymer network and the solvent are not separated in two phases, but they exist together as a gel phase. Thus, a polymer gel has both a solid-like nature stemming from a three-dimensional network and a polymer solution-like nature arising from a solvent dissolved and retained in a polymer network. This duality is the feature of polymer gels not found in other materials and the source of the uniqueness. At the same time, however, this duality often causes difficulty in understanding polymer gels. The solid nature of polymer gel is discussed based on the theory of rubber elasticity, while the liquid-like nature is presented based on the theory of polymer solutions. Therefore, to understand the basic concept of polymer gel, fundamental understanding of both is indispensable, and the harmony of both is essential.

Both rubber elasticity and polymer solution theory are based on statistical mechanics. Under ideal assumptions, both theories bring rigorous prediction by mathematical formulas for various physical property values. On the other hand, the 3D polymer network is inherently heterogeneous; this is obvious from the fact that even synthetic linear polymer chains have heterogeneous distribution in length. It is impossible to synthesize a polymer network with uniform mesh size and number of branching. Since it is not possible to accurately define the structure, it is difficult to formulate the distribution function and to adapt the statistical mechanics approach practically.

For this reason, it is difficult to understand the correlation between the structure and physical properties of a real polymer gel, and the contribution of theory to material design may be limited. However, we believe that understanding the fundamentals of polymer gels is still relevant, because the hurdle for practical application of polymer gels is high, and it is difficult to go beyond the difficulty relying only on experience. Material design based on fundamentals is indispensable to overcome this situation. Understanding the phenomenon in the form of a mathematical expression is extremely meaningful, even though we cannot observe quantitative agreement between the theory and the experimental result. Useful information is often obtained by comparing experimental results with theoretical values obtained under certain exact assumptions. It is also essential to change the degree of coarse-graining and watch over the rough sketch of physical properties using scaling theory. In this way, it is crucial to handle the heterogeneity of polymer gels. On the other hand, it is vital to deepen the fundamental understanding of polymer gels by experimentally verifying the theories using polymer gels with a well-defined structure.

Therefore, in this book, as an introduction of basic knowledge, we first explain the statistical mechanics and scaling of a polymer chain in Chapter 1 and that of polymer solution in Chapter 2. In Chapter 3, we introduce the structure of polymer gels and explain the rubber elasticity, which predicts the solid-like nature of polymer gels. In Chapter 4, we describe the swelling/deswelling, which can be understood by combining the rubber elasticity (solid-like nature) and the osmotic pressure of a polymer solution (liquid-like nature). We introduce the large deformation and fracture in Chapter 5 and the diffusion of substances in polymer gels in Chapter 6, which are essential for practical applications.

The last half of this book contains our experimental results using Tetra-PEG gels, which is a near-ideal polymer gel developed by us. We briefly explain Tetra-PEG gels in Chapter 7 and experimental results in Chapters 8–17. We examined the validity of the most of the theories presented in the first half using Tetra-PEG gels. This book was designed to be an introduction to understand polymer gels. By comparing the first half and the last half, readers can learn how to examine the models and how to utilize the models to experiments. I hope this book will help you know polymer gels.

Tokyo *Takamasa Sakai*
December 2019

Acknowledgements

I want to express my gratitude to all the students who have promoted research together. This textbook is a culmination of 12 years that I learned about polymer gels with you. Special thanks go to Takuya Katashima, Xiang Li, Takeshi Fujiyabu, Yuki Yoshikawa, and Yuki Akagi. Also, I would like to express my gratitude to Junsei Kishi, who helped to publish the original Japanese version.

I sincerely express my most substantial gratitude to Prof. Ung-il Chung, who proposed writing this book. Almost every day, he has encouraged me, "Is writing textbooks progressing? You must write every day, even little by little." I can say that this book has never been realized unless Ung-il has encouraged me.

I also thank my family, Kanako, Chiho, and Itsuki with all of my love.

Part I

Theories

Physics of Polymer Gels, First Edition. Edited by Takamasa Sakai.

1

Single Polymer Chain

Takamasa Sakai

Graduate School of Engineering, The University of Tokyo, Tokyo, Japan

1.1 General Features

A polymer gel is a three-dimensional network of polymer chains containing a large amount of solvent (Figure 1.1). When a network structure is formed only by chemical bonding, all the polymer chains are included in a single molecule; one large macromolecule traps a large number of solvent molecules. Let us calculate the molecular weight of a polymer gel. For example, 100 g of a gel with a polymer concentration of 5% contains 5 g of polymer networks. In other words, one molecule has a weight of 5 g. Because the molecular weight is given by the sum of Avogadro's number of weights of individual molecules, the molecular weight of the polymer gel is 3×10^{24} g/mol, which is extremely large. When one stretches a piece of polymer gel, all the chains forming this extremely large macromolecule are stretched, which is why the mechanical properties of polymer gels are predicted based on the simple sum of the contributions of single polymers connected to neighboring chains via crosslinks. Thus, learning the characteristics of a single polymer chain is important for understanding polymer gels. This chapter introduces some methodologies for extracting the universal characteristics of a single polymer chain.

1.1.1 Conformation of a Polymer Chain

A polymer chain is a linear molecule containing a large number of atoms. Prior to considering the shape of a polymer chain, let us focus on the local structure of a polymer composed of four carbons (Figure 1.2). When a carbon–carbon single bond is present between the monomers, the distance between each monomer is approximately 1.5 Å. Additionally, if carbons are connected by a single bond, the bond angle θ is essentially constant at 109.5°. Even if the bond length and bonding angle are constant, rotation around the bond axis, represented by ψ, is allowed, resulting in conformational flexibility. In fact, the value of ψ takes the trans ($\psi = 0°$) or gauche ($\psi = \pm 120°$) stable angles due to steric hindrance.

Let us increase the number of carbons to 100 and consider the shape of the resulting polymer chain. For example, if all the bonds take trans conformations,

Physics of Polymer Gels, First Edition. Edited by Takamasa Sakai.

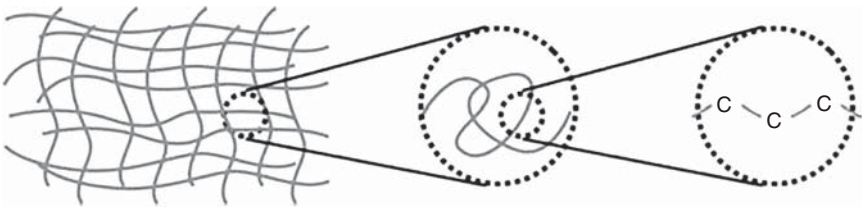

Figure 1.1 Schematic diagram of polymer gels. The polymer network consists of polymer chains connected to neighboring chains via crosslinks.

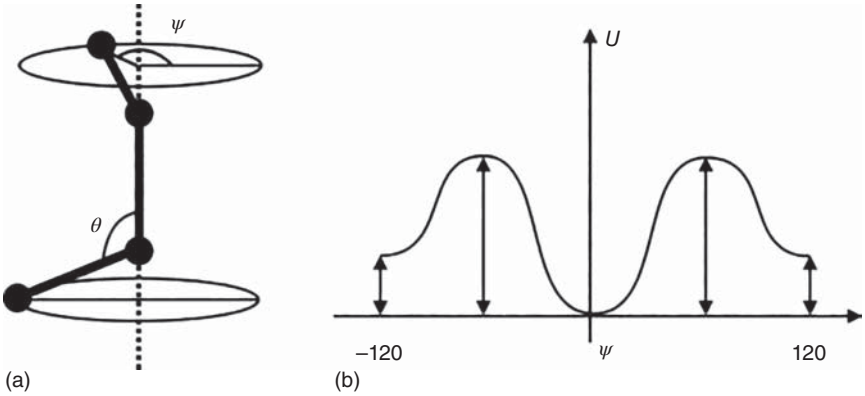

Figure 1.2 Conformation of local structures containing four carbon atoms (a) and the energy landscape (b).

the polymer chain takes an elongated form with an end-to-end distance of approximately 25 nm. Conversely, if all bonds are in gauche conformations, the polymer chain takes a helical structure, and the end-to-end distance becomes very short. Although these structures can be realized by some specific macromolecules or under specific conditions, conventional polymers contain both trans and gauche forms and have highly complicated structures. However, by applying coarse-graining concepts, sufficiently long polymer chains can be approximated to a model chain regardless of the details of the monomer unit.

1.1.2 Coarse-Graining of a Polymer Chain

Here, we introduce "coarse-graining," which is an important concept in discussing polymers. Coarse-graining is one methodology for extracting the universal characteristics of a phenomenon. Roughly speaking, coarse-graining methods intentionally shift focus away from the trivial matters for the characteristics of interest, simplify the problem, and provide the universal characteristics. Let us see an example of coarse-graining for polymer chains. The first coarse-graining is "setting the bond length as constant and the bond angle as freely rotational." This assumption represents a considerable "jump" from the discussion earlier. In principle, the bonding angle should be constant at approximately 109.5°, and the local conformation should be trans or gauche.

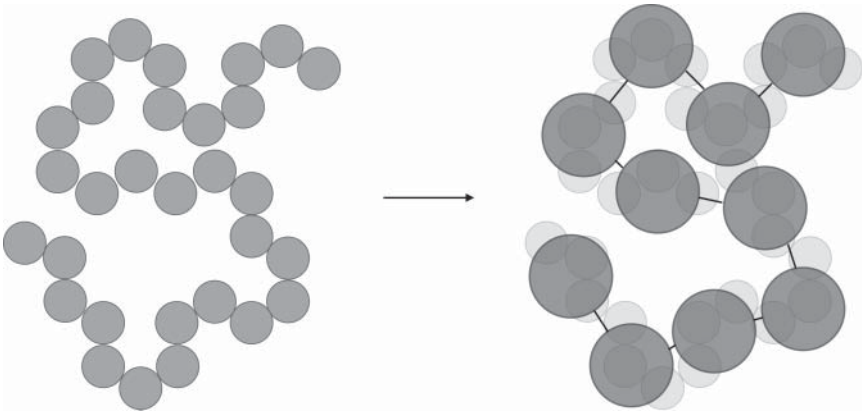

Figure 1.3 Coarse-graining of monomeric units in a polymer chain.

However, one simple idea justifies this coarse-graining. The idea is to combine some monomers together and to make a "segment." Figure 1.3 shows a schematic of making a segment from three monomers; as a result, a polymer chain can be visualized as a sequence of segments. As shown in Figure 1.3, the bonds between neighboring segments can take various angles relative to the bonds between monomers, and the individual properties of each monomer can be masked. Masking the individual properties of each monomer is of great importance in polymer physics, because only under such conditions can we extract the universal properties of the polymer chain. The length of the smallest segment that has freely rotating bonds is called the segment length, which is intrinsic to each monomer unit. Conversely, by taking the appropriate segment with the segment length, the end-to-end distance of a polymer chain is determined by considering a series of segments connected by freely rotating bonds. For simplicity, this book considers polymer chains as consisting of monomers that act as segments with freely rotating bonds, following the method of de Gennes [1]. In other words, the monomer length is the same as the segment length, and the degree of polymerization is the same as the number of segments.

1.1.3 Free Rotation Model

Chains consisting of segments with free rotation can be addressed using the free rotation chain model. Assuming that a polymer chain consists of N vectors ($\mathbf{a}_i$) of size a, the end-to-end distance ($\mathbf{r}$) of the chain is written as follows:

$$\mathbf{r} = \mathbf{a}_1 + \mathbf{a}_2 + \cdots + \mathbf{a}_N \tag{1.1}$$

Since it may be difficult to start with a three-dimensional problem, let us first consider the problem in one dimension. The one-dimensional version of this problem is actually given by the familiar problem as follows:

A point proceeds $+a$ or $-a$ with equal probabilities in one step. How far is the point from the origin after N steps?

This problem is equivalent to tossing coins in high school mathematics. In this case, the displacement, r, can be calculated as an expected value as follows:

$$\begin{aligned} r &= a\left(-N\binom{N}{0}\left(\frac{1}{2}\right)^N-(N-2)\binom{N}{1}\left(\frac{1}{2}\right)^{N-1}\left(\frac{1}{2}\right)\right. \\ &\quad \left.+\cdots+(N-2)\binom{N}{1}\left(\frac{1}{2}\right)\left(\frac{1}{2}\right)^{N-1}+N\binom{N}{0}\left(\frac{1}{2}\right)^N\right) \\ &= a\left[N\left\{-\binom{N}{0}\left(\frac{1}{2}\right)^N+\binom{N}{0}\left(\frac{1}{2}\right)^N\right\}\right. \\ &\quad \left.+(N-2)\left\{-\binom{N}{1}\left(\frac{1}{2}\right)^{N-1}\left(\frac{1}{2}\right)+\binom{N}{1}\left(\frac{1}{2}\right)\left(\frac{1}{2}\right)^{N-1}\right\}+\cdots\right]=0 \end{aligned} \tag{1.2}$$

The result of $r = 0$ is not essential. This answer is obvious from the expression of Eq. (1.2); the situations in which a point reaches $-r$ and r have equal probabilities and cancel each other. In both cases, the end-to-end distance should be considered, r. The absolute value of the displacement must be considered to correctly evaluate the size. In general, the absolute value of the displacement is obtained by the square root of the root mean square of r ($\langle r^2\rangle^{1/2}$). Let us return to the three-dimensional problem from here. For a general three-dimensional vector $\mathbf{r}$, $\langle \mathbf{r}^2\rangle$ is calculated as follows:

$$\begin{aligned} \langle \mathbf{r}^2\rangle &= \mathbf{r}\cdot\mathbf{r} = (\mathbf{a}_1+\mathbf{a}_2+\cdots+\mathbf{a}_N)(\mathbf{a}_1+\mathbf{a}_2+\cdots+\mathbf{a}_N) \\ &= \sum_{i=1}^{N}{\mathbf{a}_i}^2+\sum_{i=1}^{N}\sum_{k\neq i}^{N}\mathbf{a}_i\mathbf{a}_k = Na^2 \end{aligned} \tag{1.3}$$

Here, $\mathbf{a}_i\mathbf{a}_k = 0$ (if $i \neq k$) since each jump vector is uncorrelated ($\langle\cos\theta\rangle = 0$ because the average value of bond angle is 90°). Given that the polymer chains are isotropic, the polymer chains are considered spheres of diameter $aN^{1/2}$. In a one-dimensional problem, some people may feel uncomfortable that vectors can overlap each other. Although the overlap is highly reduced in the three-dimensional space, overlap between the monomer units is permitted under this model. This polymer chain is called an ideal chain [2–4]. This concept is analogous to an ideal gas having no volume. Of course, the overlapping of monomers is not allowed in real polymers; this model is incorrect except in special cases. Despite this assumption being unrealistic, it is the foundation for many theoretical models because the end-to-end distance of an ideal chain follows the Gaussian distribution. The Gaussian distribution is a simple and useful statistical model and thus provides physical quantities in simple forms with less difficulty than other methods. Section 1.2 shows that the Gaussian distribution successfully describes the end-to-end distance of an ideal chain.

1.2 Statistics of a Single Polymer Chain

1.2.1 End-to-End Distance of a 1D Random Walk

In Section 1.1.3, the average end-to-end distance of an ideal chain was determined based on the distribution of end-to-end distances. This section considers the probability that an ideal chain has a specific distance of x. Again, let us start with a one-dimensional problem. Assuming that the number of steps the point proceeded in the + direction is N_+ and that in the − direction is N_- in the previously mentioned one-dimensional problem, the following equations are obtained:

$$N = N_+ + N_- \tag{1.4}$$

$$x = N_+ - N_- \tag{1.5}$$

For simplicity, we can assume that the length of a step is unity and estimate the number of situations ($W(N, x)$) in the case that the point reaches x after N steps. Because sets of N_+ and N_- for arriving at x are uniquely determined from Eqs. (1.4) and (1.5), $W(N, x)$ is estimated as the number of arrangements of N_+ pieces of "+" and N_- pieces of "−" (Figure 1.4):

$$W(N,x) = \binom{N}{N_+} = \frac{N!}{(N-N_+)!N_+!} = \frac{N!}{\left(\frac{N+x}{2}\right)!\left(\frac{N-x}{2}\right)!} \tag{1.6}$$

On the other hand, the total number of possible paths in N steps is 2^N, which is calculated as the total number of situations that can occur when selecting one of the two choices N times. Thus, the probability of reaching x after N steps is expressed as follows:

$$\frac{W(N,x)}{2^N} = \frac{N!}{2^N\left(\frac{N+x}{2}\right)!\left(\frac{N-x}{2}\right)!} \tag{1.7}$$

Calculating the exact value for all N is a very painful task; however, if we make a proper approximation at a sufficiently large limit of N, this equation leads to a

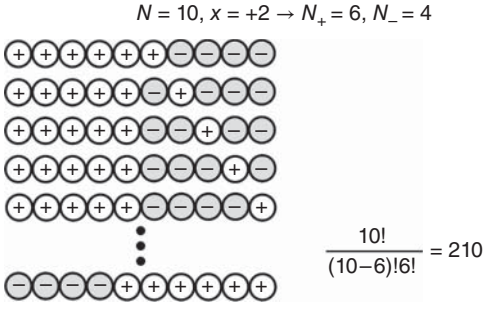

Figure 1.4 Number of situations that reach x in N steps ($N = 10$, $x = +2$).

Gaussian distribution. Let us calculate this value following the method of Rubinstein and Colby [4]. First, the natural logarithm is taken of both sides of the equation:

$$\ln\left(\frac{W(N,x)}{2^N}\right) = \ln N! - N\ln 2 - \ln\left(\frac{N+x}{2}\right)! - \ln\left(\frac{N-x}{2}\right)! \tag{1.8}$$

The last two terms are reduced to the following:

$$\begin{aligned}\ln\left(\frac{N+x}{2}\right)! &= \ln\left[\left(\frac{N}{2}+\frac{x}{2}\right)\left(\frac{N}{2}+\frac{x}{2}-1\right)\cdots\left(\frac{N}{2}+2\right)\left(\frac{N}{2}+1\right)\cdot\left(\frac{N}{2}\right)!\right] \\ &= \ln\left(\frac{N}{2}\right)! + \sum_{s=1}^{x/2}\ln\left(\frac{N}{2}+s\right) \end{aligned} \tag{1.9}$$

$$\ln\left(\frac{N-x}{2}\right)! = \ln\left(\frac{N}{2}\right)! - \sum_{s=1}^{x/2}\ln\left(\frac{N}{2}+1-s\right) \tag{1.10}$$

By substituting Eqs. (1.9) and (1.10) into Eq. (1.8), one obtains the following:

$$\begin{aligned}\ln\left(\frac{W(N,x)}{2^N}\right) &= \ln N! - N\ln 2 - 2\ln\left(\frac{N}{2}\right)! - \sum_{s=1}^{x/2}\ln\left(\frac{N}{2}+s\right) \\ &\quad + \sum_{s=1}^{x/2}\ln\left(\frac{N}{2}+1-s\right) \\ &= \ln N! - N\ln 2 - 2\ln\left(\frac{N}{2}\right)! - \sum_{s=1}^{x/2}\ln\frac{\left(\frac{N}{2}+s\right)}{\left(\frac{N}{2}+1-s\right)} \end{aligned} \tag{1.11}$$

The fourth term in Eq. (1.11) can be rewritten as the following:

$$\ln\frac{\left(\frac{N}{2}+s\right)}{\left(\frac{N}{2}+1-s\right)} = \ln\frac{\left(1+\frac{2s}{N}\right)}{\left(1+\frac{2-2s}{N}\right)} = \ln\left(1+\frac{2s}{N}\right) - \ln\left(1+\frac{2-2s}{N}\right) \tag{1.12}$$

Here, we apply an important approximation of the relationship between s and N. The maximum value of s is $N/2$, and the number of situations corresponding to this case is only 1. In most cases, s stays close to the origin (see one-dimensional walks), making it sufficiently smaller than N. Here, by ignoring the case of large s, which is unlikely, and only considering the case where $s \ll N$, the expression can be further transformed using a Taylor expansion ($\ln(1+y) \approx y$).

$$\ln\left(1+\frac{2s}{N}\right) - \ln\left(1+\frac{2-2s}{N}\right) \cong \frac{2s}{N} - \frac{2-2s}{N} = \frac{4s}{N} - \frac{2}{N} \tag{1.13}$$

Using Eq. (1.13), Eq. (1.11) can be transformed to the following:

$$\begin{aligned}\ln\left(\frac{W(N,x)}{2^N}\right) &= \ln N! - N\ln 2 - 2\ln\left(\frac{N}{2}\right)! - \sum_{s=1}^{x/2}\left(\frac{4s}{N} - \frac{2}{N}\right) \\ &= \ln N! - N\ln 2 - 2\ln\left(\frac{N}{2}\right)! - \frac{4}{N}\sum_{s=1}^{x/2} s + \frac{2}{N}\sum_{s=1}^{x/2} 1 \\ &= \ln N! - N\ln 2 - 2\ln\left(\frac{N}{2}\right)! - \frac{4}{N}\frac{\left(\frac{x}{2}\right)\left(\frac{x}{2}+1\right)}{2} + \frac{2}{N}\frac{x}{2} \\ &= \ln N! - N\ln 2 - 2\ln\left(\frac{N}{2}\right)! - \frac{x^2}{2N} \end{aligned} \tag{1.14}$$

Equation (1.14) can be reduced using the following Starling approximation:

$$N! \cong \sqrt{2\pi N}\left(\frac{N}{e}\right)^N \quad \text{for } N \gg 1 \tag{1.15}$$

$$\begin{aligned}\ln\left(\frac{W(N,x)}{2^N}\right) &= \ln N! - N\ln 2 - 2\ln\left(\frac{N}{2}\right)! - \frac{x^2}{2N} \\ &= \ln\left(\sqrt{2\pi N}\left(\frac{N}{e}\right)^N\right) - N\ln 2 - 2\ln\left(\sqrt{\pi N}\left(\frac{N}{2e}\right)^{N/2}\right) - \frac{x^2}{2N} \\ &= \ln\sqrt{2\pi N} + N\ln\frac{N}{e} - N\ln 2 - \ln\pi N - N\ln\frac{N}{2e} - \frac{x^2}{2N} \\ &= \ln\left(\sqrt{\frac{2}{\pi N}}\right) - \frac{x^2}{2N} \end{aligned} \tag{1.16}$$

As a result, the probability is given by the following:

$$\frac{W(N,x)}{2^N} = \sqrt{\frac{2}{\pi N}}\exp\left(-\frac{x^2}{2N}\right) \tag{1.17}$$

If we consider x to be a continuous value and this function to be a continuous function, Eq. (1.17) corresponds to a probability density distribution function. To investigate the function, let us integrate it from $-\infty$ to ∞:

$$\int_{-\infty}^{\infty}\frac{W(N,x)}{2^N}\mathrm{d}x = \sqrt{\frac{2}{\pi N}}\int_{-\infty}^{\infty}\exp\left(-\frac{x^2}{2N}\right)\mathrm{d}x = \sqrt{\frac{2}{\pi N}}\cdot\sqrt{2\pi N} = 2 \tag{1.18}$$

Since this calculation corresponds to calculating "the sum of probabilities," it is natural that the value of the integral is 1. The doubled integral value comes from the procedure of converting discrete x to continuous x. As shown in Table 1.1, in the lattice space, when N is an even number, the probability that x becomes odd is 0. On the other hand, if N is an odd number, the probability that x will be even is 0. Therefore, for any case, as x is changed to 1, 2, 3, …, the probability alternates between a finite value and 0 (Table 1.1). The integral value of 2 comes from simply changing the discontinuous function to a continuous function.

Table 1.1 Number of situations reaching x in N steps.

	x	−4	−3	−2	−1	0	1	2	3	4
$W(N, x)$	$N = 3$	0	1	0	3	0	3	0	1	0
	$N = 4$	1	0	4	0	6	0	4	0	1

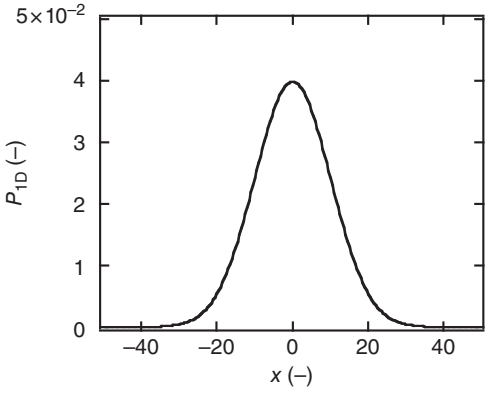

Figure 1.5 Probability density distribution function of the one-dimensional Gaussian distribution (P_{1D} with $a = 1$, $N = 100$).

By standardizing Eq. (1.17) by 2, the probability density function of a one-dimensional random walk ($P_{1D}(N, x)$) is obtained.

$$P_{1D}(N, x) = \frac{1}{\sqrt{2\pi N}} \exp\left(-\frac{x^2}{2N}\right) \tag{1.19}$$

This equation is the same as the Gaussian distribution with an average ($\langle x \rangle$) of 0 and a variance ($\langle x^2 \rangle$) of N (Figure 1.5). The general Gaussian distribution is expressed as follows:

$$f(x) = \frac{1}{\sqrt{2\pi \langle x^2 \rangle}} \exp\left(-\frac{(x - \langle x \rangle)^2}{2\langle x^2 \rangle}\right) \tag{1.20}$$

At the end of the one-dimensional problem, let Eq. (1.20) be expanded to an arbitrary step length. When the step length is a, $\langle x \rangle = 0$ and $\langle x^2 \rangle = a^2 N$, resulting in the following:

$$P_{1D}(N, x) = \frac{1}{\sqrt{2\pi a^2 N}} \exp\left(-\frac{x^2}{2a^2 N}\right) \tag{1.21}$$

1.2.2 End-to-End Distance of a 3D Random Walk

Let us expand the 1D discussion to three dimensions. In 3D space, the probability that one end is at the origin and the other at $\mathbf{r} = (r_x, r_y, r_z)$ is expressed as follows:

$$P_{3D}(N, \mathbf{r}) \mathrm{d}r_x \, \mathrm{d}r_y \, \mathrm{d}r_z = P_{1D}(N, r_x) \mathrm{d}r_x \cdot P_{1D}(N, r_y) \mathrm{d}r_y \cdot P_{1D}(N, r_z) \mathrm{d}r_z \tag{1.22}$$

By obtaining the root mean square of $\mathbf{r}$ from Eq. (1.3) and assuming the spatial isotropy, the following equation is obtained:

$$\langle \mathbf{r}^2 \rangle = \langle {r_x}^2 \rangle + \langle {r_y}^2 \rangle + \langle {r_z}^2 \rangle = Na^2$$
$$\langle {r_x}^2 \rangle = \langle {r_y}^2 \rangle = \langle {r_z}^2 \rangle = \frac{Na^2}{3} \tag{1.23}$$

Here, we focus on the x-axis component. From Eqs. (1.21) and (1.23), the following equation is obtained:

$$P_{1D}(N, r_x) = \frac{1}{\sqrt{2\pi\langle {r_x}^2 \rangle}} \exp\left(-\frac{{r_x}^2}{2\langle {r_x}^2 \rangle}\right) = \sqrt{\frac{3}{2\pi N a^2}} \exp\left(-\frac{3{r_x}^2}{2Na^2}\right) \tag{1.24}$$

The y- and z-axis components are estimated in similar ways and substituted into Eq. (1.22).

$$\begin{aligned} P_{3D}(N, \mathbf{r}) &= P_{1D}(N, r_x) \cdot P_{1D}(N, r_y) \cdot P_{1D}(N, r_z) \\ &= \left(\frac{3}{2\pi N a^2}\right)^{3/2} \exp\left(-\frac{3({r_x}^2 + {r_y}^2 + {r_z}^2)}{2Na^2}\right) \\ &= \left(\frac{3}{2\pi N a^2}\right)^{3/2} \exp\left(-\frac{3\mathbf{r}^2}{2Na^2}\right) \end{aligned} \tag{1.25}$$

Compared with Eq. (1.21), the probability density functions in one dimension and three dimensions are almost the same. However, the probability distribution that the distance between both ends becomes $|\mathbf{r}|$ differs greatly between one dimension and three dimensions. In one dimension, the probability distribution ($\mathbf{r} \neq 0$) is written as follows since the distance between the ends being $|\mathbf{r}|$ only occurs in two cases: the cases of $-r$ and $+r$.

$$Pr_{1D}(N, |\mathbf{r}|) = 2\sqrt{\frac{1}{2\pi N a^2}} \exp\left(-\frac{\mathbf{r}^2}{2Na^2}\right) = \sqrt{\frac{2}{\pi N a^2}} \exp\left(-\frac{\mathbf{r}^2}{2Na^2}\right) \tag{1.26}$$

Because there is only one situation for $\mathbf{r} = 0$, the probability distribution is given by

$$Pr_{1D}(N, |\mathbf{r}|) = \sqrt{\frac{1}{2\pi N a^2}} \exp\left(-\frac{\mathbf{r}^2}{2Na^2}\right) \tag{1.27}$$

In the case of three dimensions, we need to consider a multiplicity factor of $4\pi r^2$ because the end-to-end distance of $|\mathbf{r}|$ occurs everywhere on the spherical shell with radius $|\mathbf{r}|$. Thus, the probability distribution can be written as follows:

$$Pr_{3D}(N, |\mathbf{r}|) = 4\pi r^2 \left(\frac{3}{2\pi N a^2}\right)^{3/2} \exp\left(-\frac{3\mathbf{r}^2}{2Na^2}\right) \tag{1.28}$$

Figure 1.6 shows the probability distributions of one-dimensional and three-dimensional end-to-end distances. Their shapes are completely different from each other; in one dimension, there is a local maximum in the vicinity of $r = 0$,

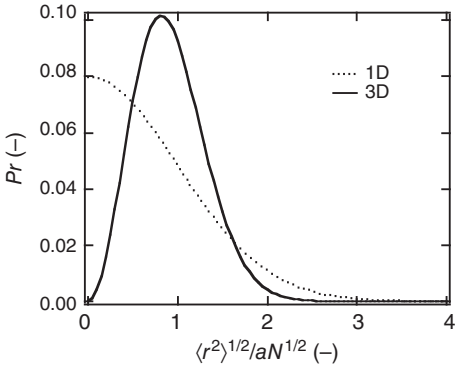

Figure 1.6 Probability distribution of end-to-end distances of one-dimensional and three-dimensional random walks.

whereas in three dimensions, there is a local maximum in the vicinity of $aN^{1/2}$. Notably, the probability that the random coil returns to the vicinity of the origin is almost 0 in three dimensions. This difference is obviously due to the multiplication factor of $4\pi r^2$, as there was no significant difference in the probability density distribution itself in one dimension and three dimensions. In three-dimensional space, only $r_x = r_y = r_z = 0$ satisfies $|\mathbf{r}| = 0$, whereas there are many combinations of r_x, r_y, r_z that satisfies ${r_x}^2 + {r_y}^2 + {r_z}^2 = |\mathbf{r}|^2$, when $|\mathbf{r}| \neq 0$. This difference in multiplicity causes the major difference in the one-dimensional and three-dimensional probability distributions.

1.2.3 Force Needed to Stretch an Ideal Chain

We then consider the force required to stretch an ideal chain. Under constant temperature and pressure, the total free energy of an ideal chain is written using enthalpy (U) and entropy (S).

$$F = U - TS \tag{1.29}$$

The change in total free energy when the end-to-end distance is extended to r is written as follows:

$$\Delta F = \Delta U - T\Delta S = \{U(N, \mathbf{r}) - U(N, 0)\} - T\{S(N, \mathbf{r}) - S(N, 0)\} \tag{1.30}$$

Here, it should be noted that the reference state is $\mathbf{r} = 0$, which is discussed in detail later. Based on the definition, entropy is expressed as the following:

$$S = k \ln \Omega \tag{1.31}$$

where Ω is the number of possible conformations of the ideal chain with a number of monomers equal to N and an end-to-end vector of $\mathbf{r}$. In contrast, by definition, Ω can be written as follows:

$$P_{3D}(N, \mathbf{r}) = \frac{\Omega(N, \mathbf{r})}{\int \Omega(N, \mathbf{r}) \mathrm{d}\mathbf{r}} \tag{1.32}$$

From Eqs. (1.31) and (1.32), one obtains the following:

$$S = k \ln \left(P_{3D}(N, \mathbf{r}) \cdot \int \Omega(N, \mathbf{r}) \mathrm{d}\mathbf{r} \right) \tag{1.33}$$

In contrast, there is no enthalpy change (ΔU) during stretching because the large deformation can be achieved by rotation around the bond axis without changing the bond lengths or bond angles. (Indeed, there is a weak energy term derived from the interactions between polymer segments, but it does not exist under the assumptions of an ideal chain.) Therefore, the energy change during the deformation mainly stems from the entropy change. This so-called entropic elasticity is completely different from the energy elasticity, which stems from the enthalpy changes of metals and ceramics. Taken together, the energy change from the deformation is given by the following:

$$\begin{aligned} -\frac{\Delta F}{T} &= S(N,\mathbf{r}) - S(N,0) = k\ln\left(P_{3D}(N,\mathbf{r})\int \Omega(N,\mathbf{r})\mathrm{d}\mathbf{r}\right) \\ &\quad - k\ln\left(P_{3D}(N,0)\int \Omega(N,\mathbf{r})\mathrm{d}\mathbf{r}\right) \\ &= k\ln\frac{P_{3D}(N,\mathbf{r})}{P_{3D}(N,0)} + k\left\{\ln\int \Omega(N,\mathbf{r})\mathrm{d}\mathbf{r} - \ln\int \Omega(N,\mathbf{r})\mathrm{d}\mathbf{r}\right\} \\ &= k\ln\frac{P_{3D}(N,\mathbf{r})}{P_{3D}(N,0)} \end{aligned} \tag{1.34}$$

Notably, $\int \Omega(N, \mathbf{r})\mathrm{d}\mathbf{r}$ is the total number of possible conformations and corresponds to 2^N in the one-dimensional problem described earlier, and this value does not depend on $\mathbf{r}$. Substituting Eq. (1.25) into Eq. (1.34), we obtain Eq. (1.35):

$$-\frac{\Delta F}{T} = k\ln\frac{P_{3D}(N,\mathbf{r})}{P_{3D}(N,0)} = k\ln\frac{\left(\frac{3}{2\pi Na^2}\right)^{3/2}\exp\left(-\frac{3r^2}{2Na^2}\right)}{\left(\frac{3}{2\pi Na^2}\right)^{3/2}} = -\frac{3kr^2}{2Na^2} \tag{1.35}$$

Finally, applying $R_0 = aN^{1/2}$, the following equation is obtained:

$$\Delta F = \frac{3kTr^2}{2Na^2} = \frac{3kT}{2}\left(\frac{r}{R_0}\right)^2 \tag{1.36}$$

Next, let us calculate the force, f, required to stretch the chain. f is obtained by differentiating the free energy change (ΔF) with displacement (r):

$$f = \frac{\partial \Delta F}{\partial r} = -T\frac{\partial S}{\partial r} = \frac{3kT}{{R_0}^2}r \tag{1.37}$$

The force is proportional to the strain, so the elasticity of the polymer follows Hooke's law. An ideal chain is a spring with a spring constant of $3kT/{R_0}^2$. This spring softens as the polymer becomes longer or the temperature decreases. Notably, the primary component of the spring constant is kT, which is the energy of simple thermal motion. Figure 1.7 is a schematic picture showing a physical representation of this phenomenon. Many children (monomers) are holding hands with each other, and each is moving freely (thermal motion). Let us consider increasing the distance between the flags being held by the children at each end by little bit. When the distance between the ends is short, it may be possible to easily separate the flags to a certain extent, but as the flags are pulled apart more and more, the resistance will increase. Imagining that if the

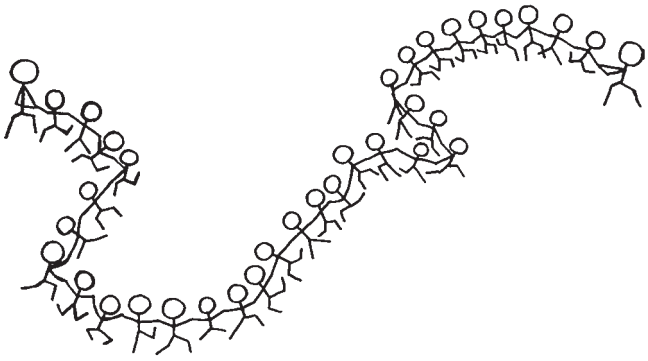

Figure 1.7 Schematic picture of a thermally fluctuating polymer chain.

movement of the children gets faster intuitively suggests that the necessary force becomes greater. Essentially, the same phenomenon occurs when stretching a polymer chain. The elastic energy of the polymer originates from the thermal fluctuations of the monomer units.

Importantly, this spring has a finite length and can be extended to a maximum of aN. As mentioned earlier, the applicability of the Gaussian distribution is limited for small deformations (Eq. (1.13)). When stretched beyond a certain point, the force diverges to values greater than what are predicted. The maximum stretchability is roughly predicted by the Kuhn model from the initial length ($aN^{1/2}$) and maximum length (aN) [5]. This equation expects that longer polymers will be more stretchable.

$$\lambda_{\max} = \frac{aN}{R_0} = \frac{aN}{aN^{1/2}} = N^{1/2} \tag{1.38}$$

Here, let us return to Eq. (1.30) again and think about why the reference condition is $r = 0$. At first glance, this appears contradictory to Eq. (1.28) and Figure 1.6. The end-to-end distance with the highest probability in three dimensions is approximately $aN^{1/2}$, and from the principle of entropy elasticity, the reference state is likely to be approximately $r = aN^{1/2}$. The reference state of $r = 0$ seems to correspond to the one-dimensional results rather than the results in three dimensions. Indeed, this is the essence of the problem. Once the two ends of the polymer are fixed and stretched, the end-to-end vector $\mathbf{r}$ is deformed only in the initial vector direction, and the axial direction will not change. Therefore, the multiplicity of $4\pi r^2$ is lost, reducing the problem to one dimension, which is why the reference state of $r = 0$. From this result, the following strange behavior is expected. When one encounters a polymer in three-dimensional space, the most stable end-to-end distance is $aN^{1/2}$. Once one pinches both ends of the chain, the chain automatically shrinks to 0 because the most stable state is $r = 0$.

Here, we introduce an example in which this phenomenon causes problems. Consider simulating a polymer network using the statistical results of the ideal chain. In three-dimensional space, ideal polymers have an average end-to-end distance of $aN^{1/2}$. We distribute ideal chains so that an average distance between

them is roughly $aN^{1/2}$ and crosslink them. This situation is similar to the situation in which prepolymers with functional groups at both ends are crosslinked by crosslinking agents. We then apply Eq. (1.36), which is the potential for single polymer strands, to each polymer chain. At that moment, the polymer chain automatically shrinks, and the polymer network collapses. In this way, if one simply applies the results based on an ideal chain, one will obtain a practically unrealistic outcome. Similar problems occur when predicting the mechanical properties of polymer networks from the mechanical properties of a single polymer chain.

Since the analytical methods shown in this section can be handled as mathematical equations, it is possible to discuss even coefficients. However, difficult mathematical formulas that are not intuitive must be solved. Additionally, although it is possible to obtain exact solutions under certain limited conditions, solving these equations will not readily provide a rough grasp of more universal behavior. For example, analytically determining the relationship between force and displacement for real polymer chains is practically impossible. On the other hand, the idea of scaling enables us to consider the behavior of polymers in the form of a power law. The scaling theory was first applied to polymer physics by Pierre-Gilles de Gennes. The scaling theory is highly suitable for "coarse-graining" the polymeric system. Using scaling theory, the universal properties of polymers have been predicted and experimentally demonstrated. In this book, analytical description, scaling description, or both are shown to be necessary. In Section 1.3, we introduce the scaling rules for an ideal chain as an introduction of scaling theory.

1.3 Scaling of a Single Polymer Chain

Roughly speaking, the scaling rule is a power law relationship expressing how the parameter of interest changes when other parameters are changed. As an example, let us consider the relationship between the radius (r) and the volume (V) of a sphere:

$$V = \frac{4}{3}\pi r^3 \tag{1.39}$$

What is the essence of this formula? Of course, although it is important for young people to remember the exact equation, it is rare for adults to estimate the exact volume of a ball. There is little possibility of encountering the following problem:

If the radius of a sphere is doubled, by what factor does the volume increase?

When solving this problem, it is not convenient to calculate the volume of the two spheres and then calculate the ratio. Instead, we only use the fact that the volume is the cube of the radius, and $2^3 = 8$. This example gives us a conceptual understanding of the power law relationship, and scaling theory focuses only on the power law relationship. The scaling law between the radius and the volume of the sphere is written as follows:

$$V \sim r^3 \tag{1.40}$$

The coefficient is eliminated, and the formula is dramatically simplified. As a result, this equation expresses the relationship between the volume of the 3D

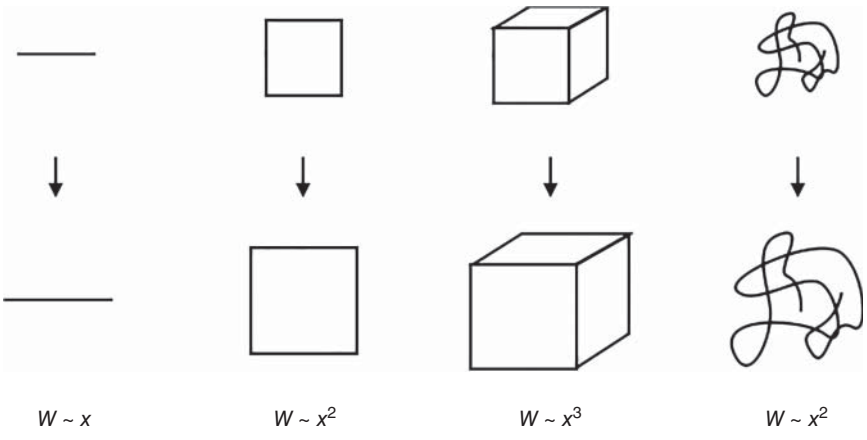

Figure 1.8 Relationship between the weight (W) and length (x) of D-dimensional objects.

object and the representative length. In this way, fine information is lost, and the relationship is generalized. This universality of the scaling fits polymer physics, and it describes the universal rules of polymer chains independent of polymeric species. Indeed, many scaling laws of polymers have been predicted and experimentally validated. Because this book only introduces important scaling laws for understanding polymer gels, I recommend reading the original textbook of de Gennes if you want to learn more. You can find at least two scaling rules earlier in this book. One is scaling for $\langle r^2 \rangle$ of an ideal chain, which is given by Eq. (1.3) as follows:

$$\langle r^2 \rangle \sim N \tag{1.41}$$

From this scaling rule, we can see the characteristics of the ideal chain. In general, an isotropic D-dimensional object has the following relationship between the characteristic length, x, and the weight, w (Figure 1.8):

$$w \sim x^D \tag{1.42}$$

For example, in one dimension, the weight is proportional to the length, and in three dimensions, the weight is proportional to the cube of the length. How does this apply to the ideal chain? Given that the degree of polymerization is proportional to the weight of a polymer chain ($w \sim N$), the following equation is obtained:

$$w \sim N \sim \langle r^2 \rangle \sim x^2 \tag{1.43}$$

The scaling rule reveals that the weight of an ideal chain is proportional to the square of the length. Thus, an ideal chain has a two-dimensional structure despite being an isotropic three-dimensional object. Objects having fractal structures have such extended dimensions, so-called the fractal dimension. Therefore, an ideal chain has a two-dimensional fractal structure.

1.3.1 Stretching of an Ideal Chain

Another important scaling rule that has already been addressed is the relationship between displacement and force in stretching of an ideal chain ($f \sim r$). In this section, scaling theory is applied to determine the force required to stretch an ideal chain. According to de Gennes, this scaling relationship is obtained from the following two conditions:

1. The length (R) after stretching depends only on tension (f), temperature (T), and the initial length (R_0).
2. Since tension (f) is constant at any point along the chain, R must be a linear function of N.

Condition 1 is used for the dimension analysis, which is based on the idea that when the unit systems of the left and right sides are compatible, the equality of the sides is physically correct. This analysis is useful for investigating the relationship between correlating parameters. Many physics teachers will tell you that formula can easily be predicted based on the units of the parameters. An example of dimension analysis is predicting that the formula for speed divides the distance by the time based on the units of speed (m/s). For dimension analysis, let us summarize the units of each physical quantity shown in Condition 1.

$$R\,(\mathrm{m}),\ \ f(\mathrm{N}),\ \ \ T(\mathrm{K}),\ \ \ R_0(\mathrm{m})$$

Since R and R_0 have the same unit system, they seem to be easy to handle, and f and T will require more consideration. For T, the units can be converted to that of energy (J = N m) in the form of kT with Boltzmann's constant (k). For f, multiplying with R forms the work (N m), which involves applying a force of f and stretching the chain by R. Notably, the initial length is 0 since it becomes a one-dimensional problem at the moment both ends are grasped. Based on these considerations, we obtain the following expression by setting the ratio of the length on the left side and the ratio of the energy on the right side:

$$\frac{R}{R_0} \sim \frac{fR}{kT} \tag{1.44}$$

Since this scaling rule is dimensionless on both sides, the dimensions of both sides are of course consistent. However, this equation does not show all possible relationships. Because both sides are dimensionless, even if one multiplies the right side, one can obtain a dimensionally correct expression. Expression (1.44) is a special case ($x = 1$) of the expression shown as follows:

$$\frac{R}{R_0} \sim \left(\frac{fR}{kT}\right)^x \tag{1.45}$$

Since an expression including this arbitrary exponent is obtained from Condition 1, the value of x in the equation derived from Condition 1 is estimated by Condition 2. Let us look at Condition 2 before determining the final scaling rule. What Condition 2 says is extremely simple. That is, "when a chain is divided in half, the force applied to both ends of each half is still f, so the elongation of each half is one-half of that of the whole chain. Therefore, the chain elongation should be

proportional to the degree of polymerization ($R \sim N$)." By applying this condition to Eq. (1.45), x can be determined. Since f and kT do not depend on R or N, they are excluded from the equation, leaving only the relevant physical quantities (R and N).

$$\frac{R}{R_0} \sim R^x \tag{1.46}$$

Rearranging the formula and applying $R_0 \sim N^{1/2}$, we obtain the following:

$$R \sim {R_0}^{\frac{1}{1-x}} \sim N^{\frac{1}{2(1-x)}} \tag{1.47}$$

According to Condition 2 ($R \sim N$), $x = 1/2$. By substituting $x = 1/2$ into Eq. (1.45), the following equation is obtained:

$$f \sim \frac{kT}{{R_0}^2} R \sim \frac{kT}{a^2 N} R \tag{1.48}$$

Although the calculation itself is simple, Eq. (1.48) is almost the same as Eq. (1.37). Let us turn our attention to the following problem. Considering only the unit system, it should be possible to set fR_0 instead of fR as the impulse in Eq. (1.45). Can we still obtain the same conclusion? In fact, the same expression can be obtained. In this way, if one can imagine, one can predict the correct scaling rule without having to solve difficult mathematical problems. This simplicity is an advantage of scaling theory, and at the same time, it can be said that the difficulty in visualizing the problem is the bottleneck. Scaling theory is particularly powerful for complex problems and is compatible with polymer gels with complex structures. Becoming comfortable with scaling theory by learning the various scaling laws in this book will be of great help.

1.3.2 Real Chains

An ideal chain could be modeled as a simple random walk such that the overlapping of monomers is allowed. However, the overlapping of monomers is of course not allowed in reality. A model chain with an excluded volume is called a real chain. Notably, a real chain is a chain modeled by simply adding the excluded volume effect to an ideal chain, but it is still different from chains that actually exist. Real chains are described in a model called a self-avoiding random walk (SAW) [6]. In a SAW, passing through a previously occupied trajectory is inhibited. Although only one condition, in which overlapping is not permitted, is added, the analysis of a SAW is substantially more difficult. For example, the one-dimensional problem cannot be simply extended as it can in ideal chains because the nature of the SAW changes substantially depending on the dimensions of the lattice. For example, in one dimension, there are only two straight paths forward, the plus and minus directions. Intuitively, the number of cases increases qualitatively in 2D and 3D. Even in the two-dimensional and three-dimensional SAWs, it is rare for both chain ends to be close to each other because of the excluded volume effect.

Correlations between close events are relatively easier to consider in the context of processes that are described probabilistically, such as SAW, but to consider

correlations between distant events is extremely difficult. For example, the condition "go forward, but do not to step on the occupied lattice point one step ahead" can be relatively easily formulated, while it is extremely difficult to formulate the condition "do not step on any lattice point that is currently occupied." Despite the difficulty, the statistical properties of SAW have been revealed using various mathematical methodologies. For example, the root-mean end-to-end distance ($\langle r^2 \rangle = {R_F}^2$) in three-dimensional space can be expressed as follows:

$$R_F = aN^{3/5} \tag{1.49}$$

For the derivation, solving difficult mathematical problems or using simulations is necessary. It may seem that compared with $R_0 = aN^{1/2}$ for an ideal chain, this equation is not very different. However, for example, when $a = 3$ Å and $N = 100$, $R_0 = 30$ Å and $R_F = 48$ Å, the difference is a factor of approximately 1.5, which suggests that the effect of overlapping inhibition is reasonably large.

1.3.3 Stretching of a Real Chain

Finally, let us consider the force needed to stretch a real chain. Similar to an ideal chain, the following physical quantities are likely related to this phenomenon:

$$R\,(\mathrm{m}), f\,(\mathrm{N}), T\,(\mathrm{K}), R_F\,(\mathrm{m})$$

The difference between the real chain and the ideal chain is only in the reference, which changed from R_0 to R_F. A similar expression is predicted for an ideal chain:

$$\frac{R}{R_F} \sim \left(\frac{fR}{kT}\right)^x \tag{1.50}$$

Here, unlike in the case of an ideal chain, we assume the chain shows spring-like behavior and resulting Hooke's law ($f \sim R$). Focusing only on the relationship between f and R, we obtain

$$R^{1-x} \sim f^x \tag{1.51}$$

To satisfy Hooke's law, it is necessary for x to equal 1/2. By substituting $x = 1/2$ into Eq. (1.50), the following equation is obtained:

$$f \sim \frac{kT}{{R_F}^2} R \sim \frac{kT}{a^2 N^{6/5}} R \tag{1.52}$$

Equation (1.52) is almost identical to that of an ideal chain, and the only difference is due to the difference between R_0 and R_F. In the case of an ideal chain, when a small force f is applied, R is proportional to N (indeed, the scaling rule was derived from this condition). This relationship indicates that the chain was stretched by tension. On the other hand, in real chains, R is proportional to the power greater than the unity of N ($R \sim N^{6/5}$). This power suggests that the tension is not constant in the chain, and the force applied to the chain is transmitted by the interactions between the units in the real chain as well.

Prior to considering stretching with a large force, we introduce a blob, which is an important concept in polymer physics. Up to this point, we considered f

as a product with reference length and as having the same units as energy or impulse. Pincus, on the other hand, introduced a virtual segment (elastic blob) with a length of ξ defined as the following [7]:

$$\xi \approx \frac{kT}{f} \tag{1.53}$$

As is obvious from the formula, ξ is the length required to give the same impulse as the thermal energy ($k_B T$) from the force f. According to the expression, ξ diverges to infinity at the limit of small forces and becomes 0 at the limit of large forces. ξ is the length at which the impulse given by the external force becomes comparable to the thermal energy. Based on Eq. (1.53), we can estimate the measure of the "small force," which is the condition described by Eq. (1.52). When the applied force is small, ξ is a chain size (not infinite), and the energy given by the force is sufficiently small compared with thermal energy; the thermal motion is not influenced by the applied force. Under this condition, the conformation of the chain is not greatly affected by the external force, and the initial statistics (the statistics of a real chain) are preserved. The initial statistics are disturbed from the point of $\xi = R_F$ because the force ($=kT/R_F$) gives impulses comparable to the thermal energy. When such a force is applied, the conformation of the chain is disturbed, and the initial statistics can no longer be used. Thus, Eq. (1.52) holds at a small f as expressed by the following equation:

$$\xi > R_F \leftrightarrow f < \frac{kT}{R_F} \tag{1.54}$$

Next, let us consider the case when a large force f is applied ($\xi \ll R_F$). First, we focus on a monomer unit in the real chain. Does a great change occur in its correlation with neighboring units? In fact, even when a large force is applied, short-range correlations between neighboring units are hardly affected, which is similar to the situation depicted in Figure 1.7; the children in the middle of the line rarely notice that they are being stretched. Instead, the correlations between groups of units are influenced by the force. The group here is the elastic blob. Inside a blob of size ξ, thermal energy dominates energy from an external force, and inside the blob, the initial conformation is preserved. On the other hand, the correlation between blobs is governed by the applied force. Therefore, under strong stretching, the blobs line up in the stretching direction (Figure 1.9). Assuming that the number of monomer units contained inside the blob is g_p, ξ

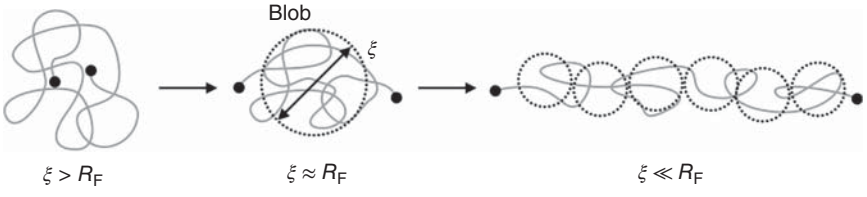

Figure 1.9 Schematic picture of stretching a real chain.

is written as follows:

$$\xi \approx a g_{\mathrm{p}}{}^{3/5} \tag{1.55}$$

Given that the number of blobs is N/g_{p}, the end-to-end distance of a chain is the following:

$$R \approx \xi \cdot \frac{N}{g_{\mathrm{p}}} \approx \xi \cdot N \cdot \left(\frac{\xi}{a}\right)^{-5/3} \approx aN\left(\frac{fa}{kT}\right)^{2/3} \tag{1.56}$$

Now, we rearrange this expression to isolate force f:

$$f \approx \frac{kT}{a}\left(\frac{R}{aN}\right)^{3/2} \tag{1.57}$$

This equation predicts that the force will be proportional to $R^{3/2}$ under a large deformation. However, this power law was not clearly observed in the stretching of a polymer chain as measured by atomic force microscopy (AFM). On the other hand, this scaling rule can be extended to the stretching of gels (Chapter 5), and that rule shows good agreement with experiments [8–10]. Based on these experimental results, the molecular weight of the polymer chain must be sufficiently long to observe the power law predicted by Eq. (1.57).

Column 1: Miscible Gels and Immiscible Gels

In this book, we discuss transparent gels, in which the constituent polymer chains are miscible with the solvent. On the other hand, in turbid gels like "tofu," not all constituent polymers are miscible. In this case, some polymers are phase-separated without solvation, forming an aggregated structure, of which size reaches the visible light region, resulting in turbidity. Therefore, turbid gels can be called immiscible gels or sponge-like gels. Immiscible gels are in between miscible gels and sponges. One of the major differences between miscible and immiscible gels is the solvent retention ability. In immiscible gels, the osmotic pressure is relatively small, because the amount of solvated component is small, leading to poor solvent retention. Therefore, when an immiscible gel is compressed, the solvent is extracted out of the gel. You may know water is easily extracted from tofu; on the other hand, it is hardly extracted from a transparent jelly.

Another difference is that immiscible gels are inherently heterogeneous due to phase separation. In this book, we started the description of polymer gels from that of a polymer chain followed by that of polymer solutions. Thus, this book implicitly treats homogeneous miscible gels. For immiscible gels, mesoscale-sized modeling may be more suitable than molecular models shown in this book; it is better to adopt the prediction based on the mesoscale fibrous structure and the mechanical properties of fibers. Of course, turbid gels like tofu are not just a sponge, but also have properties in between miscible and immiscible gels. Therefore, one needs to consider which character will appear with respect to each physical property.

References

1 de Gennes, P.G. (1979). *Scaling Concepts in Polymer Physics*. Ithaca, NY: Cornell University Press.
2 Doi, M. (1996). *Introduction to Polymer Physics*. Clarendon Press.
3 Flory, P.J. (1953). *Principles of Polymer Chemistry*. Ithaca, NY: Cornell University Press.
4 Rubinstein, M. and Colby, R.H. (2003). *Polymer Physics*. Oxford: Oxford University Press.
5 Kuhn, W. (1946). Dependence of the average transversal on the longitudinal dimensions of statistical coils formed by chain molecules. *J. Polym. Sci.* 1: 380–388.
6 Shuler, K.E. (2009). *Advances in Chemical Physics, Volume 15: Stochastic Processes in Chemical Physics*. Wiley.
7 Pincus, P. (1976). Excluded volume effects and stretched polymer chains. *Macromolecules* 9: 386–388.
8 Katashima, T., Asai, M., Urayama, K. et al. (2014). Mechanical properties of tetra-PEG gels with supercoiled network structure. *J. Chem. Phys.* 140: 074902.
9 Urayama, K. and Kohjiya, S. (1997). Uniaxial elongation of deswollen polydimethylsiloxane networks with supercoiled structure. *Polymer* 38: 955–962.
10 Urayama, K. and Kohjiya, S. (1998). Extensive stretch of polysiloxane network chains with random- and super-coiled conformations. *Eur. Phys. J. B* 2: 75–78.

2

Polymer Solution

Takamasa Sakai

Graduate School of Engineering, The University of Tokyo, Tokyo, Japan

2.1 Polymer Chains in Solution

In Chapter 1, an ideal chain and a real chain were introduced as typical polymer chains. This chapter first addresses what practical conditions will cause a polymer chain to behave as an ideal chain or a real chain. To address this problem, let us consider how much free space is inside a polymer chain. The polymer volume fraction inside the polymer chain (ϕ_{int}) indicates the ratio of the volume occupied by monomer units to the volume of the sphere with a diameter equal to the end-to-end distance of the polymer chain, R (Figure 2.1).

For example, in the case of an ideal chain, since the polymer chain consists of N monomer units with a volume of a^3 and $R = aN^{1/2}$, ϕ_{int} is expressed as follows:

$$\phi_{\text{int}} \approx \frac{a^3 N}{(aN^{1/2})^3} = N^{-1/2} \tag{2.1}$$

For a real chain, the following equation can be used:

$$\phi_{\text{int}} \approx \frac{a^3 N}{(aN^{3/5})^3} = N^{-4/5} \tag{2.2}$$

Therefore, for example, if $N = 100$, ϕ_{int} of the ideal chain and the real chain are 0.10 and 0.025, respectively. Based on these calculations, both real chains and ideal chains have swollen structures, and they become less dense as N increases. Since the monomer units are surrounded by many solvent molecules, the interactions between monomer units and solvent molecules are clearly an important factor in determining the conformation of the polymer chain.

2.1.1 Chain Swelling in a Good Solvent

From the discussion on the internal polymer volume fraction, a polymer chain includes many solvent molecules from the solution. When a good solvent coexists with a polymer, the polymer swells and takes an extended structure compared with an ideal chain. Here, we introduce Flory's approach to the swelling of an ideal chain [1].

Physics of Polymer Gels, First Edition. Edited by Takamasa Sakai.

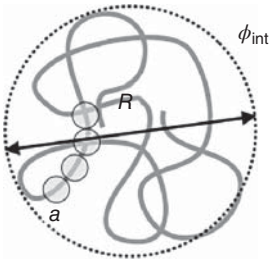

Figure 2.1 Schematic picture of a polymer chain.

When an ideal chain reaches an energy equivalent to the elastic energy (ΔF_{el} in Eq. (1.36)), the ideal chain swells. This energy is generated by the coexistence of a good solvent. In general, the free energy change (ΔF) when a polymer chain is mixed with solvent molecules is expressed as follows:

$$\Delta F = \Delta F_{el} + \Delta H_{mix} - T\Delta S_{mix} \tag{2.3}$$

This equation shows that the swelling tendency caused by the coexistence of the solvent and the restoring tendency due to entropy elasticity determine the state of the system. Let us consider the situation in which the initial end-to-end distance (R_0) changes to αR_0 due to swelling.

$$R = \alpha R_0 \tag{2.4}$$

The equilibrium state is the point where the change in total free energy due to swelling is 0.

$$\frac{\partial \Delta F}{\partial \alpha} = \frac{\partial \Delta F_{el}}{\partial \alpha} + \frac{\partial}{\partial \alpha}(\Delta H_{mix} - T\Delta S_{mix}) = 0 \tag{2.5}$$

Although we do not describe the derivation of this formula in detail, the following solution can be obtained. The method used here is similar to that of gel swelling (see Chapter 4):

$$\alpha^5 - \alpha^3 \sim \left(1 - \frac{T}{\Theta}\right) N^{1/2} \tag{2.6}$$

Here, Θ is the temperature at which the influence of the coexistence of the solvent is negligible (θ temperature). At $T = \Theta$, one obtains $\alpha = 1$, indicating that the chain maintains its initial conformation, a characteristic of an ideal chain. This state is called the θ state, and in this state, the repulsive effect of entropy and the attractive effect from the mixing enthalpy are exactly balanced. In the θ state, the monomer units and the solvent molecules are arranged randomly; the probability that a monomer exists next to another monomer unit and the probability that a solvent molecule exists next to a monomer unit can be written as the initial ϕ_{int} and $1 - \phi_{int}$, respectively.

On the other hand, at $T < \Theta$, Eq. (2.6) becomes positive, and the chain swells ($\alpha > 1$). Under this condition, it is more favorable for monomer units to interact with solvent molecules than interact with other monomer units, and the probability that a solvent molecule exists next to a monomer unit is greater than the initial $1 - \phi_{int}$, resulting in swelling. To roughly investigate the swelling behavior, let us consider the limit of a large N. Here, because the value of expression Eq. (2.6) itself

becomes extremely large, the value of α also becomes large. As a result, $\alpha^5 \gg \alpha^3$ holds, and Eq. (2.6) can be reduced to the following:

$$\alpha^5 \sim \left(1 - \frac{T}{\Theta}\right) N^{1/2}$$
$$\alpha \sim N^{1/10} \tag{2.7}$$

Substitution of this result into Eq. (2.4) gives the following:

$$R \sim N^{1/10} R_0 \sim N^{1/10} N^{1/2} \sim N^{3/5} \tag{2.8}$$

This scaling corresponds to the dependence of R of the real chain on N as shown by Eq. (1.49). In other words, when T is smaller than Θ and N is sufficiently large, the polymer chain takes the conformation of a real chain. Paradoxically speaking, no matter how good the quality of the solvent, a real chain does not swell further, meaning that the upper limit of swelling is the real chain. When conventional polymers are stably dissolved, their structures are in between an ideal chain and a real chain. Analogously, in general polymer chains comprising a miscible polymer gel take an intermediate structure between an ideal chain and a real chain.

2.1.2 Existing Conditions of an Ideal Chain and a Real Chain

Here, we summarize the situations in which the ideal chain and the real chain exist. An ideal chain was modeled by a simple random walk under the assumption that overlapping between segments is allowed. This assumption means that there is no correlation between the arrangement of monomer units and solvent molecules, which corresponds to a situation in which no repulsive forces or attractive forces exist between monomer–monomer, monomer–solvent, or segment–solvent. The simplest example with these conditions is a single polymer melt system because the only component presents in the system is the polymer, and the polymer is serving as both the solute and the solvent. Therefore, there is no entropy of mixing ($\Delta S_{\mathrm{mix}} = 0$), and the interactions between monomer–monomer, monomer–solvent, and segment–solvents are equal ($\Delta H_{\mathrm{mix}} = 0$). Notably, taking the case of $N = 100$ as an example, approximately 10 different ideal chains are within the volume of one average ideal chain in a molten system. Although this prediction was first proposed by Flory, it was not immediately accepted. However, this prediction has been verified by small-angle neutron scattering (SANS) using deuterium-labeled polymers [2].

In addition to the single polymer molten system, Eq. (2.6) indicates that at some $T = \Theta$, the polymer chain takes the conformation of the ideal chain. Generally, in a binary system, mixing is favorable because entropy increases with mixing; in other words, there are repulsive forces between molecules of the same species. To cancel this repulsive force, the enthalpy of mixing should cause certain attractive forces between molecules of the same species. The state in which these entropy and enthalpy changes cancel is the θ state. In the θ state, monomer units and solvent molecules are arranged in an uncorrelated manner, satisfying the condition of the ideal chain. To satisfy this condition in reality, solvents (called θ solvents) specific to the polymer species must be used, and these solvents can be found in the literature [3].

Real chains exist when $T < \Theta$ and $N \gg 1$; in other words, a long polymer chain in a good solvent takes the conformation of a real chain. Notably, $\alpha^5 \gg \alpha^3$ is not satisfied even at $N = 100$. Although it depends on the type of polymer, it has been experimentally shown that Eq. (1.49) holds above approximately $N = 1000$ [4, 5]. A representative example of a good solvent system is an athermal condition. The athermal condition is when $\Delta H_{\mathrm{mix}} = 0$, meaning that the total interaction enthalpies between the monomer units, between the solvents, and between the solvent and the monomer unit cancel out. As a result, the monomer units are repulsed by the contribution from the mixing entropy.

Although the ideal chain and the real chain are representative chain conformations, they are extreme conformations instead of typical conformations. Indeed, in reality, polymer chains have intermediate conformations between those of an ideal chain and a real chain. Generalizing the end-to-end distance R_0 using an index ν indicating the exclusion volume of a polymer chain is convenient.

$$R_0 \approx aN^{\nu} \tag{2.9}$$

ν is 1/2 for ideal chains and 3/5 for real chains, and conventional polymer chains take intermediate values ($1/2 \leq \nu \leq 3/5$) with some exceptions.

2.2 Effect of Concentration on the Polymer Conformation

In Section 2.1, we discussed dilute solutions in which polymers do not overlap with each other. In dilute solutions, because interactions between polymers are negligible, the picture is simple and easy to understand. However, as the concentration increases, polymers begin to interact with each other. At what concentration do polymers start interacting with each other? How will the conformations of the polymers change? In this section, we first focus on the concentration at which polymers start overlapping (the overlapping concentration, c^*, or the overlapping polymer volume fraction, ϕ^*).

2.2.1 Overlapping Concentration

The overlapping concentration is the concentration at which the polymers fill the system while maintaining the conformations they had in the dilute solution (shown in the middle of Figure 2.2). Given that the space is completely filled without overlapping, the polymer volume fraction inside the polymer envelope is identical to that of the whole system. Thus, the following scaling equation is predicted for a polymer with an exclusion volume index ν:

$$\phi^* = \phi_{\mathrm{int}} \approx \frac{a^3 N}{(aN^{\nu})^3} = N^{1-3\nu} \tag{2.10}$$

The exponent on N is $-1/2$ in the case of an ideal chain and $-4/5$ for a real chain; in general, as N increases, the polymer tends to fill the system with a lower polymer concentration. From Eqs. (2.9) and (2.10), the following statements can be derived:

- The volume occupied by one polymer with a degree of polymerization N_1 is larger than that occupied by two polymers each with a degree of polymerization of $N_1/2$.
- If N is small, it is impossible to fill the system no matter how much the concentration is increased; on the other hand, if N approaches infinity, even a single polymer can fill the system.

These facts should be confirmed by the reader by using Eq. (2.9) because these are important for discussing gelation. Notably, in a practical sense, ϕ^* is not a single concentration but a concentration range. The concentration range shown in Figure 2.2b is wide, and it can depend on how ϕ^* was estimated.

How will the conformation of the polymers change as the concentration is increased beyond ϕ^*? Let us start by considering chains in the θ solvent. In the dilute state, the chain has an end-to-end distance of $aN^{1/2}$. In the polymer melt, which is the maximum concentration, the end-to-end distance is also $aN^{1/2}$. Thus, the chain always has an end-to-end distance of $aN^{1/2}$ regardless of the concentration because entropy and enthalpy changes due to the mixing of the polymer and solvent cancel out with each other in any concentration range; there is no total energy change due to the mixing of the polymer and solvent. Therefore, as the concentration increases, ideal chains overlap one another without changing their conformation (mixed model, Figure 2.3b). This prediction has been verified by a SANS experiment using deuterium-labeled substances [2].

Turning our attention to real chains, in the dilute state, a real chain has an end-to-end distance of $aN^{3/5}$. When we decrease the fraction of the solvent, the system becomes a polymer melt, which contains only polymer chains. In a polymer melt, the polymer chains take the conformation of ideal chains regardless of their initial conformation, and the end-to-end distance is $aN^{1/2}$. Therefore, it is expected that for concentrations above ϕ^*, the end-to-end distance gradually shrinks from $aN^{3/5}$ to $aN^{1/2}$ as the concentration increases. To understand this situation, the influence of concentration on the excluded volume effect must be considered.

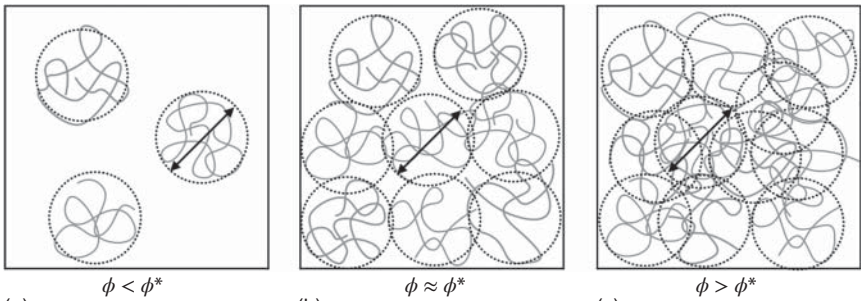

Figure 2.2 Overlapping of polymer chains in different concentration ranges: (a) dilute, (b) semidilute, and (c) concentrated regions.

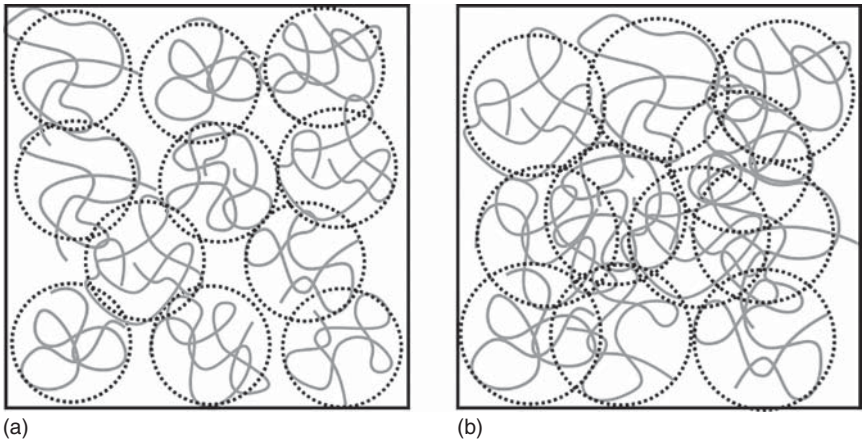

Figure 2.3 Models of polymer solutions: (a) isolated model and (b) combined model.

2.2.2 Semidilute Solution

Let us start with a dilute system in which there is enough space for the polymers to be isolated. At these concentrations, real chains rarely overlap with each other. Therefore, in the dilute state, real chains have an end-to-end distance of $aN^{3/5}$ regardless of the concentration. Next, let us consider the semidilute region above ϕ^*. In this concentration range, nowhere in the system are there isolated polymers. If interpenetration between polymers does not occur even in this state, the polymers will shrink. This model is called an isolated model (Figure 2.3a). Considering that the original size is $aN^{3/5}$ and volume contraction occurs at concentrations higher than ϕ^*, the following scaling relationship is established for the isolated model:

$$R \approx aN^{3/5}\left(\frac{\phi^*}{\phi}\right)^{1/3} \tag{2.11}$$

Here, $(\phi^*/\phi)^{1/3}$ is the ratio of the uniaxial dimension change when the volume shrinks inversely proportional to the concentration. Unlike this model, it is possible to have a conformation close to an ideal chain; at concentrations above ϕ^*, the excluded volume is no longer dominant, and the real chains overlap with each other (mixed model shown in Figure 2.3b). Indeed, many experiments on real chains in solution support the mixed model [6].

How can we draw a picture of the mixed model? First, let us focus on a polymer segment in a polymer solution with a concentration above ϕ^* (Figure 2.4). This segment obviously has the strongest interactions with its two neighboring segments because they are covalently bonded and move essentially together. This type of direct interaction among topological neighbors weakens as the distance between segments increases. Another type of interaction occurs among spatially neighboring segments that do not belong to the same polymer or are not topological neighbors even if they belong to the same polymer. Here, the problem is whether the segment can determine if the spatial neighbor belongs to the same

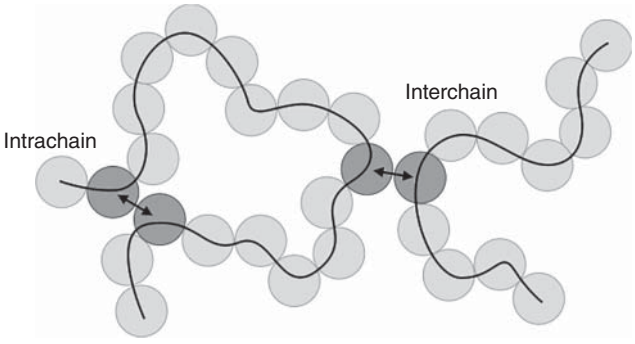

Figure 2.4 Neighboring segments in a polymer solution.

polymer but is topologically far away or if it belongs to another polymer. Ultimately, it is impossible to distinguish because of the decay in topological interactions. Therefore, selectively excluding segments contained in other polymers is impossible, and as a result, adjacent polymers overlap with each other.

2.2.3 Blobs in Semidilute Solution

Let us further consider the case of real chains at semidilute concentrations. Because interactions between segments in a real chain and solvent molecules are favored over interactions among segments, penetration with other chains is disfavored. At concentrations above ϕ^*, polymer chains are forced to penetrate into each other. Given that this applies a kind of pressure to real chains, this situation is similar to the problem of stretching a single chain (see Section 1.2.4), and the blob concept can again be used. The excluded volume is still considered to be dominant on a small scale, although polymers interpenetrate each other on a large scale due to pressure from the surrounding chains. Similar to the discussion in Section 1.2.4, the sequence of segments not involved in interpenetration where the excluded volume dominates can be considered as a blob (concentration blob). The concentration blob is visualized as the nonoverlapping sequence of segments in a snapshot of a semidilute solution (Figure 2.5).

The scaling of the blob size (ξ) is estimated by the following two required conditions:

1. For $\phi \approx \phi^*$, the blob is equivalent to an isolated chain ($\xi \approx R_F$), and ξ decreases as ϕ increases.
2. The blob size does not depend on the molecular weight of the polymer.

Condition 1 is reasonable, given that the exclusion volume of a real chain is dominant at ϕ^*. Condition 2 is reasonable because the length of the polymer chain does not influence the picture shown in Figure 2.5b. The length of the polymer containing a blob (unless it is very short) does not affect the nature of the blob or the interaction between neighboring blobs. The scaling of ξ expected from

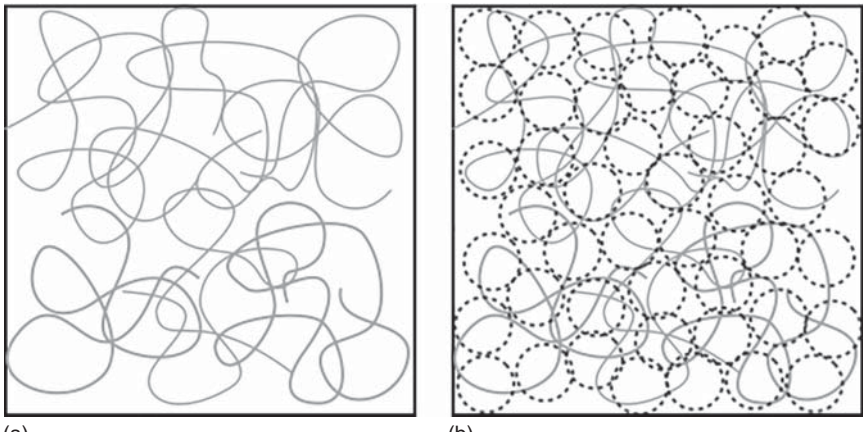

Figure 2.5 Schematic picture of a semidilute solution. A polymer solution (a) is filled with blobs shown as circles (b).

Condition 1 is as follows:

$$\xi \approx R_{\mathrm{F}} \left(\frac{\phi}{\phi^*} \right)^x \tag{2.12}$$

By substituting Eqs. (2.9) and (2.10), we achieve Eq. (2.13):

$$\xi \approx a N^{3/5} \left(\frac{\phi}{N^{-4/5}} \right)^x \tag{2.13}$$

When we focus on the power law of N, we find the following:

$$\xi \sim N^{\frac{3+4x}{5}} \tag{2.14}$$

Applying the requirement of Condition 2 ($\xi \sim N^0$), one obtains $x = -3/4$. As a result, the scaling of ξ is given as follows:

$$\xi \approx a \phi^{-3/4} \tag{2.15}$$

From this equation, concentration blobs are expected to dramatically shrink with increasing concentration. However, concentration blobs do not become shorter than a certain length; since the segments of a real chain cannot overlap, the blob size cannot be smaller than the segment size.

Next, let us consider the end-to-end distance (R) of a real chain at a semidilute concentration. The dimensions of real chains are influenced by other chains and contract slightly with increasing polymer concentration. This contraction can be predicted based on the scaling for the blobs. As shown in Figure 2.5, in a semidilute solution, the blobs are packed in a compact manner. Thus, a real chain in a semidilute solution is considered as a series of blobs. Given that the number of segments included in a blob is g_{p} and the exclusion volume effect is still dominant inside of the blob, ξ is written as follows:

$$\xi \approx a {g_{\mathrm{p}}}^{3/5} \tag{2.16}$$

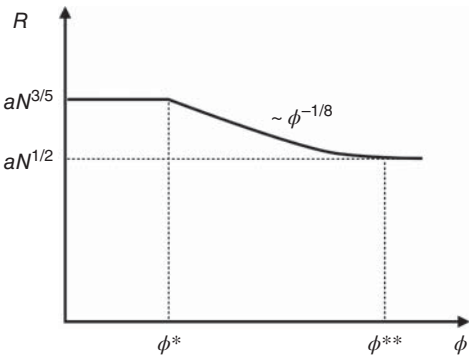

Figure 2.6 Dependence of R on ϕ for a real chain.

Notably, this expression is the same as that of elastic blobs (Eq. (1.55)). Because the number of blobs in a chain is given by N/g_p and the blobs are randomly arranged, R is represented as the following:

$$R \approx \xi \left(\frac{N}{g_p} \right)^{1/2} \tag{2.17}$$

Here, R is estimated as the size of a random walk with a step length of ξ and a number of steps of N/g_p. By substituting Eqs. (2.16) and (2.17), one obtains Eq. (2.18):

$$R \approx \xi N^{1/2} \left(\frac{a}{\xi} \right)^{5/6} \approx a N^{1/2} \phi^{-1/8} \tag{2.18}$$

The dependence of Eq. (2.18) on ϕ is much smaller than that of the isolated model (Eq. (2.5)), suggesting that the effect of surrounding polymers is not significant. Figure 2.6 illustrates how this end-to-end distance varies with increasing concentration. At dilute concentrations, $R = aN^{3/5}$ gradually shrinks in proportion to $\phi^{-1/8}$ above ϕ^* and finally reaches that of an ideal chain ($R = aN^{1/2}$). The concentration region where the chain contracts in proportion to $\phi^{-1/8}$ is called the semidilute region ($\phi^* < \phi < \phi^{**}$), and the region where $R = aN^{1/2}$ is called the concentrated region ($\phi^{**} < \phi$). The reason why the chain does not decrease beyond the size of the ideal chain is that the blob size cannot be smaller than the segment size; the segment has a clear excluded volume at any concentration. Thus, in the concentrated region, a blob is equivalent to a segment. As a result, a real chain can be represented as a random walk consisting of segments and has the same conformation as an ideal chain.

This argument can be extended for general polymers with an index ν. By substituting R_F in Eq. (2.11) for aN^ν, and assuming the blob size is independent of N, the following scaling can be obtained:

$$\xi \approx a \phi^{\frac{\nu}{1-3\nu}} \tag{2.19}$$

$$R \approx a N^{1/2} \phi^{\frac{2\nu-1}{2(1-3\nu)}} \tag{2.20}$$

2.3 Osmotic Pressure of a Polymer Solution

Since polymers comprising a polymer gel are miscible with the solvent, when the gel is immersed in the same solvent as that contained in the gel (for example, when the hydrogel is immersed in water), there is a difference in osmotic pressure between the inside and outside of the gel. Although the polymers in the gel tend to migrate into the external solution to decrease the difference in concentration, they cannot move because they are immobilized by crosslinks, which is similar to situations in which a polymer solution and a solvent are separated by a semipermeable membrane (Figure 2.7). As a result, to reduce the difference in concentrations, the solvent enters the gel, resulting in swelling. In this manner, gels can exchange solvent and substances with their environment and can change their volume in response to external stimuli, which is unlike what is seen in other materials. The key to understanding this unique swelling phenomenon is the osmotic pressure. Here, we will first discuss the osmotic pressure of the polymer solution.

The osmotic pressure (Π) is calculated as a change in the free energy of mixing (F_{mix}) when changing the number of solvent molecules (n_{B}) with a constant number of polymers in the system (n_{A}).

$$\Pi V_1 = -\left(\frac{\partial F_{\mathrm{mix}}}{\partial n_{\mathrm{B}}}\right)_{n_{\mathrm{A}}} \tag{2.21}$$

where V_1 is the molar volume of a solvent molecule. F_{mix} is determined using the difference in entropy (ΔS) and enthalpy (ΔU) before and after the mixing of the solvents and polymers.

$$F = \Delta U - T\Delta S \tag{2.22}$$

In Sections 2.3.1 and 2.3.2, we introduce the derivation of ΔS and ΔU proposed by Flory [7] and Huggins [8].

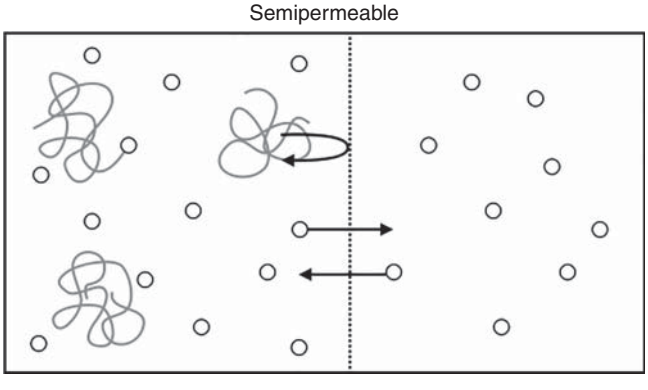

Figure 2.7 System consisting of a polymer solution and a solvent phase separated by a semipermeable membrane.

2.3.1 Entropy Change in Mixing

The entropy change when mixing polymer A and solvent B can be formulated by considering the entropy of placing each molecule in a lattice space.

We define V_A and V_B as the total volume occupied by polymer A and solvent B in the lattice, respectively. N_A and N_B are the number of lattice points occupied by each molecule (corresponding to the degree of polymerization). For simplicity, we assume that the mixing of A and B is ideal, and the volume of the system after mixing is $V_A + V_B$. Assuming that the volume of one lattice point is V_0, the number of molecules A (ν_A) and B (ν_B) can be represented as follows:

$$\nu_A = \frac{V_A}{V_0 N_A} \tag{2.23}$$

$$\nu_B = \frac{V_B}{V_0 N_B} \tag{2.24}$$

The number of lattice points occupied by A (n_A) and B (n_B) is represented by Eqs. (2.25) and (2.26), respectively:

$$n_A = \frac{V_A}{V_0} = n\phi_A \tag{2.25}$$

$$n_B = \frac{V_B}{V_0} = n\phi_B \tag{2.26}$$

where ϕ_A and ϕ_B are the volume fractions of A and B in the mixed system. The number of total lattice points ($n = n_A + n_B$) is given by the following:

$$n = \frac{V_A + V_B}{V_0} \tag{2.27}$$

The configuration entropy is represented based on the number of situations in which A and B can be arranged in the lattice (Ω).

$$S = k \ln \Omega \tag{2.28}$$

Let us consider how to arrange one lattice point of A (Figure 2.8). Given that one can choose any lattice point, the number of arrangements before mixing is n_A, and after mixing is n. Therefore, the entropy change, ΔS, during mixing can be written as follows:

$$\Delta S = k \ln n - k \ln n_A = k \ln \frac{n}{n_A} = -k \ln \phi_A \tag{2.29}$$

This equation shows that the number of cases that can be considered increases by a factor of ${\phi_A}^{-1}$ after mixing. When considering the arrangement of the next lattice point, the number of arrangements before mixing is $n_A - 1$, and after mixing, it becomes $n - 1$. Although one can express all entropy changes, these expressions are extremely difficult to handle. Therefore, we make the following two assumptions:

1. The number of arrangements of all units of polymer A increases by a factor of ${\phi_A}^{-1}$ after mixing and that of polymer B increases a factor of ${\phi_B}^{-1}$.
2. The conformational entropy of the polymers does not change during mixing.

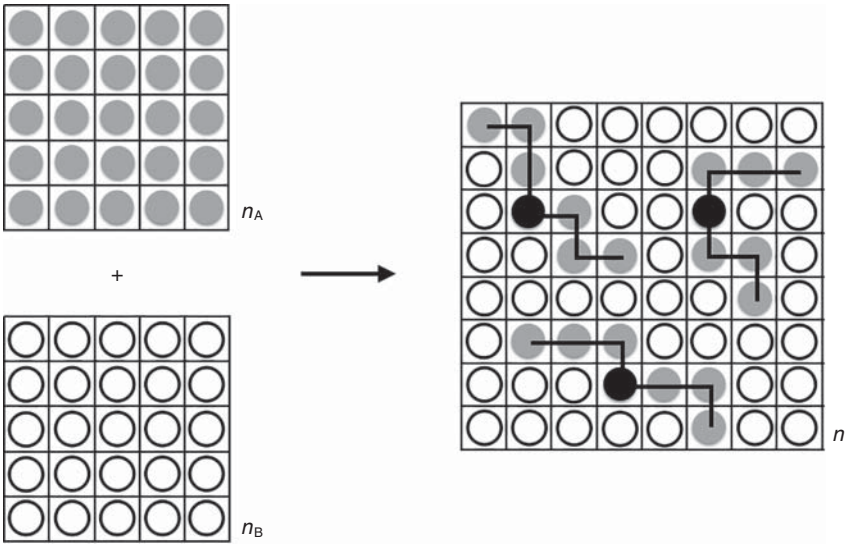

Figure 2.8 Entropy change by mixing polymers and solvents.

Assumption 1 can be rephrased as "the consequences of Eq. (2.29) can be applied even when arranging the second and subsequent units, and the entropy change during mixing is always $-k \ln \phi_A$." Assumption 2 can be rephrased as "when a unit in the center of polymer A (black circle in Figure 2.8) is arranged, the adjacent parts are automatically arranged." Of course, depending on the position of the center and the other polymers, it is often impossible to arrange other units in their original form. Even in that case, other units are arranged in an appropriate conformation with the same conformational entropy. Under these assumptions, we only consider arranging ν_A and ν_B units, which are the number of molecules A and B, respectively. Therefore, the entropy change in the system during mixing can be written as follows:

$$\Delta S_{mix} = \sum_{\nu_A} (-k \ln \phi_A) + \sum_{\nu_B} (-k \ln \phi_B) = -k(\nu_A \ln \phi_A + \nu_B \ln \phi_B) \tag{2.30}$$

The entropy change per lattice point $\Delta \overline{S}_{mix}$ is given by Eq. (2.31):

$$\Delta \overline{S}_{mix} = \frac{\Delta S_{mix}}{n} = -k \left(\frac{\phi_A}{N_A} \ln \phi_A + \frac{\phi_B}{N_B} \ln \phi_B \right) \tag{2.31}$$

Here, given that A is a polymer and B is a small molecule, $N_A = N$ and $N_B = 1$. When we define $\phi_A = \phi$ and $\phi_B = 1 - \phi$, we obtain the following:

$$\Delta \overline{S}_{mix} = -k \left(\frac{\phi}{N} \ln \phi + (1 - \phi) \ln(1 - \phi) \right) \tag{2.32}$$

In general, $\Delta \overline{S}_{mix} \geq 0$ for $0 \leq \phi \leq 1$, the entropy increases with mixing. Given that $\Delta F = \Delta U - T\Delta S$, the system is stabilized by mixing due to the effects of entropy.

2.3.2 Enthalpy Change in Mixing

The enthalpy change in mixing is estimated using a mean-field assumption. Under the mean-field assumption, segments A and B are arranged homogeneously in the system and are not correlated, and the volume fractions of segment A and solvent B in any region are equal to the average values, ϕ_A and ϕ_B. Strictly speaking, this assumption does not hold when the polymer concentration is sufficiently lower than the overlapping density ($\phi_A \ll \phi^*$) because at dilute concentrations, the segment concentration is locally high in the region where the polymer exists but is 0 in the region where no polymer exists. However, for the sake of simplicity, we accept this assumption and proceed with the discussion.

Assuming that the unit interaction energies between AA, BB, and AB are u_{AA}, u_{BB}, and u_{AB}, respectively, the interaction energies (U_A and U_B) between adjacent segments of polymer A and solvent B can be written as follows:

$$\begin{aligned} U_A &= u_{AA}\phi_A + u_{AB}\phi_B \\ U_B &= u_{AB}\phi_A + u_{BB}\phi_B \end{aligned} \tag{2.33}$$

The total interaction energy of the system, U, is given by Eq. (2.34):

$$U = \frac{zn_A U_A}{2} + \frac{zn_B U_B}{2} = \frac{zn}{2}(\phi_A U_A + \phi_B U_B) \tag{2.34}$$

where z is the number of adjacent lattice points and the factor 1/2 is introduced to account for the double counting. By substituting Eq. (2.33) into Eq. (2.34), we obtain the following:

$$\begin{aligned} U &= \frac{zn}{2}\{\phi(u_{AA}\phi + u_{AB}(1-\phi)) + (1-\phi)[u_{AB}\phi + u_{BB}(1-\phi)]\} \\ &= \frac{zn}{2}[u_{AA}\phi^2 + 2u_{AB}\phi(1-\phi) + u_{BB}(1-\phi)^2] \end{aligned} \tag{2.35}$$

This is the total interaction energy in the mixed state. Next, let us consider the interaction energy before mixing. Given that a single A phase contains n_A segments with only AA interactions, the interaction energy of a phase of segment A is given by the following:

$$\frac{zn_A}{2}u_{AA} = \frac{zn}{2}\phi u_{AA} \tag{2.36}$$

Applying the same procedure to solvent molecules B, one can obtain the total interaction energy of separated A and B phases (U_0).

$$U_0 = \frac{zn}{2}[\phi u_{AA} + (1-\phi)u_{BB}] \tag{2.37}$$

Thus, the change in total interaction energy that occurs during mixing is

$$\begin{aligned} U - U_0 &= \frac{zn}{2}[u_{AA}\phi^2 + 2u_{AB}\phi(1-\phi) + u_{BB}(1-\phi)^2] \\ &\quad - \frac{zn}{2}[\phi u_{AA} + (1-\phi)u_{BB}] \\ &= \frac{zn}{2}[-u_{AA}\phi(1-\phi) + 2u_{AB}\phi(1-\phi) - u_{BB}\phi(1-\phi)] \\ &= \frac{zn}{2}\phi(1-\phi)(2u_{AB} - u_{AA} - u_{BB}) \end{aligned} \tag{2.38}$$

The change in the interaction energy per lattice point ($\Delta\overline{U}_{\mathrm{mix}}$) is as follows:

$$\Delta\overline{U}_{\mathrm{mix}} = \frac{U - U_0}{n} = \frac{z}{2}\phi(1-\phi)(2u_{\mathrm{AB}} - u_{\mathrm{AA}} - u_{\mathrm{BB}}) \tag{2.39}$$

Here, we introduce the interaction parameter (χ) as defined by Flory.

$$\chi = \frac{z}{2}\frac{(2u_{\mathrm{AB}} - u_{\mathrm{AA}} - u_{\mathrm{BB}})}{kT} \tag{2.40}$$

Using the interaction parameter, $\Delta\overline{U}_{\mathrm{mix}}$ is represented by Eq. (2.41):

$$\Delta\overline{U}_{\mathrm{mix}} = \chi\phi(1-\phi)kT \tag{2.41}$$

2.3.3 Basic Equation of Osmotic Pressure

Based on the estimated values of entropy and enthalpy, the total energy change from mixing is given by ΔF_{mix}.

$$\begin{aligned}\Delta F_{\mathrm{mix}} &= n\Delta\overline{F}_{\mathrm{mix}} = n(\Delta\overline{U}_{\mathrm{mix}} - T\Delta\overline{S}_{\mathrm{mix}}) \\ &= nkT\left[\frac{\phi}{N}\ln\phi + (1-\phi)\ln(1-\phi) + \chi\phi(1-\phi)\right]\end{aligned} \tag{2.42}$$

We then estimate the osmotic pressure. By substituting Eq. (2.42) into Eq. (2.21), we obtain Eq. (2.43):

$$\begin{aligned}\Pi V_1 &= -\left(\frac{\partial F_{\mathrm{mix}}}{\partial n_{\mathrm{B}}}\right)_{n_{\mathrm{A}}} \\ &= -\left(\frac{\partial\left(nkT\left[\frac{\phi}{N}\ln\phi + (1-\phi)\ln(1-\phi) + \chi\phi(1-\phi)\right]\right)}{\partial n_{\mathrm{B}}}\right)_{n_{\mathrm{A}}} \\ &= -kT\left(\frac{\partial\left(\frac{n_{\mathrm{A}}}{N}\ln\phi + n_{\mathrm{B}}\ln(1-\phi) + \chi n_{\mathrm{A}}(1-\phi)\right)}{\partial n_{\mathrm{B}}}\right)_{n_{\mathrm{A}}} \\ &= -kT\left(\frac{n_{\mathrm{A}}}{N}\frac{\partial(\ln\phi)}{\partial n_{\mathrm{B}}} + \ln(1-\phi) + n_{\mathrm{B}}\frac{\partial(\ln(1-\phi))}{\partial n_{\mathrm{B}}} + \chi n_{\mathrm{A}}\frac{\partial(1-\phi)}{\partial n_{\mathrm{B}}}\right)\end{aligned} \tag{2.43}$$

in which the following relationship was used:

$$n_{\mathrm{A}} = n - n_{\mathrm{B}} = n\phi \tag{2.44}$$

The calculation was then conducted using the following relationship:

$$\left(\frac{\partial\phi}{\partial n_{\mathrm{B}}}\right)_{n_{\mathrm{A}}} = \frac{\partial\left(\frac{n_{\mathrm{A}}}{n_{\mathrm{A}}+n_{\mathrm{B}}}\right)}{\partial n_{\mathrm{B}}} = -\frac{n_{\mathrm{A}}}{(n_{\mathrm{A}}+n_{\mathrm{B}})^2} = -\frac{\phi^2}{n_{\mathrm{A}}} \tag{2.45}$$

$$\Pi V_1 = -kT\left(-\frac{\phi}{N} + \ln(1-\phi) + \frac{n_{\mathrm{B}}}{n_{\mathrm{A}}}\frac{\phi^2}{1-\phi} + \chi n_{\mathrm{A}}\left(\phi - \frac{n_{\mathrm{B}}}{n_{\mathrm{A}}}\phi^2\right)\right) \tag{2.46}$$

Finally, using the following relationship, one obtains an equation representing the osmotic pressure of polymer solutions:

$$\frac{n_B}{n_A} = \frac{1-\phi}{\phi} \tag{2.47}$$

$$\Pi V_1 = kT\left(\frac{\phi}{N} - \phi - \ln(1-\phi) - \chi\phi^2\right) \tag{2.48}$$

To understand the nature of osmotic pressure, we modify Eq. (2.48) using the Tailor series $\ln(1-\phi) \approx -\phi + \phi^2/2$.

$$\frac{\Pi V_1}{kT} = \frac{1}{N}\phi + \left(\frac{1}{2} - \chi\right)\phi^2 \tag{2.49}$$

When we focus on an extremely dilute region ($\phi < N^{-1}$), the first term dominates the osmotic pressure.

$$\frac{\Pi V_1}{kT} \approx \frac{1}{N}\phi \tag{2.50}$$

Given that ϕ/N is proportional to the molar concentration of the polymer, this equation is equivalent to the ideal gas law. Notably, there is no contribution from the enthalpy term containing χ, suggesting that the osmotic pressure is determined only by the molar concentration and is independent of the solubility of the polymer. The formal expression in Eq. (2.50) is called the van't Hoff equation and is used to measure the molecular weight of polymers from their osmotic pressure. Notably, the previously mentioned equation only holds at extremely dilute concentrations since the N of the polymer generally exceeds 100. In a region with slightly higher concentrations, it is necessary to consider the term ϕ^2. Even at such concentrations, when $\chi = 0.5$ (θ state), the second term of Eq. (2.49) cancels, and Eq. (2.50) holds. Note that the prefactor of ϕ^2 in Eq. (2.49) consists of two different components: "1/2" is the contribution of the entropy, and "χ" is the contribution of enthalpy. That is, in the θ state, the interaction energy (ΔU_{mix}) between segments cancels the 2nd-order of mixing entropy. Although Eq. (2.49) is also an approximation for small ϕ, even at $\phi = 0.1$, this approximation is too rough in some cases. At higher polymer volume fractions, terms with higher orders cannot be ignored.

2.3.4 Phase Separation of the Polymer Solution

In Section 2.3.3, we introduced the osmotic pressure of miscible systems in which the polymer and solvent molecules were randomly arranged. However, some systems show multiple phases that are not compatible with each other, i.e., phase separations. In this section, let us consider the conditions under which a certain polymer solution undergoes a phase separation. Here, we consider a case in which two phases (Phase 1 and Phase 2) with different polymer volume fractions (ϕ_1 and ϕ_2, respectively) coexist (Figure 2.9). The phases contain n_{1A} and n_{2A} polymer molecules A and n_{1B} and n_{2B} solvent molecules B, respectively.

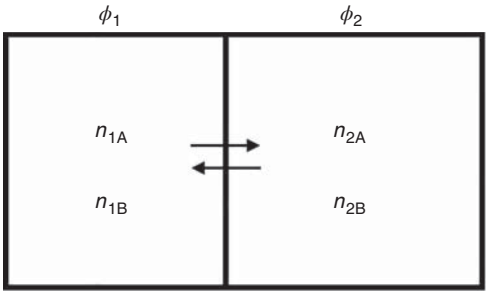

Figure 2.9 Phase separation of a polymer solution; coexistence of two phases with different compositions.

Given that this coexisting system is closed to the outside environment, the following equations can be established:

$$n_{1A} + n_{2A} = n_A$$
$$n_{1B} + n_{2B} = n_B \tag{2.51}$$

These equations show that the movement of a molecule A from Phase 1 to Phase 2 does not directly influence other molecules; molecules A and B move independently, and Eq. (2.51) does not specify the number of molecules in Phases 1 and 2. In this system, the condition of phase equilibrium is written as follows:

$$\left(\frac{\partial F_{\text{mix}}}{\partial n_{1B}}\right)_{n_{1A}} = \left(\frac{\partial F_{\text{mix}}}{\partial n_{2B}}\right)_{n_{2A}} \tag{2.52}$$

This differentiation shows the free energy change when molecule B moves among the phases, and this value is called the chemical potential ($\Delta\mu$). This equation shows that there is no energy change when molecule B moves from Phase 1 to Phase 2, which is a condition for the coexistence of two phases. By substituting Eq. (2.42) into Eq. (2.52), one obtains $\Delta\mu$.

$$\Delta\mu = \left(\frac{\partial F_{\text{mix}}}{\partial n_B}\right)_{n_A} = kT\left(\frac{\phi}{N} - \phi - \ln(1-\phi) - \chi\phi^2\right) \tag{2.53}$$

Note that the derivation method is almost the same as that of Π in the Section 2.3.3, and the only difference is that $\Delta\mu$ has the opposite sign as ΠV_1. Figure 2.10

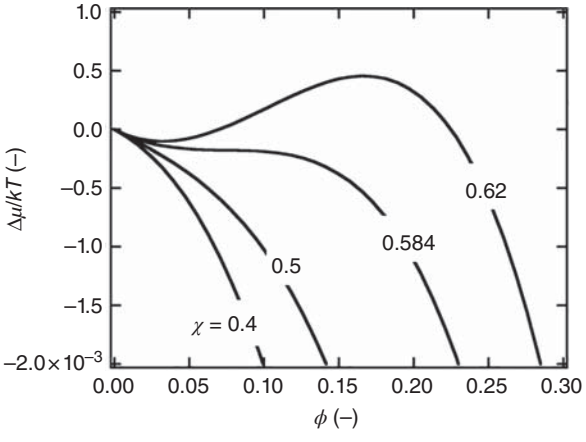

Figure 2.10 ϕ-Dependence of $\Delta\mu$ with different χ ($N = 150$). At $\chi > 0.584$, $\Delta\mu$ has a local maximum and minimum.

shows the dependence of $\Delta\mu$ on ϕ when $N = 150$. When χ is small, $\Delta\mu$ is always negative over the whole composition and monotonically decreases. That is, as the concentration of B in the system increases, the system stabilizes, so molecules A and B are miscible over the entire concentration range. On the other hand, if χ exceeds a certain threshold, as ϕ increases, the function has a local maximum after a local minimum and obviously shows two compositions with equal $\Delta\mu$. Under these conditions, two phases satisfying $\Delta\mu(\phi_1) = \Delta\mu(\phi_2)$ coexist.

The fact that Eq. (2.53) has both a local minimum and a local maximum can be explained by the following equation having two different solutions:

$$\left(\frac{\partial\Delta\mu}{\partial\phi}\right)_{T,P} = 0$$
$$\left(\frac{\partial\Delta\mu}{\partial\phi}\right)_{T,P} = -1 + \frac{1}{N} - \frac{1}{\phi - 1} - 2\chi\phi = 0$$
$$2\chi\phi^2 + \left(1 - \frac{1}{N} - 2\chi\right)\phi + \frac{1}{N} = 0 \tag{2.54}$$

Here, the condition $0 < \phi < 1$ was utilized. Let us investigate the critical value of χ at which phase separation begins to occur. The form of the function at the critical point is shown in Figure 2.10 when $\chi = 0.584$, i.e. when Eq. (2.54) has a double root. Considering that expression Eq. (2.54) is a quadratic expression of ϕ, the equation having a double root is expressed as follows:

$$\left(1 - \frac{1}{N} - 2\chi\right)^2 - \frac{8\chi}{N} = 0$$
$$\chi_c = \frac{1}{2}\left(1 + \frac{1}{N}\right) + \sqrt{\frac{1}{N}} \tag{2.55}$$

χ_c indicates the critical point at which phase separation begins to occur. As shown in Figure 2.11, χ_c decreases with increasing N, suggesting that at higher molecular weights, phase separation is more likely. Although χ_c asymptotically approaches $\chi_c = 1/2$ (under θ conditions) for extremely high N, this condition

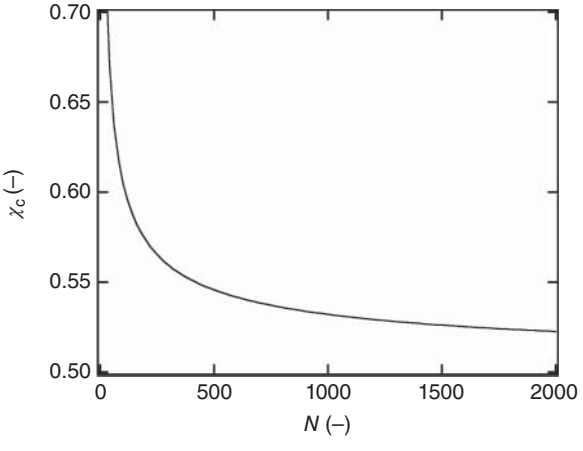

Figure 2.11 *N*-Dependence of χ_c.

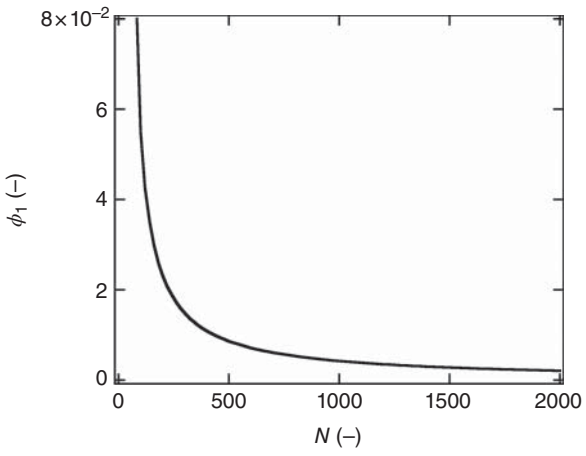

Figure 2.12 Dependence of the polymer volume fraction on N in a dilute phase (ϕ_1) ($\chi = 0.562$).

rarely holds considering that conventional polymers have N values that are at most on the order of 10^2–10^3.

Next, we focus on the condition $\chi > \chi_c$. The two distinct roots of Eq. (2.53) are represented as follows:

$$\phi = \frac{2\chi + \frac{1}{N} - 1 \pm \sqrt{\left(2\chi - \frac{1}{N} - 1\right)^2 - \frac{4}{N}}}{4\chi} \tag{2.56}$$

Here, we define the polymer volume fraction of a dilute phase as ϕ_1 and show it as a function of N (Figure 2.12). ϕ_1 decreases with increasing N, suggesting that a high molecular weight enhances the tendency toward phase separation.

2.3.5 Scaling of Osmotic Pressure

de Gennes claimed that the lattice-based mean-field theory discussed in the Section 2.3.3 fails in a good solvent, particularly at low concentrations because the chains are swollen and avoid each other at concentrations below c^*. The effect of excluded volume and even correlations caused by covalent bonding between polymer segments are not taken into consideration in this model. Since the segments are localized near the center of the polymer, the segment density is not uniform inside the polymer chain. Of course, ϕ does not include such information. de Gennes solved the problem by scaling the osmotic pressure. The osmotic pressure can be expanded to the power series of the concentration (the virial expansion).

$$\frac{\Pi}{kT} = \frac{c}{N} + B_2\left(\frac{c}{N}\right)^2 + B_3\left(\frac{c}{N}\right)^3 + O\left(\left(\frac{c}{N}\right)^4\right) \tag{2.57}$$

Here, c is the number density of the segments (m^{-3}), N is the degree of polymerization of the polymer, and B_2 and B_3 are the second and third virial coefficients, respectively. Notably, c/N is the number density of the polymers (m^{-3}). At the limit of dilution, the second and higher terms are negligible, and the osmotic pressure is proportional to the number density of the polymer, similar to the ideal gas

law (see Eq. (2.50)). However, in general, the influence of the second term, which is from the interactions between two polymers, cannot be completely ignored even at dilute concentrations ($\phi < \phi^*$). In the case of a good solvent ($\nu = 0.6$), polymers behave like a rigid sphere with radius R_F in the dilute region. Under these conditions, the second virial coefficient is a constant proportional to ${R_F}^3$, and the following equation holds:

$$\frac{\Pi}{kT} = \frac{c}{N} + (\text{constant}) \times {R_F}^3 \left(\frac{c}{N}\right)^2 + O\left(\left(\frac{c}{N}\right)^3\right) \tag{2.58}$$

The validity of this equation was experimentally examined by direct observation of Π and light scattering in many systems [9].

We now shift our focus to the semidilute region, $\phi^* < \phi \ll 1$. To estimate the scaling in this concentration range, we assume the following for Eq. (2.58):

1. In the dilute region, Π/kT is proportional to c/N (each term has the same units).
2. In the semidilute region, the contribution of the two-body interaction ($B_2 \approx {R_F}^3$) is large.
3. The main contributor to the second term in Eq. (2.58) is transformed to $c/N({R_F}^3 c/N)$, and ${R_F}^3 c/N$ is dimensionless.

Based on the previously mentioned considerations, c/N can be used as a key tool for matching units on both sides of the equation, and the power of ${R_F}^3 c/N$ is used as a dimensionless quantity, and thus the following scaling equation is obtained:

$$\frac{\Pi}{kT} = \frac{c}{N}\left({R_F}^3 \frac{c}{N}\right)^x = \frac{c}{N}\left(\frac{c}{c^*}\right)^x \tag{2.59}$$

Here, $c^* \approx N/{R_F}^3$ was utilized (see Section 2.2). As a result, the polymer concentration relative to c^* is an important factor for determining the osmotic pressure. To determine x in Eq. (2.59), requirements, such as "osmotic pressure is not dependent on the molecular weight of the polymers," must be set. This is because if the concentration is higher than c^*, the system is a mixed model, and the properties will be governed by the blob regardless of the molecular weight of the polymers. By transforming the equation using $R_F = aN^{3/5}$, the following equation can be obtained:

$$\frac{\Pi}{kT} \approx \frac{c}{N}\left({R_F}^3 \frac{c}{N}\right)^x \sim \frac{1}{N}(N^{4/5})^x \tag{2.60}$$

To eliminate the dependence on N, one should set $x = 5/4$ and obtain the following scaling:

$$\frac{\Pi}{kT} = \frac{c}{N}\left(\frac{c}{c^*}\right)^{5/4} \sim c^{9/4} \sim \phi^{9/4} \tag{2.61}$$

Finally, we investigate the relationship between the osmotic pressure and blobs. As seen in Section 2.2, blobs are an important concept in the semidilute region. Based on the dependence of the blob size on ϕ ($\xi \sim \phi^{-3/4}$), Eq. (2.61) can be transformed as follows:

$$\frac{\Pi}{kT} \sim \frac{1}{\xi^3} \tag{2.62}$$

This equation shows that the osmotic pressure is proportional to the number density of blobs, again indicating the importance of the blob concept in the semidilute region. The blob is a unit that causes osmotic pressure. This equation can be applied not only to any solution system characterized by a good solvent but also to other solutions characterized by ν as in the previous discussion.

$$\frac{\Pi}{kT} \sim \frac{1}{\xi^3} \sim \phi^{\frac{3\nu}{3\nu-1}} \tag{2.63}$$

The consequences of semidilute solutions are expected to be applicable to a wide range of polymer gels because the overlapping concentration of polymer gels, by definition, is 0 since the molecular weight of a three-dimensional network is infinite (substitute $N = \infty$ in Eq. (2.10)). Once a gel is formed, the system can be regarded as a semidilute system even if the polymer concentration is extremely low.

Column 2: Blob Size of a Polymer Gel

A blob is defined by de Gennes as correlation length of polymers in a semidiluted polymer solution. Although the concept of blob was explained by Section 2.2, it may be hard to catch the sense. Here, we provide another approach to explain the concept of blob for better understanding.

We focus on a monomer #0 contained in a polymer chain in semidilute solution. In a semidiluted solution, although it is necessary to consider a situation where a lot of polymers interpenetrate with each other, for simplicity, we depict only two polymers (marked with white and gray). The first problem is whether monomer #0 can distinguish monomer #1, which is directly connected to #0, from monomer #a, which only presents in the vicinity of #0, and belongs to another polymer.

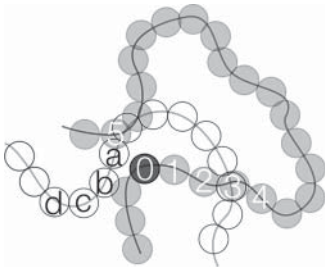

The answer is "Yes," because the interaction based on a direct connection is strong. This type of correlation based on direct connection gradually decays as going away to #2, #3, #4, and finally the interaction via direct connection is negligible in #5. Therefore, from the monomer #0, both #5 and #a exist at similar distances and cannot be distinguished from each other.

As such, there are strong "correlations" in between the two monomers that are directly connected and move with interactions, such as monomers #0 and #1.

This correlation decays with distance, and the distance at which the correlation disappears is referred to as the "correlation length" or "blob size." Thus, a blob may be rephrased as a group of monomers having effective correlations, and the size has the order of nanometers. The blob size decreases with an increase in polymer concentrations, because monomers belonging to other polymers penetrate into the polymer chain and screen out the correlation.

Next, we consider blobs of polymer gels, where the definition of the correlation length is the same with semidiluted polymer solutions. The problem is how much crosslinks influence the correlation length. There have been experimental results where only the crosslinks are added to a semidiluted polymer solution, and they have shown that the correlation length is not greatly influenced by crosslinks. This result can be understood if we consider the distance between crosslinks is larger than the blob size. In the case where only less than one crosslink exists in blob size, crosslinks do not influence the correlation length strongly. Based on the original definition, the correlation length is a parameter that reflects the solution properties, such as osmotic pressure, rather than network properties. Thus, the correlation length is not directly related to the length between neighboring crosslinks [10].

References

1 Flory, P.J. (1953). *Principles of Polymer Chemistry*. Ithaca, NY: Cornell University Press.
2 Cotton, J.P., Decker, D., Benoit, H. et al. (1974). Conformation of polymer chain in the bulk. *Macromolecules* 7: 863–872.
3 Brandrup, J., Immergut, E.H., and Grulke, E.A. (1999). *Polymer Handbook*, 4e. Wiley-Interscience.
4 Konishi, T., Yoshizaki, T., Saito, T. et al. (1990). Mean-square radius of gyration of oligo- and polystyrenes in dilute-solutions. *Macromolecules* 23 (1): 290–297.
5 Osa, M., Ueno, Y., Yoshizaki, T., and Yamakawa, H. (2001). Gyration-radius expansion factor of oligo- and poly(α-methylstyrene)s in dilute solution. *Macromolecules* 34 (18): 6402–6408.
6 Daoud, M., Cotton, J.P., Farnoux, B. et al. (1975). Solutions of flexible polymers. Neutron experiments and interpretation. *Macromolecules* 8 (6): 804–818.
7 Flory, P.I. (1942). Thermodynamics of high polymer solutions. *J. Chem. Phys.* 10 (1): 51–61.
8 Huggins, M.L. (1942). Theory of solutions of high polymers. *J. Am. Chem. Soc.* 64: 1712–1719.
9 Zimm, B.H. (1948). Apparatus and methods for measurement and interpretation of the angular variation of light scattering – preliminary results on polystyrene solutions. *J. Chem. Phys.* 16 (12): 1099–1116.
10 Nishi, K., Asai, H., Fujii, K. et al. (2014). Small-angle neutron scattering study on defect-controlled polymer networks. *Macromolecules* 47: 1801–1809.

3

Definition of Polymer Gels and Rubber Elasticity

Takamasa Sakai

Graduate School of Engineering, The University of Tokyo, Tokyo, Japan

3.1 Elasticity of Gels

In Chapters 1 and 2, we learned about the characteristics of isolated polymer chains and polymer solutions. In this chapter, we discuss the correlation between the structure and physical properties of polymer gels based on Chapters 1 and 2. As an overview of the mechanical properties of polymer gels, we first show a typical engineering stress (σ)–elongation ratio (λ) curve for the uniaxial stretching of a polymer gel (Figure 3.1). The stress and elongation ratio are the normalized force and the length of the test piece during stretching and are defined as follows:

$$\sigma = \frac{F}{S_0} \tag{3.1}$$

$$\lambda = \frac{L}{L_0} \tag{3.2}$$

Here, F is the force applied to the test piece, S_0 is the sectional area of the initial test piece, L_0 is the length of the initial test piece, and L is the length after the stretching. The strain (ε), defined in Eq. (3.3), can be used as an indicator of deformation instead of λ:

$$\varepsilon = \frac{L - L_0}{L_0} = \lambda - 1 \tag{3.3}$$

Generally, polymer gels have high deformability and can be extended by a factor of more than 10 without any damage in special cases. Such high stretchability is achieved, because the mechanical response of the polymer gel is controlled by the conformational change in the polymer chain that forms the polymer gel, i.e. rubber elasticity. Therefore, the architecture of the polymer network determines the mechanical properties of the polymer gel. Thus, clarifying the correlation between the structure and physical properties in the science of polymer gels is extremely important. For example, this correlation is important for guiding material design, and it can serve as a methodology to estimate network structures. As the latter example may be less clear, we will discuss it in more detail.

In the case of metals, for example, their atomic arrangement can be directly observed, and their physical properties are measurable. Because both their

Physics of Polymer Gels, First Edition. Edited by Takamasa Sakai.

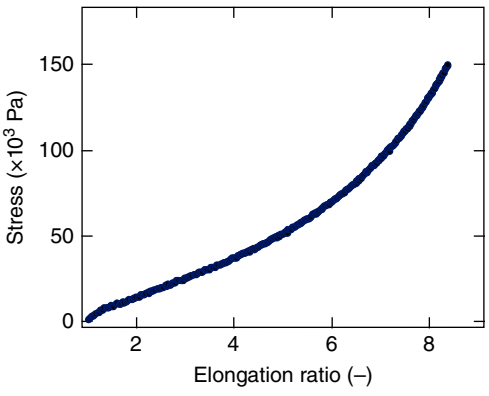

Figure 3.1 Stress–elongation curve of a hydrogel.

structure and properties are determined independently, it is possible to verify a model relating the structure to the physical properties, resulting in a full understanding of the material. When an ideal model describing the structure–property relationship is obtained, material science will then be a mature and sophisticated field.

On the other hand, the three-dimensional network of a polymer gel cannot be directly observed to date. Thus, establishing concrete models for predicting structure–property relationships is difficult. We need to begin by discussing a structure estimated from the feed conditions, which is far from the actual structure due to the inherent heterogeneity (see Section 3.8). Thus, it is difficult to discuss the structure–property relationships, and it is practically impossible to verify models. As a result, a plurality of models predicting each physical property coexist. In the strictest sense, the validities or the applicable conditions of models are currently mostly unknown. Therefore, clarifying the structure–property relationships of polymer gels through the systematic study of polymer gels with well-defined network structures is of great interest (see Part 2: Experiments).

Because the polymer network structure cannot be directly observed, the models are uncertain. However, even in this situation, it is important to know the structures of the gels. Therefore, estimating the structure based on a combination of a model and a physical property is common even today. Among the physical properties of a gel, the elastic modulus is one of the most conveniently measurable and is the parameter most frequently used to estimate the structure. In this chapter, we will first discuss the definition of polymer gels and then models for predicting the elastic modulus.

3.2 Definition of Polymer Gels

Polymer gels are "a three-dimensional polymer network structure containing a solvent". How can we experimentally confirm that polymer chains form a three-dimensional network structure? Here, we introduce two representative methods for determining the gelation using rheological and scattering experiments.

3.2.1 Criterion for Gelation by Rheology

In rheological measurements, the strain response to a certain stress and the stress response to a certain strain are measured as a function of time. For example, when a constant stress is applied to a Newtonian liquid, which is an ideal liquid, it continues to flow at a constant strain rate. On the other hand, when constant stress is applied to a Hookean elastic body, which is an ideal solid, it is deformed to a constant deformation ratio. Conversely, matter that flows at a constant strain rate is a *liquid*, while matter that deforms to a constant strain is a *solid*. Since a polymer gel is a "solid" composed of a three-dimensional network, by definition it does not flow. Here, we define gelation using the stress relaxation test, which is a representative rheological measurement.

In stress relaxation tests, a certain strain is instantly applied to a substance, and the time development of stress ($\sigma(t)$) required to maintain the strain is observed (Figure 3.2). Both polymer melts and polymer solutions exhibit elasticity over short periods. However, they flow when the observation time is increased, and finally, the stress reaches 0, which is characteristic of a "viscoelastic liquid." On the other hand, since the gel has a three-dimensional network structure, the stress does not reach 0 and remains finite even after long-term observation. Occasionally, the stress relaxes over a short period even in the gel. These behaviors are characteristic of a "viscoelastic solid." In this way, the difference between liquids (sol) and solids (gel) can be observed upon long-term observation.

In rheology, a material that has a modulus that shows a finite plateau over a long timeframe is a gel, while a material that has a relaxation modulus of 0 over a long time period is a sol. During the transition from sol to gel, the viscosity gradually increases and tends toward infinity at the sol–gel transition point. Although many researchers have attempted to evaluate the divergence point of viscosity, direct observation is difficult because of the dramatic change in viscosity near the critical point. Winter and Chambon therefore identified the critical point using dynamic viscoelasticity measurements under the sinusoidal strain [1]. The dependences of strage modulus (G') and loss modulus (G'') on frequency (ω) can be seen in the dynamic viscoelasticity measurements, and these dependences reflect the elasticity and the viscosity of the system, respectively. Here, the frequency in the dynamic measurement is inversely proportional to the observation time in

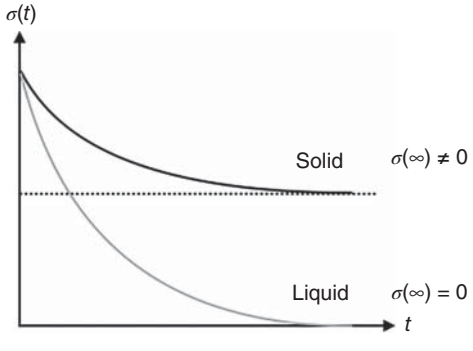

Figure 3.2 Stress relaxation behavior of a solid and a liquid.

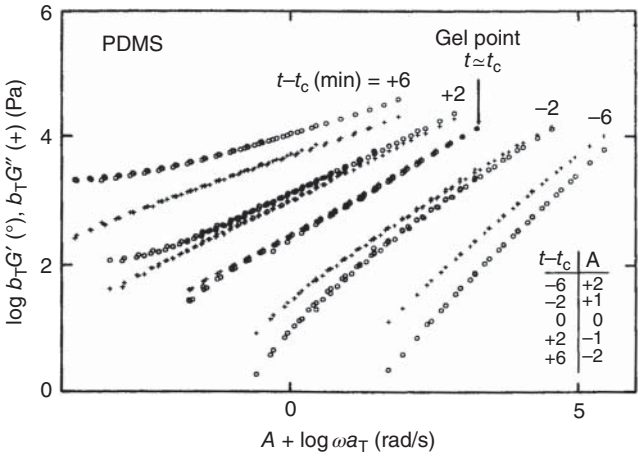

Figure 3.3 Frequency dependence of the storage modulus (G') and loss modulus (G'') of a polydimethylsiloxane (PDMS) elastomer quenched during the reaction. The curves were shifted side to side (by factor A) to avoid overlap [1].

the static measurement; long-term observation in the static measurements corresponds to low-frequency measurements in the dynamic measurements.

In dynamic measurements, liquids show terminal flow behavior, which is characteristic frequency dependences of $G' \sim \omega^2$ and $G'' \sim \omega^1$ in a low-frequency region. On the other hand, in the gel state, a plateau of G' with no frequency dependence occurs in a low-frequency region ($G' \sim \omega^0$ and $G'' \sim \omega^0$). Gels take a self-similar (fractal) structure at the gelation point, and a specific power law ($G' \approx G'' \sim \omega^\beta$) is observed. Here, the index β reflects the fractal structure. This spectrum indicates that the viscosity diverges to infinity and is observed in various gels regardless of the type of crosslinks present. This criterion for determining the gelation point is called the "Winter–Chambon criterion" (Figure 3.3).

3.2.2 Criterion for Gelation by Scattering

When we irradiate matter with light, X-ray photons, and neutrons, new light, X-rays, and neutrons will be scattered in all directions due to the interactions between the molecule and the irradiant, i.e. scattering. Because light, X-rays, and neutrons all act as waves, we can see the interference patterns of the scattered waves on a screen placed some distance away from the matter. Because the interference patterns reflect the spatial relationship among the molecules in the matter, the interference pattern provides information on the internal structure of the matter. The interference pattern changes rapidly because of the motion of the molecules. By averaging the scattering patterns over a long period (static scattering), we can obtain statistical information on the intramolecular and intermolecular interactions. Looking at the changes in the interference patterns over time (dynamic scattering) can help elucidate the molecular motion of the polymer chains.

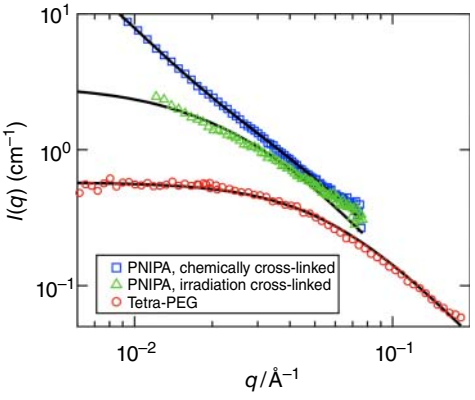

Figure 3.4 Small-angle neutron scattering of homogeneous Tetra-PEG gel and heterogeneous poly(*N*-isopropylacrylamide) gel.

Generally, the network structures of polymer gels are highly heterogeneous. Strong excess scattering, which is not observed in polymer solutions, is often observed at small scattering angles ($q < 0.01$ Å^{-1}), where q is the magnitude of the scattering vector. The scattering angles that show the excess scattering correspond to a few tens of nanometers in real space [2–4]. However, in the case of dynamic scattering for these heterogeneous networks, a clear reduction in the dynamic coherence (often called the initial amplitude) is generally observed in the time correlation function. The decrease in the dynamic coherence indicates the immobilization of the polymer chains in the observed area. The excess scattering at low scattering angles and the reduction in dynamic coherence are widely observed at sol–gel transitions and thus have been recognized as criteria for recognizing such transitions.

However, similar excess scattering is also reported in polymer solutions when the polymer chains form aggregates. In addition, a series of gels with very small excess scattering signals have been observed (Figure 3.4), suggesting that the excess scattering is not always the best indicator of a sol–gel transition [5]. Furthermore, a recent study found gelation with no excess scattering and no deterioration of the dynamic coherence. These findings suggest that the definition of gels must be reviewed.

3.3 Mesh Size of a Polymer Gel

The most popular and intuitive structural parameter for characterizing a polymer network may be mesh size. However, as mentioned earlier, direct observation is not possible with the current technology. Therefore, the mesh size is currently indirectly estimated using some assumptions. There are three methods for estimating the average mesh size:

1. Calculating from the feed concentration of a crosslinking agent or the degree of polymerization of a chain connecting neighboring crosslinking points.
2. Calculating from the elastic modulus or swelling degree.
3. Assuming the blob size obtained by the scattering experiment is equal to the mesh size.

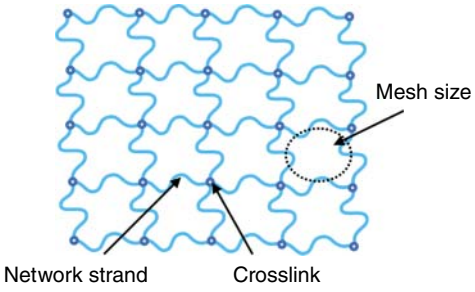

Figure 3.5 Schematic picture of a tetra-functional network.

Which method is the most suitable way to determine the mesh size of polymer gels? It depends on the properties of greatest interest; for example, these could be the extensibility or the permeability of a substance. Based on our experimental results, there is no single measure of mesh size that well characterizes both properties. Conversely, the mesh sizes estimated by methods 1–3 are all related to certain physical properties. Here, we discuss method 1 in detail.

For simplicity, let us consider the tetra-functional network structure, as shown in Figure 3.5. The distance (d) between the crosslinking points can be calculated under the assumption that all of the crosslinking agents (crosslinking agent density, c) react perfectly and are homogeneously distributed. Let us divide the reaction space into equivalent cubes with a certain volume, put crosslinking points one by one into these cubes, and connect all pairs of neighboring crosslinking points with polymer chains. Since the volume that one crosslinking point occupies is $1/c$ (m^3), the length of one side of the cube is

$$d = \left(\frac{1}{c}\right)^{1/3} \tag{3.4}$$

For example, the conventional case of $c = 1\,\mathrm{mol/m^3}$ gives d approximately 10^{-7}–10^{-8} m. Indeed, the diffusion of quantum dots (diameter of approximately 10 nm) is greatly hindered by conventional polymer gels; thus, this rough estimation method seems to give a realistic value.

Next, we try to estimate this parameter from the degree of polymerization of the chains connecting the crosslinking points (N). Consider the situation in which chains containing functional groups at both chain ends are crosslinked in their current form to generate a network. In this situation, the mesh size can be estimated as the end-to-end distance of a chain. When we set $N = 10^2$ and the monomer length (assumed to be equal to the persistence length) to 5 Å, the end-to-end distance is 5×10^{-9} m. In the case of forming a network from the monomer and the crosslinking agent, the degree of polymerization is estimated by dividing the monomer concentration by the concentration of the crosslinking agent, and the same calculation is used to obtain the distance between the crosslinking points.

Although both methods give similar mesh sizes, the two estimations are based on completely different pictures of gelation. When we use the first estimation based on c, we implicitly accept the change in conformation during the crosslinking process; the structure of the strands in the network is defined by the density of the crosslinking agent and not by the conformation of the original uncrosslinked

polymer chain. On the other hand, in the case of the second estimation based on N, the network strand is assumed to maintain its conformation during the gelation process. This assumption implies that forming a gel at a concentration below the overlapping concentration is difficult, and entanglements are trapped at high concentrations. Notably, the mesh size estimated here is that in the "as-prepared state." We can include the effects of swelling or deswelling on the mesh size by multiplying by the cube root of the volume change.

3.4 Elastic Modulus

Given that polymer networks consist of a large number of polymers, it is natural to imagine that the mechanical properties of the gel can be described as the sum of the mechanical properties of single polymer chains as introduced in Chapter 1. In particular, regarding the elastic modulus, since only a small deformation region is considered, we can treat a network strand as an ideal chain obeying a Gaussian distribution. In Section 3.4.1, we first discuss the affine network model, which models a polymer network composed of Gaussian chains, and then move to more complicated models.

3.4.1 Affine Network Model

The simplest model for describing the elastic modulus of a polymer network is the affine network model proposed by Kuhn [6]. As shown in Figure 3.6, the gel is initially in a rectangular parallelepiped with three sides of L_{x0}, L_{y0}, and L_{z0}. The end-to-end vectors of the polymer chains contained in this polymer network are $\mathbf{r}_0 = (r_{x0}, r_{y0}, r_{z0})$.

Let us consider the case where each axis of this rectangular parallelepiped is stretched by factors of λ_x, λ_y, and λ_z, making each side $\lambda_x L_{x0}$, $\lambda_y L_{y0}$, and $\lambda_z L_{z0}$, respectively. In this model, we assume that the deformation modes of the entire gel and microscopic network strand are the same (affine deformation); the

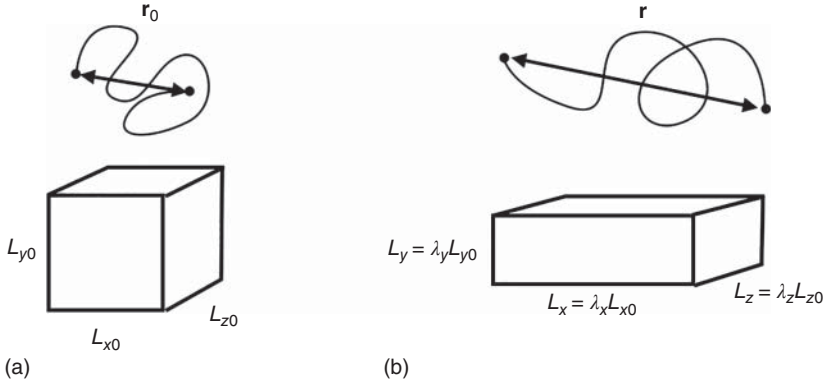

Figure 3.6 The upper two strands are network strands, and the bottom two boxes are gels. (a) Left strand and box are initial state, and (b) right strand and box are deformed state.

end-to-end vector deforms in the same manner as the macroscopic deformation and becomes $\mathbf{r} = (\lambda_x r_{x0}, \lambda_y r_{y0}, \lambda_z r_{z0})$. Consider the energy change in this network strand due to deformation. Here, assuming that network strands are ideal chains, the entropy $S(N, \mathbf{r})$ of a network strand can be written as Eq. (3.5), which is based on Eq. (1.35):

$$S(N, \mathbf{r}) = -\frac{3k\mathbf{r}^2}{2Na^2} + S(N, 0) \tag{3.5}$$

The difference in energies before and after the deformation (ΔS) is given as the following:

$$\begin{aligned}\Delta S &= S(N, \mathbf{r}) - S(N, \mathbf{r}_0) \\ &= -\frac{3k(\mathbf{r}^2 - {\mathbf{r}_0}^2)}{2Na^2} \\ &= -\frac{3k}{2Na^2}(((\lambda_x r_{x0})^2 + (\lambda_y r_{y0})^2 + (\lambda_z r_{z0})^2) - ({r_{x0}}^2 + {r_{y0}}^2 + {r_{z0}}^2)) \\ &= -\frac{3k}{2Na^2}((\lambda_x{}^2 - 1){r_{x0}}^2 + (\lambda_y{}^2 - 1){r_{y0}}^2 + (\lambda_z{}^2 - 1){r_{z0}}^2)\end{aligned} \tag{3.6}$$

Here, because the ideal chain is isotropic and ${\mathbf{r}_0}^2 = a^2 N$, we can obtain the following:

$${r_{x0}}^2 = {r_{y0}}^2 = {r_{z0}}^2 = \frac{a^2 N}{3} \tag{3.7}$$

Substituting Eq. (3.7) into Eq. (3.6), we obtain Eq. (3.8):

$$\Delta S = -\frac{k}{2}(\lambda_x{}^2 + \lambda_y{}^2 + \lambda_z{}^2 - 3) \tag{3.8}$$

When we set the total number of network strands as n, the energy change by deformation (ΔF) is given as follows:

$$\Delta F = -nT\Delta S = \frac{nkT}{2}(\lambda_x{}^2 + \lambda_y{}^2 + \lambda_z{}^2 - 3) \tag{3.9}$$

Here, let us consider uniaxial stretching behavior. The volume of polymer gel hardly changes when deformed by stress because the deformation of the polymer chain requires less energy than is required to change the volume of the solvent, which is the main constituent of the polymer gel, or than is required to squeeze the solvent out of the polymer gel. This phenomenon is called incompressibility, and the following formula holds for incompressible matters:

$$\lambda_x \lambda_y \lambda_z = 1 \tag{3.10}$$

As a result, when the polymer gel is stretched along the x-axis, the dimensions in the directions perpendicular to the stretching axis shrink. Given that the y direction and the z direction are equivalent, the deformation ratio of each axis can be written as follows:

$$\lambda_x = \lambda, \lambda_y = \lambda_z = \lambda^{-1/2} \tag{3.11}$$

By substituting Eq. (3.11) to Eq. (3.9), we obtain Eq. (3.12);

$$\Delta F = \frac{nkT}{2}(\lambda^2 + 2\lambda^{-1} - 3) \tag{3.12}$$

The differential of ΔF by the change in length in the stretching direction is the force (f_x) necessary for stretching in the uniaxial direction.

$$f_x = \frac{\partial(\Delta F)}{\partial L_x} = \frac{\partial(\Delta F)}{\partial \lambda L_{x0}} = \frac{nkT}{2L_{x0}} \frac{\partial(\lambda^2 + 2\lambda^{-1} - 3)}{\partial \lambda} = \frac{nkT}{L_{x0}}(\lambda - \lambda^{-2}) \tag{3.13}$$

Nominal stress (σ) is given by dividing f_x by the initial area of the specimen ($L_{y0}L_{z0}$),

$$\sigma = \frac{f_x}{L_{y0}L_{z0}} = \frac{nkT}{L_{x0}L_{y0}L_{z0}}(\lambda - \lambda^{-2}) = \frac{nkT}{V_0}(\lambda - \lambda^{-2}) \tag{3.14}$$

The prefactor in Eq. (3.14) is called the shear modulus, G.

$$G = \frac{nkT}{V_0} = \nu kT \tag{3.15}$$

Here, ν (m^{-3}) is the number density of the elastically effective network strands. Equation (3.15) simply tells us that the contribution of an elastically effective network strand to the elasticity is kT. The initial slope of the σ–λ relationship is obtained by differentiating Eq. (3.14) with respect to λ and substituting $\lambda = 1$.

$$\left.\frac{\partial \sigma}{\partial \lambda}\right|_{\lambda=1} = G(1 + 2\lambda^{-3})|_{\lambda=1} = 3G = E \tag{3.16}$$

Here, the initial slope, E, is called Young's modulus or the tensile elastic modulus, and $E = 3G$ for incompressible materials such as polymer gels.

Figure 3.7 shows the relationship between the stress–elongation curve derived from Eq. (3.14). As clearly shown in Figure 3.7, the relationship is not linear but instead strongly nonlinear. This relationship is a feature of entropy elasticity and is essentially different from energy elasticity, which shows a linear relation. Figure 3.7 also shows the experimentally obtained stress–elongation curve shown at the beginning of this chapter. The experimental values in small deformations are very consistent with the values predicted by Eq. (3.14). However, in the highly stretched region, the experiment deviated upward from the prediction. This shift indicates that the chain has been dramatically stretched and is no longer obeying Gaussian statistics. As discussed in Section 1.1.3, each network strand can be

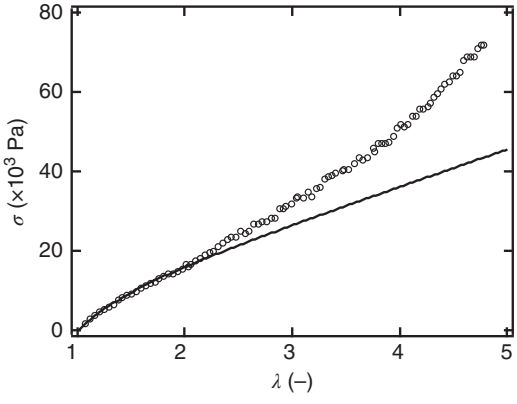

Figure 3.7 Stress–elongation curve and the prediction of neo-Hookean model.

extended to a maximum length of aN. The affine network model is correct for small deformations where Gaussian statistics are still applicable. When stretched to a certain extent, the effects of finite stretchability must be considered.

3.4.2 Phantom Network Model

The most important assumption in the affine network model is the affine deformation of the network strands. However, in reality, the deformation at the network strands can be different from the bulk deformation. Under incompressible deformation, the average position of the crosslinking points should be approximated by the values determined by the affine deformation, but the true points can fluctuate around the average positions. James and Guth proposed the phantom network model, which considers the fluctuation in the crosslinking points [7]. Here, Gaussian statistics is utilized to consider the fluctuations in the crosslinking point in the model. Here, the derivation of Rubinstein and Colby will be explained [8].

We want to know the fluctuation of a certain point $(s, \mathbf{x})$ in a three-dimensional random walk of N steps where one end is fixed at the origin and the other end is fixed at $\boldsymbol{X}$. To simplify the situation, let us first consider the one-dimensional version of this problem:

There is a 1D random walk starting from the origin and reaching X after N steps. Among all the random walks that satisfy the above conditions, what is the probability of being at point x at the sth step?

All events starting from the origin and reaching X at N steps are represented by the shaded area in the diagram of Figure 3.8. The total number of cases represented by this shaded area is defined by the probability density distribution $P_{1D}(N, X)$. Using Eq. (1.21), $P_{1D}(N, X)$ can be written as follows:

$$P_{1D}(N, X) = \frac{1}{\sqrt{2\pi a^2 N}} \exp\left(-\frac{X^2}{2a^2 N}\right) \tag{3.17}$$

We want to explore the cases of passing through (s, x) within the total possible cases. Although this trajectory is not necessarily linear, conceptually, the trajectory starts from (0, 0) and reaches (N, X) via (s, x), as shown by the arrows in Figure 3.8. To estimate the number density function, it is sufficient to consider the process of reaching x at step s and then advancing by $X - x$ with the remaining $N - s$ steps as follows:

$$\begin{aligned} P_{1D}(s, x) \cdot P_{1D}(N - s, X - x) = {} & \frac{1}{\sqrt{2\pi a^2 s}} \exp\left(-\frac{x^2}{2a^2 s}\right) \\ & \cdot \frac{1}{\sqrt{2\pi a^2 (N - s)}} \exp\left(-\frac{(X - x)^2}{2a^2 (N - s)}\right) \end{aligned} \tag{3.18}$$

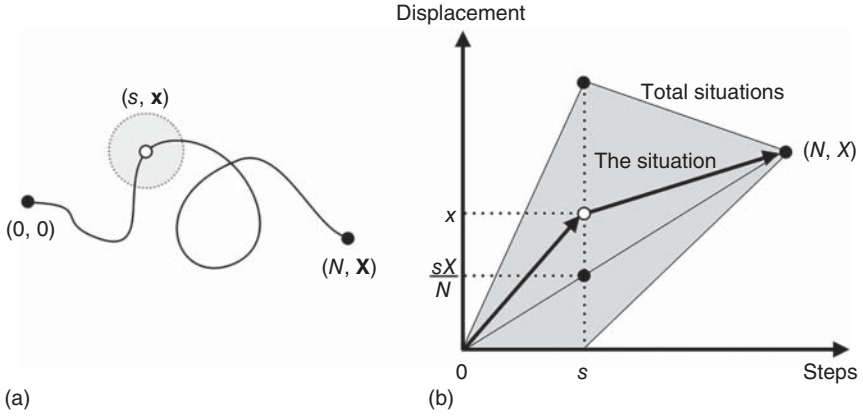

Figure 3.8 (a) A polymer chain starting from the origin and goes to X by N steps, through x by n steps. (b) Conceptual picture of a path starting from origin to (N, X) through (s, sX/N).

Thus, the probability density function is given by (3.19):

$$\begin{aligned}
&\frac{P_{1D}(s,x)\cdot P_{1D}(N-s,X-x)}{P_{1D}(N,X)} \\
&= \frac{\dfrac{1}{\sqrt{2\pi a^2 s}}\exp\left(-\dfrac{x^2}{2a^2 s}\right)\cdot\dfrac{1}{\sqrt{2\pi a^2(N-s)}}\exp\left(-\dfrac{(X-x)^2}{2a^2(N-s)}\right)}{\dfrac{1}{\sqrt{2\pi a^2 N}}\exp\left(-\dfrac{X^2}{2a^2 N}\right)} \\
&= \frac{1}{\sqrt{2\pi a^2 \frac{s}{N}(N-s)}}\exp\left(-\frac{\left(x-\frac{s}{N}X\right)^2}{2a^2\frac{s}{N}(N-s)}\right)
\end{aligned} \tag{3.19}$$

This is a Gaussian distribution with an average of sX/N and a variance of $s(N-s)/N$. This formula tells us that, given that the trajectory finally reaches X with N steps, it is reasonable that it advances to s/N of the whole course (sX/N) within s steps. That is, as conceptually shown in Figure 3.8, the straight line connecting the origin and X is likely to have been achieved. The variance is the harmonic mean (number of effective monomers: K) of s and $N-s$, which are the number of steps before and after reaching point x, respectively.

$$K = \frac{1}{\frac{1}{s}+\frac{1}{N-s}} = \frac{s}{N}(N-s) \tag{3.20}$$

In the one-dimensional random walk shown in Section 1.1.2, the variance was N, which is the total number of steps. In this case, the dispersion occurs within the steps of s, but the dispersion that occurs within the subsequent $(N-s)$ steps also influences the entire dispersion, resulting in the harmonic means

of these parameters. This conclusion does not change substantially moving to three-dimensional space, and the expression in three dimensions is as follows:

$$\left(\frac{3}{2\pi a^2 K}\right)^{3/2} \exp\left(-\frac{3\left(\mathbf{x}-\frac{s}{N}\mathbf{X}\right)^2}{2a^2K}\right) \tag{3.21}$$

The most important point in this consequence is that the variance is a^2K, which means that the fluctuation of the point (s, x) can be expressed only using K. For example, the fluctuation of the center ($s = N/2$) of a random walk of N steps is $\langle x^2\rangle^{1/2} = aN^{1/2}/2$, which is half the size of the original random walk.

Let us make a leap in our way of thinking. Focusing only on the fluctuation, the fluctuation of a certain point in an ideal chain in which both ends are fixed is equal to the fluctuation at the end of the ideal chain with of K steps. In other words, we can convert constraints from two points into equivalent constraints for one point (Figure 3.9). The chain after conversion is called "an equivalent chain." In the example of both ends-immobilized ideal chain with a degree of polymerization of N, the restraints placed on the monomer at the midpoint of the ideal chain are equivalent to those placed on the monomer at the opposite end of the equivalent chain with a degree of polymerization of $N/4$; both have the same restraints, $\langle x^2\rangle^{1/2} = aN^{1/2}/2$. With this in mind, the fluctuation of the crosslinking point can be quantitatively evaluated.

Next, let us consider a situation closer to the polymer networks. From here, for the sake of simplicity, the degree of polymerization of an ideal chain is N if there are no special considerations. When a gel is deformed, we deform the outermost layer of the gel. Thus, conceptually, we can envision a wall at the edge of the gel that deforms the same as the bulk. First, we consider the situation depicted in Figure 3.10a. Following the previous discussion, the fluctuation of the point constrained to the outer wall by the two ideal chains is equal to the fluctuation of the point constrained by an equivalent chain with $K = N/2$. If we extend another ideal chain from the point (Figure 3.10b), the fluctuation of the end point is equal to the fluctuation of the end point of the equivalent chain of $K = N + N/2 = 3N/2$. Next, let us consider the case where three ideal chains are connected to the wall (Figure 3.10c). In this case, first, two of the ideal chains are converted to an equivalent chain with $N/2$, and then, the two chains (with N and $N/2$) are further converted to an equivalent chain with $N/3$. The result of $N/3$

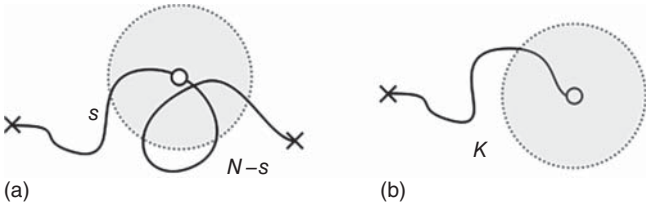

Figure 3.9 Fluctuation of a point along a polymer chain with both ends immobilized. The effect of immobilization at two points can be converted to immobilization at one point using K.

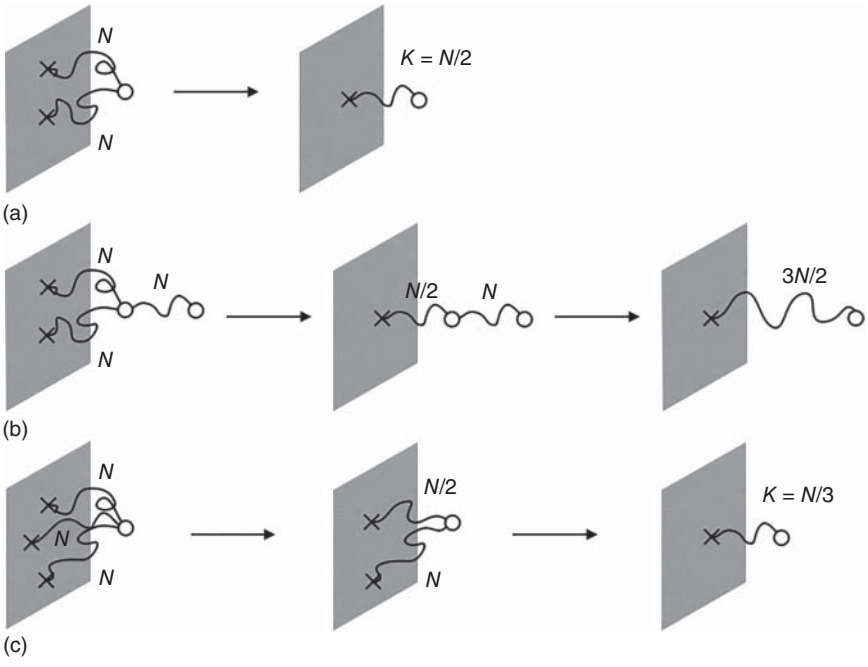

Figure 3.10 Equivalent transformations of the effects of immobilization by multiple chains to that of an effective chain.

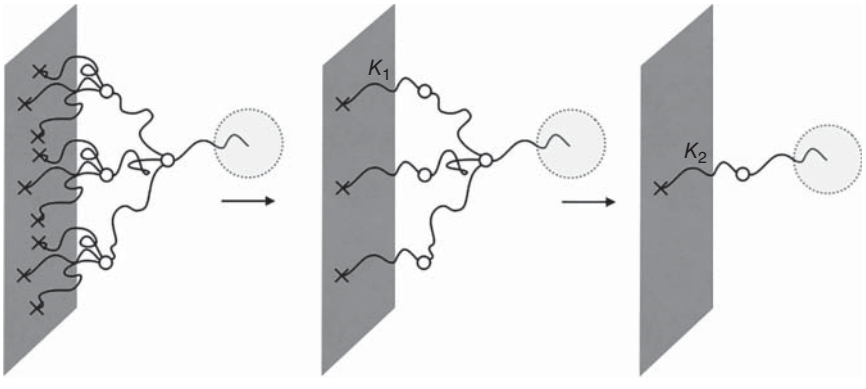

Figure 3.11 Equivalent transformation of the effect of the immobilization by a subnetwork to that of the effective chain.

can also be directly estimated as the harmonic mean of the three Ns. Therefore, in general, the fluctuation of a point connected to the wall by $f-1$ ideal chains is equal to that by an equivalent chain with $N/(f-1)$.

Next, we consider the fluctuation of a crosslinking point sufficiently distant from the wall. To investigate this problem, we consider the fluctuation of an end-point of a polymer network, as shown in Figure 3.11.

Figure 3.11 shows the region near the edge of a 4-functional polymer gel. First, the nine ideal chains connecting the crosslinking points (first generation)

to the wall are converted into three chains with a degree of polymerization K_1. Equation (3.22) is suggested by the previously mentioned discussion.

$$K_1 = \frac{1}{\frac{1}{N} + \frac{1}{N} + \frac{1}{N}} = \frac{N}{3} \tag{3.22}$$

Next, looking at the second-generation crosslinking points, they are connected to the wall by three $(K_1 + N)$-equivalent chains. These three chains are converted to an equivalent chain with the degree of polymerization K_2.

$$K_2 = \frac{1}{3}\left(\frac{N}{3} + N\right) \tag{3.23}$$

Finally, the fluctuation of the endpoint of the network is the same as that of the endpoint of an equivalent $K_2 + N$ chain.

$$K_2 + N = \frac{1}{3}\left(\frac{N}{3} + N\right) + N = N\left(1 + \frac{1}{3} + \left(\frac{1}{3}\right)^2\right) \tag{3.24}$$

Notably, the term $(1/3)^2$ is generated from the ideal chain connecting the wall to the first-generation crosslinking points. The effect of the earlier generation decreases while approaching the center of the polymer network. A simple expansion of this equation shows that the fluctuation of a point far from the wall is equivalent to that of the equivalent chain with the degree of polymerization K.

$$K = N\left(1 + \frac{1}{3} + \left(\frac{1}{3}\right)^2 + \left(\frac{1}{3}\right)^3 + \cdots\right) \tag{3.25}$$

This equation is generalized for f-functional polymer networks as follows:

$$K = N\left(1 + \frac{1}{f-1} + \left(\frac{1}{f-1}\right)^2 + \left(\frac{1}{f-1}\right)^3 + \cdots\right) \tag{3.26}$$

Because this is an infinite geometric series, it can be written as Eq. (3.27):

$$K = \frac{N}{1 - \frac{1}{f-1}} = \frac{f-1}{f-2}N \tag{3.27}$$

Because this geometric series quickly converges, roughly all crosslinking points in the polymer network can be considered to be constrained by an equivalent chain with a degree of polymerization K.

Figuring out how to best determine the elastic modulus is quite difficult even after discussing these models. However, the goal is almost complete. To estimate the elastic modulus, we focus on a network strand connecting two f-functional crosslinking points (Figure 3.12). The two crosslinking points are connected to the wall at both ends by $f-1$ effective chains with degrees of polymerization K. According to Eq. (3.22), these $f-1$ equivalent chains can be converted into an equivalent chain with the degree of polymerization $K/(f-1)$. Finally, the partial chain is included in an equivalent chain with the degree of polymerization $N + 2K/(f-1)$, which connects the wall to the wall. In other words, in the phantom network model, we consider the stretching of these virtual strands with a

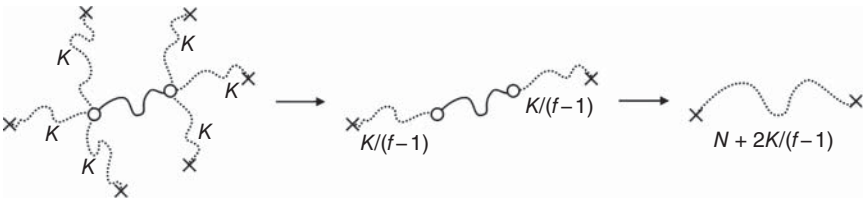

Figure 3.12 The effective chain in the phantom network model.

degree of polymerization N_{ph} instead of real network strands; it is exactly as the name suggests.

$$N_{\text{ph}} = N + \frac{2K}{f-1} = N + \frac{2}{f-1}\frac{f-1}{f-2}N = \frac{f}{f-2}N \tag{3.28}$$

Here, we utilize the conclusion of Eq. (1.35), which shows that the energy required to deform a polymer chain is inversely proportional to N. Therefore, in the phantom network model, the energy required to deform a network strand is as follows:

$$\Delta F = \frac{f-2}{f} \cdot \frac{3kT\mathbf{r}^2}{2Na^2} \tag{3.29}$$

By substituting Eq. (3.29) into the derivation of the affine network model, we can estimate the elastic modulus from the phantom network model.

$$G = \frac{f-2}{f}\nu kT = \left(\nu - \frac{2}{f}\nu\right)kT \tag{3.30}$$

Let us compare this conclusion with that of the affine network model. For the same polymer network, the affine network model always predicts a higher modulus than that predicted by the phantom network model. For example, in the case of a tetra-functional network, the elastic modulus predicted by the affine network model is double than that predicted by the phantom network model.

In the affine network model, a network strand has an energy of kT. How can we define an elastic element in the phantom network model? To understand the nature of these networks, let us consider the network structure shown in Figure 3.13. Such a strange figure is used because the influence of the edge is too strong when small networks are considered; the influence of the edge decreases with increasing network size. Because the network shown in Figure 3.13 has no edge, it is possible to extract universal properties of networks free from the edge effects. The numbers of crosslinking points (μ), network strands (ν), and independent closed cycles (cycle rank, ξ) for each system are also shown in Figure 3.13. Based on these numbers, the following relationships among these parameters are predicted [9]:

$$\nu = 2\mu \tag{3.31}$$

$$\xi = \nu - \mu + 1 \tag{3.32}$$

Equation (3.31) is derived from the fact that the network consists only of tetra-functional crosslinks. Although four network strands meet at each

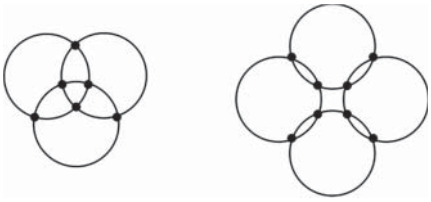

	(a)	(b)
μ	6	8
ν	12	16
ξ	7	9

Figure 3.13 Number of crosslinks (μ), network strands (ν), and independent closed cycles (ξ). Dangling chain-free network structures. Black circles indicate crosslinks.

crosslink, each strand is counted twice when counting as it is shown. Generally, for f-branched networks, the following relationship between the numbers of network strands and crosslinks holds true:

$$\mu = \frac{2}{f}\nu \tag{3.33}$$

Next, Eq. (3.32) holds for general networks without edges. In extremely large networks, such as a polymer gel, because ν, μ, and ξ are all extremely large, Eq. (3.32) can be reduced as follows:

$$\xi = \nu - \mu \tag{3.34}$$

Using Eq. (3.34), Eq. (3.30) can be reduced to the following:

$$G = (\nu - \mu)kT = \xi kT \tag{3.35}$$

This equation implies that an independent cycle has an energy of kT in the phantom network model.

3.5 Network Strands and Crosslinks

Thus far, we have introduced the affine network and the phantom network models, which describe the elastic modulus. According to these models, the elastic modulus is estimated from the values of ν and ξ. The next challenge is estimating ν and ξ. Here, we define the network strand and the crosslink in detail.

To understand the nature of this problem, we consider a cleaving process in a tetra-functional network, as shown in Figure 3.14. Initially, this network is complete and consists of 20 tetra-functional crosslinks and 49 network strands ($\nu \neq 2\mu$ due to the edge effect). When one network strand is cut (Figure 3.14a), the number of network strands decreases by 1, and two of the tetra-functional crosslinks become tri-functional crosslinks. As a result, the number of crosslinks does not change, and only the number of network strands changes (decreases by 1).

Next, another adjacent network strand is cut (Figure 3.14b). This cleavage is different from the previous case and causes a complex change. When focusing on crosslinks, not only does a tetra-functional crosslink becomes a tri-functional crosslink but also a tri-functional crosslink becomes a node, i.e. one crosslink disappears. At the same time, two network strands originally connected by a

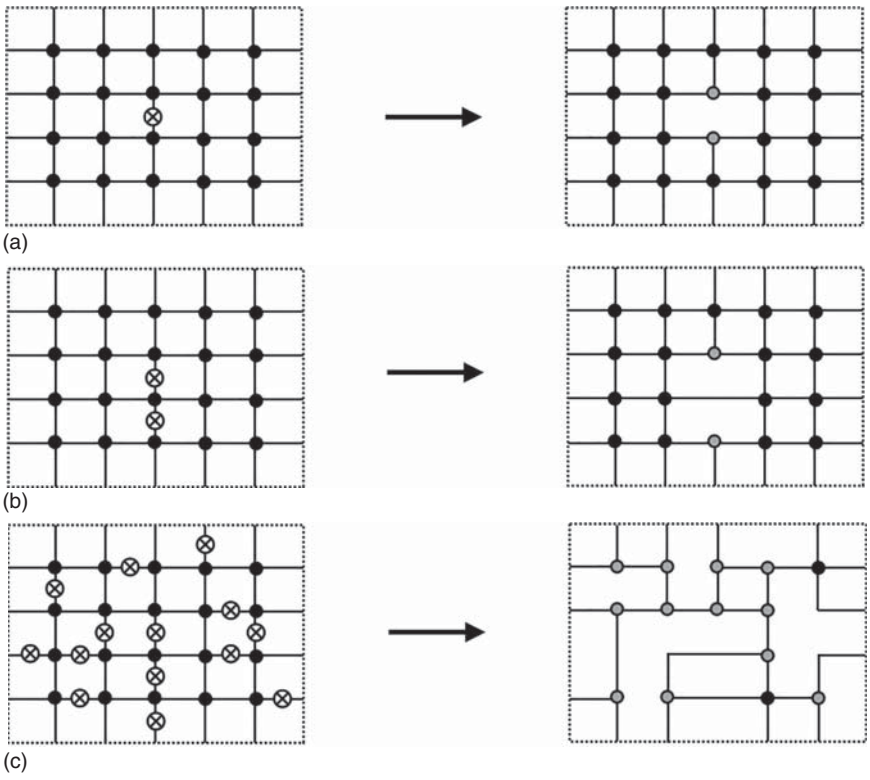

Figure 3.14 Cleavage of network strands in tetra-functional network: cleavage of (a) a strand, (b) two neighboring strands, and (c) many strands. Black and gray circles indicate 4- and 3-functional crosslinks, respectively.

crosslink become a single network strand. As a result, one crosslink and two network strands are lost by cutting this second network strand. Figure 3.14c shows the results of cutting additional network strands; many crosslinks become tri-functional or are lost, and the number of network strands decreases dramatically. It is easy to imagine that the final result will change depending on which network strands are cut.

Let us return to the original problem. What parameters can we use to calculate ν and ξ? It will be at most the concentration of a prepolymer, the functionality of the crosslinking molecule, and the conversion of the reaction between the prepolymer and the crosslinking molecule. One of the difficulties in this problem is that different ν and ξ are predicted from the same feed conditions depending on how the partial chains are connected (or cut), as shown in Figure 3.14. Therefore, estimating ν and ξ in a network is generally very difficult.

Another challenge comes from the connectivity of the network strands, but we need to consider a network on a larger scale. Let us consider the condition that a crosslinking molecule becomes a tetra-functional crosslink. Is it sufficient for the four chains connected to this molecule to be connected to different crosslinking molecules? The answer is "No" because the connected crosslinking molecules

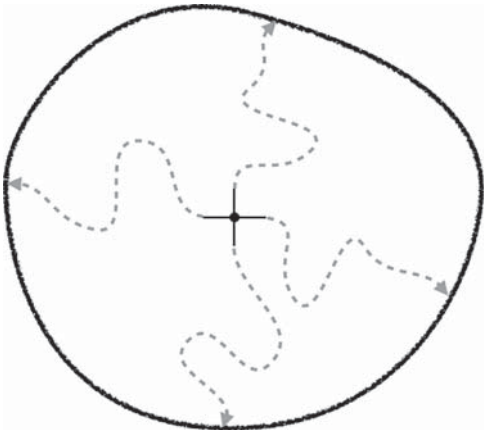

Figure 3.15 When all four arms are connected to the edge of the polymer gel, the tetra-functional molecule becomes a tetra-functional crosslink.

could not be connected anywhere. Therefore, to be connected properly, the crosslinks must be connected to the edge of the network (Figure 3.15). If all four chains extending from this crosslink are connected to the edge of the network without interruption, this crosslinking molecule is a tetra-functional crosslink. However, this definition further complicates this problem.

At the end of this section, the definitions of crosslinks and network strands are summarized. A crosslink is a branching point with three or more links to the edge of the network, and the network strand is a chain connecting two neighboring crosslinks. In either the affine network model or the phantom network model, the crosslinks are assumed to move in accordance with the macroscopic deformation. Because the network strands connecting these crosslinks obey affine deformation, they are sometimes called elastically effective chains or elastically active network chains [10].

3.5.1 Percolate Network Model

Thus far, we have discussed the difficulties in determining the concentrations of crosslinks and network strands. On the other hand, in the previously mentioned problem, if we consider a branch point ahead of a branch point ahead of a certain partial chain, the number of branches that can be connected to the edge of network increases in a geometric progression. The probability that a network strand is connected to the edge is likely to be quite high when the connectivity is high (see Figure 3.14). Indeed, if a network is ideal to some extent, it is relatively easy to estimate ν and ξ by a simple approximation [11].

Let us consider a network made from tetra-functional molecules. Functional group A is attached to the terminal of the tetra-branched polymer, and functional group A reacts with another functional group A to form a linkage. The conversion of the A–A bond forming reactions is defined as p ($0 \leq p \leq 1$). We focus on the region where the reaction is almost complete and p is close to 1 and assume the following:

At $p = 1$, a perfect lattice consisting only of tetra-functional crosslinks is formed.

Although this assumption is quite idealized because there are many degrees of freedom in the way the polymers are connected, we accept this assumption and can understand the scope of this problem. When the number density of the tetra-functional polymer is c (m^{-3}), ν and μ are given for $p = 1$ as follows:

$$\mu = c \tag{3.36}$$

$$\nu = 2c \tag{3.37}$$

These equations hold because one tetra-functional polymer forms one crosslink and two network strands. Next, the network strands are gradually cut, which is the same process as that shown in Figure 3.14. That is, when a network strand is cut, a network strand disappears, and two tetra-functional crosslinks are converted to tri-functional crosslinks. In this case, the position of the network strand to be cut next is different. There is only a small probability that the network strand to be cut next is adjacent to the first cleavage site. Thus, we can consider the same process for the second cut: a network strand disappears, and two tetra-functional crosslinks are converted to tri-functional crosslinks. How long will this process hold? The probability that two neighboring network strands are cut is approximately represented by $(1-p)^2$. This probability is, for example, 0.01 at $p = 0.9$ and 0.04 at $p = 0.8$, which can be negligible in this range of p. In the range where this process holds, ν and μ can be expressed as follows using p:

$$\mu = c \tag{3.38}$$

$$\nu = 2cp \tag{3.39}$$

The number of crosslinking points does not change and the number of network strands decreases in proportion to p. When the affine model or a phantom model is applied, in the vicinity of $p = 1$, the elastic modulus, G, is given as follows:

$$G_{\mathrm{af}} = 2pCkT \quad \text{(Affine network model)} \tag{3.40}$$

$$G_{\mathrm{ph}} = (2p-1)CkT \quad \text{(Phantom network model)} \tag{3.41}$$

3.5.2 Bethe Approximation

In Section 3.5.1, we showed that ν and μ can be estimated quite easily with the percolate network model. However, it may seem that the approximation is far from the real value; indeed, the percolate network model holds only for nearly ideal networks. Here, we introduce a different approach – Bethe approximation. While the percolate network model is top-down, Bethe approximation is a bottom-up methodology and can be utilized to estimate other parameters such as the gelation point.

In Bethe approximation, the network structure is approximated to a virtual tree-like structure [10, 12]. The tree structure is simpler than the network structure. Let us consider the situation where a network structure is made from a tetra-functional polymer by an AA-type reaction (Figure 3.16), as discussed earlier. When one or two reactions occur, what kind of species will be formed? All the possibilities are listed in Figure 3.16.

Many kinds of structures with double links and loops, which are often treated as defects, can be formed. As the number of linkages increases further, we need

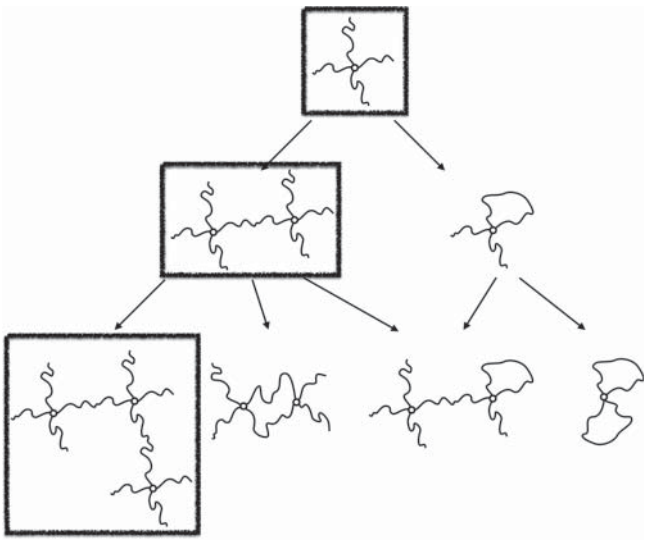

Figure 3.16 Formation of a network structure by an AA-type reaction of tetra-functional polymers.

to consider a tremendous number of situations, and it becomes impossible to evaluate all potential situations. Bethe approximation is used to simplify this problem. As shown in Figure 3.17, a real tree contains only branched structures and does not contain loops. Such a branching structure can be formed by assuming that no intramolecular reaction occurs in the reaction. Bethe approximation only considers the structures surrounded by boxes in Figure 3.16. Although this approximation is often criticized due to this simplification, this is one of the few analytical methodologies that can describe the polymer network. Notably, this methodology is a kind of mean-field approximation, and does not focus on the real tree structure. In Bethe approximation, we can make three assumptions:

1. No intramolecular reactions occur in finite-sized clusters.
2. Every functional group has the same reactivity.
3. The reactivity of the functional groups does not change with other reactions.

Assumption 1 sets Bethe structure and forms the basis of this model. The limitation to finite-sized clusters comes from the fact that it is impossible to distinguish intramolecular and intermolecular reactions in the case of an infinitely sized cluster, i.e. a gel. Assumptions 2 and 3 guarantee the constant reactivity of the functional group during gelation, which is vital for subsequent stochastic considerations.

Let us now consider the situation in which we know a certain probability, p, that the ends of branched molecules are linked, and this probability corresponds to the reaction conversion. We discuss the AA-type reaction of a tetra-functional molecule as an example. The challenge is in determining if the path extending from one arm leads to an infinite-sized cluster, as depicted in Figure 3.15. To solve this problem, we consider the event F as defined as follows:

F: A path extending from an arm does not lead to an infinite-sized cluster.

Figure 3.17 The structure of a tree with no intramolecular connections.

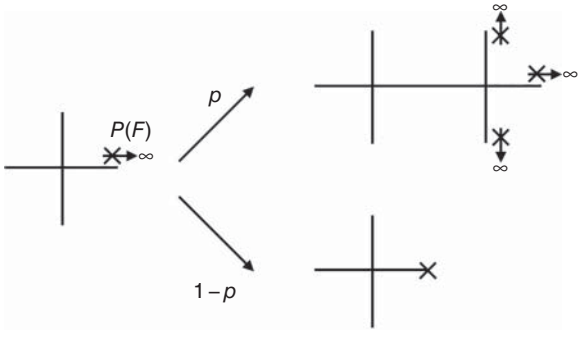

Figure 3.18 Elementary steps of an AA-type reaction of tetra-functional polymers.

The probability $P(F)$ of this event can be calculated by considering the elementary process that an arm connects to the next molecule, as shown in Figure 3.18.

For the first reaction, there are two possible situations: the arm connects to the next molecule (probability, p), and the arm does not connect to the next molecule (probability, $1 - p$). If the arm does not connect to the next molecule, this arm cannot connect to the infinite-sized network; thus, the probability of this situation is included in $P(F)$. On the other hand, if the arm is connected to the next molecule, we need to consider the three new arms from the next molecule. To eliminate the connectivity to the infinite-sized network, these three arms should each be in situation F. Therefore, the probability that the arm connects to the next molecule but does not lead to the infinite-sized network is given by $p \cdot P(F)^3$. $P(F)$ is given by the sum of these probabilities:

$$P(F) = p \cdot P(F)^3 + (1 - p) \tag{3.42}$$

This equation is a cubic function of $P(F)$ and can be transformed to the following:

$$(P(F) - 1)(p \cdot P(F)^2 + p \cdot P(F) + p - 1) = 0 \tag{3.43}$$

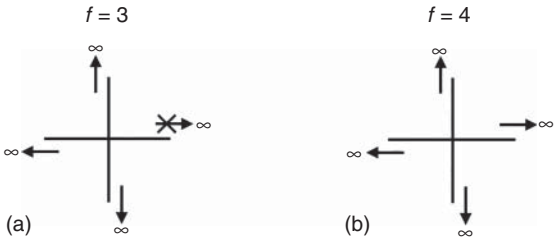

Figure 3.19 Situations in which a polymer becomes a (a) tri- or (b) tetra-functional crosslinks.

This function has three solutions, including a trivial solution of $P(F) = 1$. The solution is given by considering $0 \leq P(F) \leq 1$.

$$P(F) = \sqrt{\frac{1}{p} - \frac{3}{4}} - \frac{1}{2} \tag{3.44}$$

By using this equation, $P(F)$ can be estimated from p, which is directly measured experimentally. Once $P(F)$ is given, the probability that the original tetra-functional molecule becomes an f-functional crosslink ($P(X_f)$) is given as shown in Figure 3.19.

$$P(X_3) = \binom{4}{3} P(F)(1 - P(F))^3 \tag{3.45}$$

$$P(X_4) = (1 - P(F))^4 \tag{3.46}$$

Furthermore, the expected values of crosslinks (μ_0) and network strands (ν_0) formed from a tetra-functional molecule are represented as follows:

$$\mu_0 = P(X_3) + P(X_4) \tag{3.47}$$

$$\nu_0 = \frac{3}{2}P(X_3) + \frac{4}{2}P(X_4) \tag{3.48}$$

It should be noted that tri- and tetra-functional crosslinks are not distinguished when determining the number of crosslinks, and the duplication is taken into account when counting network strands. By taking the product of this expected value and the number density of the tetra-functional molecule, the number

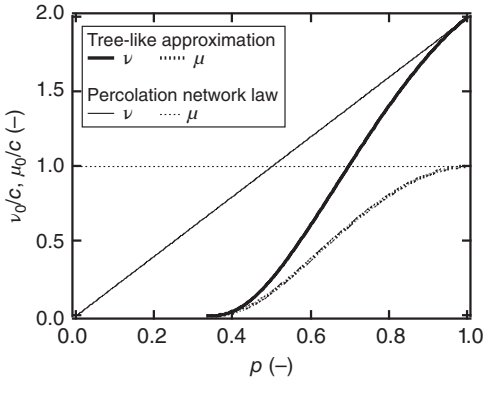

Figure 3.20 Effect of p on normalized ν_0 and μ_0.

density of crosslinks and network strands can be calculated. Furthermore, the elastic modulus can be estimated by applying the affine model or the phantom model. Here, we compare the density of the crosslinks and network strands calculated from the percolate network model and Bethe approximation. As shown in Figure 3.20, in the region of $p \approx 1$, the results are approximately the same. This result is proof that network structures can be modeled by mean-field treatment as Bethe approximation when connectivity is high and that both models can predict the structural parameters of ideal networks.

3.6 Topological Interaction

Essentially, in the models introduced so far, a network strand is the elastic element, and the elasticity of the network is described by the sum of the network strands. However, these models contain serious problems regarding the implicit stability of the network. That is, the problem of infinite contraction, which was also mentioned in Chapter 1. Since the most stable end-to-end distance of a network strand is 0, a network of finite size is unstable, and the most stable state is achieved when the volume = 0. As a result, the gel shrinks spontaneously, which causes a problem even during the gelation process. When a small amount of crosslinking occurs in solution, a local heterogeneous density distribution is generated. A denser region has higher elasticity, resulting in contraction and a further increase in the density of crosslinks. However, less dense regions will become even less dense shown in Figure 3.21. Of course, such situations may not occur in reality, and a uniform network is formed in controlled gelation processes.

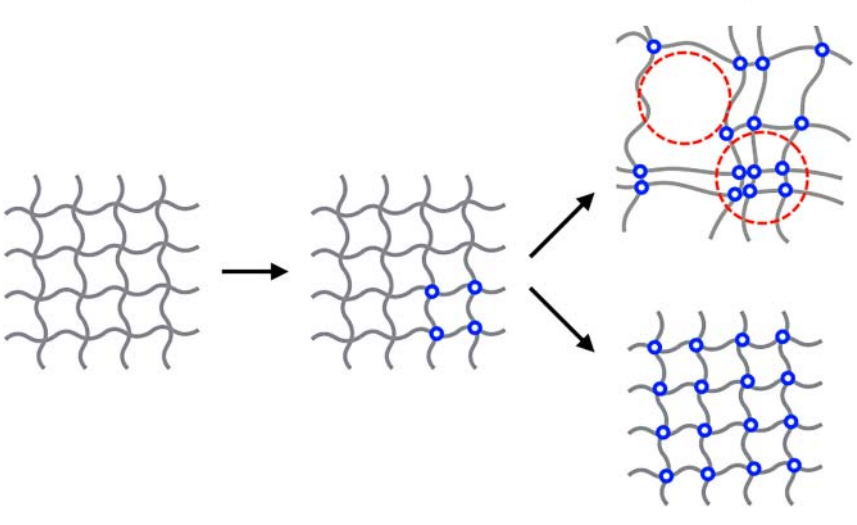

Figure 3.21 Schematic picture of the gelation reaction. Circles indicate the crosslinking points.

Figure 3.22 Topological interactions between two polymer chains (a) attractive and (b) repulsive.

Iwata et al. proposed a model describing the elasticity of a network based on the topological nature of the polymers, which solves the previously mentioned problems [13–15]. Since the details of the model are complicated, here we only introduce the concept of the model (Figure 3.22).

Indeed, the theories of elasticity introduced so far are implicitly based on the assumption that the network strands have no excluded volume and can pass through each other. Such a chain is called a phantom chain, and although the name is similar, it has no direct relationship with the phantom network model. Even in the situation where the network chains are definitely entangled, such as $\phi = 1$, we did not consider the influence of entanglement on the mechanical properties. However, in reality, a network strand has a definite excluded volume, no slip-through occurs, and entanglement has a significant influence on the mechanical properties.

As a simple example, here we consider two chains with excluded volumes. When these chains are entangled, it is impossible to pull them apart, and a force counteracting the separation is generated. The force is attractive because it works to keep the two chains entangled. However, when two nonentangled macromolecules are brought close to each other, they cannot pass through each other, and a force counteracting their interaction is generated, and this force is repulsive (Figure 3.22). Although the origin of these forces is collisions between segments of the chain (excluded volume effect), the forces can be either attractive or repulsive depending on the situation. This force is called "topological (geometric) interaction" because this force seems to maintain the initial geometric configuration of the polymer. Under this concept, an "entanglement" between network strands topologically inhibits chain motion. Of course, although no entanglements exist without an excluded volume, the excluded volume effect and entanglement are identical under this concept.

Returning to a gel network, it can be regarded as a series of ring structures (Figure 3.23). The previously mentioned concept suggest that the network structure is maintained by the repulsive force between rings, and infinite contraction does not occur. Furthermore, even if a heterogeneous distribution of crosslinks temporarily occurred during gelation, both repulsive and attractive topological forces are generated, so they cancel each other out, resulting in a homogeneous structure. When the material is deformed, an attractive force and a repulsive force becomes out of balance due to the anisotropic distribution of rings, leading to the stress. Considering the ring as a structural unit of the network solves many of the problems that arise when the network strand is used as the unit. In recent years, this model has been extended to large deformation regions, and the nonlinear behavior of rubber is well studied [16, 17]. Thus, topological interactions are an interesting concept, and they provide a good example of the potential faults of classical rubber elastic theory.

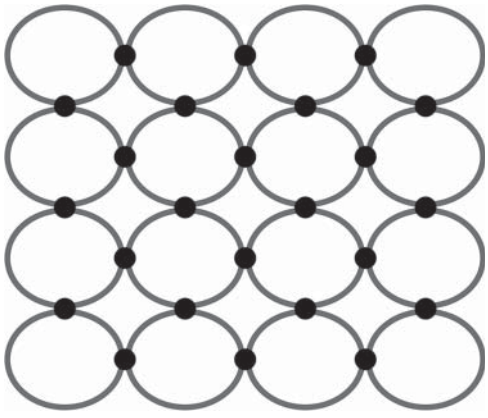

Figure 3.23 A polymer network consists of many cyclic polymers.

3.7 Sol–Gel Transition

In this chapter, we have reviewed the definition of a polymer gel and the rubber elasticity of polymer gels. Here, we briefly introduce models for theoretically predicting the sol–gel transition. As introduced in Section 3.2.1, the crosslinking reaction in a polymer solution forms a three-dimensional network structure, i.e. a polymer gel. This liquid-to-solid transition is called a sol–gel transition or simply gelation.

There are two important considerations in gelation. One is the critical point at which the gel is formed, such as the lowest concentration at which a gel can form and the lowest crosslinking density. The other is how the physical properties change approaching the critical point, such as how the viscosity increases approaching gelation and how the elastic modulus increases after gelation. Models of gelation predict the critical point and the processes that occur near the critical point. Conventional models can be roughly divided into two groups: (i) Bethe approximation, (ii) the percolation model in lattices, and (iii) simulations. In this section, we briefly explained Bethe approximation and the percolation model.

3.7.1 Gelation Threshold of Bethe Approximation

Here, we focus on predicting the gelation threshold based on Bethe approximation discussed in Section 3.5.2. Briefly, the model considers Bethe structure without intramolecular linking. Using Bethe approximation, the critical conversion (p_c) necessary for gelation can also be predicted. Here, we again consider the tetra-functional network. The gelation threshold is equivalent to the point where we can find an infinite-sized network for the first time. In the system, there is at least one arm leading to the infinite-sized network. Under these conditions, Eq. (3.43) should have a solution in the range $0 \leq P(F) \leq 1$. Given $g(P(F)) = pP(F)^2 + pP(F) + p - 1$, the condition is represented as follows:

$$\begin{aligned} &g(0)g(1) = (p-1)(3p-1) \leq 0 \\ &p \geq \frac{1}{3} \end{aligned} \tag{3.49}$$

The gel is predicted to form at $p \geq 1/3$, namely, $p_c = 1/3$. This discussion can be extended to the AA-type reaction of an f-functional polymer, and the results are as follows:

$$(P(F) - 1)\left(p \cdot \sum_{n=2}^{f} P(F)^{n-2} - 1\right) = 0 \tag{3.50}$$

The criteria for the gelation of f-functional polymers are represented as

$$p_c = \frac{1}{f-1} \tag{3.51}$$

In this way, Bethe approximation is versatile and can also be applied to AB-type reactions, which are reactions between molecules with different functionalities, and living polymerizations.

3.7.2 Gelation Threshold from the Percolation Model

The word "percolation" can mean "penetration" and "bleeding out." In the percolation model, the lattice points in a certain lattice space are marked randomly, and how the marked lattice points are connected is discussed. The growth of connected lattice points (clusters) is similar to that of polymer networks as well as the structure of oil fields and the flaring of forest fires. Gelation in the percolation model is defined as the existence of clusters passing through all the principal axes (percolation, right-hand images in Figure 3.24).

The method of percolation can be roughly divided into two pathways. One is site percolation, which randomly fills empty lattice spaces. Here, we define the

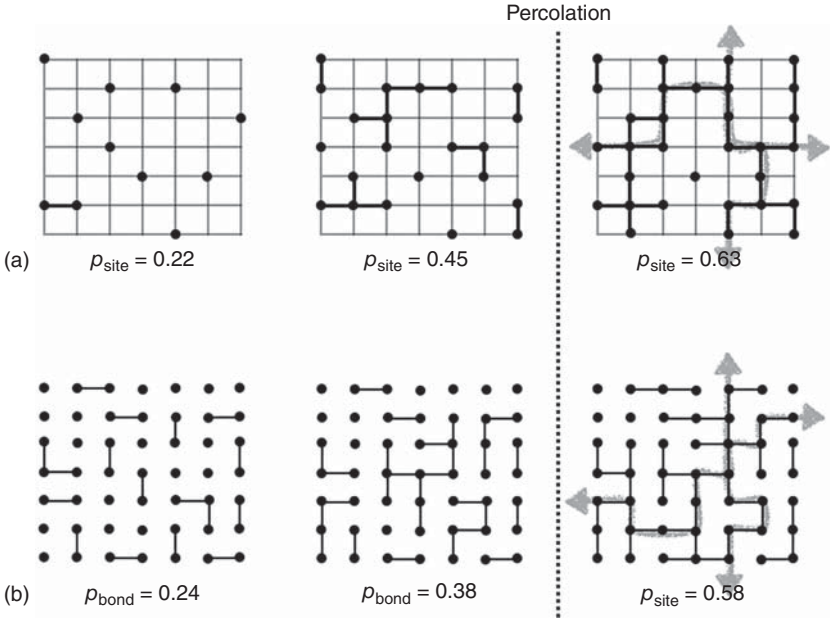

Figure 3.24 Gelation by (a) site percolation ($p_{bond} = 1$) and (b) bond percolation ($p_{site} = 1$).

probability that the site is occupied as p_{site} and the probability that the adjacent occupied sites are connected as p_{bond}. In the site percolation model, p_{site} is variable, while $p_{bond} = 1$. In other words, when neighboring sites are occupied, the sites are definitely connected. The site percolation model is appropriate for the prediction of the lowest polymer concentration forming a gel .

In the bond percolation model, $p_{site} = 1$ and p_{bond} is variable; all lattice points are occupied first, and points are bonded randomly. The bond percolation model is appropriate for a gelation from a polymer solution with a concentration higher than the overlapping concentration. Comparing these two models in a certain lattice space, it is generally more difficult for site percolation to percolate throughout the system compared with bond percolation, and site percolation has a slightly larger threshold. There is another model, called the site–bond percolation model, in which both p_{site} and p_{bond} are variables.

Finally, we compare these theoretical predictions and the experimental results. For a tetra-functional network structure, representing a conventional polymer gel, Bethe approximation ($p_c \approx 0.33$) and the bond percolation model (diamond lattice, $p_c \approx 0.39$) predict similar values. These predictions were compared with the experimental results of a gelation from an AB-type reaction of tetra-functional prepolymers and showed good agreement at concentrations above the overlap concentration (c^*) [18]. Based on this observation, p^* is expected to be constant in the concentration range above c^*. On the other hand, p^* gradually increases as the concentration decreases below c^*, and gelation was not observed below $c^*/6$. These data strongly suggest that c^* of the prepolymer is an important factor and greatly affects the gelling process.

Based on the agreement with the experimental results, the predictive models introduced here seem to have sufficient accuracy. Notably, the models address the ideal process. Therefore, in principle, it is impossible to form gels below the threshold predicted by the models. The deviation in the threshold value suggests the experimental condition deviate from those assumed in the model.

3.8 Heterogeneity of Polymer Gels

At the end of this chapter, we introduce the heterogeneity of polymer gels. What we want to emphasize here is that 3D polymer networks are inherently heterogeneous. To understand the essence of this problem, let us imagine synthesizing a unit structure of a tetra-functional network containing four branching points by the cyclization of a polymer with eight side chains, as shown in Figure 3.25.

If mutually reactive functional groups are present only at the ends, the correct (structure shown on right side of Figure 3.25) can be synthesized. However, the correct structure is rarely synthesized in cases when the concentration of macromolecules in the system is high or when each arm has reactive functional groups. In general, various unit structures (shown in Figure 3.26) can be synthesized. Therefore, it is practically impossible to synthesize an ideal polymer network, as shown in Figure 3.5, and thus polymer networks are heterogeneous.

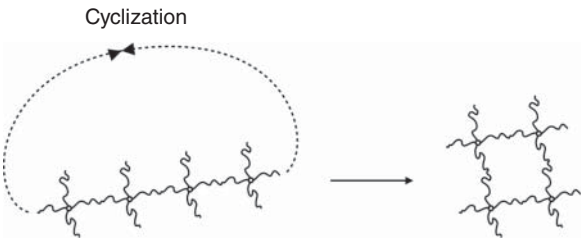

Figure 3.25 Synthesis of the unit structure of a tetra-functional network.

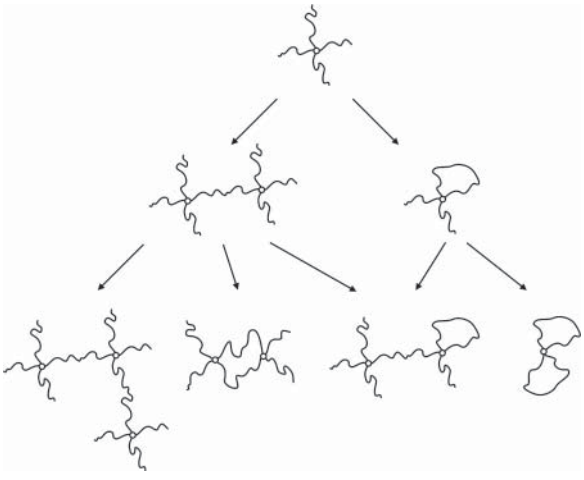

Figure 3.26 Structures formed by the AA-type reaction of tetra-functional polymers.

As a next step, we consider a more popular system, namely, preparing a polymer gel by radical copolymerization of a vinyl monomer and a divinyl crosslinker (Figure 3.27). In this reaction, mainly vinyl monomers undergo polymerization, and the divinyl crosslinkers are sparsely introduced at random. When both vinyl groups of a divinyl crosslinker react, the crosslinker becomes a crosslink, and the series of monomer units between neighboring crosslinks becomes a network strand. As immediately seen from this process, the molecular weights of network strands have a random and heterogeneous distribution. Loops and entanglements can both be formed. The size of these heterogeneous regions are similar to the sizes of the network strands; these regions are called local inhomogeneities.

In radical copolymerizations, highly branched polymeric clusters form and grow at the beginning of the reaction. As the reaction progresses further, the branched clusters grow into nanogel-like structures, and eventually they combine to form a macroscopic three-dimensional network structure. Therefore, a dense region is formed by the nanogels, and sparse regions are formed in regions where the nanogels are connected. This dense-sparse heterogeneity is considerable, and its size is approximately several tens of nanometers to several hundred nanometers. This type of heterogeneity is called global heterogeneity, and it can be confirmed by excessive scattering in light scattering analysis, small-angle neutron scattering, and so on.

On the other hand, local inhomogeneities cannot be observed directly and can be observed only as deviations in the physical properties from those predicted by

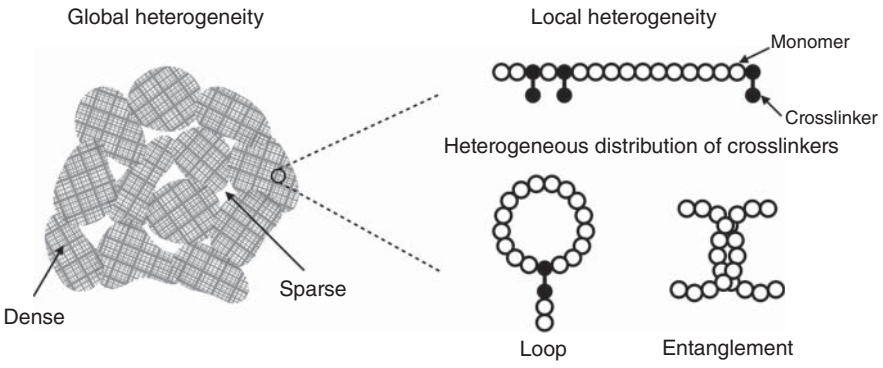

Figure 3.27 Heterogeneities in polymer gels are categorized as global or local heterogeneities.

an applicable model, making them impossible to discuss quantitatively. In recent years, some methodologies capable of directly observing local heterogeneities have been developed, and local heterogeneities are slowly being revealed [19, 20].

Column 3: Elastic Deformation and Plastic Deformation

Some materials show degrading mechanical profile in repetitive mechanical testing. The phenomenon that the mechanical profiles of deformation and recovery do not coincide with each other is called "hysteresis" (see Figure 3.28). The origin of hysteresis is energy dissipation. A solid stores energy when strain is applied. In an ideal elastic material, the stored energy is released as it is without any energy dissipation (elasticity), and the recovery profile is the same with the deforming one. The force needed to deform an ideal elastic material is determined only by "deformation ratio" at the time. An example of an ideal elastic material is the spring.

If a material shows a hysteresis, the material dissipates energy due to viscoelasticity and/or plastic deformation. We introduce viscosity prior to explaining the viscoelasticity. A matter exhibiting viscosity is generally a liquid. What determines the force needed to deform a liquid? If one imagines swimming in the

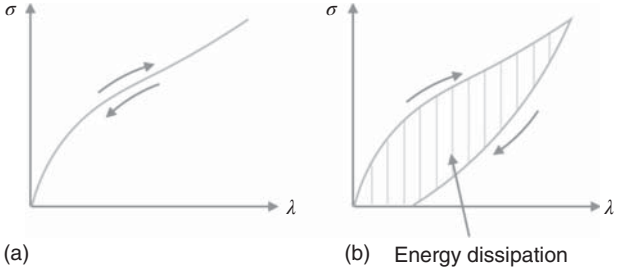

Figure 3.28 Mechanical profiles of (a) an elastic body and (b) a viscoelastic body showing hysteresis.

pool, the answer is speed. The force for deforming the viscous body is determined only by the "deformation rate" at the time, and does not relate to how much it is deformed from the initial state. Thus, even after a large deformation, the force becomes 0 after a long time; i.e. all applied energy is dissipated.

Polymer gels and polymer liquids/melts often show viscoelasticity, which includes both elasticity and viscosity. That is, they store energy in a short time range (elasticity), while the energy is dissipated and the force required for deformation decreases over time (viscosity). Thus, even during the deformation, a certain amount of energy is dissipated, resulting in a difference in mechanical profiles of deformation and recovery (hysteresis). The degree of hysteresis varies according to the relationship between the deformation rate and the time required for energy dissipation (relaxation time).

Plastic deformation is a permanent distortion and is observed above a critical stress (σ_c). The origin of plastic deformation is often due to the irreversible structural changes causing energy dissipation (such as destruction of structure). An amount of energy dissipation of a plastic body is determined only by "degree of deformation." Many of the theories introduced in this book deals with ideal elastic materials and viscoelastic materials in the equilibrium state (after a sufficiently longer time than the relaxation time). When one applies the theories to the experimental results, one must consider the effect of viscoelasticity and plastic deformation.

References

1 Winter, H.H. and Chambon, F. (1986). Analysis of linear viscoelasticity of a crosslinking polymer at the gel point. *J. Rheol.* 30: 367–382.
2 Shibayama, M., Takahashi, H., and Nomura, S. (1995). Small-angle neutron-scattering study on end-linked poly(tetrahydrofuran) networks. *Macromolecules* 28: 6860–6864.
3 Bastide, J. and Leibler, L. (1988). Large-scale heterogeneities in randomly cross-linked networks. *Macromolecules* 21: 2647–2649.
4 Shibayama, M. (1998). Spatial inhomogeneity and dynamic fluctuations of polymer gels. *Macromol. Chem. Phys.* 199: 1–30.
5 Nishi, K., Asai, H., Fujii, K. et al. (2014). Small-angle neutron scattering study on defect-controlled polymer networks. *Macromolecules* 47: 1801–1809.
6 Kuhn, W. (1946). Dependence of the average transversal on the longitudinal dimensions of statistical coils formed by chain molecules. *J. Polym. Sci.* 1: 380–388.
7 James, H.M. and Guth, E. (1949). Simple presentation of network theory of rubber, with a discussion of other theories. *J. Polym. Sci.* 4: 153–182.
8 Rubinstein, M. and Colby, R.H. (2003). *Polymer Physics*. Oxford: Oxford University Press.
9 Tanaka, F. and Ishida, M. (1996). Elastically effective chains in transient gels with multiple junctions. *Macromolecules* 29: 7571–7580.
10 Flory, P.J. (1953). *Principles of Polymer Chemistry*. Ithaca/London: Cornell University Press.

11 Nishi, K., Noguchi, H., Sakai, T., and Shibayama, M. (2015). Rubber elasticity for percolation network consisting of Gaussian chains. *J. Chem. Phys.* 143: 184905.

12 Miller, D.R. and Macosko, C.W. (1976). New derivation of post gel properties of network polymers. *Macromolecules* 9: 206–211.

13 Iwata, K. and Edwards, S.F. (1989). New model of polymer entanglement: localized Gauss integral model. Plateau modulus G_N, topological second virial coefficient $A^{\theta}{}_2$ and physical foundation of the tube model. *J. Chem. Phys.* 90: 4567–4581.

14 Iwata, K. and Kimura, T. (1981). Topological distribution functions and the second virial coefficients of ring polymers. *J. Chem. Phys.* 74: 2039–2048.

15 Iwata, K. and Ohtsuki, T. (1993). On catenate network formation by end-linking reactions. *J. Polym. Sci., Part B: Polym. Phys.* 31: 441–446.

16 Hirayama, N. and Tsurusaki, K. (2011). Topological interaction between loop structures in polymer networks and the nonlinear rubber elasticity. *Nihon Reoroji Gakk.* 39: 65–73.

17 Hirayama, N., Tsurusaki, K., and Deguchi, T. (2009). Linking probabilities of off-lattice self-avoiding polygons and the effects of excluded volume. *J. Phys. A: Math. Theor.* 42: 105001.

18 Sakai, T., Katashima, T., Matsushita, T., and Chung, U.-i. (2016). Sol–gel transition behavior near critical concentration and connectivity. *Polym. J.* 48: 629–634.

19 Lange, F., Schwenke, K., Kurakazu, M. et al. (2011). Connectivity and structural defects in model hydrogels: a combined proton NMR and Monte Carlo simulation study. *Macromolecules* 44: 9666–9674.

20 Zhong, M., Wang, R., Kawamoto, K. et al. (2016). Quantifying the impact of molecular defects on polymer network elasticity. *Science* 353: 1264–1268.

4

Swelling and Deswelling

Takamasa Sakai

Graduate School of Engineering, The University of Tokyo, Tokyo, Japan

Polymer gels contain a large number of solvent molecules and can absorb additional solvent or lose solvent from the as-prepared state. These processes are of course accompanied by volume changes in the polymer gel, i.e., swelling and deswelling. For example, a super water-absorbing polymer gel used for diapers can absorb up to 1000 times its dry weight in water. This fact shows that a polymer gel can hold a large amount of solvent and that there is a limit to how much a polymer can swell. When a hydrogel is placed in an aqueous environment, such as in the living body, either swelling or contraction generally occurs to some extent, and there is a concomitant change in volume. Therefore, it is practically important to know to what extent swelling can occur and how the physical properties change with changes in volume change. In this chapter, we discuss the swelling of polymer gels, including changes in mechanical properties due to swelling, the conditions for equilibrium swelling, and the kinetics of swelling.

4.1 Changes in the Elastic Modulus Due to Swelling/Deswelling

Here, there is a polymer gel with elastic modulus G in the as-prepared state. When the gel swells to twice its initial volume, how will the elastic modulus change? If the network is not broken and new bonds do not form upon swelling, the concentration of network strands is halved. The affine network model suggest the elastic modulus will be halved. However, experimentally, the elastic modulus is not halved; it decreases by 20–30%. This discrepancy is caused by the fact that we did not consider additional effects of the subsequent swelling process. The gel discussed here is different from a gel formed at half the polymer concentration for which G can be described by Eq. (3.15). Even if the concentrations are the same, when there are differences between the as-prepared state and the state after subsequent processes, the gels will have different elastic moduli. Notably, the physical properties of polymer gels are influenced by the two states, the state of prepara-

Physics of Polymer Gels, First Edition. Edited by Takamasa Sakai.

tion and the state of interest. In the following sections, we introduce models for predicting the changes in the elastic modulus due to swelling/deswelling based on this concept.

4.1.1 Statistical Model for Networks Consisting of Ideal Chains

According to the phantom network model, the change in total energy under deformation is as follows:

$$\Delta F = \frac{\xi_0 V_0 kT}{2}(\lambda_x{}^2 + \lambda_y{}^2 + \lambda_z{}^2 - 3) \tag{4.1}$$

Here, ξ_0 is the number density of the cycle rank, and V_0 is the volume of the gel. If ξ_0 is exchanged for ν_0, the equation is equivalent to the predictive equation from the affine network model (Eq. (3.9)). Here, we consider the process in which a cubic gel with side lengths of $L_0(=V_0{}^{1/3})$ is swollen (or shrunken) Q times to a given volume and then uniaxially stretched (Figure 4.1).

The entire elongation ratio in the stretching axis, λ_x, is given by the following:

$$\lambda_x = \alpha Q^{1/3} \tag{4.2}$$

Here, $\alpha_x = \alpha$ is the elongation ratio in the x direction of the swollen gel. Given that no volume change occurs during the stretching process ($\alpha_x\alpha_y\alpha_z = 1$), λ_y and λ_z can be represented as follows:

$$\lambda_y = \lambda_z = \alpha^{-1/2}Q^{1/3} \tag{4.3}$$

By substituting Eq. (4.1) into this equation, we obtain the following:

$$\Delta F = \frac{\xi_0 V_0 kT}{2}\{Q^{2/3}(\alpha^2 + 2\alpha^{-1}) - 3\} \tag{4.4}$$

The force f needed for stretching is obtained by differentiating ΔF by the length of the specimen after stretching, L_x.

$$\begin{aligned} f = \frac{\partial \Delta F}{\partial L_x} &= \frac{\partial\left[\frac{\xi_0 V_0 kT}{2}\{Q^{2/3}(\alpha^2 + 2\alpha^{-1}) - 3\}\right]}{\partial L_x} \\ &= \frac{\xi_0 V_0 kT}{2}\frac{\partial Q^{2/3}(\alpha^2 + 2\alpha^{-1})}{\partial(\alpha L_0 Q^{1/3})} = \frac{\xi_0 V_0 kTQ^{1/3}}{L_0}(\alpha - \alpha^{-2}) \end{aligned} \tag{4.5}$$

Here, Q was treated as constant because during stretching, the swelling degree (Q) is already set. Furthermore, given that the cross-sectional area after swelling

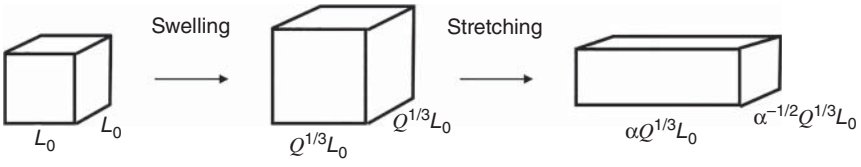

Figure 4.1 Swelling and subsequent stretching of a rectangular gel.

is ${L_0}^2Q^{2/3}$, the stress (σ) applied to the sample can be written as follows:

$$\sigma = \frac{f}{{L_0}^2Q^{2/3}} = \frac{\xi_0 kT}{2}Q^{-1/3}\frac{\partial(\alpha^2 + 2\alpha^{-1})}{\partial\alpha} = \xi_0 kTQ^{-1/3}(\alpha - \alpha^{-2}) \tag{4.6}$$

Thus, the elastic modulus of the swollen gel is represented by Eq. (4.7):

$$G = \xi_0 kTQ^{-1/3} = G_0Q^{-1/3} \tag{4.7}$$

Here, G_0 is the elastic modulus before the volume change. The elastic modulus after the volume change is in proportion to $Q^{-1/3}$ instead of Q. According to Eq. (4.7), even if the gel swells to twice its original volume, the elastic modulus is not halved but is reduced by a factor of approximately $2^{-1/3}$ ($\approx$0.8).

Let us continue with this expression a little more. Since the volume is doubled, the cycle rank is certainly halved. Considering that the cycle rank after deformation is ξ_0/Q, Eq. (4.7) can be transformed as follows:

$$G = \frac{\xi_0}{Q}(kTQ^{2/3}) \tag{4.8}$$

Given that kT is the contribution of an elastic element to the elastic modulus, it can be considered that the contribution per element is changed by a factor of $Q^{2/3}$ after the volume change. When Figure 4.1 is reviewed once again, the partial chain is uniaxially stretched by a factor of $Q^{1/3}$ by the swelling. Assuming that network strands are Gaussian chains, the energy of a network strand changes by a factor of $Q^{2/3}$ due to uniaxial stretching by a factor of $Q^{1/3}$. The change in the elastic modulus of $Q^{1/3}$ times can be obtained by considering that the contribution of each network strand changes by a factor of $Q^{2/3}$, and the concentration of the network strands is changed by a factor of Q^{-1}. Thus, if we can imagine both scaling rules, we can predict Eq. (4.7) by scaling. Using the polymer volume fractions before swelling (ϕ_0) and after (ϕ_m) and taking into account that $\xi_0 \sim \phi_0$, $Q \sim \phi_0/\phi_m$, Eq. (4.7) is transformed as follows:

$$G \sim \xi_0 Q^{-1/3} \sim \frac{\phi_0}{N}\left(\frac{\phi_0}{\phi_m}\right)^{-1/3} \sim N^{-1}{\phi_0}^{2/3}{\phi_m}^{1/3} \tag{4.9}$$

It has been experimentally confirmed that Eqs. (4.7) and (4.9) are applicable to various systems. However, as for the power law of approximately ϕ_m, powers more than 1/3 and close to 0.5 have been observed. In Section 4.1.2, we introduce a scaling approach that can explain the powers more than 1/3.

4.1.2 Scaling for Networks Consisting of Nonideal Chains

Panyukov proposed a scaling of the elastic energy for gels in swelling/deswelling as shown as follows [1]:

$$\frac{F_{el}}{kT} \sim \frac{G}{kT} \sim \frac{\phi_m}{N}\left(\frac{\lambda R_0}{R_{ref}}\right)^2 \tag{4.10}$$

Here, λ is the uniaxial elongation ratio due to the volume change, R_0 is the end-to-end distance of a network strand in the state of preparation, and R_{ref} is the reference length. Given that λ is proportional to the cube root of Q, and

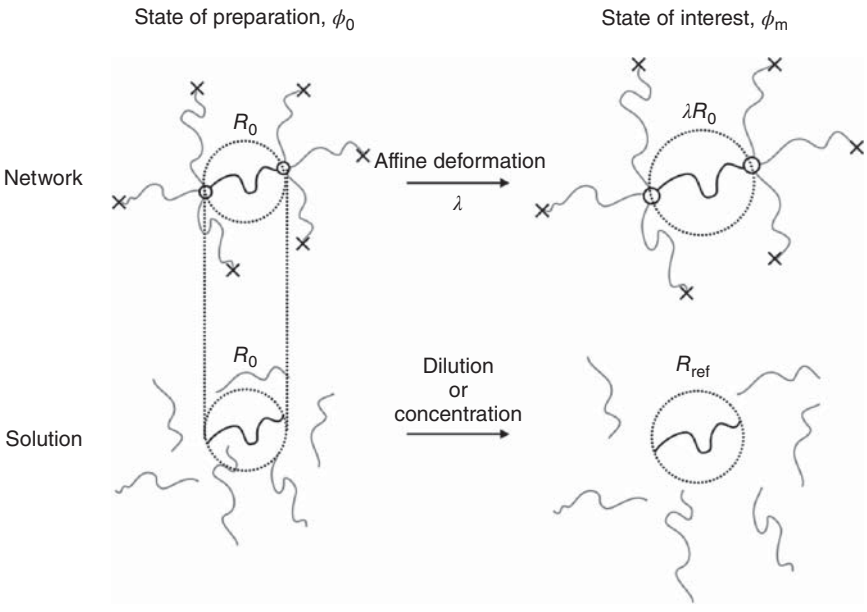

Figure 4.2 Deformation of a network and a chain during a change in concentration.

ϕ/N ($\sim\xi_0/Q$) is proportional to the number density of network strands after swelling/deswelling, Eq. (4.10) is almost the same shape as Eq. (4.8). The only difference is R_{ref} in the denominator. In Eq. (4.8), the equilibrium end-to-end distance of an ideal chain R_0 is implicitly adapted as the reference (R_{ref}); substituting $R_{ref} = R_0$ into Eq. (4.10) affords Eq. (4.9).

$$\frac{F_{el}}{kT} \sim \frac{G}{kT} \sim \frac{\phi_m}{N}\left(\frac{\lambda R_0}{R_0}\right)^2 \sim \frac{\phi_m}{N}\left(\frac{\phi_0}{\phi_m}\right)^{2/3} \sim N^{-1}{\phi_0}^{2/3}{\phi_m}^{1/3} \tag{4.11}$$

Notably here, $\lambda \sim (\phi_0/\phi_m)^{1/3}$. Thus, when we assume $R_{ref} = R_0$, Eq. (4.9) is not dependent on the characteristics of the polymer chain, which cannot explain some of the experimental results.

To explain these experimental results, Obukhov and Colby proposed a model in which R_{ref} is the equilibrium end-to-end distance of a polymer chain with a degree of polymerization N that exists in a solution with a polymer volume fraction of ϕ_m (Figure 4.2) [2]. By combining this concept with that in Eq. (4.10), nine different scaling relationships depending on polymer concentration in the states of preparation and interest can be predicted. There are three major concentration regions in the states of preparation and interest: (i) a dilute region, (ii) a semidilute region, and (iii) a concentrated region. Although it may seem complicated, the concept itself is simple. Let us learn from the fundamental idea.

In the state in which they were prepared, polymers in the solution connect with each other to form a network. The model assumes that the end-to-end distance of the polymer chain is not influenced by crosslinking and remains constant (Figure 4.2, left). Thus, R_0 is assumed to obey the expressions for the end-to-end distance of a polymer chain in solution discussed in Section 2.2.

$$R = aN^{\nu} \quad (\text{Dilute} : \phi < \phi^*) \tag{4.12}$$

$$R = aN^{\nu}\left(\frac{\phi}{\phi^*}\right)^{(2\nu-1)/2(1-3\nu)} \quad (\text{Semidilute} : \phi^* < \phi < \phi^{**}) \tag{4.13}$$

$$R = aN^{1/2} \quad (\text{Concentrated} : \phi^{**} < \phi) \tag{4.14}$$

Next, during the process of swelling/shrinking, it is assumed that the network strands are deformed in an affine manner with a change in volume (Q); polymer chains are deformed by $\lambda = Q^{1/3}$ toward an axis, and their end-to-end distances become λR_0. These results are the implication of the numerator in parenthesis in Eq. (4.10).

On the other hand, as mentioned earlier, R_{ref} is the equilibrium end-to-end distance of a polymer chain with a degree of polymerization N in a solution with a polymer volume fraction of ϕ_{m} (Figure 4.2). In other words, R_{ref} is the most stable end-to-end distance of a network strand at ϕ_{m}, excluding the effect of crosslinking. As a result, we also consider R_{ref} to follow Eqs. (4.12)–(4.14) in the same manner as R_0, and this is the basic framework of the Obukhov–Colby model. When we apply an equation to each set of conditions, we can predict the scaling relationship under each set of conditions.

Let us turn to an example: the case in which a gel is formed in a semidilute solution of polymer and swollen in the range of a semidilute region. Here, we assume real chains ($\nu = 3/5$) for simplicity, i.e. R_0 and R_{ref} can be written as follows:

$$R_0 = aN^{3/5}\left(\frac{\phi_0}{\phi^*}\right)^{-1/8} \tag{4.15}$$

$$R_{\mathrm{ref}} = aN^{3/5}\left(\frac{\phi_{\mathrm{m}}}{\phi^*}\right)^{-1/8} \tag{4.16}$$

By substituting these equations into Eq. (4.10), we obtain the following:

$$\begin{aligned}\frac{G}{kT} &\sim \frac{\phi_{\mathrm{m}}}{N}\left(\frac{\lambda R_0}{R_{\mathrm{ref}}}\right)^2 \sim \frac{\phi_{\mathrm{m}}}{N}\left(\frac{\lambda a N^{3/5}\left(\frac{\phi_0}{\phi^*}\right)^{-1/8}}{aN^{3/5}\left(\frac{\phi_{\mathrm{m}}}{\phi^*}\right)^{-1/8}}\right)^2 \\ &\sim \frac{\phi_{\mathrm{m}}}{N}\left(\frac{\phi_0}{\phi_{\mathrm{m}}}\right)^{2/3}\left(\frac{\phi_0}{\phi_{\mathrm{m}}}\right)^{-1/4} \sim N^{-1}{\phi_{\mathrm{m}}}^{7/12}{\phi_0}^{5/12}\end{aligned} \tag{4.17}$$

This equation predicts that the elastic modulus is proportional to ${\phi_{\mathrm{m}}}^{7/12}$ and that the power is approximately twice as large as that of Eq. (4.9). Next, let us consider the elastic modulus when the network is formed in the semidilute region and further swollen to the dilute region.

$$\begin{aligned}\frac{G}{kT} &\sim \frac{\phi_{\mathrm{m}}}{N}\left(\frac{\lambda R_0}{R_{\mathrm{ref}}}\right)^2 \sim \frac{\phi_{\mathrm{m}}}{N}\left(\frac{\lambda a N^{3/5}\left(\frac{\phi_0}{\phi^*}\right)^{-1/8}}{aN^{3/5}}\right)^2 \\ &\sim \frac{\phi_{\mathrm{m}}}{N}\left(\frac{\phi_0}{\phi_{\mathrm{m}}}\right)^{2/3}\left(\frac{\phi_0}{\phi^*}\right)^{-1/4} \sim N^{-1}{\phi_{\mathrm{m}}}^{1/3}{\phi_0}^{5/12}{\phi^*}^{1/4}\end{aligned} \tag{4.18}$$

In this process, the elastic modulus is expected to be proportional to $\phi_m{}^{1/3}$. When comparing Eqs. (4.17) and (4.18), the ϕ_m-dependence of the elastic modulus changes from 7/12 to 1/3. As a result, when a gel formed in a semidilute region is swollen to a dilute region, the elastic modulus is expected to show crossover at approximately ϕ^*. This crossover was experimentally observed; the power law changed in the vicinity of ϕ^* for the prepolymer [3]. Notably, the power law did not depend on whether the gel was swollen or shrunk. Essentially, the sign of the volume change does not matter; instead, what matters is if the polymer volume fraction is higher or lower than ϕ^*.

Finally, we note the limitation of this model. Equation (4.10), which is the cornerstone of this model, is correct for networks consisting of network strands following the Gaussian statistics. In the strictest sense, Hooke's law is not always correct for network strands that do not obey Gaussian statics. Let us restate here that it is difficult to describe the physical properties of general polymer gels even with scaling. In addition, according to Eq. (4.10), the end-to-end distance contracts in proportion to $\phi_m{}^{1/3}$. When the extent of contraction is too large, the end-to-end distance becomes too small compared with $aN^{1/2}$. However, such a situation is, of course, not observed in reality, and the result predicted by the scaling is not consistent with the experimental results. For this case, the more complicated situation introduced in the Section 4.1.3 must be considered.

Determining if the assumption that the prepolymers are captured into a polymer network while maintaining the end-to-end distance that they had in free solution always holds is worth considering. When we see processes forming gels from prepolymers, the previously mentioned assumption does not seem self-evident. At low concentrations, below ϕ^*, there is a possibility that the prepolymers are captured with a slightly stretched state simply by chance, and vice versa at high concentrations, above ϕ^*. On the other hand, when making a gel from monomers and crosslinkers, the polymer chains between the crosslinking points will likely form a network while maintaining R_0. Although we must pay attention to these limitations, according to the good agreement between the theoretical outcomes and experimental results, the concept itself that the elastic modulus of a polymer gel is strongly influenced by the two states, the states in which it was prepared and the state of interest, seems correct to some extent.

4.1.3 Scaling for Highly Deswollen Networks

The model introduced in the Section 4.1.2 can be applied to a wide concentration range, including the dilute, semidilute, and concentrated regions. However, as mentioned earlier, the model cannot reproduce the experimental results of highly deswollen polymer gels. Indeed, the experimental results in which the gel was formed in the dilute region and deswollen to the concentrated region were clearly different from the prediction of Eq. (4.10) [4–7]. This inconsistency is attributed to the fact that the degree of deformation is too large to be modeled with the same picture.

In the discussion earlier, the most stable end-to-end distance (R_{ref}) of a network strand contracts by $\phi^{-1/8}$ in the semidilute region and becomes a constant of $aN^{1/2}$ at concentrations above ϕ^{**}. On the other hand, the actual end-to-end distance of the network strand (the distance between the crosslinks)

affinely shrinks ($\sim\phi^{-1/3}$). Therefore, these two lengths deviate largely with strong deswelling above ϕ^{**}, and the end-to-end distance becomes considerably smaller than $aN^{1/2}$. Notably, decreasing the end-to-end distance does not significantly influence the conformation of the ideal chain. According to the discussion in Chapter 1, the energy needed to stretch the ideal chain to length R_0 is approximately kT, which does not strongly influence the conformation or the distribution of segments. Of course, this scheme is only applicable for moderate deswelling, and the distribution is influenced in the case of strong deswelling. Although the deswelling of a gel does not substantially change the conformation of the network segments, it does increase the density of crosslinks. Thus, a space occupied by a network strand is invaded by other crosslinks and other network strands during deswelling. As a result, network strands are expected to become substantially entangled with each other and form complicated structures. Notably, this interpenetrated structure is not trapped because it is solved by swelling. In addition, this interpenetrated structure can form in any gel if it is strongly deswollen. This type of interpenetrated structure is called a "supercoiled structure" (Figure 4.3).

Let us take a closer look at the supercoiled network in Figure 4.3. Two kinds of entanglements exist: trapped entanglements formed during gelation and pseudo-entanglements formed during deswelling. Related to these entanglements, the network strands can be virtually divided into two parts. One is the minimal path connecting the crosslinks on both ends; this path cannot pass through the preformed trapped entanglements. The other part is the subpart that penetrates into other crosslinks, which can be solved by pulling the strand. Rubinstein approached this problem based on this virtual division.

As is evident from Figure 4.3, the end-to-end distance of the supercoiled network strand is the same as that of the minimal path (primitive path). Here, assuming that there is no correlation between segments following the minimal path, the end-to-end distance of this path (R_{bb}) follows Gaussian statistics and R_{bb} can be predicted as follows:

$$R_{bb} \approx a{N_{bb}}^{1/2} \tag{4.19}$$

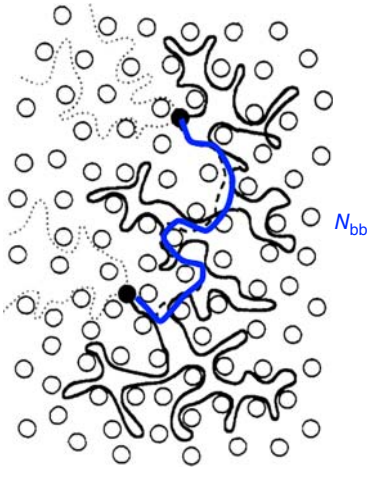

Figure 4.3 Schematic picture of a strongly deswollen network.

As the minimal chain has the same number density as the network strand, the virtual degree of polymerization (N_{bb}) and the volume fraction (ϕ_{bb}) of the minimal chain are written as follows:

$$\frac{\phi_{bb}}{N_{bb}} = \frac{\phi_m}{N} \tag{4.20}$$

Here, we assume that the supercoil occurs above the concentration at which the contribution of the entanglements to the elasticity dominates in the uncrosslinked polymer solution with polymerization degree N_{bb}. The degree of polymerization of a subchain between neighboring entanglements (N_e) in a polymer solution (ϕ_e) is represented as follows [8]:

$$\phi_e = \left(\frac{N_e}{N_{e,0}}\right)^{-\frac{1}{\alpha-1}} \tag{4.21}$$

Here, $N_{e,0}$ is the degree of polymerization of a subchain between neighboring entanglements in the polymer melt. This equation relates the concentration at which the contribution of entanglement becomes considerable (ϕ_e) and the molecular weight between neighboring entanglements (N_e). α is the exponent in the power law relationship between the rubbery plateau modulus of the entangled polymer solution and the polymer volume fraction ($\alpha = 7/3$ for a θ solvent and $\alpha = 9/4$ for a good solvent). According to this equation, one can estimate ϕ_e for a polymer chain with a degree of polymerization of N_1 by substituting N_1 into N_e. Conversely, one can estimate N_e for a polymer solution with a volume fraction of ϕ_1. Applying Eq. (4.21) to the primitive-path chain, the following equation relating N_{bb} and ϕ_{bb} is obtained:

$$\phi_{bb} = \left(\frac{N_{bb}}{N_e}\right)^{-\frac{1}{\alpha-1}} \tag{4.22}$$

We assume the use of the θ solvent in further discussions for simplicity. According to Eqs. (4.20) and (4.22), we obtain the following:

$$N_{bb} \cong {N_e}^{3/7}\left(\frac{\phi_m}{N}\right)^{-4/7} \tag{4.23}$$

Substitution of Eq. (4.23) into Eq. (4.19) gives Eq. (4.24):

$$R_{bb} \cong a{N_{bb}}^{1/2} \cong a{N_e}^{3/14}\left(\frac{\phi_m}{N}\right)^{-2/7} \tag{4.24}$$

Here, we define $\phi_{e\theta}$ as ϕ_e in θ solvent, use Eq. (4.21) for N_e, and substitute these variables into Eq. (4.23).

$$R_{bb} \cong aN^{1/2}\left(\frac{\phi_m}{{\phi_e}^{\theta}}\right)^{-2/7} \tag{4.25}$$

This equation can be used to determine R_{bb}, which is the most stable end-to-end distance of the supercoiled polymer network structure (R_{ref}).

$$R_{ref} \cong aN^{1/2}\left(\frac{\phi_m}{{\phi_e}^{\theta}}\right)^{-2/7} \tag{4.26}$$

Given that $R = aN^{1/2}$ in a conventional concentrated polymer solution, the most stable structure of the supercoiled network strand is $(\phi_m/\phi_e{}^{\theta})^{-2/7}$-times smaller than that of the polymer chain in a concentrated solution. By substituting Eq. (4.26) into Eq. (4.10), the elastic modulus of a supercoiled network is obtained.

$$\frac{G}{kT} \cong \frac{\phi}{Nb^3}\left(\frac{\phi_m}{\phi_0}\right)^{-2/3}\left(\frac{\phi_m}{\phi_e{}^{\theta}}\right)^{4/7} \sim \phi_m{}^{19/21} \tag{4.27}$$

This equation shows that the elastic modulus is proportional to $\phi_m{}^{19/21}$. Several experiments have roughly shown $G \sim \phi_m{}^{1}$, supporting the validity of this model [7]. Notably, when one simply substitutes the prediction in a concentrated region ($R_{ref} = aN^{1/2}$) to Eq. (4.10), one obtains $G \sim \phi_m{}^{1/3}$, which is completely different from experimental results. These results strongly suggest that when a network is formed in a diluted state and then strongly deswollen, a complicated structure, as discussed here, is formed.

4.2 Equilibrium Swelling

In the Section 4.1, the changes in the elastic modulus due to swelling/deswelling were discussed. Generally, when a gel in its as-prepared state is immersed in a good solvent, the gel swells because the polymer constituting the gel is miscible in the solvent and osmotic pressure is generated. If no polymer exists in the solution outside the gel, osmotic pressure occurs due to the difference in the polymer concentrations inside and outside the gel. To reduce the difference in osmotic pressure, the polymers want to elute into the outer solution; however, the polymers cannot freely elute because they are crosslinked into a network structure. As a result, instead of eluting out of the gel, the gel swells by drawing in the solvent. Swelling also decreases the elastic pressure (corresponding to the elastic modulus of the swollen gel). Although both pressures decrease with swelling, the decrease in osmotic pressure is larger than that of elastic pressure. Thus, after a certain degree of swelling, these pressures become balanced, and an equilibrium swollen state is achieved. Because the osmotic pressure is typically greater than the elastic pressure in the initial state, the gel swells. This idea has been proposed by Flory, and the conditions for equilibrium swelling can be written as follows [9]:

$$\left(\frac{\partial F_{el}}{\partial n_B}\right)_{n_A} + \left(\frac{\partial F_{mix}}{\partial n_B}\right)_{n_A} = 0 \tag{4.28}$$

Here, F_{el} and F_{mix} are the free energies of elasticity and mixing, respectively, and n_A and n_B are the number of moles of the polymer and the solvent, respectively. The criterion for equilibrium swelling is that the change in total free energy is 0 during swelling/deswelling; in other words, the change in total free energy is 0 and the number of macromolecules in the gel does not change, and only the number of solvent molecules changes.

4.2.1 Scaling Prediction of the Equilibrium Swelling

Here, we introduce a scaling prediction for the equilibrium swelling. We utilize Eq. (4.10) to determine F_{el} and Eq. (2.62) to determine F_{mix}. In scaling theory, because both F_{el} and F_{mix} are power law functions of ϕ, differentiation with respect to ϕ only divides each term by ϕ in the scaling relationship. Thus, we need to consider the following equation:

$$\frac{\frac{\phi_e}{N}\left(\frac{\lambda R_0}{R_{ref}}\right)^2}{\phi_e} \sim \frac{\phi_e^{\frac{3\nu}{3\nu-1}}}{\phi_e} \tag{4.29}$$

Here, ϕ_e is the polymer volume fraction in the equilibrium swollen state. What we want to know is the elastic modulus (G_e) in the equilibrium swelling state, which varies depending on the concentration range of the as-prepared and equilibrium swollen states, as discussed in the Section 4.1.2. As an example, let us consider a case in which a gel is made in a semidilute region ($\phi^* < \phi_0$) and swollen to a dilute region. By substituting Eqs. (4.13) and (4.12) for R_0 and R_{ref}, respectively, the following scalings are obtained for ϕ_e and G_e:

$$\phi_e \sim G_0^{\frac{9\nu-3}{6\nu+1}} \phi_0^{\frac{1-3\nu}{6\nu+1}} \tag{4.30}$$

$$G_e \sim G_0^{\frac{9\nu}{6\nu+1}} \phi_0^{\frac{-3\nu}{6\nu+1}} \tag{4.31}$$

Based on Eqs. (4.30) and (4.31), a relationship between ϕ_e and G_e is obtained:

$$G_e \sim \phi_e^{\frac{3\nu}{3\nu-1}} \tag{4.32}$$

Notably, the right side of Eq. (4.32) is equivalent to the osmotic pressure (Eq. (2.63)). Given that the left side of Eq. (4.29) was originally G_e/ϕ_e, Eq. (4.32) is directly obtained from Eq. (4.29). In other words, applying the scaling for a semidilute regime to the osmotic pressure of gels gives Eq. (4.29) a priori. Although the agreement between the experimental results and those predicted by Eq. (4.29) is often used as evidence supporting the validity of the c^* theorem proposed by de Gennes, the agreement is not correct. Instead, this agreement only suggests that the osmotic pressure of the gel is described by that of the semidilute solution.

This equation is practically important because we can estimate the important parameter ν through the following process. One can prepare a series of gels with different initial concentrations or different elastic moduli and measure their elastic moduli in their equilibrium swelling states. By plotting ϕ_e and G_e, one can estimate ν based on Eq. (4.32). Figure 4.4 shows the results of Tetra-PEG gels with different molecular weights and initial concentrations of network strands [3]. The data from the gels prepared under various conditions are on a master curve. ν was estimated from the power to be 0.56, which was close to that of a real chain. The estimated ν explained the other physical properties well, and similar results were obtained in other systems [3, 10–13], supporting the validity and usefulness of this methodology.

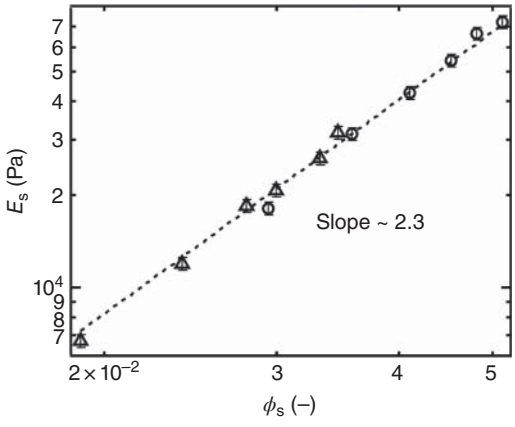

Figure 4.4 Scaling relationship between the elastic modulus (E_s) and polymer volume fraction in the equilibrium swollen state (ϕ_s).

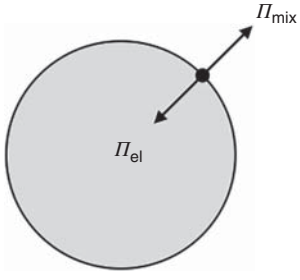

Figure 4.5 Two pressures were generated on an electrically neutral gel in a solvent: osmotic pressure (Π_{mix}) and elastic pressure (Π_{el}).

4.2.2 Statistical Mechanics of Equilibrium Swelling

Here, we consider the pressure applied to the surface of a hydrogel. In the equilibrium swollen state, these pressures should be balanced with each other. Considering an electrically neutral gel in an appropriate solvent, there are two pressures: the osmotic pressure (Π_{mix}) resulting from the difference in the polymer concentrations inside and outside of the gel and the elastic pressure due to the deformation of the polymer network (Π_{el}). Note that Π_{mix} and Π_{el} generally have opposite signs, as shown in Figure 4.5. Therefore, the conditions for equilibrium swelling are expressed as follows:

$$\Pi = \Pi_{mix} + \Pi_{el} = 0 \tag{4.33}$$

According to Chapter 2, Π_{mix} is given using ΔF_{mix} as follows:

$$\Pi_{mix} = -\frac{N_A}{V_1}\left(\frac{\partial \Delta F_{mix}}{\partial n_B}\right)_{n_A} \tag{4.34}$$

Here, N_A is Avogadro's constant, V_1 is the molar volume of the solvent, and thus N_A/V_1 is the number of solvent molecules in a unit volume. ΔF_{mix} of the gel has the following form:

$$\Delta F_{mix} = nkT[(1-\phi)\ln(1-\phi) + \chi\phi(1-\phi)] \tag{4.35}$$

The difference between Eq. (4.35) and that of the polymer solution (Eq. (2.42)) is the absence of the term ϕ/N, which is due to the extremely large N of polymer gels

($N \approx \infty$). Solving Eq. (4.34) through a process similar to that used for Eq. (2.42), Π_{mix} can be represented as follows:

$$\Pi_{\mathrm{mix}} = -\frac{N_{\mathrm{A}}kT}{V_1}(\phi + \ln(1-\phi) + \chi\phi^2) \tag{4.36}$$

Next, we consider Π_{el} to be defined as follows:

$$\Pi_{\mathrm{el}} = -\frac{N_{\mathrm{A}}}{V_1}\left(\frac{\partial \Delta F_{\mathrm{el}}}{\partial n_{\mathrm{B}}}\right)_{n_{\mathrm{A}}} \tag{4.37}$$

This equation is similar to that of Π_{mix} (Eq. (4.34)) and represents the change in the elastic energy when the number of solvent molecules increases while the number of network strands in the gel remains constant. Assuming that the network strands are ideal chains and follow the affine network model, ΔF_{el} is represented as the following:

$$\Delta F_{\mathrm{el}} = \frac{\nu_0 V_0 kT}{2}(\lambda_x{}^2 + \lambda_y{}^2 + \lambda_z{}^2 - 3 - \ln(\lambda_x\lambda_y\lambda_z)) \tag{4.38}$$

Compared with Eq. (3.9), one notices that the term $\ln(\lambda_x\lambda_y\lambda_z)$ has appeared. The origin of this term is the change in entropy when arranging network strands in the network, which was proposed by Flory [9]. Notably, this term does not influence the discussion in Chapter 3 because we only consider the isovolumetric transformation ($\lambda_x\lambda_y\lambda_z = 1$), i.e. $\ln(\lambda_x\lambda_y\lambda_z) = 0$. Notably, in the phantom network model, the term $\ln(\lambda_x\lambda_y\lambda_z)$ does not exist because the crosslinks fluctuate, and arranging the network strands is apparently unnecessary. Given that the swelling is isotropic, the following condition is applied to Eq. (4.38):

$$\lambda_x = \lambda_y = \lambda_z = \lambda = Q^{1/3} = \left(\frac{V}{V_0}\right)^{1/3} \tag{4.39}$$

Here, V_0 is the initial volume of the gel.

$$\Delta F_{\mathrm{el}} = \frac{3\nu_0 V_0 kT}{2}(\lambda^2 - 1 - \ln\ \lambda) \tag{4.40}$$

The differentiation affords the following:

$$\left(\frac{\partial \Delta F_{\mathrm{el}}}{\partial n_{\mathrm{B}}}\right)_{n_{\mathrm{A}}} = \left(\frac{\partial \Delta F_{\mathrm{el}}}{\partial \lambda}\right)_{n_{\mathrm{A}}}\left(\frac{\partial \lambda}{\partial n_{\mathrm{B}}}\right)_{n_{\mathrm{A}}} = \frac{3\nu_0 V_0 kT}{2}(2\lambda - \lambda^{-1})\left(\frac{\partial \lambda}{\partial n_{\mathrm{B}}}\right)_{n_{\mathrm{A}}} \tag{4.41}$$

To calculate $\partial\lambda/\partial n_{\mathrm{B}}$, the following relationship is used:

$$\lambda^3 = \frac{V}{V_0} = \frac{V_0 + n_{\mathrm{B}}V_1}{V_0} \tag{4.42}$$

By differentiating Eq. (4.42) by n_{B}, one obtains the following:

$$3\lambda^2\left(\frac{\partial \lambda}{\partial n_{\mathrm{B}}}\right)_{n_{\mathrm{A}}} = \frac{V_1}{V_0} \tag{4.43}$$

Substituting this equation into Eq. (4.41), the following equation is obtained:

$$\left(\frac{\partial \Delta F_{\mathrm{el}}}{\partial n_{\mathrm{B}}}\right)_{n_{\mathrm{A}}} = \nu_0 V_1 kT\left(\lambda^{-1} - \frac{1}{2}\lambda^{-3}\right) \tag{4.44}$$

Thus, Π_{el} is represented by Eq. (4.45):

$$\Pi_{el} = \nu_0 N_A kT \left(\frac{1}{2}\lambda^{-3} - \lambda^{-1}\right) = \nu_0 N_A kT \left(\frac{1}{2}\left(\frac{\phi}{\phi_0}\right) - \left(\frac{\phi}{\phi_0}\right)^{1/3}\right) \quad (4.45)$$

Here, the following relationship was used:

$$\lambda = \left(\frac{V}{V_0}\right)^{1/3} = \left(\frac{\phi_0}{\phi}\right)^{1/3} \quad (4.46)$$

Finally, by combining Eqs. (4.33), (4.36) and (4.45) with $\phi = \phi_e$, the conditions for equilibrium swelling can be represented as follows:

$$\begin{aligned} \Pi &= -\frac{N_A kT}{V_1}(\phi_e + \ln(1-\phi_e) + \chi\phi_e{}^2) \\ &\quad + \nu_0 N_A kT \left(\frac{1}{2}\left(\frac{\phi_e}{\phi_0}\right) - \left(\frac{\phi_e}{\phi_0}\right)^{1/3}\right) = 0 \\ \nu_0 &= \frac{\phi_e + \ln(1-\phi_e) + \chi\phi_e{}^2}{V_1\left(\frac{1}{2}\left(\frac{\phi_e}{\phi_0}\right) - \left(\frac{\phi_e}{\phi_0}\right)^{1/3}\right)} \end{aligned} \quad (4.47)$$

Based on the phantom network model, we obtain the following:

$$\xi_0 = -\frac{\phi_e + \ln(1-\phi_e) + \chi\phi_e{}^2}{V_1\left(\frac{\phi_e}{\phi_0}\right)^{1/3}} \quad (4.48)$$

Note that the second term in the denominator of Eq. (4.47) does not exist in Eq. (4.48), which reflects the absence of an entropic term due to the arrangement of the network strands ($\ln(\lambda_x\lambda_y\lambda_z)$). Although the Flory–Rehner model is popular, it is difficult to intuitively understand from the formula. To understand this model visually, Π_{mix} and $-\Pi_{el}$ are plotted against Q in Figure 4.6. The intersections in this graph are points where $\Pi_{mix} + (-\Pi_{el}) = 0$, indicating equilibrium swelling states. Here, we show two Π_{mix} values with different χ and four Π_{el} values with different elastic moduli based on different models. For each combination of Π_{mix} and $-\Pi_{el}$, we only find a single intersection. These results indicate that according to Eq. (4.47), only one unique equilibrium swelling state can be achieved from these initial conditions. As the values of χ or G_0 decrease, the intersection moves to larger values of Q, suggesting large swelling. This result is consistent with the intuitive understanding that soft gels and gels in good solvents swell substantially. It is also interesting that Π_{el} does not increase but decreases with swelling ($Q > 1$) because the stretching of the network strands due to swelling (positive effect) and the reduction of network strand density due to swelling (negative effect) cancel each other out. On the other hand, Π_{mix} decreases monotonically with decreasing ϕ, resulting in a balance between Π_{mix} and $-\Pi_{el}$. Notably, although Π_{el} behaves quite differently in the affine and phantom network models, the difference does not significantly influence the equilibrium swelling ratio (Q_e). As these models may be oversimplified, it is not essential to discuss the validity of each model here. A qualitative discussion is possible in the region where Q_e is small because the values of Π_{el} predicted by the two models are substantially different.

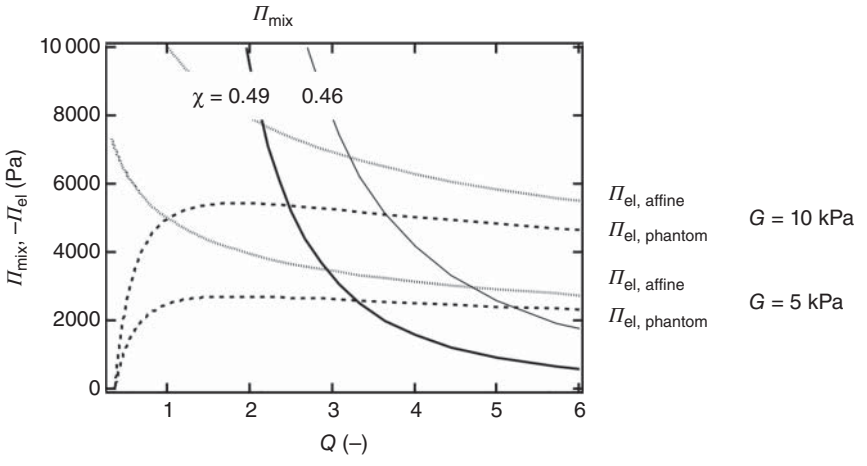

Figure 4.6 Π_{mix} and $-\Pi_{el}$ as a function of Q ($\phi_0 = 0.1$, $V_1 = 1.8 \times 10^{-5}$ m^3/mol). Each crosspoint indicates equilibrium conditions.

As described earlier, there are some pitfalls in the practical operation of Eq. (4.47). This equation has reproduced various experimental results to some extent. On the other hand, the parameter χ, which should be determined for each combination of polymer and solvent, depends on the degree of polymerization of the network strands, the number of branches, and even the initial polymer concentration [14–17]. Equation (4.47) is derived under the assumption that the free energy and elastic energy of mixing are represented by Eqs. (4.35) and (4.40), respectively. Therefore, all the deviations of the real system from the assumption are considered in parameter χ. Therefore, it is not essential to estimate the number density of network strands from χ and Q_e based on Eq. (4.47); it is more direct and accurate to measure the elastic modulus by mechanical measurements and estimate the number density of the network strands. One example of a promising use of the Flory–Rehner equation is to estimate a change in an elastic modulus over time from the degree of swelling. We can estimate χ from the initial values of G and Q_e and set χ as a fixed parameter during the swelling caused by degradation [18, 19]. We discuss the application of the Flory–Rehner model to predict the degradation behavior in Chapters 4 and 16.

Notably, Eqs. (4.47) or (4.48) cannot reproduce the volume phase transition; there is always only one intersection of Π_{mix} and $-\Pi_{el}$ (Figure 4.6), and the coexistence of the two phases is not reproduced. To reproduce the volume phase transition, we need to introduce a concentration-dependent χ term or the osmotic pressure of fixed ions. Finally, we compare Eq. (4.47) with the conventional Flory–Rehner model written in a general polymers textbook.

$$\nu_{dry} = \frac{\phi_e + \ln(1-\phi_e) + \chi\phi_e^{\,2}}{V_1\left(\frac{1}{2}\phi_e - \phi_e^{\,1/3}\right)} \tag{4.49}$$

The major differences are that the left side is clearly from the dry material and that ϕ_0 has disappeared from the denominator. This difference is caused by the conditions considered by Eqs. (4.47) and (4.49), i.e. whether the initial state is a

melt ($\phi_0 = 1$) or contains a solvent ($\phi_0 < 1$). The reason for the subscript "dry" is that the conventional expression focuses only on elastomers, which do not contain solvent. The difference in the denominator is simply caused by the difference in the initial conditions. Because the denominator expresses the change in elastic energy due to deformation, the displacement by swelling ($Q_e = \phi_0/\phi_e$) is a key term. Indeed, by setting $\phi_0 = 1$, Eq. (4.47) is reduced to Eq. (4.49); thus, Eq. (4.49) is simply a special case of Eq. (4.47) ($\phi_0 = 1$).

4.3 Volume Phase Transition

4.3.1 Electrically Neutral Gels

Some kinds of polymer gels undergo discontinuous volume changes when the solvent quality is slightly changed. This phenomenon was first observed by Tanaka and was named the volume phase transition phenomenon [20]. For example, during heating, hydrogels made from poly(*N*-isopropylacrylamide) (PNIPAAm) shrink discontinuously at approximately 32 °C (Figure 4.7). How can we predict this volume phase transition phenomenon?

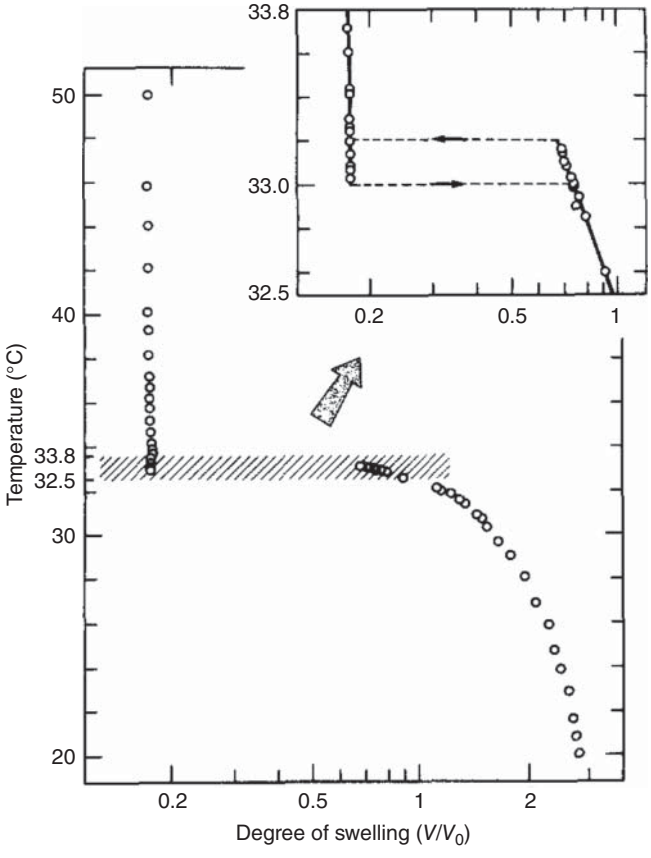

Figure 4.7 Temperature-dependence of volume of a PNIPAAm hydrogel [21].

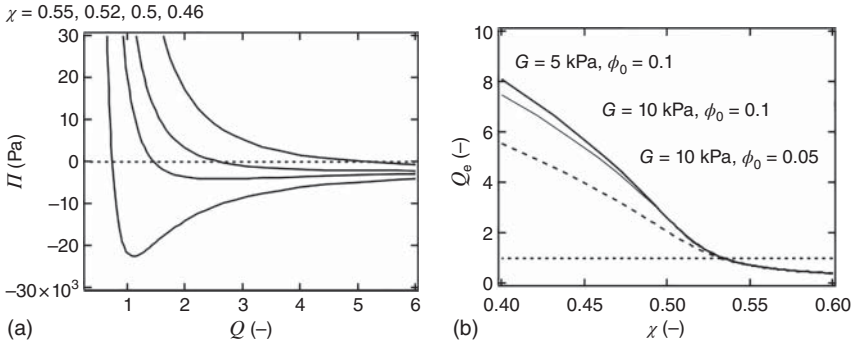

Figure 4.8 (a) Q-Dependence of Π and (b) χ-dependence of Q_e.

In Section 4.2, we learned that polymer gels swell in good solvents and shrink in poor solvents. Figure 4.8a shows the dependency of Π $(=\Pi_{mix} + \Pi_{el})$ when χ changes (given by Eq. (4.47)). Unlike Section 4.2, since Π is plotted directly, the intersection with $\Pi = 0$ indicates the equilibrium swelling (Q_e). As χ increases, Q_e gradually decreases, and when $Q_e < 1$ in a region where χ is sufficiently high, the gel shrinks. By solving Eq. (4.47) for χ, we can quantitatively predict the effect of χ on Q_e. Figure 4.8b shows the relationships of Q_e and χ when G and ϕ_0 are changed. No discontinuous change, as shown in Figure 4.7, is reproduced, and Q_e is always continuous with changing χ. That is, the changes predicted by Eq. (4.47) are continuous, and the discontinuous phase transition cannot be reproduced.

The simplest way to reproduce the volume phase transition is to introduce the ϕ-dependence of χ as follows:

$$\chi = \chi_1(T) + \chi_2\phi \tag{4.50}$$

This type of dependence is not unrealistic and has been confirmed in some polymers, including PNIPAAm [22]. The ϕ-dependent χ completely differentiates the Q-dependence of Π, which has both a local minimum and maximum (Figure 4.9).

As shown in Figure 4.9, as χ_1 increases, the number of points where $\Pi = 0$ changes from 1 ($\chi_1 = 0.46$) to 3 ($\chi_1 = 0.475$) to 1 ($\chi_1 = 0.49$) again. When the number of points where $\Pi = 0$ is 1, only one stable state exists. On the other

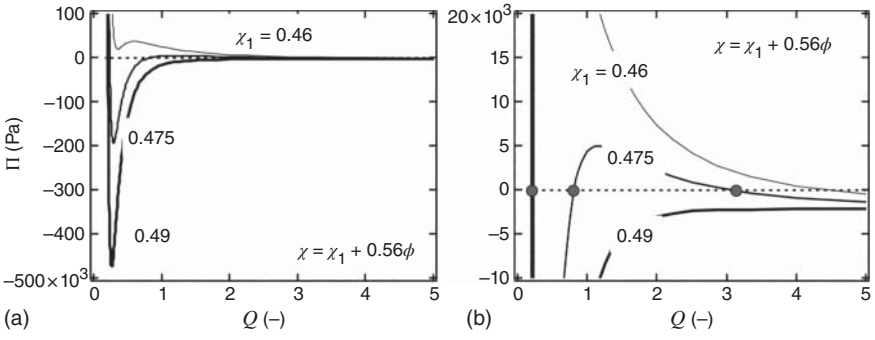

Figure 4.9 Q-Dependence of Π at various values of χ_1 and a fixed χ_2 of 0.56. Panel (b) is an enlarged view of (a).

hand, when there are three such points, three sets of equilibrium conditions seem to exist. However, not all three sets of conditions are stable.

The bulk modulus (K), which is defined in Eq. (4.51), indicates the stability of the system:

$$K = \phi\left(\frac{\partial \Pi}{\partial \phi}\right)_T \tag{4.51}$$

K indicates the pressure needed to change the volume of the gel by squeezing out the solvent. When $K < 0$, the gel spontaneously shrinks and is not stable. Thus, the condition $K > 0$ must be met for the material to exist as a solid. To investigate the Q-dependence of K, we first calculate the following partial differential:

$$\frac{\partial Q}{\partial \phi} = \frac{\partial\left(\frac{\phi_0}{\phi}\right)}{\partial \phi} = -\phi_0 \phi^{-2} \tag{4.52}$$

Substituting Eq. (4.52) to Eq. (4.51) gives the following:

$$K = \phi\left(\frac{\partial \Pi}{\partial \phi}\right)_T = \phi\left(\frac{\partial \Pi}{\partial Q}\right)_T \left(\frac{\partial Q}{\partial \phi}\right)_T = -\phi_0 \phi^{-1}\left(\frac{\partial \Pi}{\partial Q}\right)_T \tag{4.53}$$

Given that $\phi_0 \phi > 0$, the region where the slope of the $\Pi - Q$ relationship is positive is unstable (see Figure 4.9). Thus, only the two points on the end points are stable, and the middle region is unstable. In the unstable region, the gel is not stable, and phase separation spontaneously occurs (spinodal decomposition).

Figure 4.10 shows the dependence of the equilibrium swelling ratio (Q_e) on χ_1. The solid line is obtained by substituting Eq. (4.50) into Eq. (4.47), and the spinodal region is obtained from the condition $\partial \Pi / \partial \phi < 0$. As a result, decreasing the solvent quality induces a discontinuous volume change at approximately $\chi_1 = 0.48$, while increasing the solvent quality induces a discontinuous volume changes at approximately $\chi_1 = 0.46$, which shows hysteresis behavior. We can observe a slight hysteresis in the case of the PNIPAAm hydrogel shown in Figure 4.7. Because the solvent quality decreases with increasing temperature in many systems, the $Q_e - T$ graph is similar to the graph shown in Figure 4.10 [21].

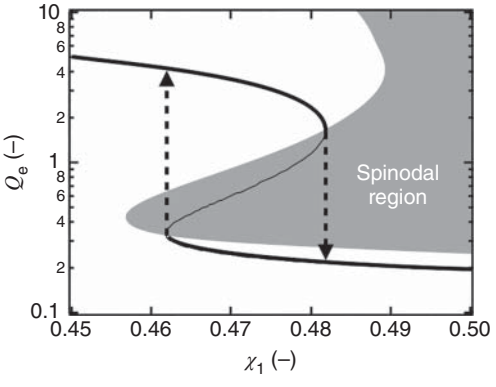

Figure 4.10 χ_1-Dependence of the equilibrium swelling ratio (Q_e).

4.3.2 Electrically Charged Gels

Although we discussed the volume phase transition of neutral gels in Section 4.3.1, few neutral gels show volume phase transitions. On the other hand, volume phase transitions are common in electrically charged gels. Indeed, volume phase transitions were first observed in a partially hydrolyzed acrylamide gel [20]. When the density of the fixed charge is relatively low, the electrostatic repulsive force between the fixed charges is negligible, and the osmotic pressure based on the Donnan effect is dominant. By considering this effect, the volume phase transition can be theoretically predicted, even if χ is not dependent on ϕ.

When the gel has a fixed charge, the same amount of oppositely charged counterions penetrate into the gel to maintain the electrical neutrality of the gel phase. As a result, the ion concentration in the gel is greater than that of the external solution by the concentration of fixed charges. This effect is called the Donnan effect. Assuming that there are f fixed charges per network strand, the osmotic pressure derived from the counterions (Π_{ion}) is by the following:

$$\Pi_{\text{ion}} = \nu_0 \frac{\phi}{\phi_0} fkT \tag{4.54}$$

Thus, the total pressure of charged gels is given by Eq. (4.55):

$$\begin{aligned}\Pi &= \Pi_{\text{mix}} + \Pi_{\text{el}} + \Pi_{\text{ion}} \\ &= kT\left[-\frac{1}{V_1}(\phi + \ln(1-\phi) + \chi\phi^2) + \nu_0\left\{\left(f+\frac{1}{2}\right)\left(\frac{\phi}{\phi_0}\right) - \left(\frac{\phi}{\phi_0}\right)^{1/3}\right\}\right]\end{aligned} \tag{4.55}$$

This pressure value includes all the pressures generated in the polymer gel and is called the equation of state for polymer gels [23].

Figure 4.11 shows the contribution of each pressure as a function of ϕ (other parameters are set in the range of conventional gels). Π_{el} has a relatively smaller influence on the total pressure than do Π_{mix} and Π_{ion}. Notably, the impact of Π_{ion} is quite large even if only a few ions are present per network strand ($f = 5$, 10 in Figure 4.11).

Figure 4.12 shows the conditions where the volume phase transition occurs. The osmotic pressure only greatly increases when several fixed charges are added

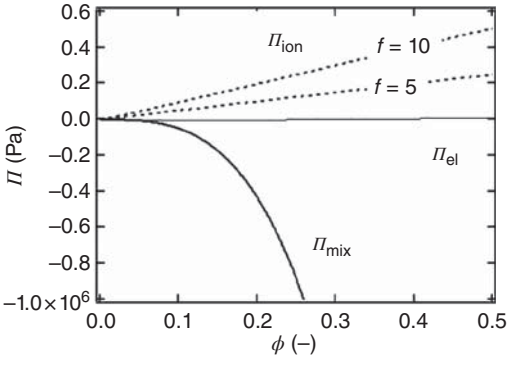

Figure 4.11 ϕ-Dependence of Π_{mix}, Π_{ion}, and Π_{el} ($\chi = 0.5$, $\phi_0 = 0.05$, and $G = 10\,000$ Pa).

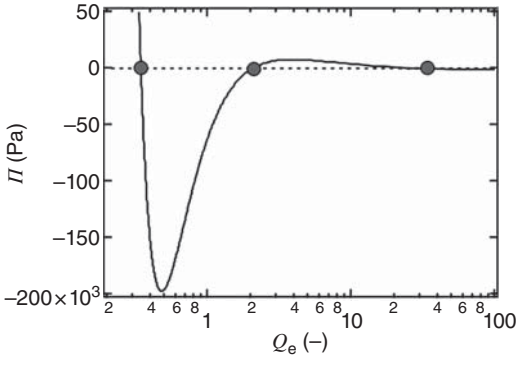

Figure 4.12 Q-Dependence of Π under conditions where a phase separation occurs ($f = 10$, $\phi_0 = 0.05$, $\chi = 0.65$, and $G = 10\,000$ Pa).

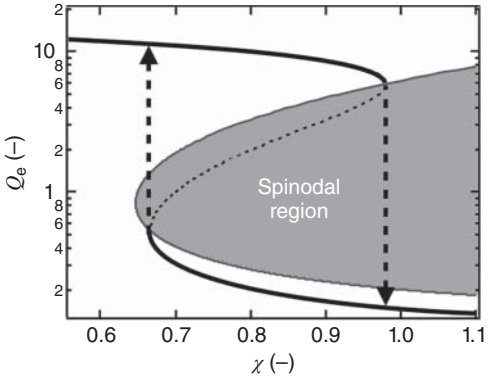

Figure 4.13 χ-Dependence of Q_e for an electrically charged gel ($\phi_0 = 0.1$ and $f = 5$).

per network strand, and this generates three apparent stable points ($\Pi = 0$). Similar to the case of a neutral gel, the intersection in the middle is unstable, and the volume phase transition occurs between the stable points at each end. Figure 4.13 shows the volume phase transition behavior of a charged gel ($\phi_0 = 0.1$ and $f = 3$). The volume of the swollen phase is considerably larger than that in the case of a neutral gel, suggesting that the osmotic pressure generated by the counterion concentration is large. Again, note that this large swelling is not caused by repulsion between charges fixed in the network but by the effect of the counterion. Due to their high swellability, charged gels have been used practically as water-absorbing materials for disposable diapers and water retaining agents for soils.

4.4 Swelling/Shrinking Kinetics

In Sections 4.2 and 4.3, we learned that gels swell or shrink depending on solvent quality. The next consideration is how fast the gel swells or shrinks. To solve this problem, the gel must be considered as a continuum, and the equation of motion can be solved [24]. First, let us consider the displacement vector $\mathbf{u}(\mathbf{r})$ when the three-dimensional elastic body undergoes an arbitrary deformation.

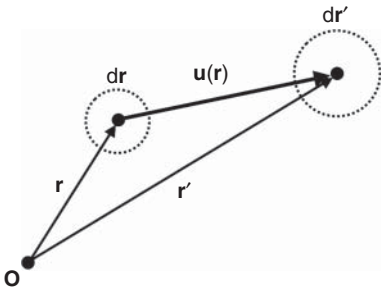

Figure 4.14 Deformation of a point from **r** to **r′**.

The displacement vector defines the displacement between a point (**r**) and the other point (**r′**) (Figure 4.14).

$$\mathbf{r}' = \mathbf{r} + \mathbf{u}(\mathbf{r}) \tag{4.56}$$

The displacement of a point at **r** (d**r**) is given in Eq. (4.57):

$$\mathbf{r}' + \mathrm{d}\mathbf{r}' = \mathbf{r} + \mathrm{d}\mathbf{r} + \mathbf{u}(\mathbf{r} + \mathrm{d}\mathbf{r}) \tag{4.57}$$

By substituting Eq. (4.56) into Eq. (4.47), one can obtain the following:

$$\mathrm{d}\mathbf{r}' = \mathrm{d}\mathbf{r} + \mathbf{u}(\mathbf{r} + \mathrm{d}\mathbf{r}) - \mathbf{u}(\mathbf{r}) \tag{4.58}$$

Here, we define **r** and **u** as follows:

$$\mathbf{r} = \begin{pmatrix} x_1 \\ x_2 \\ x_3 \end{pmatrix}, \quad \mathbf{u} = \begin{pmatrix} u_1 \\ u_2 \\ u_3 \end{pmatrix} \tag{4.59}$$

$$\begin{aligned} \mathrm{d}\mathbf{r}' &= \mathrm{d}\mathbf{r} + \begin{pmatrix} \dfrac{\partial u_1}{\partial x_1}\mathrm{d}x_1 + \dfrac{\partial u_1}{\partial x_2}\mathrm{d}x_2 + \dfrac{\partial u_1}{\partial x_3}\mathrm{d}x_3 \\ \dfrac{\partial u_2}{\partial x_1}\mathrm{d}x_1 + \dfrac{\partial u_2}{\partial x_2}\mathrm{d}x_2 + \dfrac{\partial u_2}{\partial x_3}\mathrm{d}x_3 \\ \dfrac{\partial u_3}{\partial x_1}\mathrm{d}x_1 + \dfrac{\partial u_3}{\partial x_2}\mathrm{d}x_2 + \dfrac{\partial u_3}{\partial x_3}\mathrm{d}x_3 \end{pmatrix} \\ &= \mathrm{d}\mathbf{r} + \begin{pmatrix} \dfrac{\partial u_1}{\partial x_1} & \dfrac{\partial u_1}{\partial x_2} & \dfrac{\partial u_1}{\partial x_3} \\ \dfrac{\partial u_2}{\partial x_1} & \dfrac{\partial u_2}{\partial x_2} & \dfrac{\partial u_2}{\partial x_3} \\ \dfrac{\partial u_3}{\partial x_1} & \dfrac{\partial u_3}{\partial x_2} & \dfrac{\partial u_3}{\partial x_3} \end{pmatrix} \begin{pmatrix} \mathrm{d}x_1 \\ \mathrm{d}x_2 \\ \mathrm{d}x_3 \end{pmatrix} \\ &= \mathrm{d}\mathbf{r} + \tilde{\mathbf{u}} \cdot \begin{pmatrix} \mathrm{d}x_1 \\ \mathrm{d}x_2 \\ \mathrm{d}x_3 \end{pmatrix} \end{aligned} \tag{4.60}$$

Because the distance between two points changes from d**r** to d**r′**, the second term in the right hand of Eq. (4.60) clearly indicates the strain.

The tensor $\tilde{\mathbf{u}}$ indicates the strain of the continuum and is called the relative deformation tensor. Any deformation described by $\tilde{\mathbf{u}}$ consists of contributions

from isotropic volumetric deformation ($\tilde{\mathbf{u}}_{\mathrm{vol}}$), isovolumetric deformation ($\tilde{\mathbf{u}}_{\mathrm{eq}}$), and rotation ($\tilde{\mathbf{u}}_{\mathrm{rot}}$). Because rotation is not a deformation, the pure deformation is represented by $\tilde{\mathbf{u}}_{\mathrm{def}}$.

$$\tilde{\mathbf{u}}_{\mathrm{def}} = \tilde{\mathbf{u}} - \tilde{\mathbf{u}}_{\mathrm{rot}} = \tilde{\mathbf{u}}_{\mathrm{vol}} + \tilde{\mathbf{u}}_{\mathrm{eq}} \tag{4.61}$$

Each tensor is represented as follows:

$$\tilde{\mathbf{u}}_{\mathrm{def}} = \begin{pmatrix} u_{11} & u_{12} & u_{13} \\ u_{21} & u_{22} & u_{23} \\ u_{31} & u_{32} & u_{33} \end{pmatrix} \quad \text{with } u_{ik} = \frac{1}{2}\left(\frac{\partial u_k}{\partial x_i} + \frac{\partial u_i}{\partial x_k}\right) \tag{4.62}$$

$$\tilde{\mathbf{u}}_{\mathrm{rot}} = \frac{1}{2}\begin{pmatrix} 0 & \dfrac{\partial u_1}{\partial x_2} - \dfrac{\partial u_2}{\partial x_1} & \dfrac{\partial u_1}{\partial x_3} - \dfrac{\partial u_3}{\partial x_1} \\ \dfrac{\partial u_2}{\partial x_1} - \dfrac{\partial u_1}{\partial x_2} & 0 & \dfrac{\partial u_2}{\partial x_3} - \dfrac{\partial u_3}{\partial x_2} \\ \dfrac{\partial u_3}{\partial x_1} - \dfrac{\partial u_1}{\partial x_3} & \dfrac{\partial u_3}{\partial x_2} - \dfrac{\partial u_2}{\partial x_3} & 0 \end{pmatrix} \tag{4.63}$$

$$\tilde{\mathbf{u}}_{\mathrm{vol}} = \frac{1}{3}\left(\frac{\partial u_1}{\partial x_1} + \frac{\partial u_2}{\partial x_2} + \frac{\partial u_3}{\partial x_3}\right)\begin{pmatrix} 1 & 0 & 0 \\ 0 & 1 & 0 \\ 0 & 0 & 1 \end{pmatrix} = \frac{1}{3}\mathrm{div}\,\mathbf{u}\begin{pmatrix} 1 & 0 & 0 \\ 0 & 1 & 0 \\ 0 & 0 & 1 \end{pmatrix} \tag{4.64}$$

$$\tilde{\mathbf{u}}_{\mathrm{eq}} = \begin{pmatrix} u_{11} & u_{12} & u_{13} \\ u_{21} & u_{22} & u_{23} \\ u_{31} & u_{32} & u_{33} \end{pmatrix} - \frac{1}{3}\mathrm{div}\,\mathbf{u}\begin{pmatrix} 1 & 0 & 0 \\ 0 & 1 & 0 \\ 0 & 0 & 1 \end{pmatrix} \tag{4.65}$$

So far, we have discussed the basics of describing strain on a continuum. We then consider the kinetics of deformation with a focus on the minute volume element of the continuum. The equation of motion for a minute volume element moving in a fluid is given by the following equation:

$$\rho\frac{\partial^2}{\partial t^2}\mathbf{u} = \nabla\cdot\tilde{\boldsymbol{\sigma}} - f\frac{\partial}{\partial t}\mathbf{u}$$
$$\tilde{\boldsymbol{\sigma}} = \begin{pmatrix} \sigma_{11} & \sigma_{21} & \sigma_{31} \\ \sigma_{12} & \sigma_{22} & \sigma_{32} \\ \sigma_{13} & \sigma_{23} & \sigma_{33} \end{pmatrix} \tag{4.66}$$

where ρ is the density, f is the friction between the gel network and the solvent, and $\tilde{\boldsymbol{\sigma}}$ is the stress tensor. The value of σ_{ik}, which is a component of $\tilde{\boldsymbol{\sigma}}$, is the stress in the k-direction working on the surface orthogonal to the i-direction. The left side of Eq. (4.66) is the product of the weight of the minute element and the acceleration, the first term on the right side is the force applied to the minute element, and the second term is the viscous resistance. Because the volume change in the gel is slow and is a semistatic process, the acceleration is approximated as 0, and the following equation is obtained:

$$\frac{\partial}{\partial t}\mathbf{u} = \frac{1}{f}\nabla\cdot\tilde{\boldsymbol{\sigma}} \tag{4.67}$$

The stress tensor is given by the following equation using the bulk modulus (K) and shear modulus (G):

$$\tilde{\boldsymbol{\sigma}} = 3K\tilde{\mathbf{u}}_{\mathrm{vol}} + 2G\tilde{\mathbf{u}}_{\mathrm{eq}} \tag{4.68}$$

Each element of the tensor is given as follows:

$$\sigma_{ik} = K\nabla\cdot\mathbf{u}\delta_{ik} + 2G\left(u_{ik} - \frac{1}{3}\nabla\cdot\mathbf{u}\delta_{ik}\right) \tag{4.69}$$

The first term of Eq. (4.69) is the stress due to the volume change, and the second term is that due to the shear deformation. We then solve Eq. (4.67)

$$\frac{\partial}{\partial t}\mathbf{u} = \frac{1}{f}\nabla\cdot\tilde{\boldsymbol{\sigma}} = \frac{1}{f}\begin{pmatrix}\sigma_{11} & \sigma_{12} & \sigma_{13}\\ \sigma_{21} & \sigma_{22} & \sigma_{23}\\ \sigma_{31} & \sigma_{32} & \sigma_{33}\end{pmatrix}\begin{pmatrix}\frac{\partial}{\partial x_1}\\ \frac{\partial}{\partial x_2}\\ \frac{\partial}{\partial x_3}\end{pmatrix} = \frac{1}{f}\begin{pmatrix}\frac{\partial\sigma_{11}}{\partial x_1} + \frac{\partial\sigma_{12}}{\partial x_2} + \frac{\partial\sigma_{13}}{\partial x_3}\\ \frac{\partial\sigma_{21}}{\partial x_1} + \frac{\partial\sigma_{22}}{\partial x_2} + \frac{\partial\sigma_{23}}{\partial x_3}\\ \frac{\partial\sigma_{31}}{\partial x_1} + \frac{\partial\sigma_{32}}{\partial x_2} + \frac{\partial\sigma_{33}}{\partial x_3}\end{pmatrix} \tag{4.70}$$

When we focus on the x_1 direction, the following equation is obtained from Eqs. (4.63) and (4.70):

$$\begin{aligned}
&\frac{\partial\sigma_{11}}{\partial x_1} + \frac{\partial\sigma_{12}}{\partial x_2} + \frac{\partial\sigma_{13}}{\partial x_3}\\
&= \frac{\partial}{\partial x_1}\left\{K\left(\frac{\partial u_1}{\partial x_1} + \frac{\partial u_2}{\partial x_2} + \frac{\partial u_3}{\partial x_3}\right) + \frac{2}{3}G\left(2\frac{\partial u_1}{\partial x_1} - \frac{\partial u_2}{\partial x_2} - \frac{\partial u_3}{\partial x_3}\right)\right\}\\
&\quad + G\frac{\partial}{\partial x_2}\left(\frac{\partial u_2}{\partial x_1} + \frac{\partial u_1}{\partial x_2}\right) + G\frac{\partial}{\partial x_3}\left(\frac{\partial u_3}{\partial x_1} + \frac{\partial u_1}{\partial x_3}\right)\\
&= \left(K + \frac{G}{3}\right)\frac{\partial}{\partial x_1}\left(\frac{\partial u_1}{\partial x_1} + \frac{\partial u_2}{\partial x_2} + \frac{\partial u_3}{\partial x_3}\right) + G\left(\frac{\partial^2 u_1}{\partial {x_1}^2} + \frac{\partial^2 u_2}{\partial {x_2}^2} + \frac{\partial^2 u_3}{\partial {x_3}^2}\right)\\
&= \left(K + \frac{G}{3}\right)\frac{\partial}{\partial x_1}\nabla\mathbf{u} + G\Delta\mathbf{u}
\end{aligned} \tag{4.71}$$

By solving the x_2 and x_3 directions with similar processes, one obtains the following:

$$\frac{\partial}{\partial t}\mathbf{u} = \frac{1}{f}\nabla\cdot\tilde{\boldsymbol{\sigma}} = \frac{1}{f}\begin{pmatrix}\left(K + \frac{G}{3}\right)\frac{\partial}{\partial x_1}\nabla\mathbf{u} + G\Delta\mathbf{u}\\ \left(K + \frac{G}{3}\right)\frac{\partial}{\partial x_2}\nabla\mathbf{u} + G\Delta\mathbf{u}\\ \left(K + \frac{G}{3}\right)\frac{\partial}{\partial x_3}\nabla\mathbf{u} + G\Delta\mathbf{u}\end{pmatrix} \tag{4.72}$$

For simplicity, here we consider a spherical-shaped gel, which gives a deformation vector ($\mathbf{u}$) with the following form:

$$\mathbf{u}(\mathbf{r}, t) = u(r, t)\frac{\mathbf{r}}{r} \tag{4.73}$$

Here, $\mathbf{r}/r$ is the unit vector parallel to $\mathbf{r}$. Because the deformation only depends on the distance from the origin r, due to the symmetric nature of the sphere, $u(r, t)$

is the essential function governing the deformation of any point in the gel. Due to the high symmetry, the following equation holds:

$$\frac{\partial}{\partial x_1} = \frac{\partial}{\partial x_2} = \frac{\partial}{\partial x_3} = \frac{\partial}{\partial r} \tag{4.74}$$

Using Eq. (4.74), Eq. (4.73) can be reduced:

$$\frac{\partial u(r,t)}{\partial t}\frac{\mathbf{r}}{r} = \frac{1}{f}\left(\left(K + \frac{\mu}{3}\right)\frac{\partial}{\partial r}\nabla u(r,t) + G\Delta u(r,t)\right)\frac{\mathbf{r}}{r} \tag{4.75}$$

Thus, Eq. (4.76) can be obtained:

$$\frac{\partial u(r,t)}{\partial t} = \frac{1}{f}\left[\left(K + \frac{\mu}{3}\right)\frac{\partial}{\partial r}\nabla u(r,t) + G\Delta u(r,t)\right] \tag{4.76}$$

Due to the symmetry of the sphere, Eq. (4.77) holds:

$$\frac{\partial}{\partial r}\nabla = \Delta \tag{4.77}$$

Finally, one obtains the following equation:

$$\frac{\partial u(r,t)}{\partial t} = \frac{1}{f}\left(K + \frac{4G}{3}\right)\frac{\partial}{\partial r}\nabla u(r,t) = D\frac{\partial}{\partial r}\left[\frac{1}{r^2}\frac{\partial}{\partial r}(r^2 u)\right] \tag{4.78}$$

Notably, we applied ∇ for the 3D polar coordinate system and neglected the partial derivative of the rotation angle due to the symmetry of the sphere. Because of its similarity to the diffusion equation, this equation is called the "swelling equation," and D is called the collective diffusion coefficient of gels.

$$D = \frac{K + \frac{4G}{3}}{f} \tag{4.79}$$

To solve Eq. (4.78), we focus on the initial conditions ($t = 0$). We set the initial radius as a_0 and the equilibrium radius as a_∞, and we consider the strain of a point from the initial to the equilibrium state. Notably, the strain is defined by setting the equilibrium state as the reference condition (Figure 4.15) because the initial condition is not stable and is therefore not suitable for use as the reference condition. In other words, the initial condition is a deformed state; the pressure of Π_0 compresses the radius of the sphere from a_∞ to a_0 in the initial condition. Thus, the strain of a point, which has a distance r from the origin in the equilibrium swollen state, in the initial condition ($t = 0$) is given as follows:

$$u(r,0) = (a_\infty - a_0)\frac{r}{a_\infty} = \Delta a\frac{r}{a_\infty} \tag{4.80}$$

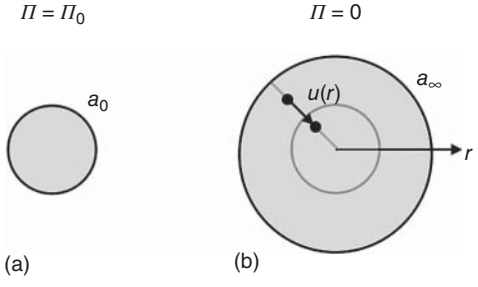

Figure 4.15 (a) Initial state (deformed) and (b) equilibrium state (undeformed) of a gel.

Because this strain is caused by the pressure Π_0, the following equation holds:

$$\Pi_0 = K \cdot \frac{\mathrm{d}V}{V} = K \cdot 3\frac{\mathrm{d}r}{r} = 3K \cdot \frac{u(r,0)}{r} = 3K \cdot \frac{\Delta a}{a_\infty} \tag{4.81}$$

To achieve the boundary condition, we focus on the force working on the surface of the sphere in the radial direction. The deformation in the radial direction contains contributions from the isotropic volumetric deformation ($\mathrm{d}u_{\mathrm{vol}}/\mathrm{d}r$) and the isovolumetric deformation ($\mathrm{d}u_{\mathrm{eq}}/\mathrm{d}r$), similar to Eq. (4.61).

$$\frac{\mathrm{d}u}{\mathrm{d}r} = \frac{\mathrm{d}u_{\mathrm{vol}}}{\mathrm{d}r} + \frac{\mathrm{d}u_{\mathrm{eq}}}{\mathrm{d}r} \tag{4.82}$$

The volumetric deformation is given as follows and is similar to Eq. (4.64):

$$\frac{\mathrm{d}u_{\mathrm{vol}}}{\mathrm{d}r} = \frac{1}{3}\mathrm{div}\, u = \frac{1}{3}\frac{1}{r^2}\frac{\mathrm{d}}{\mathrm{d}r}(r^2 u) = \frac{1}{3}\left(\frac{\mathrm{d}u}{\mathrm{d}r} + \frac{2u}{r}\right) \tag{4.83}$$

Based on Eqs. (4.82) and (4.83), $\mathrm{d}u_{\mathrm{eq}}/\mathrm{d}r$ is represented as follows:

$$\frac{\mathrm{d}u_{\mathrm{eq}}}{\mathrm{d}r} = \frac{2}{3}\left(\frac{\mathrm{d}u}{\mathrm{d}r} - \frac{u}{r}\right) \tag{4.84}$$

Given that u_{vol} is deformation in the radial direction and u_{eq} is deformation in the surface direction, the stress in the radial direction (σ_{rr}) is given by Eq. (4.85):

$$\begin{aligned}\sigma_{\mathrm{rr}} &= 3K\frac{\mathrm{d}u_{\mathrm{vol}}}{\mathrm{d}r} + 2G\frac{\mathrm{d}u_{\mathrm{eq}}}{\mathrm{d}r} \\ &= K\left(\frac{\mathrm{d}u}{\mathrm{d}r} + \frac{2u}{r}\right) + 2G \cdot \frac{2}{3}\left(\frac{\mathrm{d}u}{\mathrm{d}r} - \frac{u}{r}\right) \\ &= \left(K + \frac{4}{3}G\right)\frac{\mathrm{d}u}{\mathrm{d}r} + 2\left(K - \frac{2}{3}G\right)\frac{u}{r}\end{aligned} \tag{4.85}$$

The initial conditions are set as when the gel is immersed in the solution, the gel surface is the free-end and the stress applied to the gel surface is 0.

$$\sigma_{\mathrm{rr}}|_{r=a} = 0 \tag{4.86}$$

By solving Eq. (4.78) using Eqs. (4.81) and (4.86) as boundary and initial conditions, respectively, the following solution is obtained:

$$u(r,t) = \sum_n F_n(r)\exp(-D{k_n}^2 t) \tag{4.87}$$

Here, $F_n(r)$ and k_n are represented as follows:

$$F_n(r) = -6\frac{\Delta a}{a_\infty}\frac{(-1)^n}{k_n}\left[\frac{\cos\, k_n r}{k_n r} - \frac{\sin\, k_n r}{(k_n r)^2}\right] \tag{4.88}$$

$$k_n = \frac{n\pi}{a_\infty} \tag{4.89}$$

Now, we want to know the deformation of the gel surface over time ($a(t)$), which is represented by using the deformation of the gel surface ($u(a_\infty, t)$).

$$a(t) = a_\infty + u(a_\infty, t) \tag{4.90}$$

The function $u(a_\infty, t)$ is given using Eqs. (4.87)–(4.89).

$$\begin{aligned} u(a_\infty, t) &= -6\Delta a \sum_n \frac{(-1)^n}{n\pi}\left[\frac{\cos\, n\pi}{n\pi} - \frac{\sin\, n\pi}{(n\pi)^2}\right] \exp(-Dk_n{}^2 t) \\ &= -6\Delta a \sum_n \frac{1}{(n\pi)^2} \exp\left(-D\left(\frac{n\pi}{a_\infty}\right)^2 t\right) \\ &= -\Delta a \sum_n \frac{6}{(n\pi)^2} \exp\left(-n^2 \frac{t}{\tau_1}\right) \\ &= -\Delta a \sum_n u_n \end{aligned} \tag{4.91}$$

Here, τ_1 is the longest relaxation time, and u_n is defined as follows:

$$\tau_1 = \frac{a_\infty{}^2}{\pi^2 D} \tag{4.92}$$

$$u_n = \frac{6}{(n\pi)^2} \exp\left(-n^2 \frac{t}{\tau_1}\right) \tag{4.93}$$

To visualize the time-evolution of $u(a_\infty, t)$, we consider the characteristics of u_n. Figure 4.16 plots $u(a_\infty, t)$ and u_n $(n = 1, 2, 5)$ normalized with Δa against t/τ_1. As is clear from the form of the equation, the absolute value of u_n decays, and the decay rate increases as n increases. From this graph, one can see that the influence of u_n with $n \geq 2$ on the slow relaxation behavior $(t > \tau_1)$ is negligible. As a result, the volume change in the spherical gel can be approximated using u_1.

$$\frac{a_\infty - a(t)}{a_\infty - a_0} \cong \frac{6}{\pi^2} \exp\left(-\frac{t}{\tau_1}\right) \tag{4.94}$$

Experimentally, τ_1 is obtained as the slope of the plot of $\log(a_\infty - a(t))/(a_\infty - a_0)$ against t over a long time scale. Notably, τ_1 is proportional to $a_\infty{}^2$ (Eq. (4.92)); the rates of swelling and shrinking decrease as the size of the gel increases.

The collective diffusion coefficient (D) obtained from the aforementioned swelling measurement showed good agreement with the collective diffusion coefficient measured by dynamic light scattering (DLS). By using the

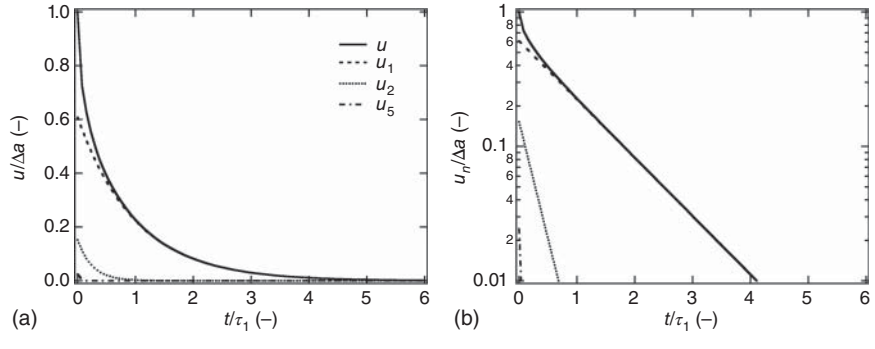

Figure 4.16 (a) $u(a_\infty, t)$ normalized by Δa. (b) Dependence of $u_n/\Delta a$ on t/τ_1 $(n = 1, 2, 5)$.

Einstein–Stokes equation for D (see Section 6.2.1), one obtains a correlation length, ξ.

$$\xi = \frac{k_B T}{6\pi\eta D} \tag{4.95}$$

where η is the viscosity of the solvent. Although this value is sometimes confused with the mesh size, it is not correct to relate ξ to the so-called mesh size because the density of the crosslinks and network strands are directly related to the shear modulus (G), as shown in Chapter 3. Instead, based on Eq. (4.79), ξ strongly relates to the bulk modulus, K, and the friction coefficient between the solvent and the polymer network, f. The blob size, which is defined by Eq. (4.95), is similar to that of the polymer solutions introduced in Eqs. (2.15) and (2.62) (see Section 15.3).

4.5 Degradation of Polymer Gels

The decomposition behavior of materials is roughly divided into two types: surface degradation and bulk degradation. Surface degradation, as its name suggests, is degradation through surface erosion; an example of surface degradation is the dissolution of rock sugar in water. Most solid materials show surface degradation. On the other hand, polymer gels often show bulk degradation. Bulk degradation occurs not from the surface but occurs when the entire body degrades homogeneously. Polymer gels contain a large amount of solvent, and the diffusion of small molecules inside the gel is not much different from that in an aqueous solution. Therefore, when a gel is degraded by a stimulus, there is no difference between the surface and the inside of the gel, resulting in bulk degradation. Bulk degradation is specific to polymer gels. In Sections 4.5.1 and 4.5.2, we explain the two representative bulk degradation behaviors of polymer gels.

4.5.1 Degradation by Cleavage of Specific Bonds

How does the shape of the gel change during bulk degradation? To capture the essence of the problem, we consider the following simple example: a hydrogel having a nearly ideal four-branched network structure with one easily cleaved bond per network strand with a fraction of r_{deg}. Let us consider the situation where hydrolysis progresses. When a gel is in the as-prepared state, the gel first swells, as discussed in Section 4.2. Since swelling and hydrolysis occur simultaneously, it is necessary to consider the relationship between the relaxation time of the swelling and the half-life of the hydrolyzable bonds. Here, we assume that the size of the gel is sufficiently small, and the relaxation time of gel swelling is sufficiently smaller than the half-life time of the bonds of interest. Indeed, when the size of the gel is 1 mm, the time scale for reaching the swelling equilibrium is approximately several minutes according to Eq. (4.92) ($D \approx 10^{-7}$ cm^2/s for conventional gels) [25]. Thus, we can focus on a simple process in which the gel reaches an equilibrium swollen state a few minutes after being immersed in water, and then hydrolysis gradually cleaves the network strands. The cleavage

of the network strands decreases the connectivity of the network, i.e. the elastic modulus (or elastic pressure) is decreased. As a result, the initial equilibrium between the elastic pressure and the osmotic pressure collapses after a certain period. To this point, we have assumed the process in which the swelling is sufficiently faster than the dissociation. Therefore, when the elastic modulus decreases, the gel swells and reaches an equilibrium immediately. This process is bulk degradation; the gel swells during degradation and eventually completely dissolves. Assuming that the hydrolysis obeys pseudo-first-order kinetics with a rate constant of k_{deg}, the probability of a network strand still connecting neighboring junction points (p) at a certain time (t) is given as follows:

$$p(t) = p_0 \cdot (1 - r_{\mathrm{deg}} + r_{\mathrm{deg}} \exp(-k_{\mathrm{deg}} t)) \tag{4.96}$$

where p_0 is the value of p at preparation ($t = 0$) and $p_0 = 1$ for ideal networks. According to the phantom network model (Eq. (3.35)) and Bethe approximation (Eqs. (3.47) and (3.48)), the change in the elastic modulus over time, $G(t)$, is represented as follows;

$$\begin{aligned} G(t) = \xi kT &= \left(\frac{1}{2}P(X_3) + P(X_4)\right) ckT \\ &= (1 + P(F))(1 - P(F))^3 ckT \\ &= \left(\frac{3}{2} - \sqrt{\frac{1}{p(t)} - \frac{3}{4}}\right)^3 \left(\frac{1}{2} + \sqrt{\frac{1}{p(t)} - \frac{3}{4}}\right) ckT \end{aligned} \tag{4.97}$$

where c (m^{-3}) is the number density of the tetra-functional unit. Given that the elastic pressure is always balanced with the osmotic pressure, ξ and the swelling ratio (Q) are related by Eq. (4.98):

$$\xi = -\frac{\frac{\phi_0}{Q} + \ln\left(1 - \frac{\phi_0}{Q}\right) + \chi\left(\frac{\phi_0}{Q}\right)^2}{V_1 Q^{1/3}} \tag{4.98}$$

We measured the degradation of a tetra-functional polymer gel with $p_0 \approx 0.9$ with different r_{deg} and estimated the change in ξ over time based on Eq. (4.98) [18]. The time-evolution of ξ was well reproduced by Eqs. (4.96) and (4.97) with a universal constant of k_{deg}. In addition, the critical connectivity ratio where a gel turned into a sol ($p_{\mathrm{c}} \approx 0.46$) was estimated based on the time at which the gel was completely dissociated (t_{deg}). This value was somewhat higher than the critical connectivity ratio of the diamond lattice and that calculated based on Bethe approximation ($p_{\mathrm{c}} \approx 0.33$; see Section 3.6.1). Thus, when an appropriate set of k_{deg} and p_{c} is used, it is possible to quantitatively reproduce the degradation behavior of gels (see Section 16.1).

Finally, we note the limitations of this treatment. First, the elution of the sol fraction is not considered. The proportion of the polymer eluting from the gel (sol fraction, ϕ_{sol}) can be roughly estimated using Bethe approximation. ϕ_{sol} is the probability that no arms of any of the four branch units are connected to the gel body, and this parameter is expressed as follows:

$$\phi_{\mathrm{sol}} = P(F)^4 = \left(\sqrt{\frac{1}{p} - \frac{3}{4}} - \frac{1}{2}\right)^4 \tag{4.99}$$

Because ϕ_{sol} is negligible when p is relatively high, the polymer volume fraction of the gel is well estimated as ϕ_0/Q, which is consistent with the assumption of Eq. (4.98). Second, the region where the elastic modulus is well reproduced by Bethe approximation is also limited to a high p region. Experimental results confirmed that this treatment worked well with $p > 0.75$ for the tetra-functional network [26]. Taken together, it is important to limit the range of fit using Eqs. (4.96) and (4.97) to the initial degradation; in the case of a four-branched network, the region should be limited to roughly the range from an initial cycle rank, ξ_0, to $\xi_0/2$ (corresponding to the region $p > 0.75$).

4.5.2 Degradation by Cleavage of Nonspecific Bonds

In Section 4.5.1, the degradation was caused by a readily cleavable site existing in a network strand. This section addresses the degradation behavior of polymer networks without easily cleavable bonds. This modeling enables us to predict the long-term stability of relatively stable gels. We model the polymer network consisting of the network strands with chemically stable bonds, such as carbon–carbon single bonds or ether bonds. Even these stable bonds have small but finite decomposition rate constants (k_m) and decompose to a considerable extent during long-term usage.

In Section 4.5.1 on site-specific cleavage, there was only one easily cleavable site per network strand, and the cleavage of a bond broke the connection between neighboring crosslinks. In other words, the cleavage of a bond is enough to break the connection between neighboring crosslinks. However, in the case of nonspecific cleavage, all bonds in a strand must be maintained to preserve the connection between neighboring crosslinks. The probability that the neighboring crosslinks connected by a network strand with the degree of polymerization N being still connected after time t is represented as follows [19]:

$$[\exp(k_m t)]^N = \exp(N k_m t) = \exp(k_{net} t) \tag{4.100}$$

Here, we assume that all bonds are cleaved by a pseudo-first-order reaction (k_m: decomposition rate constant). Equation (4.100) shows that the degradation of "a network strand" follows pseudo-first-order decomposition with a decomposition rate constant $k_{net} = N k_m$. Since N is conventionally on the order of 100, this model predicts that a network strand will decompose at a rate approximately 100 times that of a bond. Thus, we cannot ignore degradation even for a polymer gel consisting of stable chemical bonds. To examine this model, we prepared several different polymer gels with different N and performed accelerated degradation experiments. Based on an analysis similar to that used in Section 4.5.1, a relationship between k_{net} and N was estimated from the change in the swelling degree as a function of time. The values of k_{net} and N are linearly related, suggesting that Eq. (4.100) reproduces the decomposition behavior of the polymer gel well. Again, k_{net} is conventionally on the order of $100k_m$; nonspecific decomposition has a significant effect and must be considered for the long-term usage of gel.

Column 4: Diffusions of Polymer Network During Swelling

The swelling equation is based on a unique concept that defines the swelling as a diffusion process of a polymer network to the external solvent phase, not the diffusion process of solvent molecules to the gel phase. The swelling equation is established by solving the equation of motion for a unit volume of polymer network:

$$\frac{\partial u(r,t)}{\partial t} = \frac{1}{f}\left(K + \frac{4G}{3}\right)\frac{\partial}{\partial r}\nabla u(r,t) = D\frac{\partial}{\partial r}\left[\frac{1}{r^2}\frac{\partial}{\partial r}(r^2 u)\right] \tag{4.78}$$

$$D = \frac{K + \frac{4G}{3}}{f} \tag{4.79}$$

where D is cooperative diffusion coefficient, K is bulk modulus, G is elastic modulus, and f is a parameter indicating the friction between polymer network and solvent molecule. Based on Eq. (4.79), D can be estimated from three parameters, K, G, and f. Notably, although K and G are well-defined parameters, f is not conventional well-defined parameter. The unit of f is $(\mathrm{N\,s})/\mathrm{m}^4$, and different from that of conventional friction coefficient (–). Tanaka proposed that f of hydrogel was estimated from water permeation experiments, where one measured the permeation of water through a gel membrane with applying pressure. Based on f estimated from the water permeation measurement, one can estimate D based on Eq. (4.79) (D_{WP}).

Some authors examined D_{WP} in comparison with Ds estimated by other two representative methods. One is the estimation from swelling experiments using Eqs. (4.94) and (4.92) (D_{SW}):

$$\frac{a_\infty - a(t)}{a_\infty - a_0} \cong \frac{6}{\pi^2}\exp\left(-\frac{t}{\tau_1}\right) \tag{4.94}$$

$$\tau_1 = \frac{{a_\infty}^2}{\pi^2 D} \tag{4.92}$$

Although this is a direct estimation of D, one needs to assume that D is constant during swelling, which is unlikely to hold in a large swelling.

Another method is based on DLS proposed by Shibayama. Generally, scattering from a gel contains two components from dynamic network fluctuation (D_{DLS}) and static heterogeneity. By analyzing a several tens of scattering data of the gel, one can remove the contribution from static heterogeneity and extract that from dynamic fluctuation. Although this methodology is another direct estimation of D, the detected motion is a thermal fluctuation based on Brownian motion, which can be different from translational motion in swelling.

Previous works observed rough agreement of these three Ds; however, the number of samples were not large enough and full comparison of three Ds was not performed. Recently, we have compared three Ds (D_{WP}, D_{SW}, and D_{DLS})

of a series of polymer gels with tuned polymer concentration and molecular weight of network strand. We found that D_{SW} and D_{DLS} well corresponded with each other; while D_{WP} showed different trend. In addition, the results of D_{SW} and D_{DLS} well fit in with the concept of cooperative diffusion coefficient. On the other hand, the deviation of D_{WP} from the other Ds has been most likely due to the misestimation of f, which governs the "permeation of water" not the "permeation of polymer network." Conversely, this deviation supports the original idea of Tanaka that the swelling is governed by the diffusion of polymer network, which is qualitatively different from that of water molecules [27, 28].

References

1 Panyukov, S.V. (1990). Scaling theory of high elasticity. *Zh. Eksp. Teor. Fiz.* 98: 668–680.
2 Obukhov, S.P., Rubinstein, M., and Colby, R.H. (1994). Network modulus and superelasticity. *Macromolecules* 27: 3191–3198.
3 Sakai, T., Kurakazu, M., Akagi, Y. et al. (2012). Effect of swelling and deswelling on the elasticity of polymer networks in the dilute to semi-dilute region. *Soft Matter* 8: 2730–2736.
4 Urayama, K., Kawamura, T., and Kohjiya, S. (2009). Structure–mechanical property correlations of model siloxane elastomers with controlled network topology. *Polymer* 50: 347–356.
5 Urayama, K. and Kohjiya, S. (1997). Uniaxial elongation of deswollen poly-dimethylsiloxane networks with supercoiled structure. *Polymer* 38: 955–962.
6 Urayama, K., Yokoyama, K., and Kohjiya, S. (2000). Low-temperature behavior of deswollen poly(dimethylsiloxane) networks. *Polymer* 41: 3273–3278.
7 Katashima, T., Asai, M., Urayama, K. et al. (2014). Mechanical properties of tetra-PEG gels with supercoiled network structure. *J. Chem. Phys.* 140: 074902.
8 Ferry, J.D. (1980). *Viscoelastic Properties of Polymers*. Wiley.
9 Flory, P.J. (1953). *Principles of Polymer Chemistry*. Ithaca, NY: Cornell University Press.
10 Hild, G., Okasha, R., Macret, M., and Gnanou, Y. (1986). Relationship between elastic modulus and volume swelling degree of polymer networks swollen to equilibrium in good diluents, 4. Interpretation of experimental results on the basis of scaling concepts. *Makromol. Chem.* 187: 2271–2288.
11 Katashima, T., Chung, U.-i., and Sakai, T. (2015). Effect of swelling and deswelling on mechanical properties of polymer gels. *Macromol. Symp.* 358: 128–139.
12 Richards, R.W. and Davidson, N.S. (1986). Scaling analysis of mechanical and swelling properties of random polystyrene networks. *Macromolecules* 19: 1381–1389.
13 Zrinyi, M. and Horkay, F. (1987). On the elastic modulus of swollen gels. *Polymer* 28: 1139–1143.

14 Gnanou, Y., Hild, G., and Rempp, P. (1987). Molecular-structure and elastic behavior of poly(ethylene oxide) networks swollen to equilibrium. *Macromolecules* 20: 1662–1671.

15 Benoit, H., Strazielle, C., and Benmouna, M. (1988). An evaluation of the Flory χ-parameter as a function of concentration using the polymer solution scattering theory. *Acta Polym.* 39: 75–79.

16 Candau, F., Strazielle, C., and Benoit, H. (1976). Use of osmotic pressure to study linear and branched polystyrenes in solution – determination of thermodynamic parameters. *Eur. Polym. J.* 12: 95–103.

17 Peppas, N.A. and Merrill, E.W. (1976). Determination of interaction parameter χ_1 for poly(vinyl alcohol) and water in gels crosslinked from solutions. *J. Polym. Sci., Part A: Polym. Chem.* 14: 459–464.

18 Li, X., Tsutsui, Y., Matsunaga, T. et al. (2011). Precise control and prediction of hydrogel degradation behavior. *Macromolecules* 44: 3567–3571.

19 Li, X., Kondo, S., Chung, U.-i., and Sakai, T. (2014). Degradation behavior of polymer gels caused by nonspecific cleavages of network strands. *Chem. Mater.* 26: 5352–5357.

20 Tanaka, T. (1978). Collapse of gels and critical endpoint. *Phys. Rev. Lett.* 40: 820–823.

21 Hirokawa, Y. and Tanaka, T. (1984). Volume phase transition in a nonionic gel. *J. Chem. Phys.* 81: 6379–6380.

22 Vidyasagar, A., Majewski, J., and Toomey, R. (2008). Temperature induced volume-phase transitions in surface-tethered poly(*N*-isopropylacrylamide) networks. *Macromolecules* 41: 919–924.

23 Katayama, S., Hirokawa, Y., and Tanaka, T. (1984). Reentrant phase transition in acrylamide-derivative copolymer gels. *Macromolecules* 17: 2641–2643.

24 Tanaka, T. and Fillmore, D.J. (1979). Kinetics of swelling of gels. *J. Chem. Phys.* 70: 1214–1218.

25 Kamata, H., Chung, U.-i., and Sakai, T. (2013). Shrinking kinetics of polymer gels with alternating hydrophilic/thermoresponsive prepolymer units. *Macromolecules* 46: 4114–4119.

26 Nishi, K., Chijiishi, M., Katsumoto, Y. et al. (2012). Rubber elasticity for incomplete polymer networks. *J. Chem. Phys.* 137: 224903.

27 Tanaka, T., Hocker, L.O., and Benedek, G.B. (1973). Spectrum of light scattered from a viscoelastic gel. *J. Chem. Phys.* 59: 5151–5159.

28 Fujiyabu, T., Toni, F., Li, X. et al. (2018). Three cooperative diffusion coefficients describing dynamics of polymer gels. *Chem. Commun.* 54: 6784–6787.

5

Deformation and Fracture

Takuya Katashima and Takamasa Sakai

Graduate School of Engineering, The University of Tokyo, Tokyo, Japan

5.1 Description of Deformation

In this section, we first discuss the strain tensor, which is an important concept for understanding deformation. The strain tensor is a tensor describing the general deformation of a continuum. Some people may think that it is sufficient to describe deformation with a 3D vector because we deform the material in 3D space. Although this is correct in a certain sense, a 3D vector is generally insufficient to describe the deformation in 3D, unless the vector is appropriate (indeed, all 3D deformations can be described with three independent variables called invariants).

5.1.1 Displacement Vector

The external force "moves" and "deforms" the object. The movement and deformation of a continuum can be described using a set of vectors. The initial position vector ($\mathbf{P}_0$) of a certain point (A) in the continuum is represented as follows:

$$\mathbf{P}_0 = \sum_{i=1}^{3} P_i^0 \mathbf{e}_i \quad (i = 1, 2, 3) \tag{5.1}$$

Here, $\mathbf{e}_i$ is the unit basis vector along each coordinate axis. The point is shifted to position $\mathbf{P}$ after deformation.

$$\mathbf{P} = \sum_{i=1}^{3} P_i \mathbf{e}_i \tag{5.2}$$

Here, the displacement vector $\mathbf{u}$ before and after the deformation can be written as follows:

$$\mathbf{u}(x_1, x_2, x_3) = \mathbf{P} - \mathbf{P}_0 \tag{5.3}$$

Physics of Polymer Gels, First Edition. Edited by Takamasa Sakai.

5.1.2 Strain Tensor

Focusing on the two squares shown by the dotted lines in Figure 5.1, although the original shapes are the same, they are deformed differently depending on their initial alignment. In other words, the angles were preserved, and only the lengths were changed in the upper rectangle, whereas both the angles and lengths were changed in the lower rectangle. As shown in Figure 5.1, deformations can be classified into two types: changes in lengths and changes in angles. In continuum mechanics, these deformations are called "normal strain" and "shear strain," respectively. In Section 5.1.2.1, we introduce how to describe these strains using displacement vectors.

5.1.2.1 Normal Strain

Normal strains are simple elongations and compressions and contain independent strains in the x_1, x_2, and x_3 directions in three dimensions. For the sake of simplicity, we first consider the 1D deformation of a line segment (length $\mathrm{d}x_1$) with an end-to-end vector, x_1 and $x_1 + \mathrm{d}x_1$. Due to the deformation, the coordinate of the left end is moved from x_1 to $x_1 + u_1(x_1)$, where $u_1(x_1)$ is the displacement vector (Figure 5.2). Given that the elongation strain in the axial direction is ε_1, the length of the deformed segment is $(1 + \varepsilon_1)\mathrm{d}x_1$. The coordinates of the right end of the deformed segment are written as $x_1 + u_1(x_1) + (1 + \varepsilon_1)\mathrm{d}x_1$ or $x_1 + \mathrm{d}x_1 + u_1(x_1 + \mathrm{d}x_1)$.

Based on these two different expressions, we can obtain the following expression for ε_1:

$$\varepsilon_1 = \frac{u_1(x_1 + \mathrm{d}x_1) - u_1(x_1)}{\mathrm{d}x_1} \tag{5.4}$$

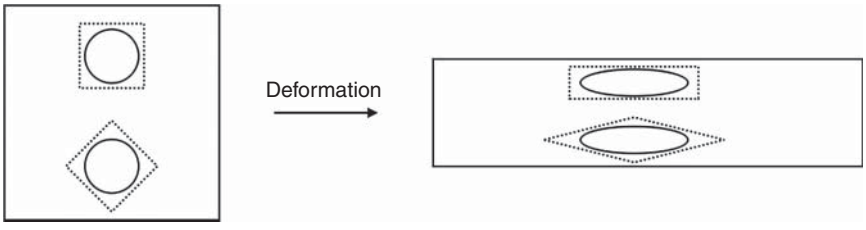

Figure 5.1 Deformation of materials. Even under the same deformation, different shapes appear to show different deformations.

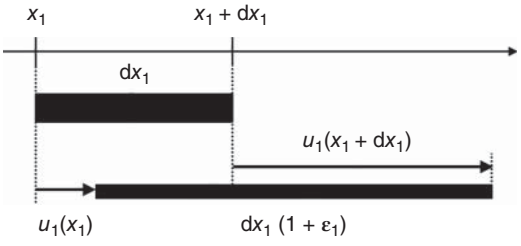

Figure 5.2 Deformation of a 1D object by a normal strain.

When the length of the segment approaches 0, the strain at a certain point, which indicates a local expansion or contraction, can be obtained from the following:

$$\lim_{dx_1 \to 0} \varepsilon_1 = \lim_{dx_1 \to 0} \frac{u_1(x_1 + dx_1) - u_1(x_1)}{dx_1} = \frac{du_1}{dx_1} \tag{5.5}$$

This argument can be extended to arbitrary points (x_1, x_2, x_3) in 3D materials, and the strain at a certain point can be written as follows:

$$\varepsilon_1(x_1, x_2, x_3) = \lim_{dx_1 \to 0} \frac{u_1(x_1 + dx_1) - u_1(x_1)}{dx_1} = \frac{\partial u_1}{\partial x_1} \tag{5.6}$$

Notably, we do not need to consider the partial derivatives of u_1 with respect to the other directions (x_2 and x_3) for ε_1.

5.1.2.2 Shear Strain

Shear strain represents the deformation of an angle. An example of pure shear deformation is a deformation of a square to a parallelogram on a 2D surface (Figure 5.3). Here, we consider the situation in which the lengths of the lines do not change and that the lines along the x_1 and x_2 axes are tilted by angles of α and $-\beta$ from their initial directions, respectively (for angular changes, anticlockwise is defined as positive). In this deformation, a point (x_1, x_2) is moved to ($x_1 + u_1(x_1, x_2)$, $x_2 + u_2(x_1, x_2)$). If the angular change is minute, the following equation can be obtained:

$$\alpha \simeq \sin\alpha = \frac{u_2(x_1 + dx_1) - u_2(x_1)}{dx_1} \tag{5.7}$$

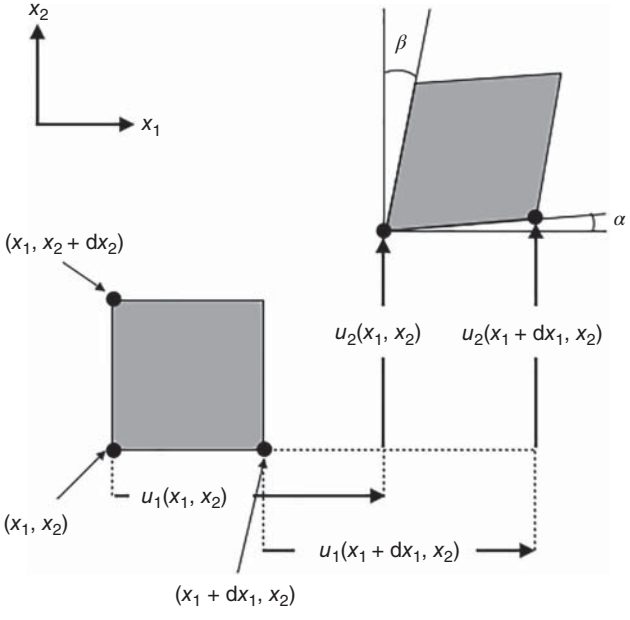

Figure 5.3 Deformation of a rectangle by shear strain.

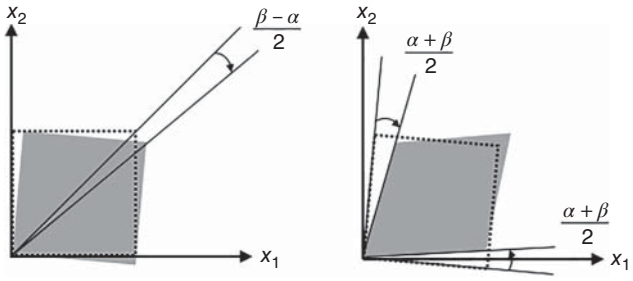

Figure 5.4 Shear strain can be divided into two processes: (a) rotation and (b) deformation.

Furthermore, as dx_1 approaches 0, the shear strain of a certain point, which indicates the distortion of the point, can be obtained as Eq. (5.8):

$$\lim_{dx_1 \to 0} \alpha = \lim_{dx_1 \to 0} \frac{u_2(x_1 + dx_1) - u_2(x_1)}{dx_1} = \frac{\partial u_2}{\partial x_1} \tag{5.8}$$

Similarly, we can calculate β as Eq. (5.9):

$$\beta = \frac{\partial u_1}{\partial x_2} \tag{5.9}$$

Notably, the deformation by angles of α and β do not always contribute to pure "deformation." For example, in the case of $\alpha = -\beta$, the shape is unchanged, and the square is only rotated by α. In this way, rotations are incorporated into shear strains, and these should be removed to extract the pure deformation component. The deformation shown in Figure 5.4 can be divided into two processes, namely, a rotation and a shear deformation, as shown as follows:

1. Rotation by $(\beta - \alpha)/2$ clockwise with retention of the shape.
2. Rotating both sides of the square by $(\alpha + \beta)/2$ in opposite directions while maintaining the side lengths.

The first process is not deformation, and the second process is shear deformation.

This division may be intuitive when you imagine the deformation of a solid. To purely deform a solid, you need to apply the same force from both sides as solids rotate when you apply a force from only one side. The previously mentioned second process is similar to the pure deformation of a solid. In general, when two sides rotate by α and β, the rotation component is $(\beta - \alpha)/2$ and the deformation component is $(\alpha + \beta)/2$. Based on this treatment, the deviations from the x_1 and x_2 axes must be the same as $(\alpha + \beta)/2$.

In the diagram shown in Figure 5.4, the deformation strains in the direction perpendicular to the x_1 and x_2 axes are called ε_{12} and ε_{21}, respectively. ε_{12} indicates how much the vector in the x_1 direction rotates toward the x_2 direction and can be described as follows:

$$\varepsilon_{12}(x_1, x_2, x_3) = \varepsilon_{21}(x_1, x_2, x_3) = \frac{\alpha + \beta}{2} = \frac{1}{2}\left(\frac{\partial u_1}{\partial x_2} + \frac{\partial u_2}{\partial x_1}\right) \tag{5.10}$$

Here, we slightly change the notation of the nominal strain.

$$\varepsilon_1(x_1, x_2, x_3) = \varepsilon_{11}(x_1, x_2, x_3) = \frac{1}{2}\left(\frac{\partial u_1}{\partial x_1} + \frac{\partial u_1}{\partial x_1}\right) \tag{5.6'}$$

In conclusion, deformations are represented as a strain tensor composed of nine components.

$$\begin{aligned}\varepsilon_{ij} &= \frac{1}{2}\left(\frac{\partial u_i}{\partial x_j} + \frac{\partial u_j}{\partial x_i}\right) \\ &= \begin{pmatrix} \dfrac{\partial u_1}{\partial x_1} & \dfrac{1}{2}\left(\dfrac{\partial u_1}{\partial x_2} + \dfrac{\partial u_2}{\partial x_1}\right) & \dfrac{1}{2}\left(\dfrac{\partial u_1}{\partial x_3} + \dfrac{\partial u_3}{\partial x_1}\right) \\ \dfrac{1}{2}\left(\dfrac{\partial u_2}{\partial x_1} + \dfrac{\partial u_1}{\partial x_2}\right) & \dfrac{\partial u_2}{\partial x_2} & \dfrac{1}{2}\left(\dfrac{\partial u_2}{\partial x_3} + \dfrac{\partial u_3}{\partial x_2}\right) \\ \dfrac{1}{2}\left(\dfrac{\partial u_3}{\partial x_1} + \dfrac{\partial u_1}{\partial x_3}\right) & \dfrac{1}{2}\left(\dfrac{\partial u_3}{\partial x_2} + \dfrac{\partial u_2}{\partial x_3}\right) & \dfrac{\partial u_3}{\partial x_3} \end{pmatrix}\end{aligned} \tag{5.11}$$

Because the rotation mode has been removed, the deformation tensor is symmetric ($\varepsilon_{ij} = \varepsilon_{ji}$); six of the nine variables are independent strain components.

5.1.3 Principal Direction and Strain

Again, focusing on Figure 5.1, a circle is transformed into an ellipse regardless of the position, while squares arranged at different angles are transformed into different shapes. In other words, different coordinate systems give different stress tensors for deformation, and one can find a concise description of deformation with an appropriate coordinate system. Under an appropriate coordinate system, any deformation can be represented by only normal strains. The directions of the appropriate coordinate system are called the "nominal directions of strain."

For example, even shear deformation can be converted into simple elongational deformation. As shown in Figure 5.5, a square deforms to a rhombus by a shear deformation under an orthogonal coordinate system of x_1 and x_2. On the other hand, if the coordinate system is taken into an orthogonal coordinate system consisting of x_1' and x_2' parallel to the two diagonal lines, this deformation is converted to an elongation and a compression in the x_1' and x_2' directions, respectively. In this way, any deformation can be represented by normal strains.

Next, we will start from where the nominal directions of strain are represented by element vectors $\mathbf{x}_1$, $\mathbf{x}_2$, and $\mathbf{x}_3$. Under the coordinate system, shear deformation

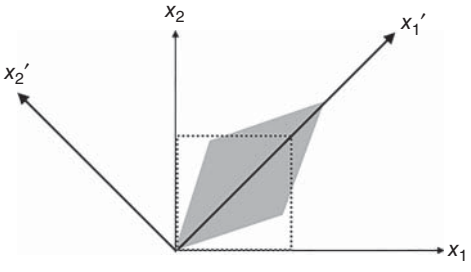

Figure 5.5 Shear strain can be regarded as a normal strain under an appropriate coordinate system.

is not generated on any surfaces, and only deformation in the normal direction is generated. Therefore, the amount of deformation in the nominal direction (δx_i) can be expressed as follows:

$$1 + \frac{\delta x_i}{x_i} = \lambda_i \text{ (constant)} \tag{5.12}$$

Here, λ_i is the elongation ratio with respect to the ith nominal direction (principal strain) and is related to the strain tensor (ε_{ij}) as follows:

$$\begin{pmatrix} \varepsilon_{11} & \varepsilon_{12} & \varepsilon_{13} \\ \varepsilon_{21} & \varepsilon_{22} & \varepsilon_{23} \\ \varepsilon_{31} & \varepsilon_{32} & \varepsilon_{33} \end{pmatrix} \mathbf{x}_1 = \lambda_1 \mathbf{x}_1 \tag{5.13}$$

Indeed, by solving Eq. (5.13) for a general $\mathbf{x}_i$ and λ_i, one can find a set of three $\mathbf{x}_i$ and λ_i pairs. This operation mathematically corresponds to finding eigenvalues/eigenvectors of the distortion tensor.

$$\begin{pmatrix} \varepsilon_{11} - \lambda & \varepsilon_{12} & \varepsilon_{13} \\ \varepsilon_{21} & \varepsilon_{22} - \lambda & \varepsilon_{23} \\ \varepsilon_{31} & \varepsilon_{32} & \varepsilon_{33} - \lambda \end{pmatrix} = 0$$

$$\{(\varepsilon_{11} - \lambda)(\varepsilon_{22} - \lambda)(\varepsilon_{33} - \lambda) + \varepsilon_{12}\varepsilon_{23}\varepsilon_{31} + \varepsilon_{13}\varepsilon_{21}\varepsilon_{32}\}$$
$$- \{\varepsilon_{13}(\varepsilon_{22} - \lambda)\varepsilon_{31} + \varepsilon_{23}\varepsilon_{32}(\varepsilon_{11} - \lambda) + (\varepsilon_{33} - \lambda)\varepsilon_{12}\varepsilon_{21}\} = 0 \tag{5.14}$$

Since $\varepsilon_{ij} = \varepsilon_{ji}$ because of its symmetry, it can be transformed as follows:

$$\lambda^3 - (\varepsilon_{11} + \varepsilon_{22} + \varepsilon_{33})\lambda^2 + (\varepsilon_{22}\varepsilon_{33} + \varepsilon_{33}\varepsilon_{11} + \varepsilon_{11}\varepsilon_{22} - {\varepsilon_{11}}^2 - {\varepsilon_{22}}^2 - {\varepsilon_{33}}^2)\lambda$$
$$+ \begin{vmatrix} \varepsilon_{11} & \varepsilon_{12} & \varepsilon_{13} \\ \varepsilon_{12} & \varepsilon_{22} & \varepsilon_{23} \\ \varepsilon_{13} & \varepsilon_{23} & \varepsilon_{33} \end{vmatrix} = 0 \tag{5.15}$$

This equation is a cubic equation of λ and has three real roots when $\lambda > 0$.

$$\lambda^3 - I_1\lambda^2 + I_2\lambda + I_3 = 0 \tag{5.16}$$

When substituting the three roots of Eq. (5.16) into Eq. (5.13), three vectors in the directions of the nominal strain ($\mathbf{x}_i$), which are called the principal axes, are obtained.

Let us summarize the process discussed here. For any deformation tensor, it is possible to determine three sets of principal axes ($\mathbf{x}_i$) and principal strain (λ_i). Since $\mathbf{x}_i$ is fixed if λ_i is determined, any deformation can be described by only three λ_i values. Since λ_i is a solution of Eq. (5.16), if I_1, I_2, and I_3 are determined, three λ_i values are also determined. In other words, the deformation is defined by I_1, I_2, and I_3 as shown as follows:

$$I_1 = \varepsilon_{11} + \varepsilon_{22} + \varepsilon_{33} = {\lambda_1}^2 + {\lambda_2}^2 + {\lambda_3}^2 \tag{5.17}$$

$$I_2 = \varepsilon_{22}\varepsilon_{33} + \varepsilon_{33}\varepsilon_{11} + \varepsilon_{11}\varepsilon_{22} - {\varepsilon_{11}}^2 - {\varepsilon_{22}}^2 - {\varepsilon_{33}}^2$$
$$= {\lambda_1}^2{\lambda_2}^2 + {\lambda_2}^2{\lambda_3}^2 + {\lambda_3}^2{\lambda_1}^2 \tag{5.18}$$

$$I_3 = \begin{vmatrix} \varepsilon_{11} & \varepsilon_{12} & \varepsilon_{13} \\ \varepsilon_{12} & \varepsilon_{22} & \varepsilon_{23} \\ \varepsilon_{13} & \varepsilon_{23} & \varepsilon_{33} \end{vmatrix} = {\lambda_1}^2{\lambda_2}^2{\lambda_3}^2 \tag{5.19}$$

Equations (5.17)–(5.19) are obtained by comparing Eqs. (5.15) and (5.16). Since I_i is identical for the deformations, it is called "invariant of deformation." I_i can be calculated from Eqs. (5.17)–(5.19) even if we use any set of strains (not the principal strains); determination of a set of invariants is much easier than determining the set of principal strains. The physical meanings of I_1, I_2, and I_3 are the average deformation ratio in one direction, the average change in surface area, and the volume change due to deformation. In other words, any deformation is defined by these three parameters.

5.2 Phenomenological Description of the Strain Energy Density Function

Energy is required to homogeneously deform an elastic body. The free energy stored in a unit volume is called the strain energy density function (W function). Because all deformations are defined by the invariants, the W function should be a function of the invariants ($W = W(I_1, I_2, I_3)$). Soft materials, such as gels and rubbers, have much lower elastic modulus values compared with their bulk modulus values, which indicates volumetric compression is difficult. Thus, they do not show apparent volumetric changes under moderate stress (incompressibility, $I_3 = 1$), and only two invariants (I_1 and I_2) determine the deformation. Based on this background, Mooney has proposed a W function as a polynomial function of $(I_1 - 3)$ and $(I_2 - 3)$ [1].

$$W = \sum_{i,j=0}^{\infty} C_{ij}(I_1 - 3)^i(I_2 - 3)^j \tag{5.20}$$

The subtraction of "3" from I_1 and I_2 comes from the initial condition ($I_1 = I_2 = 3$ in the initial undeformed condition). Because Eq. (5.20) has such large number of combinations, conventionally only some of terms are used. For example, if $C_{ij} = 0$ except for C_{10}, one obtains

$$W = C_{10}(I_1 - 3) \tag{5.21}$$

Equation (5.21) has the same function as the neo-Hookean model (Eq. (3.9)) derived from a molecular picture [2]. This equation is known to reproduce the mechanical properties of dilute gel. The W function consisting only of linear I_1 and I_2 terms is called the Mooney model [1].

$$W = C_1(I_1 - 3) + C_2(I_2 - 3) \tag{5.22}$$

Here, C_1 and C_2 are constants. Because the effect of the C_2 term is remarkable in a concentrated polymer network system such as rubber, the C_2 term is generally attributed to entanglements. Although the Moony model can reproduce the uniaxial stretching behavior of rubber to some extent, the results of the biaxial stretching test cannot be reproduced, as discussed later. To precisely reproduce the experimental results, higher-order terms are required. Thus, the Mooney model is not sufficient to reproduce a wide range of mechanical properties of polymer networks [3–7].

Here, we introduce two famous phenomenological W functions. One is the Ogden model, which is a function with power series of λ_x, λ_y, and λ_z [8].

$$W = \sum_n \frac{\mu_n}{\gamma_n}(\lambda_x{}^{\gamma_n} + \lambda_y{}^{\gamma_n} + \lambda_z{}^{\gamma_n} - 3) \tag{5.23}$$

The other is the Gent model [9], which takes into account the finite extensibility of the chain. Gent attempted to reproduce the strain hardening behavior due to the chain elongation effect by using a natural logarithm.

$$W = -\frac{G}{2}J_{\mathrm{m}} \ln\left(1 - \frac{I_1 - 3}{J_{\mathrm{m}}}\right) \tag{5.24}$$

Here, J_{m} is the value of $I_1 - 3$ at maximum extension. The relationship between nominal stress and the elongation ratio under uniaxial stretching is as follows:

$$\sigma = G(\lambda_x - \lambda_x{}^{-2})\left(1 - \frac{\lambda_x{}^2 - 2\lambda_x{}^{-1} - 3}{\lambda_{\mathrm{max}}{}^2 - 2\lambda_{\mathrm{max}}{}^{-1} - 3}\right)^{-1} \tag{5.25}$$

λ_{max} is the maximum elongation ratio under uniaxial stretching. When approaching $\lambda = \lambda_{\mathrm{max}}$, the stress diverges to infinity. Although the Gent model is a phenomenological model, it is focused on the finite extensibility of the network strands. From this viewpoint, this model is a semiphenomenological model with a molecular picture. These phenomenological models are very useful in discussing the relationship between stress and the elongation ratio without relying on a particular molecular picture.

5.2.1 Estimation of the Strain Energy Density Function

In Section 5.2, we introduced the neo-Hookean model and the Mooney model. They are the only models based on a simple assumption that the W function can be written as the sum of the invariants of the deformation tensor. Reproducing all the experimental results with these models is basically impossible. Therefore, it is also important to estimate the W function from the experimental results. Here, we describe a phenomenological method to estimate the W function from experimental results.

Uniaxial deformations, including stretching and compression, are among the most popular deformation modes. Indeed, many studies have investigated W functions based on these uniaxial deformation results. However, notably, such experimental results are insufficient to investigate W functions. The filled region in Figure 5.6 shows the physically accessible deformation range of I_1 and I_2 under isovolumetric deformation. Among all the deformation regions, uniaxial stretching, and compression cover only limited regions, which are indicated by a single solid line. Thus, an estimation of the W function based only on uniaxial experiments can be incorrect. Even the W functions that can reproduce the uniaxial stretching behavior cannot reproduce stress–strain curves for other deformations, including biaxial stretching. To estimate the W function

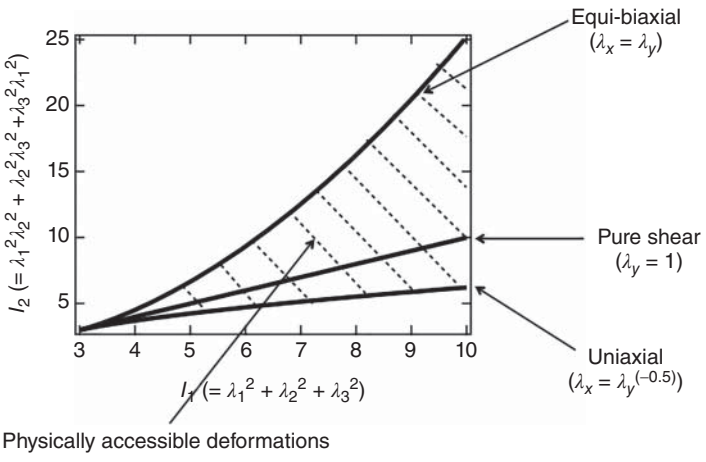

Figure 5.6 Relationships between I_1 and I_2 under isovolumetric deformation.

phenomenologically, stress–strain relationships in a wide range of deformations must be considered.

To estimate the W functions, equi-biaxial and pure shear deformations are often utilized. Biaxial stretching is a deformation mode in which a sample is isotropically stretched in two directions, the x and y directions ($\lambda_x = \lambda_y$). Under pure shear deformation, a sample is only stretched in the x direction, and initial dimension in the y direction ($\lambda_y = 1$) is maintained. The application of such a deformation seems difficult to achieve; it requires a biaxial stretching apparatus in which the sample is independently stretched along two axes.

The Rivlin–Saunder method is a method for estimating a W function based on various stress–strain curves. The method first estimates $\partial W/\partial I_1$ and $\partial W/\partial I_2$ with respect to the experimental values λ_x and λ_y according to Eq. (5.26). The values of $\partial W/\partial I_1$ and $\partial W/\partial I_2$ are plotted against I_1 and I_2, respectively. By integrating these equations with respect to I_1 and I_2, one can estimate W:

$$\frac{\partial W}{\partial I_1} = \frac{1}{2({\lambda_x}^2 - {\lambda_y}^2)}\left[\frac{{\lambda_x}^3\sigma_x}{{\lambda_x}^2 - (\lambda_x\lambda_y)^2} - \frac{{\lambda_y}^3\sigma_y}{{\lambda_y}^2 - (\lambda_x\lambda_y)^2}\right]$$
$$\frac{\partial W}{\partial I_2} = \frac{1}{2({\lambda_x}^2 - {\lambda_y}^2)}\left[\frac{\lambda_x\sigma_x}{{\lambda_x}^2 - (\lambda_x\lambda_y)^2} - \frac{\lambda_y\sigma_y}{{\lambda_y}^2 - (\lambda_x\lambda_y)^2}\right] \tag{5.26}$$

Figure 5.7 shows $\partial W/\partial I_1$ and $\partial W/\partial I_2$ for a poly dimethyl siloxane (PDMS) elastomer against $(I_1 - 3)$ and $(I_2 - 3)$. As shown in Figure 5.7, each partial differential forms a plane surface, suggesting that W can be described by the following power expansion up to the second order of $I_1 - 3$ and $I_2 - 3$:

$$W = C_{10}(I_1 - 3) + C_{01}(I_2 - 3) + C_{11}(I_1 - 3)(I_2 - 3) + C_{20}(I_1 - 3)^2 + C_{02}(I_2 - 3)^2 \tag{5.27}$$

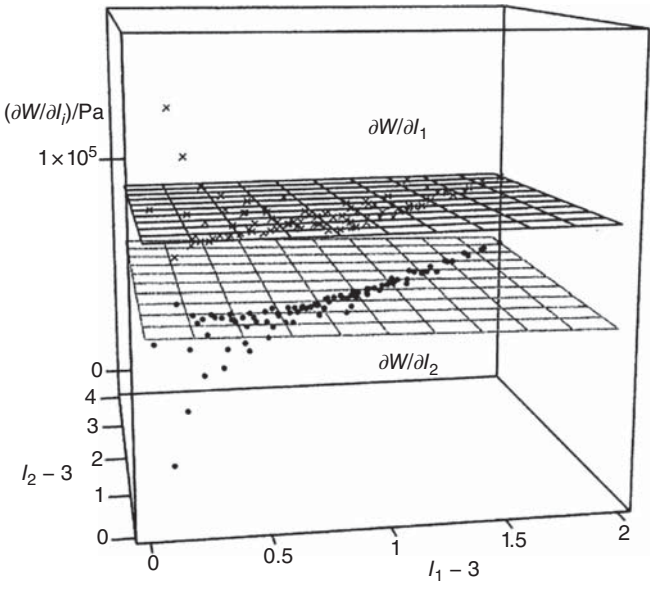

Figure 5.7 Partial differential quantity by I_1 and I_2 of the W function of a PDMS elastomer. Source: Kawamura et al. 2001 [28]. Reproduced with permission of American Chemical Society.

By substituting Eq. (5.27) into Eq. (5.26), the following equations are obtained:

$$\frac{\partial W}{\partial I_1} = C_{10} + C_{11}(I_2 - 3) + 2C_{20}(I_1 - 3)$$
$$\frac{\partial W}{\partial I_2} = C_{01} + C_{11}(I_1 - 3) + 2C_{02}(I_2 - 3) \tag{5.28}$$

Each coefficient can be determined from the slope and intercept of the plot in Figure 5.7. This result strongly suggests that general stress–strain curves cannot be reproduced by the neo-Hookean model or the Mooney–Rivlin model, and at least the second-order terms of I_1 and I_2 are necessary. In particular, the term I_2 generates a force acting in a direction (y or z axes) perpendicular to the stretching direction (x axis), which is not considered in conventional molecular models because it is difficult to take into account such cross-coupling effects in molecular models.

Biaxial stretching tests for polymer gels have been well studied by Urayama, and cross-couplings in gels with various structures have been discussed. A pure shear deformation (stretching in the x direction while maintaining the dimension in the y direction) is one of the best deformation modes for observing cross-coupling effects; the contribution of the cross-coupling can be observed as the stress along the y axis. Figure 5.8 shows the results of pure shear deformation of a slide-ring gel [10] with movable crosslinks, conventional polyacrylamide gel (PAAm gel) [10], and Tetra-PEG gel [11, 12]. The vertical axis shows the stress ratio (σ_y/σ_x), the nominal stress in the y direction is normalized by that in the x direction, and

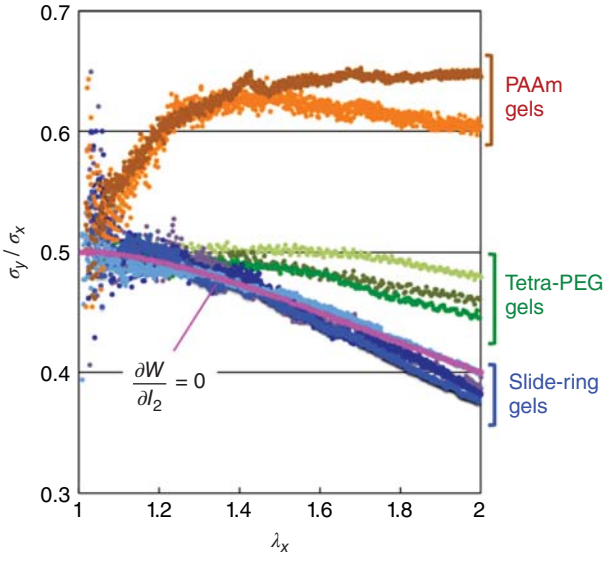

Figure 5.8 Stress ratio under pure shear deformation (σ_y/σ_x) against the elongation stress ratio in the x direction (λ_x). Source: Urayama 2016 [29]. Reproduced with permission of John Wiley and Sons.

the horizontal axis shows the elongation ratio in the x direction. The solid line in Figure 5.8 shows the prediction by the neo-Hookean model, where the W function consists only of the I_1 term $\left(\frac{\partial W}{\partial I_2} = 0\right)$. Indeed, all the models based only on I_1 show the same prediction as the neo-Hookean model. Thus, if there is no cross-coupling effect, the experimental data should be on this line.

For acrylamide gels, the stress ratio was far from what was predicted by the I_1-based model, suggesting that the contribution of the I_2 term in the W function is significant. This deviation is expected to be due to the heterogeneity of PAAm gels, including the entanglements. On the other hand, the stress ratio of the Tetra-PEG gel is much lower than that of PAAm gels but is higher than the ratio predicted by the model. Furthermore, the upward deviation increased with increasing polymer concentration. Based on this analysis, the effect of cross-coupling disappears when extrapolating the network concentration to 0. Thus, the cross-coupling in the Tetra-PEG gel is attributed to the nonideality of the networks, such as the excluded volume effect of the network strands. For the slide-ring gel, the stress ratio was consistent with the model prediction regardless of the crosslinking density. This behavior has been attributed to the fact that the crosslinking points move, which homogeneously disperses the stress, attenuating the cross-coupling. Although recent works have shown that the effect of cross coupling depends on the crosslinking structure, the subject has not been fully elucidated. Discussions about the interpretation of the physical meaning of phenomenally derived W functions are ongoing.

5.3 Molecular Models for the Strain Energy Density Function

In this section, we introduce some representative strain energy density functions based on molecular pictures. The W functions of the molecular models are generally estimated by setting the elastic free energy of a single chain under certain assumptions and integrating each free energy. Notably, the molecular models introduced here show only limited agreement with experimental results, and there are no models that can accurately reproduce a series of experimental results, including biaxial stretching data. This disagreement, however, does not diminish the importance of molecular models because the ultimate goal is to clarify the molecular picture. Therefore, it is important to know the essence of the major molecular models.

5.3.1 Neo-Hookean Model

Pioneering works in modeling the elasticity of rubber were conducted by Kuhn, and these models were later expanded to large deformation regions. Among the series of models, we introduce the neo-Hookean model, which is the simplest model [1, 13, 14]. This model is based on the following assumptions:

i. The polymer network has ν chains per unit volume. Here, the chain refers to the polymer segment between the crosslinks.
ii. The mean square end-to-end distance of all chains in the undeformed state is the same as that of the uncrosslinked free chains.
iii. Deformations are not accompanied by volume changes.
iv. The deformation ratio of the bulk corresponds to that of microscopic chains (affine deformation).
v. The conformation of each chain is described by Gaussian statistics, and the total entropy of the network can be described as the sum of the entropies of the chains.

Under these assumptions, the entropy change due to deformation is calculated as follows. The cubic unit lattice is deformed by λ_x, λ_y, and λ_z in the x, y, and z directions, respectively. From Eq. (3.8), the entropy change, Δs, of a single chain by deformation is given as follows:

$$\Delta s = s - s_0 = -k\frac{3}{2Na^2}\left\{\left\{{\lambda_1}^2 - 1\right\}{x_0}^2 + \left\{{\lambda_2}^2 - 1\right\}{y_0}^2 + \left\{{\lambda_3}^2 - 1\right\}{z_0}^2\right\} \quad (5.29)$$

According to assumption (v), the total entropy change in ν chains can be described as a simple sum of Eq. (5.29) for each chain. The total entropy change, ΔS, can be written as follows:

$$\Delta S = \sum \Delta s = -k\frac{3}{2Na^2}\left\{\left\{{\lambda_1}^2 - 1\right\}\sum {x_0}^2 + \left\{{\lambda_2}^2 - 1\right\}\sum {y_0}^2 + \left\{{\lambda_3}^2 - 1\right\}\sum {z_0}^2\right\} \quad (5.30)$$

$\sum {x_0}^2$ refers to the sum of the end-to-end square distances in the x_0 direction of ν chains. Because the undeformed chain is isotropic, $\sum {x_0}^2$ is written as follows:

$$\sum {x_0}^2 = \sum {y_0}^2 = \sum {z_0}^2 = \frac{1}{3}\sum {r_0}^2 \quad (5.31)$$

Assuming that the root-mean and the mean square are equal, the following equation is obtained:

$$\sum {r_0}^2 = \nu \overline{{r_0}^2} \tag{5.32}$$

Here, $\overline{{r_0}^2}$ is the mean square length of the chain. By substituting Eqs. (5.31) and (5.32) into Eq. (5.30), one obtains the following equation:

$$\Delta S = -\frac{\nu k}{2Na^2} {r_0}^2 \left\{ {\lambda_1}^2 + {\lambda_2}^2 + {\lambda_3}^2 - 3 \right\} \tag{5.33}$$

Since the relationship ${r_0}^2 = a^2 N$ is obtained from assumption (ii), Eq. (5.33) is converted to Eq. (5.34);

$$\Delta S = -\frac{1}{2} \nu k ({\lambda_1}^2 + {\lambda_2}^2 + {\lambda_3}^2 - 3) \tag{5.34}$$

This expression does not contain N, indicating that the entropy change in the polymer network does not directly depend on the length of the chains, which is another indication that even if chains of different lengths coexist in the gel, the equation holds. Thus, this equation is applicable to polymer gels formed from random crosslinking processes. Using Eq. (5.34), we can directly estimate the Helmholtz energy of the whole system. Assuming that there is no change in internal energy due to deformation, the change in the free energy, W, due to deformation can be written as $W = -T\Delta S$. Thus, the following equation is obtained:

$$W = \frac{1}{2} \nu k T ({\lambda_1}^2 + {\lambda_2}^2 + {\lambda_3}^2 - 3) \tag{5.35}$$

Equation (5.35) can be rewritten as follows:

$$W = \frac{G}{2} ({\lambda_1}^2 + {\lambda_2}^2 + {\lambda_3}^2 - 3) \tag{5.36}$$

$$G = \nu k T \tag{5.37}$$

Although the derivations are different, these equations are the same as Eqs. (3.12) and (3.15).

5.3.2 Inverse Langevin Model

The neo-Hookean model assumes that the segment distribution *always* follows the Gaussian distribution. Thus, this model cannot be applied to highly stretched chains, which do not obey Gaussian statistics. Indeed, upward deviations have been observed in many experimental results, and this effect is called the finite extensibility effect. The pioneering statistical model that considers the finite extensibility effect is the inverse Langevin model proposed by Kuhn and Grün [15]. They modeled the relationship between the stress and the segment orientation based on analogy to the relationship between an applied electric field and the dipole orientation.

Figure 5.9 shows a freely jointed chain consisting of n bonds with $+q$ and $-q$ charges at the ends. In the absence of an external force, these segments are randomly distributed, and there is no correlation between adjacent segments. When

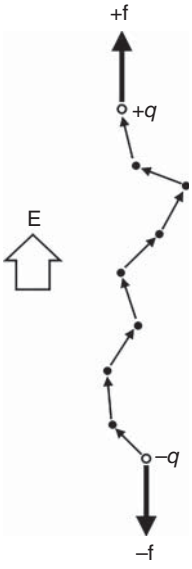

Figure 5.9 Deformation of polymer chains with a charged group at each end under an electric field.

an electric field, E, is applied in the z direction, forces of $\mathbf{f} = q\mathbf{E}$ and $-\mathbf{f} = q\mathbf{E}$ are applied to the positive and negative charges, respectively.

The energy stored in the chain (U) is proportional to the end-to-end vector ($\mathbf{R}$).

$$U = -q\mathbf{E} \cdot \mathbf{R} = -\mathbf{f} \cdot \mathbf{R} = -\mathbf{f} \cdot R_1 \tag{5.38}$$

R_1 is the normal in the x_1 direction of $\mathbf{R}$. Since the number of chain conformations, ω, follows the Boltzmann distribution, it can be written as follows:

$$\omega = \exp\left(-\frac{U}{kT}\right) \tag{5.39}$$

Thus, the distribution function, Ω, corresponding to the sum of all the conformations is expressed as follows:

$$\Omega = \sum_{\text{states}} \omega = \sum_{\text{states}} \exp\left(\frac{fR_1}{kT}\right) \tag{5.40}$$

In the case of a freely jointed chain, the number of conformations is determined by the variety of bond angles. Given the spherical coordinates for each bond, Ω is represented using two deflection angles, θ and φ.

$$\Omega = \sum_{\text{states}} \exp\left(\frac{fR_1}{kT}\right) = \int \exp\left(\frac{fR_1}{kT}\right) \prod_{i=1}^{N} \sin\,\theta_i \, \mathrm{d}\theta_i \, \mathrm{d}\varphi_i \tag{5.41}$$

Additionally, R_1 is expressed using the bond length a and θ.

$$R_1 = \sum_{i=1}^{N} a \cos\theta_i \tag{5.42}$$

By substituting Eq. (5.42) into Eq. (5.41), one obtains the following relationship:

$$\begin{aligned}\Omega &= \int \exp\left(\frac{fa}{kT}\sum_{i=1}^{N}\cos\,\theta_i\right)\prod_{i=1}^{N}\sin\,\theta_i\,\mathrm{d}\theta_i\,\mathrm{d}\varphi_i \\ &= \left[\int_0^{\pi} 2\pi\,\sin\,\theta_i\,\exp\left(\frac{fa}{kT}\cos\,\theta_i\right)\mathrm{d}\theta_i\right]^N \\ &= \left[\frac{2\pi}{fa/kT}\left\{\exp\left(\frac{fa}{kT}\right)-\exp\left(-\frac{fa}{kT}\right)\right\}\right]^N \end{aligned} \tag{5.43}$$

Combining Eq. (5.44) with Eq. (5.43) provides Eq. (5.45):

$$\sinh x = \frac{\exp(x)-\exp(-x)}{2} \tag{5.44}$$

$$\Omega = \left[\frac{4\pi\sinh\left(\frac{fa}{kT}\right)}{\frac{fa}{kT}}\right]^N \tag{5.45}$$

Based on this distribution function, the Gibbs free energy ($F = -kT\ln\Omega$) can be expressed as a function of f.

$$F = -kNT\left[\ln\left(4\pi\sinh\left(\frac{fa}{kT}\right)\right)-\ln\left(\frac{fa}{kT}\right)\right] \tag{5.46}$$

The average end-to-end distance $\langle R\rangle$ is calculated as a derivative of F with respect to f, which gives the following equation:

$$\begin{aligned}\langle R\rangle &= -\frac{\partial F}{\partial f} = \frac{\partial}{\partial f}kNT\left[\ln\left(4\pi\,\sinh\left(\frac{fa}{kT}\right)\right)-\ln\left(\frac{fa}{kT}\right)\right] \\ &= kNT\left\{\frac{1}{4\pi\,\sinh\left(\frac{fa}{kT}\right)}4\pi\,\cosh\left(\frac{fa}{kT}\right)\frac{a}{kT}-\frac{1}{fa/kT}\frac{a}{kT}\right\} \\ &= bN\left\{\coth\left(\frac{fa}{kT}\right)-\frac{1}{fa/kT}\right\}\end{aligned} \tag{5.47}$$

The term inside of the parentheses is the Langevin function (Eq. (5.48)):

$$\mathcal{L}(x) = \coth(x) - \frac{1}{x} \tag{5.48}$$

$$\mathcal{L}\left(\frac{fa}{kT}\right) = \frac{\langle R\rangle}{aN} \tag{5.49}$$

Given that $aN = R_{\max}$, the force can be written as a function of the elongation ratio:

$$f = \frac{kT}{a}\mathcal{L}^{-1}\left(\frac{\langle R\rangle}{R_{\max}}\right) \tag{5.50}$$

This equation is called the inverse Langevin model, and its shape is shown in Figure 5.10 with that of the Gaussian chain (Eq. (1.37)). Although $R_{\max}$ is

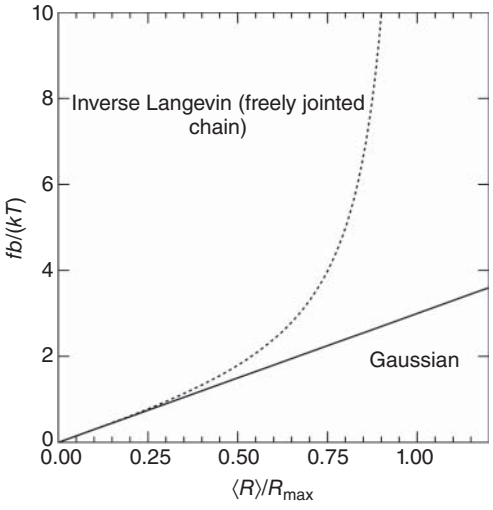

Figure 5.10 Relationship between force and strain of the Gaussian and Langevin chains.

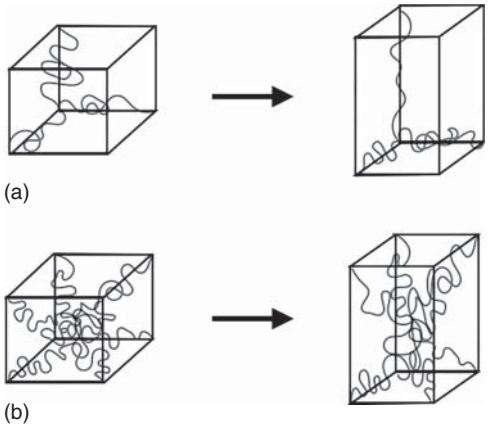

Figure 5.11 Schematic illustration of the (a) three- and (b) eight-chain models.

not included in Eq. (1.37), R_{max} is set to aN when normalizing R. In the small deformation region, both the Langevin and Gaussian chains show a linear relationship between stress and the elongation ratio (Hooke's law). The Gaussian chain shows a linear relationship over a wide range of deformations, even at $R/R_{max} > 1$. On the other hand, strain hardening is observed in the Langevin chain, and the values diverge at $R/R_{max} = 1$.

Since the entropy of a single chain is successfully estimated, the entropy of a network can be calculated as a simple sum of the contributions of each network strand. Unlike Gaussian chains, in the case of Langevin chains, the arrangement of the network strands influences the entropy of the network. The popular arrangements are the three-chain model [16] and the eight-chain model [17] (Figure 5.11).

Although we do not explain the calculation process in detail, we note here that the arrangements of chains are simply for calculation purposes. Notably, these models do not truly represent the tri-functional or octa-functional crosslinking systems. The arrangement defined here is only virtual, and it allows the effective

deformation of chains during a macroscopic deformation to be estimated. The three-chain model develops Eq. (5.50) for three dimensions. In this model, the chains are equally divided in the orthogonal coordinate directions of the x, y, and z axes, and each contribution is calculated; two of the three chains are assumed to be compressed during stretching. On the other hand, the eight-chain model considers eight chains extending from the center toward each vertex of a cube; all the chains are deformed in the same manner. The stress–elongation relationships in uniaxial deformation as predicted from the three-chain model (Eq. (5.51)) and eight-chain model (Eq. (5.52)) are shown as follows:

$$\sigma = G\sqrt{N}\left(\lambda_1 \mathscr{L}^{-1}\left(\frac{\lambda_1}{\sqrt{N}}\right) - {\lambda_1}^{-2}\mathscr{L}^{-1}\left(\frac{{\lambda_1}^{-2}}{\sqrt{N}}\right)\right) \tag{5.51}$$

$$\sigma = GN\mathscr{L}^{-1}\left(\frac{\lambda_{\text{chain}}}{\sqrt{N}}\right)\left(\frac{{\lambda_1}^2 - {\lambda_1}^{-1}}{\lambda_{\text{chain}}}\right)$$

$$\lambda_{\text{chain}} = \frac{1}{\sqrt{3}}({\lambda_1}^2 + {\lambda_2}^2 + {\lambda_3}^2)^{1/2} \tag{5.52}$$

5.4 Scaling for Large Deformation

In Section 5.3, we introduced the estimation of the stress–elongation relationship based on W functions. Despite the qualitative difference between phenomenological and molecular models, both have drawbacks that require further discussion. The molecular models do not show complete agreement with experimental results, while the phenomenological models do not provide the molecular interpretation. Thus, at this stage, neither approach has achieved great success. In this section, we coarse-grain the problem and introduce the scaling approach to the large deformations.

Here, we apply the scaling for the stretching of a single polymer chain as discussed in Chapter 1 to polymer networks. In Section 1.3.3, a real chain was stretched, and the relationship between the blob size, ξ, and the number of segments in the blob, g_{p}, is given by Eq. (1.55):

$$\xi \approx a{g_{\text{p}}}^{3/5} \tag{1.55}$$

The power of 3/5 reflects that the fractal dimension of the real chain is 5/3. Thus, Eq. (1.55) can be expanded to general chains with fractal dimension D.

$$\xi \approx a{g_{\text{p}}}^{1/D} \tag{5.53}$$

A process similar to what was discussed in Chapter 1 provides us with the following relationship for a strongly stretched polymer chain:

$$f \approx \frac{kT}{a}\left(\frac{R}{aN}\right)^{\frac{1}{D-1}} \tag{5.54}$$

Here, f is the force applied per single chain and corresponds to the nominal stress, σ, which is the force per unit cross-sectional area in the network. On the

other hand, the elongation ratio R/aN is not directly correlated to the uniaxial elongation ratio, λ, of the network; the situation in which all partial chains are stretched by a factor of λ is realized only by the isotropic volume change by a factor of λ^3 because the network strands are somewhat compressed in the direction perpendicular to the stretching direction in the isovolumetric deformation.

To account for this feature, we need to return to the W function. Here, we assume that the W function of the polymer network has the same scaling as the neo-Hookean model, which is the simplest model ($W \sim I_1$). When one assumes isovolumetric and isotropic deformation, the following equation is obtained:

$$W(I_1) \sim I_1 \sim ({\lambda_1}^2 + {\lambda_2}^2 + {\lambda_3}^2 - 3) \sim (\lambda^2 + 2\lambda^{-1} - 3) \tag{5.55}$$

The stress σ is determined as a partial derivative of W with respect to λ.

$$\sigma = \frac{\partial W}{\partial \lambda} \sim (\lambda - \lambda^{-2}) \tag{5.56}$$

According to this result, the stress is proportional to $(\lambda - \lambda^{-2})$ in the region where the effect of the finite extensibility is negligible. This result is similar to the results obtained from Eqs. (1.48) and (1.52), which are the scaling rules describing the extension behavior of ideal and real chains, respectively. When extracting only the parts of interest from Eqs. (1.48) and (1.52), the following scaling is obtained:

$$f \sim R \sim \lambda \tag{5.57}$$

This equation indicates that the force, f, is proportional to the elongation ratio, λ. That is, the λ term for a single chain corresponds to that of $(\lambda - \lambda^{-2})$ for a polymer network. The λ^{-2} term reflects the correction of the effect of compression in the perpendicular direction.

As a result, by replacing (R/aN) in Eq. (5.54) with $(\lambda - \lambda^{-2})$ and f with σ, the scaling rule for a single polymer chain is converted to that for a polymer network.

$$\sigma \sim \left(\lambda - \lambda^{-2}\right)^{\frac{1}{D-1}} \tag{5.58}$$

Using Eq. (5.58), the stress–strain behavior in the large deformation region can be predicted based on the fractal dimension of the network strands. Indeed, a power law was observed in several polymer gel and rubber systems and was well reproduced with reasonable fractal dimensions [18–20].

5.5 Fracture Behavior of Polymer Gels

In this section, we have discussed the changes in stress under deformation. A polymer gel cannot be stretched infinitely and breaks with a certain degree of stretching, which has not been explicitly discussed thus far. Some models, such as the Gent model and the inverse Langevin model, have the maximum elongation ratio, λ_{max}, as a parameter, while many models, such as the Mooney model, do not have this parameter. One of the reasons for the absence of λ_{max} is that introducing the higher-order terms of I_1 and I_2 is sufficient for "only reproducing the stress–elongation curve." Notably, there are subtle differences between λ_{max} set to reproduce the stretching curve and λ_{max} estimated experimentally as

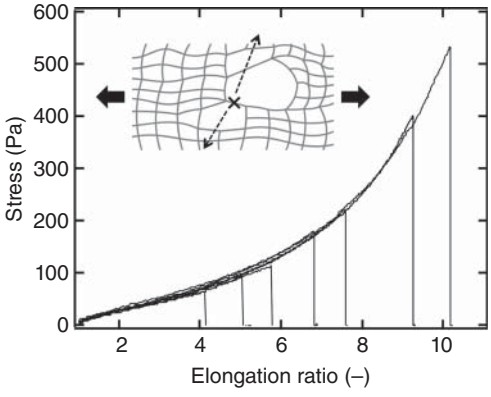

Figure 5.12 Stress–elongation curves of Tetra-PEG gel prepared under the same conditions ($n = 7$).

the breaking point. To capture the nuance, we show the stress–elongation curves of seven gels fabricated from the same condition (Figure 5.12). The stress–strain curves are almost identical. Thus, one representative λ_{max} is enough to reproduce the curve with a model. On the other hand, the actual fracture points are scattered. In contrast to λ_{max} for reproducing the stress–elongation curve, it is difficult to specify a value of λ_{max} that indicates at what point the gel breaks, which is practically important because conventional polymer gels are brittle.

In general, fractures of solid materials can be mainly divided into two groups. One is called "ductile fracture," which conventionally shows large deformation before the fracture. Ductile fracture features a large plastic deformation observed as a residual strain and a permanent set. Iron is a representative material that shows ductile fracture. The other is "brittle fracture" in which there is little or no plastic deformation before the fracture. Glasses or ceramics are representative materials showing brittle fracture. Another feature of brittle materials is the large variation in fracture points. Although polymer gels can be substantially deformed, they conventionally show brittle fracture. One of exceptions is the "double network gel" developed by Gong and Kurokawa, which solved the inevitable problem of hydrogels. Although we do not mention the details here, please refer to the papers published by these researchers [21, 22]. Here, we discuss brittle polymer gels showing λ_{max} values that vary substantially. The models predicting practical fracture points are completely different from the discussion based on W functions. Hereafter, we introduce the Griffith model and the Lake–Thomas model as representative models of fracture.

5.5.1 Griffith Model

A fracture in a brittle material can be rephrased as a process creating two or more new surfaces from one solid with external work. When an external force is applied to an elastic body with a crack, the crack propagates gradually. During crack propagation, the strain energy of the elastic body decreases and corresponds to the surface energy of the newly formed surface. In 1921, Griffith hypothesized that fracture occurs at the point where the decrease in elastic strain energy and the increase in surface energy of the newly formed surface are equal [23]. By

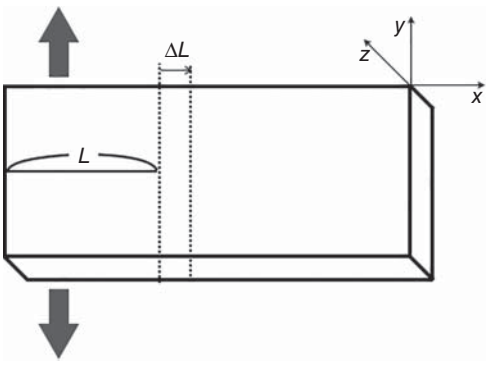

Figure 5.13 Elastic body with a crack of length *L*. Cracks propagate along the *x* axis.

releasing energy while maintaining the equilibrium between the strain energy and the surface energy, the crack propagates, resulting in macroscopic destruction.

The conditions for material fracture are determined from the energy needed to propagate a crack with length, L, by ΔL (Figure 5.13). When the crack propagates by ΔL, the surface energy of the newly formed surface (U_{surf}) is represented as follows:

$$U_{\text{surf}} = 2\gamma \Delta L \tag{5.59}$$

Here, γ is the surface energy per unit area, and the coefficient "2" indicates that two surfaces (upper and lower) are formed. On the other hand, the released elastic strain energy (U_{el}) is represented as follows:

$$U_{\text{el}} = \frac{\Delta L^2 \pi \sigma}{4E} \tag{5.60}$$

Here, σ is the external force, and E is the Young's modulus. Crack propagation is achieved when the decrease in the elastic strain energy and the increase in the surface energy of the newly formed surface are balanced.

$$\frac{\mathrm{d}U_{\text{surf}}}{\mathrm{d}L} = \frac{\mathrm{d}U_{\text{el}}}{\mathrm{d}L} \tag{5.61}$$

The minimum stress required for a crack propagation σ_0 is calculated by substituting Eqs. (5.59) and (5.60) into Eq. (5.61).

$$\sigma_0 = \left(\frac{4\gamma E}{\pi L}\right)^{1/2} \tag{5.62}$$

Griffith mentioned "cracks start to propagate when an external force σ_0 is applied to a brittle material with a crack of length L."

5.5.2 Lake–Thomas Model

The Griffith model is a model based on thermodynamics, and it is still widely used today. Although the Griffith model is undoubtedly correct as a basic formula, the fracture energy of a polymeric material such as natural rubber is much larger than that predicted by the model. In 1967, Lake and Thomas proposed that the problem is ignorance of the molecular structure of polymers in the vicinity of

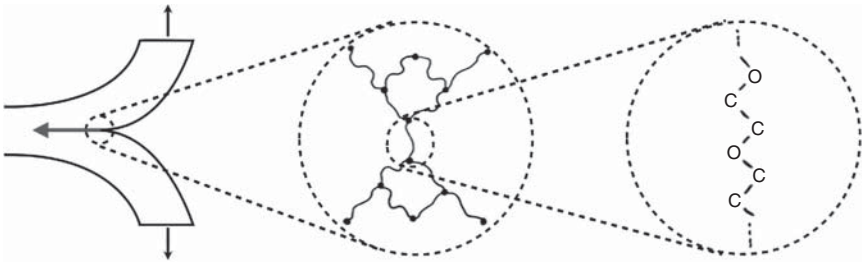

Figure 5.14 Schematic picture of the Lake–Thomas model.

the crack, and they estimated the fracture energy from "the energy required to break the partial chain at the crack tip" [24]. The essence of the Lake–Thomas model is "one cannot stretch only a specific chemical bond in a polymer chain by macroscopic deformation."

Here, we consider a situation in which there is apparently a polymer network in the vicinity of a crack tip (Figure 5.14). There are many network strands in the plane in which the crack will propagate. Thus, to propagate the crack, all the partial chains crossing the section must be broken. Let us focus on one partial chain crossing the section. An energy of approximately 400 kJ/mol, which is the approximate binding energy of a single bond, seems to be sufficient. However, now we simply extend the network strand and thus cannot concentrate the energy only on certain bonds. Instead, we can only stretch all bonds in the strands uniformly. Thus, the strand is cleaved when each bond stores an energy equivalent to the bond energy of the weakest bond, and the weakest bond then breaks; all bonds must be extended to some extent to break a bond. Based on the preceding discussion, the energy required to break a strand is represented as NU, where U is the bond energy of the weakest bond, and N is the degree of polymerization of a strand. Because typical degrees of polymerization are on the order of 100, the energy required to break a strand is much higher than that for a bond.

Next, let us expand this view slightly and consider other strands directly connected to the fracturing chain. Similarly, it is also impossible to fully extend only one strand without influencing strands that are directly connected. It is reasonable to think that the connected strands are also stretched to some extent. In reality, the force is most concentrated on the partial chain at the crack tip and decays as the distance increases. In a region sufficiently far from the tip, the deformation is the same as that in the bulk. For simplicity, we assume that a uniform stress concentration occurs only in a region with a certain length L and that other regions have the same deformation as that in the bulk. Then, the number of chains that are ultimately stretched is νL, which is obtained by multiplying the number density of network strands, ν, by the displacement length, L. (Note that the dimensions of cross section are originally divided because it is calculated per cross-sectional area.) As a result, the energy required to propagate a crack, T_0, is obtained by multiplying the number of network strands that are ultimately stretched by the energy needed to break a strand.

$$T_0 = (3/8)^{1/2} \nu LNU \tag{5.63}$$

Originally, L is roughly considered as the length of a strand, and the fracture energy of rubber has been well reproduced. When we assume that the network strand is an ideal chain, the length scales as $L \sim N^{1/2}$. Given that $G \sim \nu \sim \phi/N \sim N^{-1}$ following the scaling of the elastic modulus (in the case of rubber, $\phi = 1$), the following scaling relationship is established:

$$T_0 \sim \nu N^{1/2} N \sim N^{1/2} \sim G^{-1/2} \tag{5.64}$$

This scaling suggests that toughness decreases with increasing stiffness. This scaling has been validated experimentally for rubbers [25]. Recently, the exact form of Eq. (5.63) was validated experimentally for Tetra-PEG gel; L was approximately the end-to-end distance of a network strand [26, 27].

5.6 Mesh Size Estimated from Elastic Modulus and Finite Extensibility

We introduce a study investigating the correlation between mesh sizes and finite extensibilities. In Section 5.6, we introduced a methodology to estimate the mesh size from the elastic modulus. The estimated mesh size can be used to predict other physical properties. For example, when the mesh size increases, the extensibility is expected to increase according to the Kuhn model (see Section 1.2.3); in other words, soft gels are expected to show high extensibilities. If this estimation is always correct, large deformation behavior can be predicted based on the small deformation behavior.

Among the methods for estimating the mesh size from the elastic modulus, the simplest one is using the affine network model (assumption 1).

$$G = \nu k_B T \tag{3.15}$$

By using this equation, the density of network strands ν (m^{-3}) is estimated from the elastic modulus. When we assume that "all constitutive polymers act as network strands" (assumption 2), the following equation holds:

$$\nu = \frac{c}{m_{mono} N_c} N_A \tag{5.65}$$

Here, c (g/m^3) is the polymer concentration in the gel, m_{mono} (g/mol) is the molecular weight per monomeric unit, and N_A is Avogadro's number (mol^{-1}). According to Eqs. (3.15) and (5.65), N_c (g/mol), which is the average degree of polymerization of network strands, can be estimated from G.

Assuming that "the network strands behave as ideal chains having monomer units as segments" (assumption 3), the mesh size (r_{mesh}) can be calculated with Eq. (5.66):

$$r_{mesh} = a {N_c}^{1/2} \tag{5.66}$$

Notably, these three assumptions are fairly ideal and may differ from reality. For example, if the phantom network model (Eq. (3.35)) is used instead of the affine network model, the number of network strands in a four-branched network is estimated to be approximately twice as high. The presence of dangling chains

is not consistent with assumption 2. Of course, network strands are not always ideal chains, which is not consistent with assumption 3. Although such problems exist, this method is often used because of its simplicity. The essential problem is whether the mesh sizes estimated from the elastic modulus correctly correlate with other physical properties, such as extensibility and permeability. In the following, we introduce a study investigating the correlation between the elastic modulus and the extensibility.

The authors compared the elastic modulus and the extensibility for a Tetra-PEG gel. Tetra-PEG gel, which is composed of polyethylene glycol (Tetra-PEG) with a tetra-armed structure (Figure 5.15), is prepared by mixing solutions of two Tetra-PEG precursors with mutually reactive end groups. Because many data have suggested that Tetra-PEG gels have extremely homogeneous network structures, they are promising model systems for examining theoretical models. Furthermore, when the Tetra-PEG gel was prepared near c^* of the prepolymer, the elastic modulus corresponds well with the predictions of the tree-like approximation and the phantom network model (see Sections 3.3.2 and 3.4.2). By changing the connectivity of the Tetra-PEG gel prepared near c^*, at least assumption 1 (applicability of the phantom network model) holds, and we can focus on assumptions 2 and 3.

Figure 5.16a shows the elastic modulus, G, as a function of the connectivity, p, of the Tetra-PEG gel. The connectivity was determined from the reaction conversion between the ends of the four-armed precursors, which was directly measured spectroscopically. The reduction of p led to a decrease in G even though the polymer concentration was constant. According to assumption 2, N_c can be estimated from G using Eq. (3.35) based on the tree-like approximation. Figure 5.16b shows the calculated values of N_c as a function of p. N_c increased by a factor of approximately 3 due to the decrease in p. The classical Kuhn model predicts that N_c and the maximum elongation ratio (λ_{max}) have a scaling relationship of $\lambda_{max} \sim {N_c}^{1/2}$. Therefore, based on the previously mentioned estimation, an increase in N_c likely leads to an increase in λ_{max}.

Next, we experimentally estimated λ_{max} of these gels. Indeed, the direct measurement of λ_{max} is generally difficult because λ_{max} fluctuates greatly among samples, as discussed in Section 5.5. Therefore, we estimated λ_{max} based on the shape of the stress–elongation curves. When we assume that network strands behave

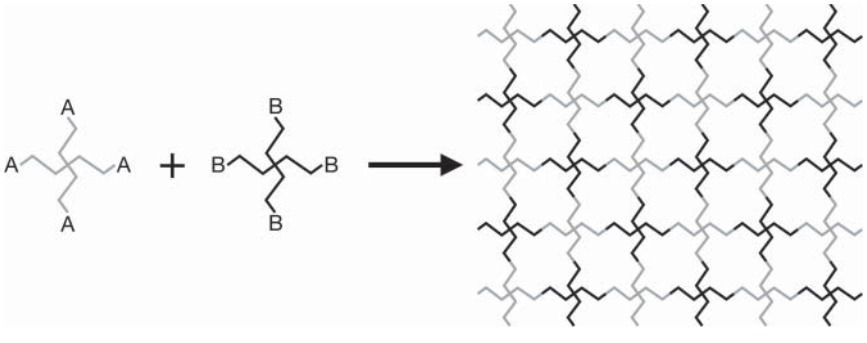

Figure 5.15 Schematic illustration of a Tetra-PEG gel.

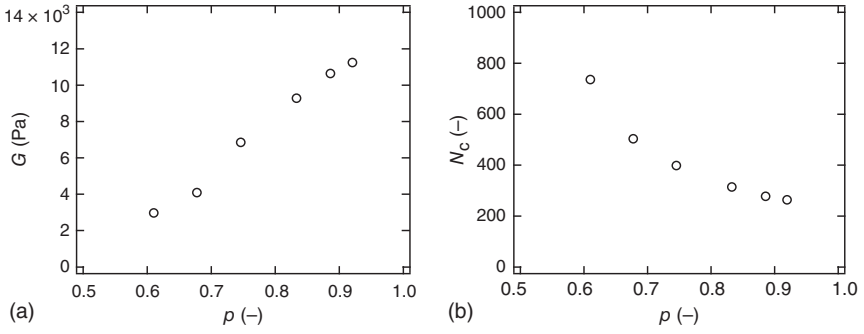

Figure 5.16 (a) Elastic modulus *G* as a function of *p*. (b) Degree of polymerization of network strands (*N*) estimated by different methodologies.

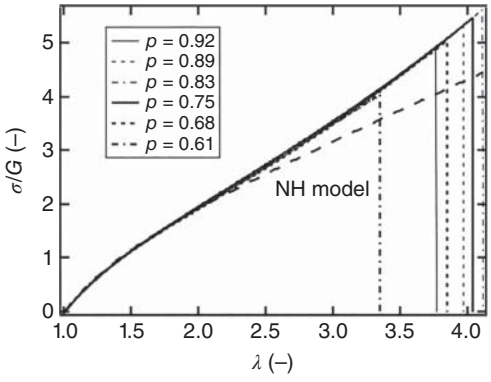

Figure 5.17 Normalized stress–elongation curves of Tetra-PEG gels with various *p*.

as ideal chains and are infinitely stretchable, the stress–strain curve can be represented by the neo-Hookean model.

$$\sigma = G(\lambda - \lambda^{-2}) \tag{3.14'}$$

However, in reality, the lengths of the network strands are finite, and the conformation changes from the ideal chain to the stretched conformation along the stretching direction. As a result, the stress–strain curve deviates upward from the values predicted using Eq. (3.14′).

Figure 5.17 shows the stress–strain curves of gels with different *p*. Here, to ignore the change in elastic modulus and focus on the deviation from Eq. (3.14′), we normalized the stress by the elastic modulus. In contrast to the aforementioned prediction, there is no significant difference in the shape of the stress–strain curves due to differences in connectivity. The elastic modulus and stretchability are completely decoupled in this system. This result can be attributed to the failure of assumptions 2 or 3. Because the difference in the chain conformation cannot explain this breakage, assumption 2 should be discarded, i.e. not all constitutive polymers act as network strands.

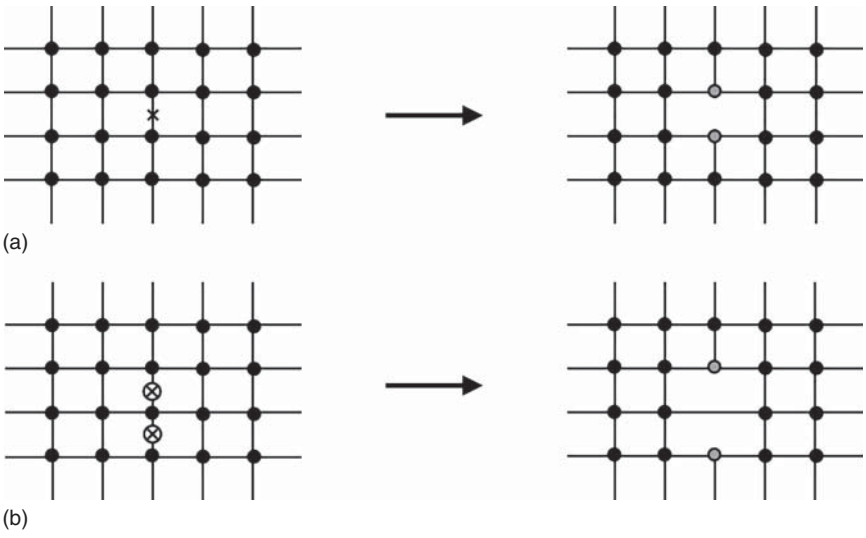

Figure 5.18 (a) Structural changes in a network following strand cleavage and (b) that in a network in which two neighboring strands are cleaved (black circle, tetra-functional crosslink; gray circle, tri-functional crosslink; cross, breakage site).

These experiments reproduced the process in which defects were gradually introduced into a regular network, where assumption 2 is likely to fail. Figure 5.18a shows a schematic illustration of the structural changes in a network following strand cleavage. The scission of a strand generates two dangling chains, and two tetra-functional junctions are converted into two tri-functional junctions, which can still act as active crosslinks. This event only decreases the number of elastically effective chains, ν, and does not change N_c. This conjecture is consistent with the experimental result that the maximum elongation ratio, which should be a function of the strand length, does not depend on the connectivity.

N_c increased when defects were further introduced and adjacent strands were broken, as shown in Figure 5.18b. This discussion is similar to the percolate network model introduced in Section 3.4.1 and corresponds to the region $p > 0.75$ in the tetra-functional network structure.

As described earlier, when connectivity is relatively high, the strand length does not change with the introduction of defects and does not affect the extensibility. This result demonstrates the risks of blind acceptance of the assumption that "all constitutive polymers act as network strands." Under this assumption, we tend to overestimate the value of N_c because the dangling chains, which do not function effectively in a network, are assumed to function as effective network strands. Of course, this method is important due to its convenience, and the mesh size predicted by this method roughly predicts the diffusion behavior of substances with sizes similar to the mesh size. However, it is also important to know the limitations of this system.

Column 5: Linear Viscoelasticity and Nonlinear Viscoelasticity

Viscoelasticity measurement is a powerful tool for understanding the dynamics and properties of polymer gels. The viscoelasticity measurement introduces an anisotropy to the material by strain (or stress) and then observes the recovery process with a characteristic time, which is related to a molecular motion in the material. Therefore, the magnitude of applied strain (or stress) is an important factor, and viscoelasticity is categorized into "linear" and "nonlinear" depending on the magnitude.

Linear viscoelasticity measurement is a method of observing the viscoelastic response under a small strain (or stress). Since the applied strain hardly changes the structure of the material, the energy is relaxed by the pure thermal motion of constituent molecules. Since the network structure forming the polymer gel is usually in an equilibrium state and is fluctuated by the thermal energy, the relaxation process from mechanical perturbation is similar to that from thermal perturbation. Therefore, in the linear viscoelastic region, there is no difference in the dissipation between different deformation modes; for example, the same results are observed even when the strain is changed, and whether the specimen is compressed or stretched. Conversely, we can experimentally determine the linear viscoelastic region as a region where the viscoelastic response does not change regardless of strains. Thus, in conventional experiments using rheometer, one should start from changing the strain with a constant stress and then determine the linear viscoelastic region.

On the other hand, in nonlinear viscoelasticity measurements, one observes the viscoelastic response under large strain (or stress). Since the applied strain greatly changes the molecular structure and molecular motion in the specimen, the relaxation process is different from that from thermal perturbation. Under such circumstances, there is no universal relationship between viscoelastic responses in different deformation modes; for example, shear and tensile measurements show qualitatively different results. One should take special attention whether the experimental range is in linear or nonlinear regions.

References

1 Mooney, M. (1940). A theory of large elastic deformation. *J. Appl. Phys.* 11: 582–592.
2 Flory, P.J. (1953). *Principles of Polymer Chemistry*. Ithaca, NY: Cornell University Press.
3 Kawamura, T., Urayama, K., and Kohjiya, S. (2002). Multiaxial deformations of end-linked poly(dimethylsiloxane) networks. III. Effect of entanglement density on strain-energy density function. *J. Polym. Sci., Part B: Polym. Phys.* 40: 2780–2790.

4 Kawamura, T., Urayama, K., and Kohjiya, S. (2003). Multiaxial deformations of end-linked poly(dimethylsiloxane) networks. 5. Revisit to Mooney–Rivlin approach to strain energy density function. *J. Soc. Rheol. Jpn.* 31: 213–217.

5 Urayama, K. (2006). An experimentalist's view of the physics of rubber elasticity. *J. Polym. Sci., Part B: Polym. Phys.* 44: 3440–3444.

6 Urayama, K., Kawamura, T., and Kohjiya, S. (2001). Multiaxial deformations of end-linked poly(dimethylsiloxane) networks. 2. Experimental tests of molecular entanglement models of rubber elasticity. *Macromolecules* 34: 8261–8269.

7 Urayama, K., Kawamura, T., and Kohjiya, S. (2003). Multiaxial deformations of end-linked poly(dimethylsiloxane) networks. 4. Further assessment of the slip-link model for chain-entanglement effect on rubber elasticity. *J. Chem. Phys.* 118: 5658–5664.

8 Ogden, R.W. (1972). Large deformation isotropic elasticity – correlation of theory and experiment for incompressible rubberlike solids. *Proc. R. Soc. London, Ser. A* 326: 565.

9 Gent, A.N. (1996). A new constitutive relation for rubber. *Rubber Chem. Technol.* 69: 59–61.

10 Kondo, Y., Urayama, K., Kidowaki, M. et al. (2014). Applicability of a particularly simple model to nonlinear elasticity of slide-ring gels with movable cross-links as revealed by unequal biaxial deformation. *J. Chem. Phys.* 141: 134906.

11 Katashima, T., Urayama, K., Chung, U.-i., and Sakai, T. (2012). Strain energy density function of a near-ideal polymer network estimated by biaxial deformation of tetra-PEG gel. *Soft Matter* 8: 8217–8222.

12 Katashima, T., Urayama, K., Chung, U.-i., and Sakai, T. (2015). Probing the cross-effect of strains in non-linear elasticity of nearly regular polymer networks by pure shear deformation. *J. Chem. Phys.* 142: 174908.

13 Allen, G., Kirkham, M.J., Padget, J., and Price, C. (1971). Thermodynamics of rubber elasticity at constant volume. *Trans. Faraday Soc.* 67: 1278–1292.

14 Gumbrell, S.M., Mullins, L., and Rivlin, R.S. (1953). Departures of the elastic behaviour of rubbers in simple extension from the kinetic theory. *Trans. Faraday Soc.* 49: 1495–1505.

15 Kuhn, W. and Grün, F. (1942). Beziehungen zwischen elastischen Konstanten und Dehnungsdoppelbrechung hochelastischer Stoffe. *Kolloid Z.* 101: 248–271.

16 Wang, M.C. and Guth, E. (1952). Statistical theory of networks of non-Gaussian flexible chains. *J. Chem. Phys.* 20: 1144–1157.

17 Arruda, E.M. and Boyce, M.C. (1993). A 3-dimensional constitutive model for the large stretch behavior of rubber elastic-materials. *J. Mech. Phys. Solids* 41: 389–412.

18 Katashima, T., Asai, M., Urayama, K. et al. (2014). Mechanical properties of tetra-PEG gels with supercoiled network structure. *J. Chem. Phys.* 140: 134906.

19 Urayama, K. and Kohjiya, S. (1997). Uniaxial elongation of deswollen polydimethylsiloxane networks with supercoiled structure. *Polymer* 38: 955–962.

20 Urayama, K. and Kohjiya, S. (1998). Extensive stretch of polysiloxane network chains with random- and super-coiled conformations. *Eur. Phys. J. B* 2: 75–78.

21 Gong, J.P., Katsuyama, Y., Kurokawa, T., and Osada, Y. (2003). Double-network hydrogels with extremely high mechanical strength. *Adv. Mater.* 15: 1155–1158.

22 Gong, J.P. (2010). Why are double network hydrogels so tough? *Soft Matter* 6: 2583–2590.

23 Griffith, A.A. (1921). The phenomena of rupture and flow in solids. *Philos. Trans. R. Soc. London, Ser. A* 221: 163–198.

24 Lake, G.J. and Thomas, A.G. (1967). The strength of highly elastic materials. *Proc. R. Soc. London, Ser. A* 300: 108–119.

25 Gent, A.N. and Tobias, R.H. (1982). Threshold tear strength of elastomers. *J. Polym. Sci., Part B: Polym. Phys.* 20: 2051–2058.

26 Akagi, Y., Sakurai, H., Gong, J.P. et al. (2013). Fracture energy of polymer gels with controlled network structures. *J. Chem. Phys.* 139: 144905.

27 Sakai, T., Akagi, Y., Kondo, S., and Chung, U.-i. (2014). Experimental verification of fracture mechanism for polymer gels with controlled network structure. *Soft Matter* 10: 6658–6665.

28 Kawamura, T., Urayama, K., and Kohjiya, S. (2001). Multiaxial deformations of end-linked poly(dimethylsiloxane) networks. 1. Phenomenological approach to strain energy density function. *Macromolecules* 34: 8252–8260.

29 Urayama, K. (2016). New aspects of nonlinear elasticity of polymer gels and elastomers revealed by stretching experiments in various geometries. *Polym. Int.* 66: 195–206.

6

Mass Transport in Polymer Gels

Xiang Li[1] *and Takamasa Sakai*[2]

[1] *Institute for Solid States Physics, The University of Tokyo, Tokyo, Japan*
[2] *Graduate School of Engineering, The University of Tokyo, Tokyo, Japan*

6.1 Thermal Motion and Brownian Motion

In solution, solvent molecules move randomly, and their average kinetic energy is determined by the temperature. Since the motion of the solvent molecules originates from heat transfer, the motion is called thermal motion. According to the molecular kinetic theory of gasses, the average velocity ($\langle v \rangle$) of solvent molecules is expressed as follows when ignoring the interactions between solvent molecules:

$$\langle v \rangle = \left(\frac{2k_B T}{m} \right)^{-1/2} \tag{6.1}$$

where k_B is the Boltzmann constant, T is the absolute temperature, and m is the mass of the molecules. According to Eq. (6.1), the average velocity ($\langle v \rangle$) of water molecules can be as large as approximately 500 m/s at room temperature. On the other hand, if the same calculation is carried out for colloidal particles with a size of 100 nm, $\langle v \rangle$ is approximately 1×10^{-3} m/s, which is 6 orders of magnitude smaller than that of water. However, for colloidal particles, the actual diffusion coefficient (D), which is a measure of the dynamics and is roughly proportional to the average velocity, is only 3 orders of magnitude smaller; the colloidal particles move much faster than what is predicted by Eq. (6.1).

The concept of the Brownian motion was originally developed to address the gap between the theory and reality. Because colloidal particles are much larger than solvent molecules and their kinetics are slow, colloidal particles constantly collide with the small solvent molecules moving with thermal motion. If these collisions occur uniformly from all directions, the forces will cancel each other out, and the colloidal particles will stay in their initial position. However, in reality, the collisions are not uniform, and the colloidal particles are continuously subjected to imbalanced random forces. The collisions with the small solvent molecules lead to disordered motion in colloidal particles, called Brownian motion [1].

Physics of Polymer Gels, First Edition. Edited by Takamasa Sakai.

6.1.1 Diffusion Coefficient and Relaxation Time

To understand the Brownian motion of colloidal particles, let us first consider a simple one-dimensional problem in which the particles move randomly by a distance $+a$ or $-a$ in every constant time interval Δt [2]. Although it is possible to use a random distance and a random time interval, we leave these parameters constant to avoid complexity and to help the reader understand the essence of the motion. Given that the position of a particle at time t is $x(t)$, the displacement of the particle from $t = 0$ will be $(x(t) - x(0))$. The average of the displacement of many particles (ensemble average) is expressed as follows:

$$\langle x(t) - x(0) \rangle = \sum_{i}^{h} \langle a_i \rangle = 0 \tag{6.2}$$

where a_i is the movement vector of the ith step, and $\langle\rangle$ denotes the ensemble average. Since the direction of travel in each step is random, $\langle a_i \rangle = 0$, similar to the conformation of the random coil discussed in Chapter 1. Thus, we again focus on the mean squared displacement ($\langle [x(t) - x(0)]^2 \rangle$) instead of $\langle x(t) - x(0) \rangle$. After time t, the particle will move $h = t/\Delta t$ steps, and the mean squared displacement is expressed as follows:

$$\begin{aligned} \langle [x(t) - x(0)]^2 \rangle &= \left\langle \left(\sum_{i}^{h} a_i \right) \left(\sum_{j}^{h} a_j \right) \right\rangle = \left\langle \sum_{i}^{h} {a_i}^2 + \sum_{j}^{h} \sum_{j \neq i}^{h-1} a_i a_j \right\rangle \\ &= \sum_{i}^{h} \langle {a_i}^2 \rangle = \frac{a^2}{\Delta t} t \end{aligned} \tag{6.3}$$

In this calculation, we use the fact that the mean of two uncorrelated values is 0 ($\langle a_i a_j \rangle = 0$), similar to the conformation of the random coil. As a result, $\langle [x(t) - x(0)]^2 \rangle$ is proportional to the elapsed time, t, with a proportionality constant of $(a^2/\Delta t)$. The proportionality constant is called a self-diffusion coefficient or simply a diffusion coefficient (D), and it indicates how easy the particles diffuse in the solution.

$$\langle [x(t) - x(0)]^2 \rangle \equiv 2Dt \tag{6.4}$$

Now, we extend this discussion to three dimensions. Let the position of the particle at time t be a vector $\mathbf{r}(t)$. Since the x, y, and z directions are equivalent, a three-dimensional problem is the simple expansion of the one-dimensional problem (Eq. (6.4)).

$$\langle [\mathbf{r}(t) - \mathbf{r}(0)]^2 \rangle = \langle [x(t) - x(0)]^2 + [y(t) - y(0)]^2 + [z(t) - z(0)]^2 \rangle = 6Dt \tag{6.5}$$

The diffusion coefficient is the parameter used to quantitatively evaluate the diffusion of substances for many applications, such as the drying speed of laundry and the release rate of the drugs. For low-molecular-weight substances with a diameter less than 1 nm, such as oxygen and ethanol molecules, the diffusion coefficients in aqueous solutions are on the order of 1×10^{-9} (m^2/s); for typical proteins such as albumin ($R_h = 4$ nm), $D \sim 5 \times 10^{-11}$ (m^2/s); and for polystyrene

beads ($R_h = 50$ nm), $D \sim 5 \times 10^{-12}$ (m^2/s) at room temperature. Another parameter for characterizing diffusion is the relaxation time, which is defined as the time to travel a distance equal to its size (R).

$$\tau \equiv \frac{R^2}{6D} \tag{6.6}$$

6.1.2 Diffusion and Migration

While *diffusion* is a random motion caused by the thermal motion of surrounding small molecules, *migration* is a directive particle motion caused by external forces, such as electric, magnetic, and gravity fields. When an external field is applied, particles in a solution are accelerated and move along the direction of the external field. On the other hand, moving particles experience friction with the solvent molecules depending on their velocity. Thus, at a certain velocity (terminal velocity), the external force and the friction force balance, and the particle motion reaches equilibrium. In particular, with a sufficiently small external force, the particle moves linearly in response to the external force (F), and the terminal velocity (v) is proportional to the applied force [3].

$$v \equiv \mu F \tag{6.7}$$

where the proportionality constant μ is called mobility, which is a measure of the ease by which particles migrate in the medium. The reciprocal of μ is the friction coefficient, ζ, which is a measure of the difficulty by which particles migrate in the medium.

$$\zeta \equiv \frac{1}{\mu} \tag{6.8}$$

According to the fluctuation–dissipation theorem by Einstein, the mobility is related to the diffusion coefficient as follows:

$$D = \mu k_B T = \left(\frac{1}{\zeta}\right) k_B T \tag{6.9}$$

Einstein's relation indicates that the friction on a particle under an external force is the same as that on the particle when the particle undergoes Brownian motion.

6.2 Diffusion in Dilute Polymer Solutions

6.2.1 Diffusion of a Hard Sphere

Thus far, we have discussed the basics of diffusion and migration, which are independent of particle size and shape. Here, we focus on the details and consider the diffusion of a rigid sphere. In the case of a large rigid sphere in a dilute solution such as a colloidal suspension, the diffusion follows Stokes' resistance law; the rigid sphere moving at a velocity v is subject to friction force (f) as shown as follows [1]:

$$f = 6\pi\eta_0 R_h v \tag{6.10}$$

where η_0 is the zero-shear viscosity of the solvent and R_h is the hydrodynamic radius of the rigid sphere. The hydrodynamic radius is the radius of a hydrodynamically equivalent sphere of the diffusing substances. For a rigid particle, the hydrodynamic radius is the same as the particle radius. When solvent molecules or counterions are absorbed on the particle surface, the hydrodynamic radius becomes larger than the particle radius. Since the thickness of the adsorption layer on the particle surface does not depend on the particle size, when the particle is small (<10 nm), the effect of the layer is large, and the hydrodynamic radius is much larger than the particle radius.

When the velocity of the particles reaches the terminal velocity, the friction force and the external force are balanced ($F = f$). In this equilibrium, the following relation holds between the diffusion coefficient and the hydrodynamic radius of the particles, according to Eqs. (6.7), (6.9), and (6.10):

$$D = \frac{k_B T}{6\pi\eta_0 R_h} \tag{6.11}$$

This formula is derived from Stokes' law and Einstein's relation and is called the Stokes–Einstein equation. Equation (6.11) is commonly used to estimate the hydrodynamic radii of particles from their diffusion coefficients, which can be measured by dynamic light scattering and other techniques. Notably, the Stokes–Einstein equation assumes that the particles are much larger than the solvent molecules and that there are no particle–particle interactions. Therefore, when the size of the particles and the solvent molecules are similar or the particle concentration is relatively high, the Stokes–Einstein equation breaks. Practically, to estimate the true hydrodynamic radius, a series of measurements must be performed at low colloidal concentrations and D is then extrapolated to a concentration of 0.

6.2.2 Rouse Model

The Rouse model was the first model developed to describe the diffusion behavior of polymers. The model regards a polymer as a series of N beads connected by $N-1$ springs. There are no hydrodynamic interactions between the beads, and each bead is subject to the same friction from solvent molecules [4]. Thus, the friction coefficient of the entire polymer (ζ_R) is equal to the sum of the friction coefficients of the individual beads (ζ_0), $\zeta_R = N\zeta_0$. Based on Eqs. (6.8) and (6.9), the diffusion coefficient is inversely proportional to the number of beads in the polymer.

$$D = \frac{k_B T}{N\zeta_0} \sim N^{-1} \tag{6.12}$$

Figure 6.1 shows a conceptual illustration of the Rouse model, in which the solvent molecules pass through the polymer and interact with each bead independently. Regardless of the conformation of the polymer (see Chapter 2), D is always represented by Eq. (6.12).

The Rouse model fails to reproduce the diffusion in dilute polymer solutions [5]. This discrepancy suggests that the hydrodynamic interactions of a polymer coil

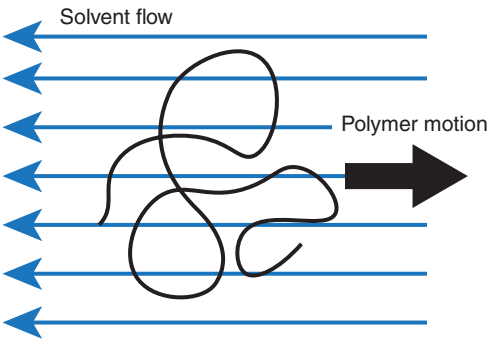

Figure 6.1 Conceptual illustration of the Rouse model. Solvent molecules flow through the polymer chain.

are essential in dilute solution. On the other hand, in concentrated polymer solutions, the polymers mutually penetrate each other, and the hydrodynamic interactions are screened out. In this case, the Rouse model reproduces the dynamics of polymers well. However, in a concentrated solution, the effects of entanglement must also be considered. When the entanglement is not negligible, "reptation" dominates the diffusion process.

6.2.3 Zimm Model

The Zimm model was also developed to describe the diffusion behavior of polymers in solution [4]. In the Zimm model, polymers are considered as a series of beads and springs similar to the Rouse model. One difference is the presence of hydrodynamic interactions between beads, which are not considered in the Rouse model. As a result of the hydrodynamic interactions, solvent molecules inside the polymer coil are trapped and diffuse along with the polymer. Based on this concept, the polymer can be regarded as a rigid sphere consisting of polymer chains and solvent molecules (Figure 6.2).

Following the Zimm model, we obtain the following relations for dilute polymer solutions:

$$D = \frac{k_{\mathrm{B}}T}{6\pi\eta R_{\mathrm{h}}} \sim \begin{cases} N^{-1/2}, & \text{for ideal chain} \\ N^{-3/5}, & \text{for real chain} \end{cases} \tag{6.13}$$

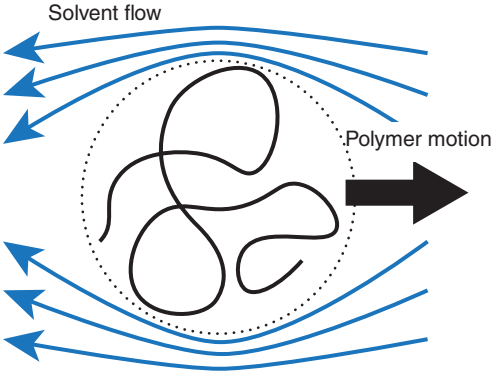

Figure 6.2 Conceptual diagram of the Zimm model. Solvent molecules can only pass around the outside of the polymer chains.

These equations well reproduce the diffusion behavior of polymer chains, especially in dilute solutions [5]. Notably, in the Zimm model, the N-dependence of D changes with the quality of the solvent because the size of the polymer scales with N as $R \sim N^{-3/5}$ in good solvent and $R \sim N^{-1/2}$ in θ solvent.

6.3 Diffusion in Semidilute Polymer Solutions and Polymer Gels

In a semidilute solution, the polymers penetrate into each other, and the polymer solution can be treated as a transient and pseudonetwork structure that changes over time (see Chapter 2). On the other hand, polymer gels with covalent crosslinkers have permanent and definite network structures. Substances such as colloid particles, drug molecules, and linear polymer chains diffusing inside these networks interact with the network in various ways, including direct collisions and hydrodynamic interactions. These interactions hinder the diffusion of substances. Although numerous models have been developed to describe the hindrance, each model can only reproduce a small portion of the experimental results. Thus, even now, there is no clear molecular picture to predict diffusion in networks [6, 7].

Here, we focus on five popular models: (i) the obstruction model that treat the network structure as real obstacles, (ii) hydrodynamic models that ignore the direct interactions with networks and only consider the hydrodynamic interactions, (iii) free volume models that assume that substances diffuse through free volumes of solvent molecules and polymers in the network structures, (iv) reptation models that consider that guest polymer chains move through the tubes formed by polymer networks, and (v) entropic trapping models that assume that the guest polymer chains jump between the cages formed by polymer networks. The first three models were originally designed for the diffusion of rigid particles, and the latter two models are for polymer chains. As mentioned in the Zimm model, when the guest polymer chain is sufficiently smaller than the mesh size, the polymers can be regarded as rigid spheres; thus, the first three models are also useful when the guest polymer chains are small.

6.3.1 Obstruction Model

One of the most intuitive ways of considering diffusion in a polymer network is regarding the polymer network as a real obstacle for diffusing substances. The diffusing substances are only allowed to move to the next position when they find a pore larger than their own radius. Many models have been developed based on this concept, such as the Maxwell–Fricke model and the Mackie–Meares model. Among these models, the most famous model was proposed by Ogston [8] (Figure 6.3).

The Ogston model simplifies the network structure and treats it as an assembly of rigid rods dispersed randomly in the solution. These rigid rods are immobilized

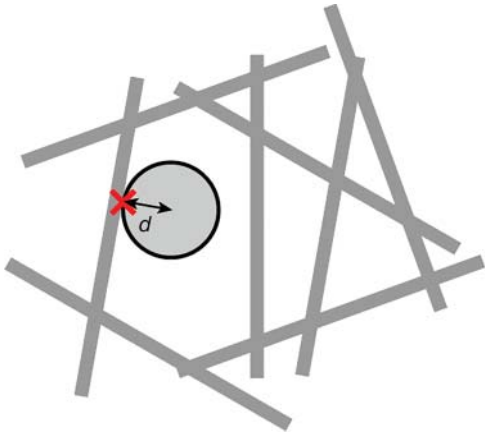

Figure 6.3 Conceptual diagram of the Ogston model.

in space. In the solution, the probability ($f(d)$) of finding another rod for the first time at a distance d from the first rod found is given by Eq. (6.14):

$$f(d) = 4\pi z L_l d \ \exp(-2\pi z L_l (d + L_s)^2) \tag{6.14}$$

where z is the number density of rods, L_l is the length of the rods, and L_s is the width of the rods. The probability of a particle finding a pore larger than itself ($P(R)$) in the network is equal to the integral of Eq. (6.14) from R to infinity.

$$P(R) = \int_R^\infty f(d)\mathrm{d}d = \exp\left[-2\pi z L_l {L_s}^2 \left(\frac{R}{L_s} + 1\right)^2\right] = \exp(-K\phi) \tag{6.15}$$

where R is the radius of the particle, K ($=2\pi(R/L_s + 1)^2$) is the retardation coefficient, and ϕ ($=z L_l {L_s}^2$) is the polymer volume fraction. Generally, in obstruction models, the diffusion coefficient is considered to be proportional to $P(R)$.

$$D = D_0 P(R) = D_0 \ \exp(-K\phi) \tag{6.16}$$

where D_0 is the diffusion coefficient of the particles in a pure solvent without any obstacles. The Ogston model was later generalized for obstacles of different shapes.

$$K \sim \begin{cases} \left(\frac{R}{L_s} + 1\right)^1, & \text{for planes} \\ \left(\frac{R}{L_s} + 1\right)^2, & \text{for rods} \\ \left(\frac{R}{L_s} + 1\right)^3, & \text{for spheres} \end{cases} \tag{6.17}$$

According to the definition, $P(R)$ indicates the available volume in the network for particles. Therefore, it is natural to consider $P(R)$ as the partition coefficient of particles between the gel and solvent; the concentration of particles in the gel should be $P(R)$ times less than that in the adjacent pure solvent if there are no additional chemical interactions between the network and particles. Because both the diffusion and partition coefficients are dependent on $P(R)$, the diffusion process has a strong correlation with the partition process.

6.3.2 Hydrodynamic Model

In hydrodynamic models, the network structure indirectly interacts with the particles via solvent molecules. In this concept, the network structure itself is not an obstacle to the particles. In most hydrodynamic models, polymer networks are simplified as rods or connected beads of which roles are just to slow the flow of the solvent molecules. This hydrodynamic effect results in a substantial increase in the local viscosity and a retardation in the diffusion of the particles.

A representative model based on hydrodynamic interactions was proposed by Cukier [9]. Cukier assumed polymer chains in the network to be connected by the solid spheres and estimated the total friction exerted by the rigid spheres in a fluid. According to Stokes' law, the friction coefficient (ζ_a) exerted by one sphere is as follows:

$$\zeta_a = 6\pi\eta_0 a \tag{6.18}$$

where a is the hydrodynamic radius of a sphere. Applying a Rouse model-like picture, the total friction coefficient is a simple sum of the friction coefficients of each component.

$$\kappa^2 = \frac{n_a \zeta_a}{\eta_0} \tag{6.19}$$

where κ is called the screening constant, which is a measure of hydrodynamic interactions, n_a is the total number of spheres constituting the network, and η_0 is the viscosity of the pure solvent. By simply assuming the number of monomers is proportional to the number of spheres, ϕ is proportional to n_a, and a scaling relation of $\kappa \sim \phi^{1/2}$ is obtained. On the other hand, one can assume that the mesh or blobs in the network generate hydrodynamic interactions, instead of monomers. By using the concept of blobs, Freed and Edwards derived a scaling relation $\kappa \sim \phi$ for the ideal chain, and de Gennes derived $\kappa \sim \phi^{3/4}$ for real chains [9].

Although it is difficult to calculate the frictional coefficient (ζ_D) between the diffusing substances and the network even with the previously mentioned assumptions, it is most likely approximated by an exponential function as shown as follows:

$$\frac{\zeta_D}{\zeta_{D0}} = \exp(\kappa R) \tag{6.20}$$

where ζ_D and ζ_{D0} are the friction coefficients of diffusing particles in the polymer network and in pure solvent, respectively. According to Einstein's expression (Eq. (6.9)), the diffusion coefficient has a reciprocal relationship with the friction coefficient. Therefore, the preceding equation can be rewritten as follows:

$$\frac{D}{D_0} = \exp(-\kappa R) \tag{6.21}$$

As a consequence, a similar expression for the obstacle model can be derived. However, notably, the retardation here originates from the indirect hydrodynamic interactions.

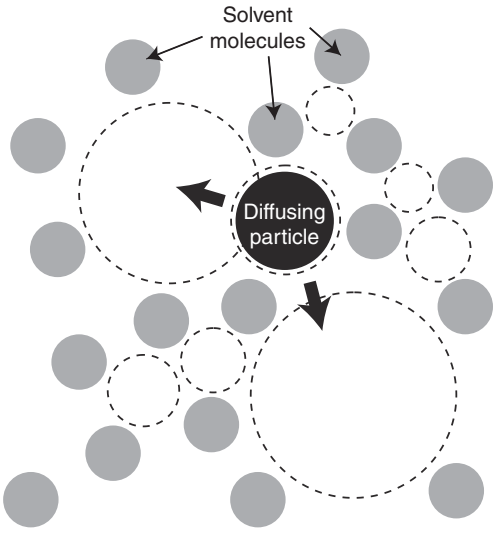

Figure 6.4 Conceptual diagram of the free volume model. Since the solvent molecules thermally fluctuate, the spatial distribution of the free volume varies with time.

6.3.3 Free Volume Model

Free volume is a vacuum that exists between molecules where no substance exists. It might sound weird to image such space in a solution; however, for example, even in a metallic crystal with a hexagonal close-packed structure, the material has 26% voids, i.e. vacuum. There are free volumes in a solvent, a polymer solution and even in a polymer melt. In a two-component system such as a polymer solution, both the solvent and polymer have free volumes. The free volume of a material is defined as the difference between the occupied volume at a given temperature and that at absolute 0. Because the molecules always undergo thermal motion at finite temperatures, the local free volume between molecules changes over time. Free volume models assume that a diffusing substance can leave its initial position only when it finds a free volume larger than itself (Figure 6.4). Notably, free volume models depict a completely different picture from the obstacle models and hydrodynamic models, and particles are considered to diffuse through the region "occupied by the solvent."

The probability of finding a free volume with a size larger than d, $P(d)$, in a pure solvent is expressed as follows by Cohen and Turnbull [6]:

$$P(d) = A \ \exp\left(\frac{-xd}{V_{\mathrm{f}}}\right) \tag{6.22}$$

where A and x are constants and V_{f} is the sum of the free volumes in the solution. Fujita assumed the mobility of particles with size R in a pure solvent to be proportional to $P(R)$ as $\mu \sim P(R)$ and estimated the diffusion coefficient using the Einstein equation.

$$D \sim Ak_{\mathrm{B}}T \ \exp\left(\frac{-xR}{V_{\mathrm{f}}}\right) \tag{6.23}$$

Yasuda et al. later extended this idea to polymer solutions. Since the free volume in a polymer solution is influenced by both the solvent and polymer chains, the

total of free volume in the system is rewritten as follows:

$$V_f = (1 - \phi)V_{fs} + \phi V_{fp} \tag{6.24}$$

where V_{fs} and V_{fp} are the free volumes of pure solvent and pure polymer, respectively. When the fraction of free volume from the solvent molecules is much larger than that from the polymer chains, the total free volume can be approximated as $V_f \approx (1 - \phi)V_{fs}$. By using this approximation for Eqs. (6.23) and (6.24), the diffusion coefficient of a substance in the presence of the polymer solution can be derived as shown.

$$\frac{D}{D_0} = \exp\left(-\frac{xR}{V_{fs}}\left(\frac{\phi}{1-\phi}\right)\right) \tag{6.25}$$

where D_0 is the diffusion coefficient in a pure solvent, which is equal to $\exp(-xR/V_{fs})$. In free volume theory, the substances are assumed to diffuse through the free volume of solvent molecules. Although the spatial distribution of free volumes derived from solvent molecules changes with time due to thermal motion, the average size of the free volume should be comparable to the size of the solvent molecules. Therefore, free volume models cannot be applied to molecules much larger than solvent molecules (e.g. proteins and polymer chains).

6.3.4 Reptation Model

All the models introduced so far assume that the diffusing substances are rigid bodies. Low-molecular-weight substances, proteins, colloid particles, or small guest polymers are suitable substances for these models. However, for large polymer chains that entangle with the surrounding polymer networks, e.g. a polymer chain in a polymer melt or gel, the diffusion process is predicted to have qualitative differences. Indeed, some experiments have found that large guest polymer chains diffuse in a polymer network much faster than predicted by the previously mentioned models. The diffusion coefficient was a power law relation with respect to the molecular weight of the guest chains rather than an exponential relation. de Gennes proposed a completely different picture; the polymer chains do not diffuse as a rigid sphere, but reptate in the network like snakes [3].

In the reptation model, a guest polymer chain is constrained by a virtual tube in a polymer network. The guest polymer chain is allowed to escape only from the ends of the tube (Figure 6.5). Although the ends of the polymer chain can freely move to new positions, as soon as the head moves, the tube is elongated to cover the head, and the remaining part of the chain is only allowed to follow the trajectory of the head. In this model, the thickness and the length of the tube are the key parameters for determining the diffusion coefficient of the guest chain. Because the chain moves along the tube, all the segments of the chain experience friction from the wall of the tube; the diffusion is treated using the one-dimensional Rouse model along the tube. Therefore, the mobility along the tube (μ_t) is inversely proportional to the chain length, and the diffusion coefficient along the tube (D_t) is obtained based on the Einstein equation.

$$D_t = \mu_t k_B T \sim N^{-1} \tag{6.26}$$

Figure 6.5 Conceptual diagram of the reptation model. The black dot is a crosslinking point or entanglement point, and the chain is constrained from a pseudotube made by these crosslinking points, and movement along the tube is permitted.

The subscript "t" denotes the motion along the tube. The relaxation time is given by Eq. (6.27):

$$\tau_{\mathrm{t}} \simeq \frac{L^2}{D_{\mathrm{t}}} \sim N^3 \tag{6.27}$$

where L is the tube length, which is proportional to the chain length.

Now we are ready to discuss diffusion in three dimensions. Because the guest chain has a random coil conformation, it is natural to assume that the constraint tube also has a random coil conformation. However, there should not be any difference in the relaxation time of the three-dimensional and one-dimensional systems because the relaxation time is defined as the time to move a distance the size of the guest chain. Therefore, the relaxation time of three-dimensional diffusion remains as shown.

$$\tau = \tau_{\mathrm{t}} \sim N^3 \tag{6.28}$$

If R is the typical length (e.g. end-to-end distance) of the tube in three dimensions, the diffusion coefficient can be derived from the relaxation time as follows:

$$D \simeq \frac{R^2}{\tau} \sim \begin{cases} N^{-2}, & \text{for ideal chain} \\ N^{-1.8}, & \text{for real chain} \end{cases} \tag{6.29}$$

Here, Eqs. (1.3) and (1.49) are used to derive the N-dependence of the end-to-end distance of the ideal chain and the real chain. The reptation model reproduced the observed N-dependence of a guest chain in a concentrated polymer solution and a polymer melt. Notably, the reptation model is the only model predicting a power law form of the N-dependence of the diffusion coefficient among the five major models introduced in this section; only the reptation model leads to a qualitatively different result from other models. To further improve the reptation model, the effects of dissociation and reconstruction of the tube were taken into account in the constraint release model, and the fluctuation of the tube length by thermal fluctuations was taken into account in the reptation with the fluctuation model. All these models predict a power law relation between the diffusion coefficient and the chain length [2].

6.3.5 Entropic Trapping Model

Finally, we introduce the entropic trapping model [10]. In this model, the polymer network is approximated as a series of pores connected by narrow paths

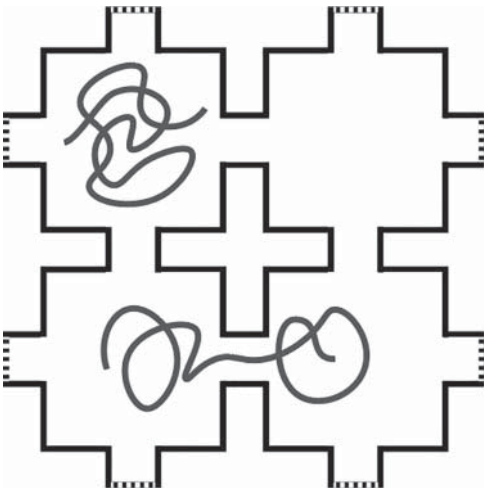

Figure 6.6 Conceptual diagram of the entropic trapping model.

(Figure 6.6). The guest chain is smaller than the size of the pores but larger than the paths. Thus, to diffuse in the polymer network, the guest chain must pass through the small paths. When the chain stays in the paths, the conformational entropy of the chain decreases, leading to an entropic barrier to chain diffusion.

Given that the partition coefficient (P) of the chains in between the pores and the paths follows the Boltzmann distribution, P is represented using the difference in the free energies of the chain in the two spaces (ΔF).

$$P = \frac{\phi_{\text{small}}}{\phi_{\text{bulk}}} \sim \exp\left(-\frac{\Delta F}{k_{\text{B}}T}\right) a$$
$$\phi = \phi_{\text{small}} + \phi_{\text{bulk}} \tag{6.30}$$

ϕ is the total polymer volume fraction of the guest chain, ϕ_{small} and ϕ_{bulk} are polymer volume fractions of the chain contained in the path and the pore, respectively. Although Eq. (6.30) holds only when the polymer chain is smaller than both the path and pore, we neglect these details and use Eq. (6.30) to illustrate the concept of the entropic trapping model.

When we accept the proportionality between the partition and diffusion coefficients, the following expression is obtained:

$$\frac{D}{D_0} = P = \exp\left(-\frac{\Delta F}{k_{\text{B}}T}\right) \tag{6.31}$$

ΔF is discussed by Casassa for ideal chains and by Daoud and de Gennes for real chains. Letting d_{c} be the typical size of the narrow paths, one obtains $\Delta F \sim N d_{\text{c}}^{-2}$ for ideal chains and $\Delta F \sim N d_{\text{c}}^{-5/3}$ for real chains. Muthukumar further developed this discussion and performed several simulation studies with various spaces. Because it is difficult to correlate the pores and paths with substructures in a real polymer network, we cannot quantitatively compare the entropic trapping model with the experimental data. The entropic trapping model has been used to explain scalings with a much stronger exponent ($D \sim N^{-2}$–N^{-4}) than that of the reptation model, which is often experimentally consistent with strongly entangled systems.

Column 6: Effects of Mesh Sizes on Mass Transport

The mesh size of gel is an intuitive and important parameter for predicting mass transport in gels. Indeed, most of the models of mass transport introduced in this chapter are built based on "mesh size." Although there are several methods to estimate the mesh size, there is no clear answer yet.

Figure 6.7a shows a simplified polymer network found in common textbooks and papers as well as a polymer network slightly closer to reality. Although no one has observed the network structure of a gel, one may understand the illustration (Figure 6.7b) is more realistic by considering that the network strands are random coil-like and that a gel is a semi-diluted system. What is the mesh size imagined from such a picture? A mesh size estimated from a molecular weight of network strand, a blob size, or a mesh size estimated from elastic modulus?

What we know at the present time is that important parameters depend on the size of diffusion molecules (see Chapter 13). According to the previous papers, the diffusion of small molecules (e.g. water molecules) is determined only by polymer concentration (or blob size), and there is negligible influence of crosslinking. When the molecular weight of the diffusion molecule reaches about 1000 g/mol, the influence of the crosslinks becomes apparent, showing the obstacle model-like behavior [11]. With further increase in molecular weight, both the reptation-like and obstacle-like behaviors are observed, and the polymer concentration and the crosslinking density independently influence the diffusion. Therefore, it seems to be difficult to discuss mass transport with a single concept of mesh size [12, 13].

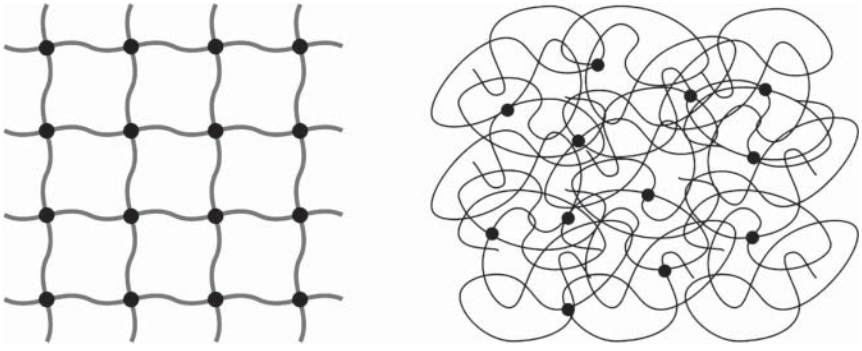

Figure 6.7 Schematic pictures of polymer networks: (a) too simplified version and (b) more realistic version.

References

1 Cussler, E.L. (2009). *Diffusion: Mass Transfer in Fluid Systems*. Cambridge University Press.

2 Rubinstein, M. and Colby, R.H. (2003). *Polymer Physics*. Oxford University Press.
3 de Gennes, P.G. (1979). *Scaling Concepts in Polymer Physics*. Cornell University Press.
4 Doi, M. and Edwards, S.F. (1986). *The Theory of Polymer Dynamics*. Clarendon Press.
5 Tetraoka, I. (2002). *Polymer Solutions*. Wiley.
6 Cohen, M.H. and Turnbull, D. (1959). Molecular transport in liquids and glasses. *J. Chem. Phys.* 31: 1164–1169.
7 Masaro, L. and Zhu, X.X. (1999). Physical models of diffusion for polymer solutions, gels and solids. *Prog. Polym. Sci.* 24 (5): 731–775.
8 Ogston, A.G. (1958). The spaces in a uniform random suspension of fibres. *Trans. Faraday Soc.* 54: 1754.
9 Cukier, R.I. (1984). Diffusion of Brownian spheres in semidilute polymer solutions. *Macromolecules* 17 (2): 252–255.
10 Muthukumar, M. and Baumgaertner, A. (1989). Effects of entropic barriers on polymer dynamics. *Macromolecules* 22 (4): 1937–1941.
11 Li, X., Khairulina, K., Chung, U.-I., and Sakai, T. (2013). Migration Behavior of Rodlike dsDNA Under Electric Field in Homogeneous Polymer Networks. *Macromolecules* 46: 8657–8663.
12 Li, X., Khairulina, K., Chung, U.-i., and Sakai, T. (2014). Electrophoretic mobility of double-stranded DNA in polymer solutions and gels with tuned structures. *Macromolecules* 47: 3582–3586.
13 Khairulina, K., Li, X., Nishi, K. et al. (2015). Electrophoretic mobility of semi-flexible double-stranded DNA in defect-controlled polymer networks: mechanism investigation and role of structural parameters. *J. Chem. Phys.* 143: 234904.

Part II

Experiments

Physics of Polymer Gels, First Edition. Edited by Takamasa Sakai.

7

Tetra Gel as a Near-Ideal Polymer Network

Takamasa Sakai

Graduate School of Engineering, The University of Tokyo, Tokyo, Japan

7.1 Ideal Polymer Network

A polymer gel consists of a three-dimensional polymer network swollen in solvent and is applied to various products, such as contact lenses, adhesion barrier, and soil modifiers. For practical applications, independent control of their various physical properties, such as gelation time, stiffness, toughness, stretchability, swelling, mass transport, and degradation, is required. However, simultaneously establishing all the properties in the required range is difficult because of the uncontrollability stemming from the heterogeneous nature of the polymer network [1–3]. The heterogeneity even hinders experimental verification of the theories predicting the physical properties and makes it impossible to understand the physics of polymer gels at the molecular level. The challenge in understanding the nature of polymer networks has a long history, and many attempts have been made to develop an ideal polymer network free from any heterogeneity [4–8]. Hild proposed four requirements for an ideal polymer network [4]:

(i) The lengths of all network strands should be identical.
(ii) The functionality of crosslinking points should be constant throughout the entire network.
(iii) The conformation of the network strands should obey Gaussian statistics.
(iv) The network should be homogeneous macroscopically as well as microscopically.

Thus, deviations from this definition are regarded as heterogeneities: heterogeneous distributions in strand length, network strands, and functionality and abnormal statistics of network strands. Notably, these requirements are for only network structures characterized by chemical crosslinks and ignore the other features of the polymer network, i.e. trapped entanglement between network strands. Because trapped entanglements are introduced in an uncontrolled manner and are difficult to quantify, the trapped entanglements should be regarded as heterogeneities as well. Thus, we add the following requirement:

(v) The network strands should not entangle with each other.

Physics of Polymer Gels, First Edition. Edited by Takamasa Sakai.

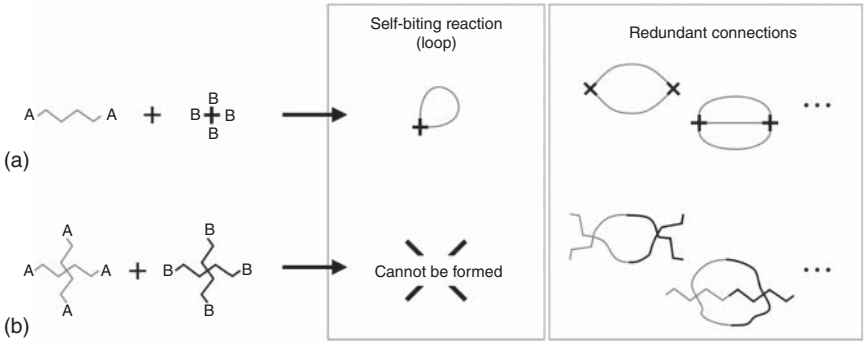

Figure 7.1 Heterogeneities formed in (a) end-crosslinking and (b) crosslink coupling.

One of the strongest rationales for this requirement is that most of the basic theories model a simple polymer network formed by chemical crosslinks and do not consider the effect of trapped entanglements.

A classic model network is synthesized from a monodisperse linear prepolymer with functional groups on both ends and a multifunctional crosslinker (Figure 7.1a and 7.2a) [4, 6]. The functional groups of the prepolymer react with those of the crosslinker to form a network structure. Notably, in general, a solvent was not used. The monodispersity of the prepolymer contributes to (i) the narrow distribution in strand length, and the defined functionality of the crosslinker contributes to (ii) the well-defined functionality of the crosslinks. In addition, (iii) the structure of polymers in a polymer melt generally obeys the Gaussian distribution [7, 9]. When the two components are mixed homogeneously, requirement (iv) may be satisfied. The only problem with this method is the deviation from requirement (v); the prepolymers strongly entangle under such a condensed condition [7, 9]. Indeed, it is expected that the contribution of trapped entanglements to physical properties is expected to be comparable to or to surpass that of chemical crosslinks, masking the effect of the chemical crosslinks. Therefore, suppressing the entanglements is important for the fundamental understanding of polymer networks.

Dilution is the simplest method to suppress entanglements, and a polymer network containing a diluent is called a polymer gel [9–11]. By definition, when the polymer solution is diluted below the overlap concentration of the polymer (c^*), the entanglements between polymers are eliminated. On the other hand, the coexistence of a diluent brings about drawbacks related to requirements (ii) and (iii) (Figure 7.1a). The intramolecular reaction is more likely to occur in the diluted system than in the concentrated system, resulting in the formation of ineffective or redundant connections [12–14]. Regarding mechanical properties, these imperfect connections are expected to make the mechanical properties lower than those expected from perfect connections; in particular, the self-biting loop is never stretched by any deformation and does not contribute to the mechanical properties. Thus, imperfect connections decrease the net functionality of the crosslinks, resulting in deviation from requirement (ii). In addition, the coexistence of a diluent changes the conformation of the polymer

chain, resulting in deviation from requirement (iii). However, when a θ-solvent for the polymer is used, the polymer chain adopts an ideal conformation, meeting requirement (iii). Therefore, the inevitable difficulty in this design lies in requirement (ii). Thus, a molecular design that reduces imperfect connections is key to developing a model polymer network with a diluent.

7.2 Tetra-PEG Gel

Recently, we have developed a molecular design that effectively reduces imperfect connections (AB-type crosslink coupling, Figure 4.1b) [1]. In the coupling process, two mutually reactive tetra-functional polyethylene glycols (Tetra-PEGs) react with each other in a solvent. This molecular design includes three key aspects to suppress the heterogeneity. First, compared with those in conventional model networks, the possible intramolecular connections in our design are limited, resulting in a drastic reduction in the number of imperfect connections. In particular, the self-biting loop, which does not contribute to the elasticity, cannot be formed in this design. Second, the polymer concentration is set near the overlap concentration of Tetra-PEG to suppress entanglements. Third, the reaction rate is tuned to allow the mutually reactive Tetra-PEGs to be mixed homogeneously. Compared with the design of conventional hydrogels, this molecular design realizes high reaction conversion values (~95%) and strongly suppresses the heterogeneity [1, 2, 15–17]. Thus, Tetra-PEG gel is currently one of the most promising candidates for a model network system. In the following Chapters 8–17, I briefly present the structure of Tetra-PEG gel and discuss the following physical properties: gelation, stiffness, toughness, stretchability, swelling, mass transport, and degradation. Because most of the theories are explained in the previous Chapters 1–6, I put a special focus on experiments and comparisons between experimental results and theoretical predictions. Throughout the discussion, I attempt to clarify the current understanding of polymer gels.

7.3 Structure Tuning of Tetra-PEG Gels

Tetra-PEG gel is formed by Tetra-PEGs with mutually reactive functional groups; one combination is thiol (SH)-terminated and maleimide (MA)-terminated Tetra-PEGs [18], and another combination is amine (NH_2)-terminated and activated ester (OSu)-terminated Tetra-PEGs [1]. Based on our previous works, different end functional groups do not strongly influence the gel structure or properties. A slight difference in swellability is observed, most likely due to the difference in hydrophobicity of the resultant linkages between Tetra-PEGs. Although hydrolysis of the OSu group decreases the reaction conversion (p) in the latter combination, the reaction conversion can be increased up to 90% by tuning the reaction condition properly [15]. These differences can be included in the analysis by tuning χ and p according to Sections 3.4 and 4.2.

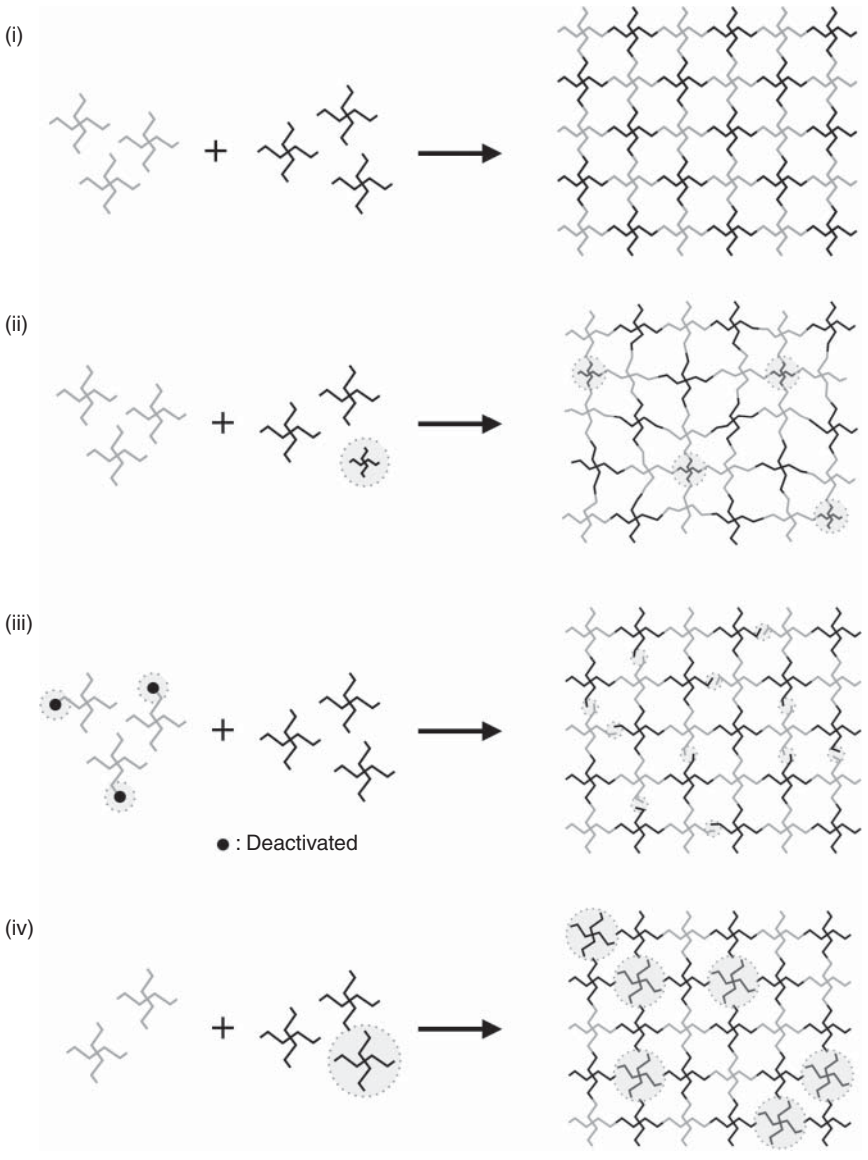

Figure 7.2 Schematic illustrations of (i) Conventional Tetra-PEG gels, (ii) a bimodal Tetra-PEG gel, (iii) a conversion-tuned Tetra-PEG gel, and (iv) a fraction-tuned Tetra-PEG gel.

Therefore, different end functional groups do not qualitatively influence the physical properties of the gels. In the following, wherein we do not focus on the different functional groups, mutually reactive Tetra-PEG prepolymers are termed Tetra-PEG-A and Tetra-PEG-B.

Basically, one can control the structure of Tetra-PEG gels by tuning the molecular weights and concentrations of the Tetra-PEG prepolymers. Representative variations in Tetra-PEG gels include the following: (i) conventional Tetra-PEG

gel [1, 19], (ii) bimodal Tetra-PEG gel [20], (iii) conversion-tuned Tetra-PEG gel [21], and (iv) fraction-tuned Tetra-PEG gel (Figure 7.2) [22]:

(i) Conventional Tetra-PEG gels are made from equimolar amounts of Tetra-PEG-A and Tetra-PEG-B with the same molecular weights. Conventionally, the molecular weights of Tetra-PEGs (M_w) are tuned from 5, 10, and 20–40 kg/mol, and the resultant gels are named 5k, 10k, 20k, and 40k Tetra-PEG gels, respectively. Because the molecular weight of an arm of Tetra-PEG is one-fourth of the entire molecular weight, the molecular weight of the resultant network strand is half of the molecular weight of Tetra-PEG. For example, the 10k Tetra-PEG gel has a network strand with a molecular weight of 5 kg/mol. The initial polymer volume fraction (φ_0) is another parameter in conventional Tetra-PEG gels and mainly governs the number density of network strands (ν) and crosslinks (μ). Notably, the molecular weight and number density of the network strands, which often strongly correlate with each other, can be independently tuned in this design.

(ii) Bimodal Tetra-PEG gels have a bimodal distribution in strand length. To introduce this bimodality, one needs to mix three kinds of Tetra-PEGs. When one mixes 5k Tetra-PEG-A, 20k Tetra-PEG-A, and 5k Tetra-PEG-B, the resultant polymer network has strand lengths of 2.5 and 6.25 kg/mol. By tuning the ratio between 5k and 20k Tetra-PEGs while maintaining the equimolar condition between the A and B functional groups, one can tune the ratio of bimodal network strands.

(iii) Conversion-tuned (p-tuned) Tetra-PEG gels have a controlled fraction of connected arms (p). To tune p, Tetra-PEG–OSu is used. Tetra-PEG–OSu hydrolyzes in aqueous environments and consequently loses its reactivity with Tetra-PEG–NH_2. Thus, one can tune p by using partially hydrolyzed Tetra-PEG–OSu and Tetra-PEG–NH_2. The tuning of p is expected to have a minimal effect on the polymer network structure; it should just connect the arm ends in the system while maintaining the polymeric species. Using this control scheme, one can change only ν and μ without changing φ_0 or M_w. Notably, the reaction between A and B is complete; p-tuned Tetra-PEG gels are obtained as the "equilibrium" of the reaction. A p-tuned Tetra-PEG gel with $p = p_1$ can be considered a replica of a conventional Tetra-PEG gel at a reaction conversion of p_1, which is a point in a "dynamic" process. This difference in state can differentiate these two gels, although we have not clearly observed this differentiation in our experiments.

(iv) Fraction-tuned (r-tuned) Tetra-PEG gels are another system with a controlled p. In this system, one mixes Tetra-PEG-A and Tetra-PEG-B under unequal molar conditions indicated by the ratio of Tetra-PEG-A to total Tetra-PEGs (r). Assuming a complete reaction between A and B, $p = 2r$ ($r < 0.5$). Although this control scheme is experimentally easier than the approach based on p-tuned Tetra-PEG gels, it features a complication related to the distribution of connections. In the p-tuned system, connections distribute homogeneously, while connections in the r-tuned system concentrate near the minor species. This difference is quantitatively

predicted by the Bethe approximation (Section 3.4.2). Based on the Bethe approximation, these systems have negligible differences in the region $p > 0.7$, while the deviation increases with a decrease in p. The deviation is maximum at the gelation point: for p-tuned system gels, the gelation point is at $p = 1/3$, and for r-tuned system gels, the gelation point is at $p = 0.19$.

References

1 Sakai, T., Matsunaga, T., Yamamoto, Y. et al. (2008). Design and fabrication of a high-strength hydrogel with ideally homogeneous network structure from tetrahedron-like macromonomers. *Macromolecules* 41 (14): 5379–5384.
2 Sakai, T. (2014). Experimental verification of homogeneity in polymer gels. *Polym. J.* 46 (9): 517–523.
3 Shibayama, M. (1998). Spatial inhomogeneity and dynamic fluctuations of polymer gels. *Macromol. Chem. Phys.* 199 (1): 1–30.
4 Hild, G. (1998). Model networks based on "endlinking" processes: synthesis, structure and properties. *Prog. Polym. Sci.* 23 (6): 1019–1149.
5 Rempp, P., Herz, J., Hild, G., and Picot, C. (1975). Tailor-made networks: synthesis and properties. *Pure Appl. Chem.* 43 (1–2): 77–96.
6 Beinert, G., Belkebir-Mrani, A., Herz, J. et al. (1974). New crosslinking processes. *Faraday Discuss. Chem. Soc.* 57: 27–34.
7 Beltzung, M., Picot, C., Rempp, P., and Herz, J. (1982). Investigation of the conformation of elastic chains in poly(dimethylsiloxane) networks by small-angle neutron scattering. *Macromolecules* 15 (6): 1594–1600.
8 Mark, J.E. and Llórente, M.A. (1980). Model networks of end-linked polydimethylsiloxane chains. 5. Dependence of the elastomeric properties on the functionality of the network junctions. *J. Am. Chem. Soc.* 102 (2): 632–636.
9 de Gennes, P.G. (1979). *Scaling Concepts in Polymer Physics*. Ithaca, NY: Cornell University Press.
10 Colby, R.H., Fetters, L.J., Funk, W.G., and Graessley, W.W. (1991). Effects of concentration and thermodynamic interaction on the viscoelastic properties of polymer solutions. *Macromolecules* 24 (13): 3873–3882.
11 Rubinstein, M. and Helfand, E. (1985). Statistics of the entanglement of polymers: concentration effects. *J. Chem. Phys.* 82 (5): 2477–2483.
12 Kawamoto, K., Zhong, M., Wang, R. et al. (2015). Loops versus branch functionality in model click hydrogels. *Macromolecules* 48 (24): 8980–8988.
13 Wang, R., Alexander-Katz, A., Johnson, J.A., and Olsen, B.D. (2016). Universal cyclic topology in polymer networks. *Phys. Rev. Lett.* 116 (18): 1–5.
14 Zhong, M., Wang, R., Kawamoto, K. et al. (2016). Quantifying the impact of molecular defects on polymer network elasticity. *Science* 353 (6305): 1264–1268.
15 Akagi, Y., Gong, J.P., Chung, U.-i., and Sakai, T. (2013). Transition between phantom and affine network model observed in polymer gels with controlled network structure. *Macromolecules* 46 (3): 1035–1040.

16 Matsunaga, T., Sakai, T., Akagi, Y. et al. (2009). Structure characterization of Tetra-PEG gel by small-angle neutron scattering. *Macromolecules* 42 (4): 1344–1351.
17 Matsunaga, T., Sakai, T., Akagi, Y. et al. (2009). SANS and SLS studies on tetra-arm PEG gels in as-prepared and swollen states. *Macromolecules* 42 (16): 6245–6252.
18 Nishi, K., Fujii, K., Chung, U.-i. et al. (2017). Experimental observation of two features unexpected from the classical theories of rubber elasticity. *Phys. Rev. Lett.* 119 (26): 267801.
19 Kondo, S., Chung, U.-i., and Sakai, T. (2014). Effect of prepolymer architecture on the network structure formed by AB-type crosslink-coupling. *Polym. J.* 46 (1): 14–20.
20 Kondo, S., Sakurai, H., Chung, U.-i., and Sakai, T. (2013). Mechanical properties of polymer gels with bimodal distribution in strand length. *Macromolecules* 46 (17): 7027–7033.
21 Akagi, Y., Katashima, T., Sakurai, H. et al. (2013). Ultimate elongation of polymer gels with controlled network structure. *RSC Adv.* 3 (32): 13251–13258.
22 Sakai, T., Katashima, T., Matsushita, T., and Chung, U.-i. (2016). Sol-gel transition behavior near critical concentration and connectivity. *Polym. J.* 48 (5): 629–634.

8

Sol-Gel Transition

Takamasa Sakai

Graduate School of Engineering, The University of Tokyo, Tokyo, Japan

8.1 Determination of Sol–Gel Transition by Rheometry

As discussed in Chapter 3, one can determine whether a system of interest is sol or gel by means of rheology. We tuned the fraction of a Tetra-PEG prepolymer (r) while maintaining the polymer molecular weight and concentration and observed the gelation process. Figure 8.1 shows the ω-dependence of G' and G'' for mixtures of Tetra-PEG prepolymers at various r values [1]. At a low r ($r < r_c$) far from stoichiometry, the system showed terminal relaxation behavior, $G' \sim \omega^2$ and $G'' \sim \omega^1$, suggesting that the system is a liquid. With an increase in r, both slopes decreased and eventually became the same at a critical point ($r = r_c$), which is the gelation point, according to the Winter–Chambon criterion [2]. After the gelation point ($r > r_c$), G' became larger than G'' and shows a plateau at low frequencies. This behavior indicates that the system is fully percolated and the system is in the gel state.

8.2 Phase Diagram

According to the Winter–Chambon criterion [2], we estimated the critical gelation ratios (r_c) at different polymer volume fractions (Figure 8.2) [1]. Circles and crosses indicate gel and sol, respectively, and the sol–gel transition point (r_c) is in a interstice between the circles and crosses. The critical molar ratio (r_c) increased with a decrease in ϕ_0 and approached stoichiometry ($r = 0.50$). This result suggests that higher reaction conversion is required for percolation in a more dilute system.

To discuss the exact reaction conversion at the critical gelation point (p_c), the reaction conversion must be measured. We performed ^{1}H NMR measurements and confirmed that approximately 95% of Tetra-PEG–OSu present in the solution reacts with excess Tetra-PEG–NH_2, regardless of ϕ_0. Here, it should be noted that NMR cannot be applied to the gel system because the diffusion of the chains is restricted by crosslinking. Thus, the values of p_c are estimated

Physics of Polymer Gels, First Edition. Edited by Takamasa Sakai.

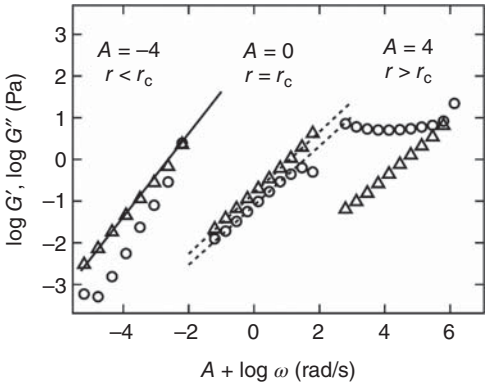

Figure 8.1 The values of G' and G'' as a function of ω in $\phi_0 = 0.034$ (circles, G'; triangles, G''). The solid line is a guideline showing the relationship $G'' \sim \omega^1$. The dashed lines are the fitting curves showing the relationship $G' \approx G'' \sim \omega^{0.69}$. The curves were shifted sideways (factor A) to avoid overlap. Source: Reproduced with permission from Sakai et al. [1]. Copyright 2016, Nature Publishing Group.

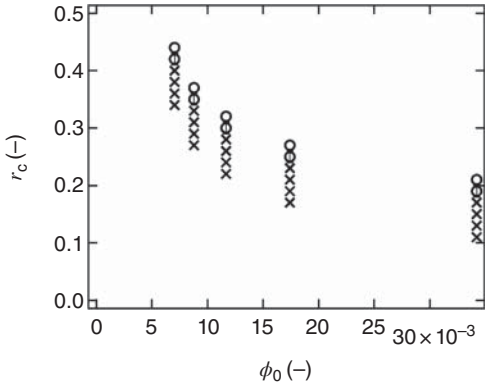

Figure 8.2 Phase diagram of a nonstoichiometric Tetra-PEG system (circle, gel; cross, sol). Source: Reproduced with permission from Sakai et al. [1]. Copyright 2016, Nature Publishing Group.

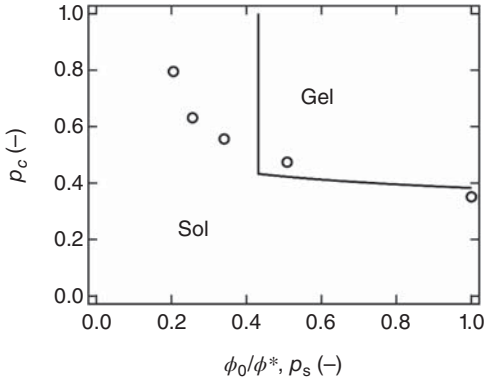

Figure 8.3 The critical reaction conversion (p_c) as a function of the polymer volume fraction in the preparation state normalized by the overlapping volume fraction (ϕ_0/ϕ^*). The solid line represents the prediction of the site–bond percolation model. Source: Reproduced with permission from Sakai et al. [1]. Copyright 2016, Nature Publishing Group.

from the extrapolation of each set of sol data with the same ϕ_0. Figure 8.3 shows the concentration dependence of p_c [1]. Here, the polymer volume fraction (ϕ_0) is normalized by the overlap volume fraction (ϕ^*). The value of p_c decreased with an increase in ϕ_0/ϕ^*, reflecting the difficulty in gelation at a low ϕ_0/ϕ^*. In our system, the lowest concentration at which the gel was formed (critical concentration) was approximately $\phi^*/5$. This result indicates that a gel can be

formed far below the overlap concentration of the prepolymers. We further discuss the gelation in the dilute region in Chapter 14.

Here, we compare the experimental phase diagram with the phase diagram predicted by site–bond percolation model (see Section 3.6.2). Monte Carlo simulations of site–bond percolation in 2D and 3D lattices provided the empirical relationships between the fraction of occupied sites (p_s) and the fraction of connected neighbor sites (p_b) as [3]

$$\frac{\log p_s}{\log {p_s}^*} + \frac{\log p_b}{\log {p_b}^*} = 1 \tag{8.1}$$

where ${p_s}^*$ and ${p_b}^*$ are the critical fractions in the pure site and bond percolations, respectively. In the case of a three-dimensional diamond lattice, ${p_s}^* = 0.43$, and ${p_b}^* = 0.39$ [4]. By definition, ${p_s}^*$ seems to correspond to ϕ_0/ϕ^* in the experimental system. In addition, the definition of p_b is different from the definition of the experimental reaction conversion (p). The experimental p value is defined as the ratio of the reacted arms to all the arms; on the other hand, p_b is the probability of forming a bond with a neighboring site "only if the neighboring site is occupied." Thus, the experimentally estimated p^* value corresponds to the probability that neighboring sites are occupied and a bond is formed between neighboring sites, $p_c = p_b p_s$.

The experimentally estimated $p_c - \phi_0/\phi^*$ values (symbols) and $p_c - p_s$ predicted by the model (solid line) are shown in Figure 8.3. One of the features of the model prediction is the discontinuous change in p_c at $p_s = 0.43$. At this point, all the neighboring sites are bonded ($p_b = 1$ and $p_c = 0.43$), and the system is just percolated; however, below this point, the number of occupied sites is insufficient for percolation. This significant difference between p_b and p_c originates from the restriction of the lattice, where only neighboring sites can be bonded. This discrepancy is discussed in detail in Chapter 14. On the other hand, when we focus on the region $p_s \approx 1$, the experimentally estimated p_c value is close to the value predicted by the bond percolation model. In addition, p_c does not further decrease with an increase in ϕ_0/ϕ^*. This correspondence strongly suggests that the bond percolation model in an appropriate lattice can be applied to the semidilute to the concentrated region of the prepolymers.

8.3 Fractal Dimension at the Critical Point

In Section 8.2, we discussed the sol–gel phase diagram and failure of the site–bond percolation model in the low ϕ_0 region. To investigate the reason for this failure, we investigated the network structure at p_c by means of the fractal dimension. Figure 8.4 shows the critical behaviors at various preparation concentrations ($\phi_0 = 0.0087$–0.034) [1]. In each critical condition, the power-law relationship ($G' \approx G'' \sim \omega^u$) was observed. The value of u increased with dilution, corresponding to previous studies.

Dynamic scaling theory [5] expresses u as [6, 7]

$$u = \frac{z}{z + k} \tag{8.2}$$

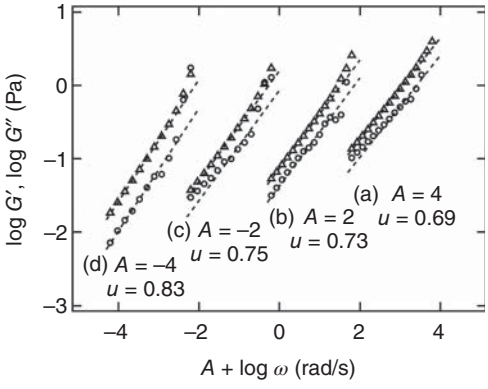

Figure 8.4 The values of G' and G'' as a function of ω for samples prepared at (a) $\phi_0 = 0.034$, (b) $\phi_0 = 0.017$, (c) $\phi_0 = 0.011$, and (d) $\phi_0 = 0.0087$. The dashed lines are the fitting curves showing the relationship $G' \approx G'' \sim \omega^u$. The curves were shifted sideways (factor A) to avoid overlap. Triangles and circles represent the loss and storage moduli, respectively. Source: Reproduced with permission from Sakai et al. [1]. Copyright 2016, Nature Publishing Group.

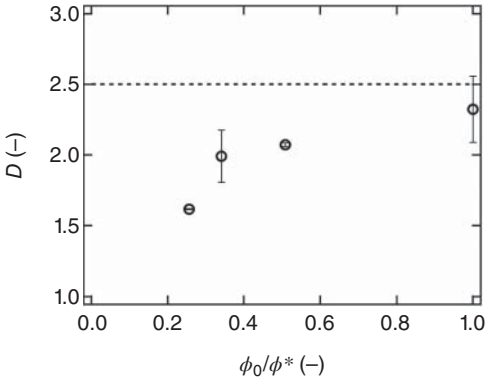

Figure 8.5 The ϕ_0/ϕ^*-dependence of D. The dashed line represents the prediction of the percolation theory. Circles represent the fractal dimension estimated from the slope of the storage and loss moduli at the critical point. Source: Reproduced with permission from Sakai et al. [1]. Copyright 2016, Nature Publishing Group.

Here, z and k are the critical exponents for the equilibrium elastic modulus and zero-shear viscosity near the critical point, respectively. When the excluded volume effect is dominant, Eq. (8.2) is reduced to the following [8–10]:

$$u = \frac{d}{D+2} \tag{8.3}$$

Here, D and d represent the fractal dimension and the spatial dimension ($d = 3$), respectively. According to Eq. (8.3), we can estimate the fractal dimension of the percolated structure at p_c from u. Figure 8.5 displays D plotted against ϕ_0/ϕ^*. The value of D at $\phi_0/\phi^* = 1$ ($D = 2.3$) is close to the prediction of the conventional percolation model for the diamond lattice ($D = 2.5$) [2]. In the dilute region, D deviates downward from the prediction of the percolation model. This deviation also indicates the inapplicability of the lattice-based percolation model to the concentration region below ϕ^*. To understand the sol–gel transition in dilute regions, we need to remove the restriction of lattices and consider the diffusion of sites.

Aggregation theory is a popular theory describing network formation from diffusing particles [11, 12]. The theory includes two representative models: monomer–cluster and cluster–cluster aggregation models. The monomer–cluster aggregation model describes the process by which monomer particles

freely diffuse and agglomerate into a cluster that is immobilized in space [13]. In addition, the cluster–cluster aggregation model considers the process in which both the clusters and monomers diffuse, collide with each other, and form aggregates. Because this theory considers the diffusion of the particles, it is expected to better reproduce the experiments in the dilute region than the monomer–cluster aggregation model. According to three-dimensional Monte Carlo simulations, the fractal dimensions of the percolation cluster in the reaction-limited monomer–cluster and cluster–cluster aggregation processes were reported to be 3.00 and 2.10, respectively [14]. In addition, the fractal dimensions in the diffusion-limited monomer–cluster and cluster–cluster aggregation processes were reported to be 2.50 and 1.78, respectively [12]. Our experimental value in the lower ϕ_0 region ($D = 1.6$) is close to that predicted by the diffusion-limited cluster–cluster aggregation (DLCCA) process. This result may suggest that the network formation process changes from lattice-based percolation to aggregation processes with dilution. This shift is likely to be caused by the fact that dilution increases the distance between prepolymers and prepolymers need to diffuse to react with other prepolymers.

Here, we make a conjecture on the percolated network structure formed at $\phi_0/\phi^* = 1/5$. First, even at such a low ϕ_0, the reaction conversion was up to 0.9. To achieve such a high conversion with limited spatial neighbors, intensive intramolecular reactions should occur between the spatial neighbors. Double or triple linkages between neighbors result in the formation of a chain-like structure that is locally oriented and has a low fractal dimension similar to that of the real chain. This prediction is supported by the abnormally low fractal dimension ($D = 1.6$), which is close to that of the real chain ($D = 1.7$).

8.4 Critical Behavior of Elastic Modulus

The elastic modulus (G) near the critical region is expected to follow a power law as

$$G \sim |p - p_c|^f \tag{8.4}$$

where p is the reaction conversion. The Bethe approximation predicts $f = 3$ [15, 16], whereas de Gennes and Daoud predict $f = 1.9$ and 2.6, respectively [17, 18]. Experiments showed scattered f values ranging from 2 to 4 [19–28]. Thus, the validity of these predictions is still unclear [29]. In addition, most of the analyses did not fully examine Eq. (8.4) because of the difficulty in quantifying p. Indeed, parameters such as time ($|t - t_c|$) or temperature ($|T - T_c|$) during the gelation process have been used instead of $|p - p_c|$. Here, t_c and T_c are defined as the time and temperature at the critical point, respectively.

In the case of a Tetra-PEG gel, we can directly measure p during the reaction process by means of ultraviolet–visible spectroscopy while at the same time measuring the viscoelasticity by means of a rheometer. Thus, we can estimate the time-dependent relationship between G and $p - p_c$, as shown in Figure 8.6 [30]. Here, we determined p_c as p at the time when the storage modulus and loss

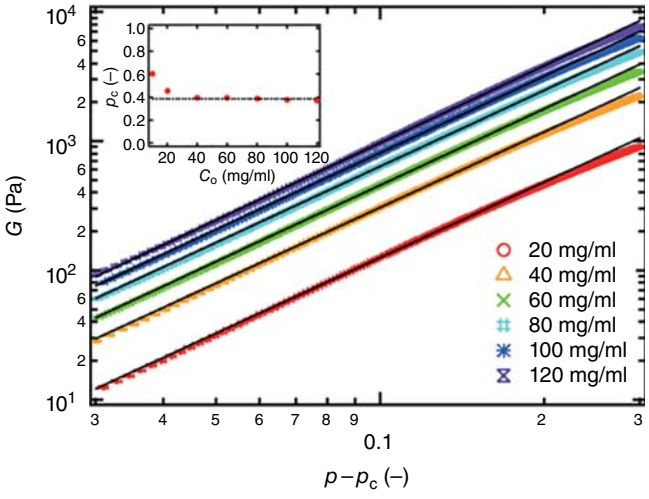

Figure 8.6 Critical behavior of *G*. The solid lines are a power law fitted the data. Inset: Initial polymer concentration (C_0) dependence of p_c. Source: Reproduced with permission from Nishi et al. [30]. Copyright 2017, American Physical Society.

modulus crossed over in the rheological measurements. Prior to the experiment, we confirmed that this criterion gave almost the same p_c as those predicted by the Winter–Chambon criterion [2]. To observe the critical behavior, the range of $p - p_c$ is set so that the storage modulus is not dependent on frequency and follows the power law. In this range, we can identify the storage modulus as *G* because the storage modulus is much larger than the loss modulus. The obtained power law ($f = 1.95 \pm 0.05$) was similar to the prediction of de Gennes ($f = 1.9$), regardless of the initial polymer concentration. These data suggest that the elasticity of gels is analogous to the conductivity of a resistor network, as proposed by de Gennes.

8.5 Reaction Kinetics of a Gelling System

The chemical reaction of Tetra-PEG–NH_2 with Tetra-PEG–OSu involves (i) aminolysis between the amine group and activated ester, (ii) hydrolysis of the activated ester, and (iii) protonation equilibrium of the terminal NH_2 group. NH_2 is in equilibrium with the equilibrium constant $K_a = [-NH_2][H^+]/[-NH_3^+]$. Notably, only the neutral amine group reacts with the activated ester group to form the amide bond, whereas the protonated amine group does not react due to the absence of an unshared electron pair. Therefore, the reaction rate equation is described as follows [31]:

$$\frac{-\mathrm{d}[-NH_2]_{\mathrm{total}}}{\mathrm{d}t} = k_{\mathrm{gel}}[-NH_2][-NHS] = k_{\mathrm{gel}} f [-NH_2]_{\mathrm{total}}[-NHS] \tag{8.5}$$

$$\frac{-\mathrm{d}[-NHS]}{\mathrm{d}t} = k_{\mathrm{gel}} f [-NH_2]_{\mathrm{total}}[-NHS] + k_{\mathrm{hyd}}[-NHS] \tag{8.6}$$

Here, $[-NH_2]_{total}$ is defined as the total concentration (mol/dm^3) of amine groups, i.e. $[-NH_2]_{total} = [-NH_2] + [-NH_3^+]$. k_{hyd}, k_{gel}, and f denote the rate constant for hydrolysis, the rate constant for gelation, and the fraction of neutral amines to total amines, i.e. $f = [-NH_2]/[-NH_2]_{total} = K_a/(K_a + [H^+])$, respectively. The K_a value was determined by potentiometric titration of a Tetra-PEG–NH_2 solution to be $10^{-9.27}$ mol/dm^3 [32]. On the basis of the previously mentioned rate equations, we evaluate k_{gel} in the following Section 8.5.2.

8.5.1 Hydrolysis Kinetics of Tetra-PEG–OSu

Figure 8.7a shows UV spectra for the hydrolysis kinetics of Linear-PEG–OSu ($M_w = 5$ kg/mol, $\phi = 0.0044$) [31]. The peak intensity observed at 260 nm, which was assigned to the dissociated NHS group, gradually increased as the gelation reaction progressed, indicating that the hydrolysis reaction proceeded.

$$[NHS^-](t) = \frac{[-NHS]_0}{A_{260}(\infty)} A_{260}(t) \tag{8.7}$$

Here, $A_{260}(\infty)$ and $A_{260}(t)$ denote the peak intensity at 260 cm^{-1} at the end of reaction and at time t, respectively. We thus estimated the hydrolysis rate constant, k_{hyd}, by least-squares fitting analysis on the basis of the following rate equation: $-d[-NHS]/dt = d[NHS^-]/dt = k_{hyd}[-NHS]$. The k_{hyd} values for Tetra-PEG–NHS of $M_w = 10$, 20, and 40 kg/mol were estimated to be 2.1×10^{-4}, 1.8×10^{-4}, and 1.9×10^{-4} s^{-1}, respectively, and that for Linear-PEG–NHS was estimated to be 2.8×10^{-4} s^{-1} (Figure 8.7b) [31]. These values were used as the fixed parameters in the following fitting analysis.

8.5.2 Gelation Kinetics of Tetra-PEG Gel

Figure 8.8 shows the concentration dependence of the kinetic traces of $[NHS^-]$ for (a) 5k Linear-PEG, (b) 10k Tetra-PEG gel, (c) 20k Tetra-PEG gel, and (d)

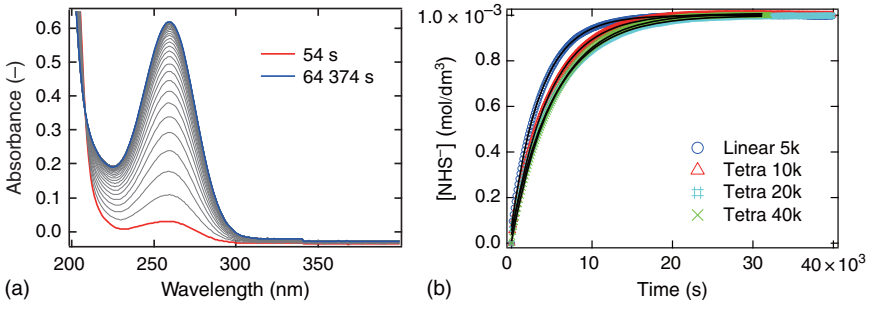

Figure 8.7 (a) Time dependence of UV spectra for the hydrolysis of Linear-PEG ($\phi = 0.044$) in a solution containing 0.2 M phosphate buffer (pH 7.0). The time interval of the data shown in this figure is 1200 s. (b) Kinetic traces obtained for the hydrolysis of NHS-terminated PEG at 260 nm as a function of time. The solid lines are results from fitting with Eq. (8.6) and $k_{gel} = 0$. Source: Reproduced with permission from Nishi et al. [31]. Copyright 2014, American Chemical Society.

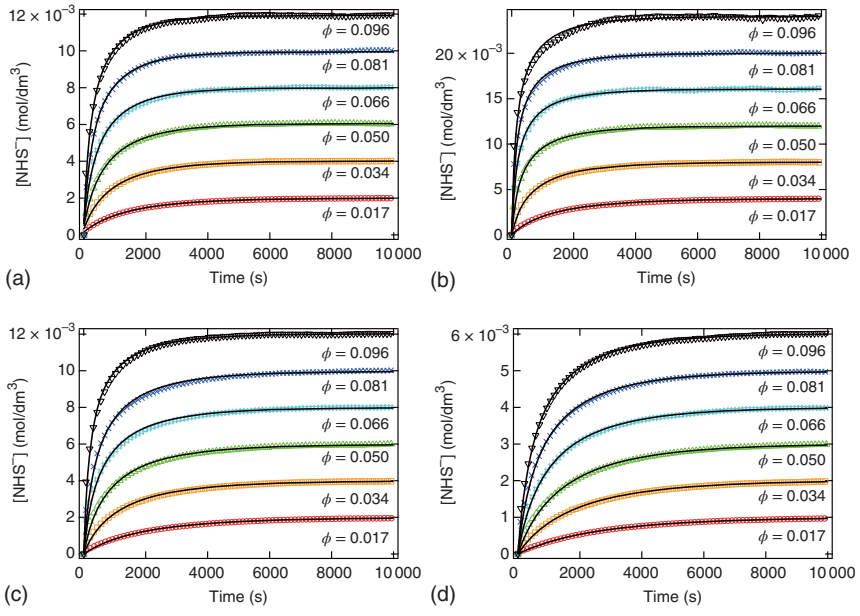

Figure 8.8 Kinetic trace obtained for the gelation of (a) 5k Linear-PEG, (b) 10k Tetra-PEG gel, (c) 20k Tetra-PEG gel, and (d) 40k Tetra-PEG gel. The solid lines are the results from fitting with Eqs. (8.5) and (8.6). Source: Reproduced with permission from Nishi et al. [31]. Copyright 2014, American Chemical Society.

40k Tetra-PEG gel [31]. The solid lines in Figure 8.8 show the theoretical curves obtained from fitting analysis using Eqs. (8.5) and (8.6), which roughly agree with the observed data from reaction initiation to near completion. The observed data are roughly represented by the fitted lines, regardless of gelation threshold.

From the fitting analysis, the gelation rate constants k_{gel} were successfully estimated for all the systems (Figure 8.9) [31]. The k_{gel} values of the Tetra-PEG gels are almost constant regardless of the polymer volume fraction and prepolymer

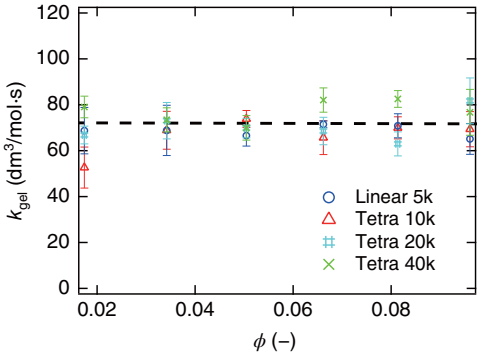

Figure 8.9 k_{gel} plotted against polymer concentration ϕ for 5k Linear-PEG, 10k Tetra-PEG gel, 20k Tetra-PEG gel, and 40k Tetra-PEG gel. Source: Reproduced with permission from Nishi et al. [31]. Copyright 2014, American Chemical Society.

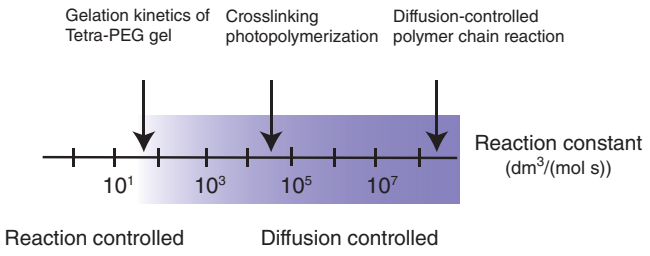

Figure 8.10 Comparison of reaction rate constants of the gelation of a Tetra-PEG gel, crosslinking photopolymerization, and a diffusion-controlled polymer chain reaction. Source: Reproduced with permission from Nishi et al. [31]. Copyright 2014, American Chemical Society.

molecular weight and are close to those for the Linear-PEG system. Furthermore, the reaction rate constant corresponds to the aminolysis rate of a low-molecular weight system ($\approx$50.9 $dm^3/(mol\,s)$) and is 10^7–10^8 times smaller than that of diffusion-controlled reactions of polymer solutions. These results strongly suggest that these reactions are reaction limited; the reaction rate of amide bond formation is much slower than the collision rate of the terminal OSu and amine groups (Figure 8.10) [31].

Here, we compare the diffusion-limited and reaction-limited cases for AB-type crosslink coupling. In the case of a diffusion-limited reaction, the reaction rate between A and B is much faster than diffusion motion. Therefore, A and B react just after encountering each other, and the local concentration of A and B at a specific time is suddenly frozen. As a result, the transient concentration heterogeneity is frozen, leading to spatial inhomogeneity. In addition, under such a high reaction rate, it is impossible to mix A and B solutions homogeneously before gelation. On the other hand, in the case of a reaction-limited reaction, the reaction rate between A and B is much slower than diffusion motion. Therefore, the A and B prepolymers diffuse and homogenize throughout the system, resulting in efficient and uniform gelation.

References

1 Sakai, T., Katashima, T., Matsushita, T., and Chung, U. (2016). Sol–gel transition behavior near critical concentration and connectivity. *Polym. J.* 48 (5): 629–634.
2 Winter, H.H. and Chambon, F. (1986). Analysis of linear viscoelasticity of a crosslinking polymer at the gel point. *J. Rheol.* 30 (2): 367–382.
3 Yanuka, M. and Englman, R. (1990). Bond-site percolation: empirical representation of critical probabilities. *J. Phys. A: Math. Gen.* 23 (7): L339–L345.
4 Xu, X., Wang, J., Lv, J.P., and Deng, Y. (2014). Simultaneous analysis of three-dimensional percolation models. *Front. Phys.* 9 (1): 113–119.
5 Martin, J.E., Adolf, D., and Wilcoxon, J.P. (1989). Viscoelasticity near the sol–gel transition. *Phys. Rev. A: At. Mol. Opt. Phys.* 39 (3): 1325–1332.

6 Winter, H.H. (1987). Evolution of rheology during chemical gelation. *Prog. Colloid Polym. Sci.* 75 (1): 104–110.

7 Hess, W., Vilgis, T.A., and Winter, H.H. (1988). Dynamical critical behavior during chemical gelation and vulcanization. *Macromolecules* 21 (8): 2536–2542.

8 Muthukumar, M. (1985). Dynamics of polymeric fractals. *J. Chem. Phys.* 83 (6): 3161–3168.

9 Muthukumar, M. (1989). Screening effect on viscoelasticity near the gel point. *Macromolecules* 22 (12): 4656–4658.

10 Randrianantoandro, H., Nicolai, T., Durand, D., and Prochazka, F. (1997). Viscoelastic relaxation of polyurethane at different stages of the gel formation. 1. Glass transition dynamics. *Macromolecules* 30 (19): 5893–5896.

11 Kolb, M., Botet, R., and Jullien, R. (1983). Scaling of kinetically growing clusters. *Phys. Rev. Lett.* 51 (13): 1123–1126.

12 Meakin, P. (1983). Diffusion-controlled cluster formation in 2–6-dimensional space. *Phys. Rev. A: At. Mol. Opt. Phys.* 27 (3): 1495–1507.

13 Witten, T.A. and Sander, L.M. (1981). Diffusion-limited aggregation, a kinetic critical phenomenon. *Phys. Rev. Lett.* 47 (19): 1400–1403.

14 Eden, M. (1961). A two-dimensional growth process. In: *Proceedings of the Fourth Berkeley Symposium on Mathematical Statistics and Probability, Volume 4: Contributions to Biology and Problems of Medicine* (ed. J. Neyman), 223–239. Berkeley, CA: University of California Press.

15 Rubinstein, M. and Colby, R.H. (2003). *Polymer Physics*. Oxford: Oxford University Press.

16 de Gennes, P.G. (1979). *Scaling Concepts in Polymer Physics*. Ithaca, NY: Cornell University Press.

17 de Gennes, P.G. (1976). On a relation between percolation theory and the elasticity of gels. *J. Phys. Lett.* 37 (1): 1–2.

18 Daoud, M. and Coniglio, A. (1981). Singular behaviour of the free energy in the sol–gel transition. *J. Phys. A: Math. Gen.* 14 (8): L301–L306.

19 Tokita, M. and Hikichi, K. (1987). Mechanical studies of sol–gel transition: universal behavior of elastic modulus. *Phys. Rev. A: At. Mol. Opt. Phys.* 35 (10): 4329.

20 Axelos, M.A.V. and Kolb, M. (1990). Crosslinked biopolymers: experimental evidence for scalar percolation theory. *Phys. Rev. Lett.* 64 (12): 1457.

21 Devreux, F., Boilot, J.P., Chaput, F. et al. (1993). Crossover from scalar to vectorial percolation in silica gelation. *Phys. Rev. E* 47 (4): 2689.

22 Fadda, G.C., Lairez, D., and Pelta, J. (2001). Critical behavior of gelation probed by the dynamics of latex spheres. *Phys. Rev. E: Stat. Phys. Plasmas Fluids Relat. Interdiscip. Top.* 63 (6): 061405.

23 Adam, M., Delsanti, M., Durand, D. et al. (1981). Mechanical properties near gelation threshold, comparison with classical and 3d percolation theories. *Pure Appl. Chem.* 53 (8): 1489–1494.

24 Adam, M., Delsanti, M., and Durand, D. (1985). Mechanical measurements in the reaction bath during the polycondensation reaction, near the gelation threshold. *Macromolecules* 18 (11): 2285–2290.

25 Martin, J.E., Adolf, D., and Wilcoxon, J.P. (1988). Viscoelasticity of near-critical gels. *Phys. Rev. Lett.* 61 (22): 2620.
26 Colby, R.H., Gillmor, J.R., and Rubinstein, M. (1993). Dynamics of near-critical polymer gels. *Phys. Rev. E* 48 (5): 3712.
27 Lusignan, C.P., Mourey, T.H., Wilson, J.C., and Colby, R.H. (1995). Viscoelasticity of randomly branched polymers in the critical percolation class. *Phys. Rev. E* 52 (6): 6271.
28 Lusignan, C.P., Mourey, T.H., Wilson, J.C., and Colby, R.H. (1999). Viscoelasticity of randomly branched polymers in the vulcanization class. *Phys. Rev. E: Stat. Phys. Plasmas Fluids Relat. Interdiscip. Top.* 60 (5): 5657.
29 Xing, X., Mukhopadhyay, S., and Goldbart, P.M. (2004). Scaling of entropic shear rigidity. *Phys. Rev. Lett.* 93 (22): 225701.
30 Nishi, K., Fujii, K., Chung, U. et al. (2017). Experimental observation of two features unexpected from the classical theories of rubber elasticity. *Phys. Rev. Lett.* 119 (26): 1–5.
31 Nishi, K., Fujii, K., Katsumoto, Y. et al. (2014). Kinetic aspect on gelation mechanism of tetra-PEG hydrogel. *Macromolecules* 47 (10): 3274–3281.
32 Kurakazu, M., Katashima, T., Chijiishi, M. et al. (2010). Evaluation of gelation kinetics of tetra-PEG Gel. *Macromolecules* 43 (8): 3935–3940.

9

Structural Analysis by Light and Neutron Scattering

Takamasa Sakai[1] *and Xiang Li*[2]

[1] *Graduate School of Engineering, The University of Tokyo, Tokyo, Japan*
[2] *Institute for Solid States Physics, The University of Tokyo, Tokyo, Japan*

The end-to-end distance of a network strand in a gel is typically in a size range of a few to several tens of nanometers. This length scale is far below the diffraction limit of visible light. In addition, the network strands fluctuate in the solvent on a time scale of milliseconds due to their thermal motion. This size and dynamics make it impossible to observe the network structure by general optical microscopes. Modern atomic force microscopy (AFM) with fast tapping mode allows direct observation of soft materials with subnanometer resolution [1], while the observable region is limited to the surface of the samples. Transmission electron cryomicroscopy (Cryo-TEM) with a fast cooling system recently visualized immiscible network structures such as thick gelatin bundles in a gelatin gel [2], while it is still challenging to observe miscible networks and other soft materials because a single polymer chain is almost transparent to electrons. The most popular technique for probing the nanostructure of soft materials, including gels, is scattering measurements with light, X-rays, and neutrons [3]. The photons and neutrons scattered by the gel network form interference patterns, reflecting the spatial distribution of the polymer chains. Here, we introduce several results of scattering from a Tetra-PEG gel. All the data shown in the following text were obtained on a small angle neutron scattering (SANS) instrument, SANS-U, installed in the Japan Research Reactor-3 (JRR-3).

9.1 Scattering Curves of Tetra-PEG Gels

The scattering profiles of Tetra-PEG gels are shown in Figure 9.1. In the case of the as-prepared 5k Tetra-PEG gel, anomalous strong scattering exists for $q < 0.01$ Å^{-1}, indicating that there are spatial defects with a characteristic size larger than 50 nm. However, in all the other gels, this anomalous scattering was not observed. Based on the scattering profiles, most of the Tetra-PEG gels were spatially homogeneous, at least in the size range smaller than 100 nm.

Physics of Polymer Gels, First Edition. Edited by Takamasa Sakai.

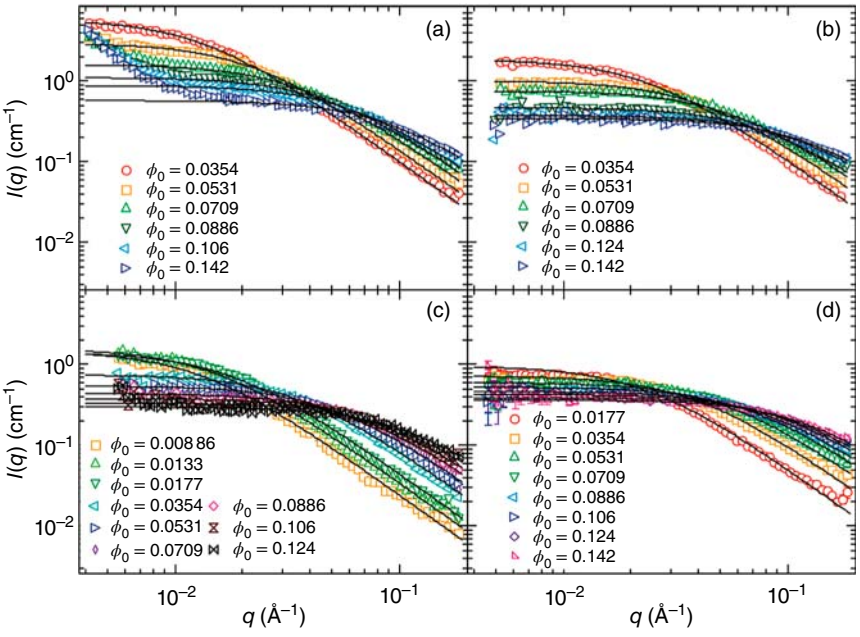

Figure 9.1 Scattering intensity curves of Tetra-PEG gels at various preparation concentrations: (a) 5k, (b) 10k, (c) 20k, and (d) 40k Tetra-PEG gels. Source: Reproduced with permission from Matsunaga et al. [5]. Copyright 2009, American Chemical Society.

The solid curves are the model fits with the Ornstein–Zernike (OZ) function (Eq. (9.1)) [4]:

$$I(q) = \frac{(\Delta\rho)^2 RT\phi^2}{N_A M_{os}} \frac{1}{1+\xi^2 q^2} \tag{9.1}$$

Here, R is the gas constant, T is the absolute temperature, M_{os} is the longitudinal modulus of the gel, and ξ is the correlation length of a gel network (Column 2). In contrast to the single-contact theory, which is a molecular-based model, the OZ function is derived on the basis of thermodynamics. The $I(0)$ values obtained from the OZ function fit to the data of the Tetra-PEG gels are obviously a decreasing function of ϕ (Figure 9.1), suggesting that all gels are in a semidilute regime. This result is a natural outcome because the polymerization degree of the gel network is infinitely large and c^* is close to 0. This statement is also supported by the osmotic pressure observed in Chapter 14. The correlation length of the gel network estimated from the OZ fit is shown in Figure 9.2. The correlation length is almost independent of the molecular weight of the prepolymers. For the 40k Tetra-PEG gel, ξ agrees well with a scaling prediction for a semidilute solution with a good solvent, $\xi \sim \phi^{-0.75}$. Notably, the values of ξ estimated from the OZ function strongly depend on the fitting range. Strictly speaking, the OZ function should be only applied when $q < \xi^{-1}$ or $I > 0.5I(0)$. The relatively large variation in the scaling relation in Figure 9.2 may originate from the fitting range.

In addition to the as-prepared state, we studied the equilibrium-swollen Tetra-PEG gels [5]. Notably, the degree of spatial heterogeneity is enhanced by

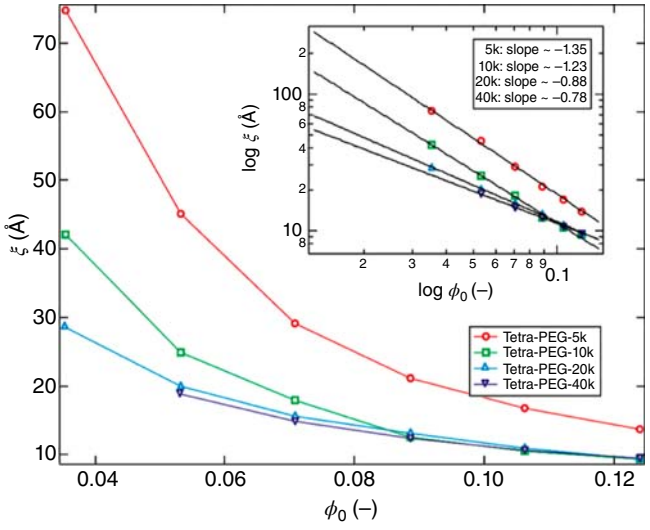

Figure 9.2 Correlation length of Tetra-PEG gels as a function of preparation concentration. Source: Reproduced with permission from Matsunaga et al. [5]. Copyright 2009, American Chemical Society.

swelling because swelling causes sparse regions to become more diluted and dense region to become less diluted. To our surprise, even the structural factors in swollen gels (data not shown here) in the SANS regime can be represented by OZ-type scattering functions, irrespective of the molecular weight. This anomalous result indicated that the spatial heterogeneity was negligible in fully swollen Tetra-PEG gels in the q-range of SANS ($0.006 < q < 0.2\,\text{Å}^{-1}$), which corresponds to a length scale of $3 < d < 100\,\text{nm}$ in real space.

However, when the q-range comes into the light scattering regime ($q < 0.003\,\text{Å}^{-1}$, corresponding to a length scale in real space of $d > 200\,\text{nm}$), strong anomalous scattering was observed for all Tetra-PEG gels (Figure 9.3 for $q\xi < 0.1$). Similar anomalous scattering has been commonly observed in

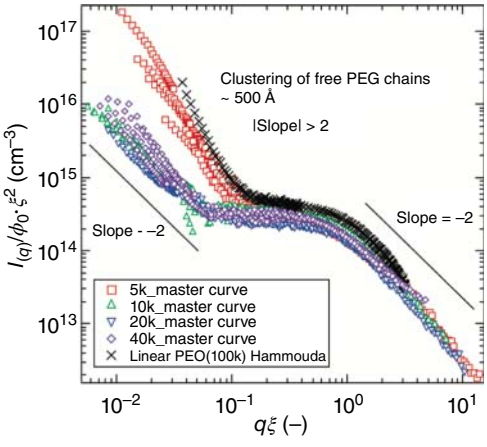

Figure 9.3 Static light scattering and SANS data are plotted as a function of $q\xi$ for four Tetra-PEG gels with different molecular weights. All the gels are measured in the as-prepared state. Source: Reproduced with permission from Matsunaga et al. [5]. Copyright 2009, American Chemical Society.

polymer gels, although it was usually observed immediately from the size of ξ, i.e. $q\xi \leq 1$. Thus, compared with conventional polymer gels, Tetra-PEG gels have significantly suppressed spatial homogeneity. We must note that linear PEG solutions displayed similar low-q anomalous scattering, which is attributed to the large-scale aggregates of PEG chains. In the linear chain study, the contribution of this anomalous low-q scattering was found to strongly depend on the solvent and chemical structure of the end groups of the PEG chains.

9.2 Scattering Curves of Stretched Tetra-PEG Gels

We performed SANS measurements on Tetra-PEG gels under stretching [6]. A pioneering work on the structure analysis of a deformed network was performed by Benoit using SANS in a contrast-matched polystyrene system to correlate the microstructure and the macroscopic deformation [7, 8]. However, the heterogeneity of the gel network made the data analysis difficult. Figure 9.4 shows a series of 2D scattering patterns of a Tetra-PEG gel prepared at $\phi = 0.11$ with a molecular weight of 40k. The gel was uniaxially stretched to various strain ratios ($\lambda = 1 - 5$). The scattering patterns acquired with different detector distances (sample to detector distance (SDD), 2 and 8 m) at $\lambda = 1.0$ were almost isotropic. Slightly anisotropic SANS patterns were observed when SDD = 2 m at a higher strain ratio ($\lambda > 3$). However, compared with the anisotropy in conventional gels, which show clear butterfly patterns even at very small λ values, this anisotropy is quite small. The 2D SANS patterns were reduced to 1D I–q profiles by taking the parallel and perpendicular sectional average and

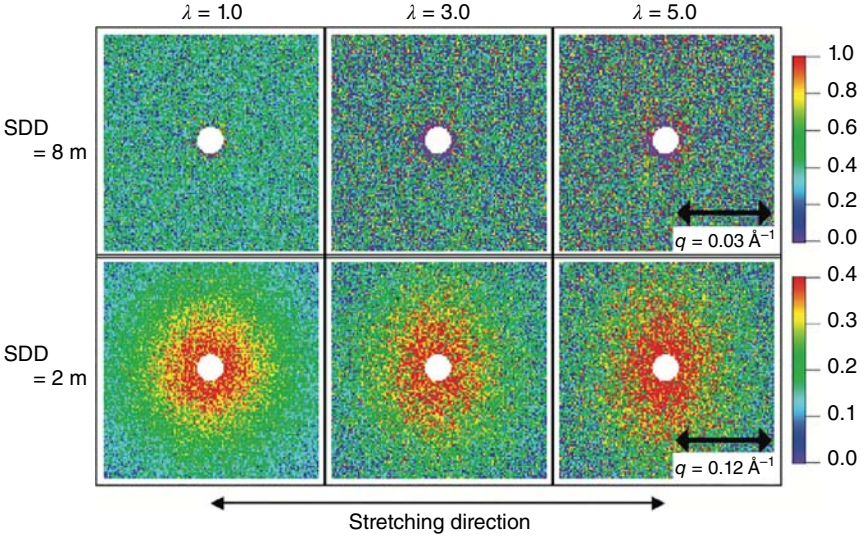

Figure 9.4 2D scattering profile of a Tetra-PEG gel under uniaxial deformation. The gel was prepared at $\phi = 0.11$ with a molecular weight of 40k. Each image was measured for 10 minutes under a fixed strain ratio. Source: Reproduced with permission from Matsunaga et al. [6]. Copyright 2011, American Chemical Society.

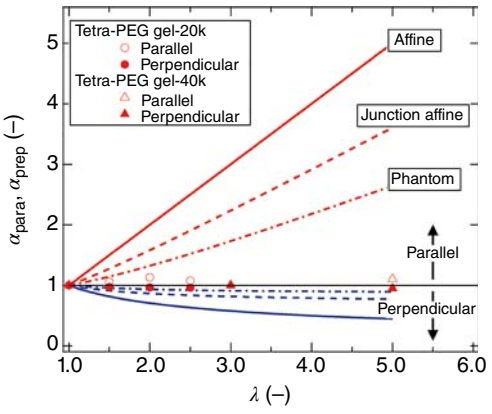

Figure 9.5 Variation in microscopic deformation ratios (α_{para} and α_{perp}) as a function of macroscopic strain ratio (λ) of Tetra-PEG gels (circles and triangles). The theoretical lines predicted by the affine (solid line), junction-affine (dashed line), and phantom chain (chain line) models are shown as guides. Source: Reproduced with permission from Matsunaga et al. [6]. Copyright 2011, American Chemical Society.

subsequently analyzed with the OZ function to obtain the stretched blob size in each direction.

Figure 9.5 shows the microscopic deformation ratios, α_{para} and α_{perp}, as a function of the macroscopic strain ratio, λ. The microscopic deformation ratios denote the deformation ratio of the blob size with respect to the blob size in the undeformed state ($\lambda = 1$). In comparison to the theoretically predicted variations for chain stretching, i.e. affine, junction-affine, and phantom network models, the variations in α_{para} and α_{perp} were negligibly small. This result suggests that the blob size, which is a typical size of the concentration fluctuation, is insensitive to the conformational changes of polymer chains, at least at the strain ratio tested in the study. Since the polymer chains are definitely stretched to an extent much larger the values of α_{para} and α_{perp}, the use of blob size to probe the chain deformation may be inappropriate. One needs to label a small number of network strands with deuterium in order to visualize the chains by means of neutron scattering. Then, one can know the relationship between macroscopic and microscopic deformations and examine the models of rubber or gel elasticity.

References

1 Yang, H., Wang, Y., Lai, S. et al. (2007). Application of atomic force microscopy as a nanotechnology tool in food science. *J. Food Sci.* 72: R65–R75.

2 Marmorat, C., Arinstein, A., Koifman, N. et al. (2016). Cryo-imaging of hydrogels supermolecular structure. *Sci. Rep.* 6: 25495.

3 Roe, R.J. (2000). *Methods of X-Ray and Neutron Scattering in Polymer Science*. Oxford University Press.

4 Matsunaga, T., Sakai, T., Akagi, Y. et al. (2009). Structure characterization of tetra-PEG gel by small-angle neutron scattering. *Macromolecules* 42 (4): 1344–1351.

5 Matsunaga, T., Sakai, T., Akagi, Y. et al. (2009). SANS and SLS studies on tetra-arm PEG gels in as-prepared and swollen states. *Macromolecules* 42 (16): 6245–6252.

6 Matsunaga, T., Asai, H., Akagi, Y. et al. (2011). SANS studies on tetra-PEG gel under uniaxial deformation. *Macromolecules* 44 (5): 1203–1210.
7 Benoit, H., Decker, D., Duplessix, R. et al. (1976). Characterization of polystyrene networks by small-angle neutron scattering. *J. Polym. Sci., Part B: Polym. Phys.* 14: 2119–2128.
8 Tsay, H.M. and Ullman, R. (1988). Small-angle neutron scattering of crosslinked polystyrene networks. *Macromolecules* 21: 2963–2972.

10

Elastic Modulus

Takamasa Sakai and Yuki Yoshikawa

Graduate School of Engineering, The University of Tokyo, Tokyo, Japan

Elastic modulus (G) is one of the most representative physical properties of polymer gels. The affine and phantom network models predict G as functions of the number density of elastically effective chains (ν) and the number density of crosslinks (μ) (Section 3.3).

$$G_{\mathrm{af}} = \nu kT \tag{3.15′}$$

$$G_{\mathrm{ph}} = (\nu - \mu)kT \tag{3.35′}$$

where k is the Boltzmann constant and T is the absolute temperature. The difference between these models is how they address the fluctuation of crosslinks. The affine network model assumes that crosslinks are fixed to the gel body and that the deformation of network strands perfectly follows the macroscopic deformation. By contrast, the phantom network model assumes that crosslinks fluctuate and that the deformation of the network strands is attenuated. For a perfect tetra-functional polymer network, the G predicted by the affine network model is double than that predicted by the phantom network model. Despite such significant differences, the validity or the condition for the establishment of these models remain unknown.

10.1 Effect of Connectivity

Tuning the connectivity (the reaction conversion) induces the minimum variation in the system, i.e. there is no change in the substances included in the system, and the only difference is whether the chain ends are connected or not. Therefore, compared with other structural parameters, i.e. strand length and polymer concentration, the connected fraction is expected to have a simple influence on the physical properties. Therefore, p is appropriate as the first parameter to be tuned for understanding the structure–property relationship.

To investigate the effect of the connectivity (p) on G, we investigated the evolution of G during the gelation process by means of rheometry and ultraviolet–visible spectroscopy. G and p were recorded as a function of

Physics of Polymer Gels, First Edition. Edited by Takamasa Sakai.

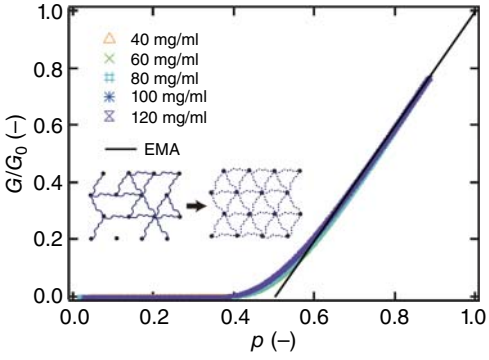

Figure 10.1 Comparison between the experimental results for a Tetra-PEG gel and the results predicted by EMA regarding the p dependence of G/G_0. Source: Reproduced with permission from Nishi et al. [1]. Copyright 2017, American Physical Society.

time (t), and then the G–p relationship was obtained using t as an intermediary. This method enables us to experimentally obtain a continuous G–p relationship. Figure 10.1 shows the relationship between G/G_0 and p [1]. Notably, G_0 is the extrapolation of G at $p = 1$ based on the percolated network model (Section 3.4.1). All data for the 20k Tetra-PEG gels with different initial polymer concentrations (C_0) fall onto a single curve, which corresponds to the values predicted by effective-medium approximation (EMA). EMA was first developed to describe the conductivity of a bond-disordered conductance network [2] and was later improved to describe the rubber elasticity of a Gaussian chain network [3]. As shown in the inset of Figure 10.1, EMA converts a disordered network with elastic constant g_0 into an averaged ideal network with elastic constant g_m. Assuming that the average fluctuation of the crosslinks is 0 under the balance of tension, G/G_0 is described as the following equation in the range of large p values ($p > 0.75$ in the tetra-branched network).

$$G/G_0 = \frac{g_m}{g_0} = \frac{p - 2/z}{1 - 2/z} \tag{10.1}$$

where z is the degree of branching in the network. Notably, the G/G_0–p relationship in EMA agrees well with the G/G_0–p relationship in the phantom network model (Section 3.3.2) with the Bethe approximation (Section 3.4.2) [1]. In other words, the p dependence of G/G_0 is successfully described by the phantom network model as [1]

$$G = g(\nu - \mu)kT = gG_{\mathrm{ph}} \tag{10.2}$$

where g is the proportionality constant. The values of $g(=G/G_{\mathrm{ph}})$ are larger than unity and increase with an increase in C_0 (Figure 10.2). For further discussion on g, we investigated the effect of the polymer concentration and molecular weight of the network strands.

10.2 Effect of the Polymer Concentration and Network Strand Length

We performed stretching measurements on Tetra-PEG gels with different C_0 values and prepolymer molecular weights [4]. The value of p was almost

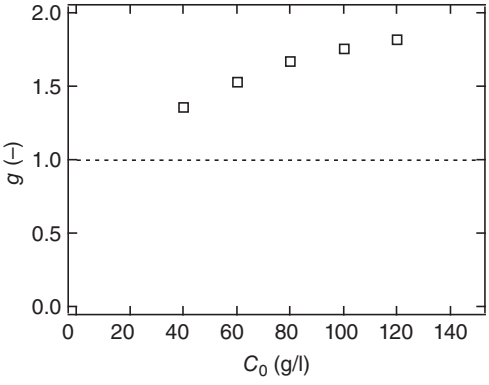

Figure 10.2 $g(=G/G_{ph})$ as a function of C_0 in the 20k Tetra-PEG gel. The dashed line shows $g = 1$, i.e. $G = G_{ph}$.

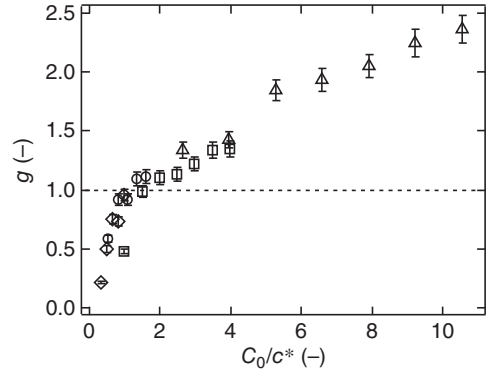

Figure 10.3 g as a function of C_0/c^* in Tetra-PEG gels (Tetra-PEG gel 5k, ◇ 10k, ○; 20k, □; 40k, Δ). The dashed line shows $g = 1$, i.e. $G = G_{ph}$.

constant at approximately $p = 0.9$, although there was slight fluctuation among the samples. Notably, this change in p is accounted for in the calculation of G_{ph} according to the Bethe approximation. Figure 10.3 shows the relationship between g $(=G/G_{ph})$ and C_0/c^*, where c^* is the overlap polymer concentration of the prepolymers (Section 2.2.1). The prediction of the phantom network model is a flat line showing $g = 1$ (dashed line). In this plot, all data roughly collapsed onto a single curve, suggesting that C_0/c^* is the parameter governing g. In the entire range tested, g increased with an increase in C_0/c^*. It should be noted that $g = 1$; in other words, G agrees well with the prediction of the phantom network model at approximately $C_0 = c^*$. Previously, the upward deviation from the prediction of the phantom network model ($g > 1$) has often been attributed to the existence of trapped entanglements. However, the phantom-like p dependence, the ultimate stretched ratio monotonically increasing with an increase in polymer concentration (Chapter 11), and the fracture energy obeying the Lake–Thomas model (Chapter 12) strongly suggest that this supposition is not the case. The transition to the affine network model is also not the case because we observed the phantom-like p dependence. At this point, we predict that this increase in g is caused by suppression of the fluctuation of the network strands (conceptually similar to the affine network model) or simply by the overlapping of network strands (conceptually similar to the topological interaction). In addition, in

the range of $C_0 < c^*$, g decreased more steeply with a decrease in C_0/c^*. The downward deviation from the prediction of the phantom network model in the dilute region may be due to the formation of elastically ineffective connections (Section 3.7).

References

1 Nishi, K., Fujii, K., Chung, U.-i. et al. (2017). Experimental observation of two features unexpected from the classical theories of rubber elasticity. *Phys. Rev. Lett.* 119 (26): 267801.

2 Kirkpatr, S. (1973). Percolation and conduction. *Rev. Mod. Phys.* 45 (4): 574–588.

3 Nishi, K., Noguchi, H., Sakai, T., and Shibayama, M. (2015). Rubber elasticity for percolation network consisting of Gaussian chains. *J. Chem. Phys.* 143 (18): 184905.

4 Akagi, Y., Gong, J.P., Chung, U.-i., and Sakai, T. (2013). Transition between phantom and affine network model observed in polymer gels with controlled network structure. *Macromolecules* 46 (3): 1035–1040.

11

Large Deformation

Takamasa Sakai and Takuya Katashima

Graduate School of Engineering, The University of Tokyo, Tokyo, Japan

As discussed in Section 5.2, the stress–strain relationship in polymer networks is determined by the strain energy density (W) function; σ_i is the partial derivative of W with respect to λ_i:

$$\sigma_i = \frac{\partial W}{\partial \lambda_i} \tag{5.56}$$

where σ_i and λ_i ($i = x, y, z$) are the nominal stress and the principal stretch ratio, respectively, along the x, y, and z axes. In the past half-century, many types of phenomenological or molecular models for W have been proposed [1, 2]. Although these models have been vigorously examined, full understanding of the W in polymer networks has not been obtained due to the following two major problems: One stems from the limitation in the deformation range of conventional mechanical testing, and the other stems from the inhomogeneities in polymer networks. To overcome these problems, we performed general biaxial and uniaxial stretching tests on a series of Tetra-PEG gels with precisely controlled network structures [3–5].

11.1 Estimation of Strain Energy Density Function

To investigate the strain energy density function, we performed general biaxial stretching measurements (see Section 5.2.1). The biaxial stretching measurement was carried out on square sheets of Tetra-PEG gels in the as-prepared state. The stress–strain relationships obtained here corresponded to the equilibrium relationships without time effects because no appreciable relaxation in stress was observed after the imposition of a constant large strain at the experimental crosshead speed of 1.0 mm/s. The biaxial tester can stretch the samples independently in the two orthogonal directions (x and y directions) and measure the tensile force in each direction as a function of the principal ratios λ_i ($i = x, y$). We employed here the three types of biaxial deformation: equi-biaxial (EB) stretching, pure shear (PS), and unequi-biaxial (UB) stretching. Under EB stretching, the samples were equally elongated in the x and y directions ($\lambda_x = \lambda_y$).

Physics of Polymer Gels, First Edition. Edited by Takamasa Sakai.

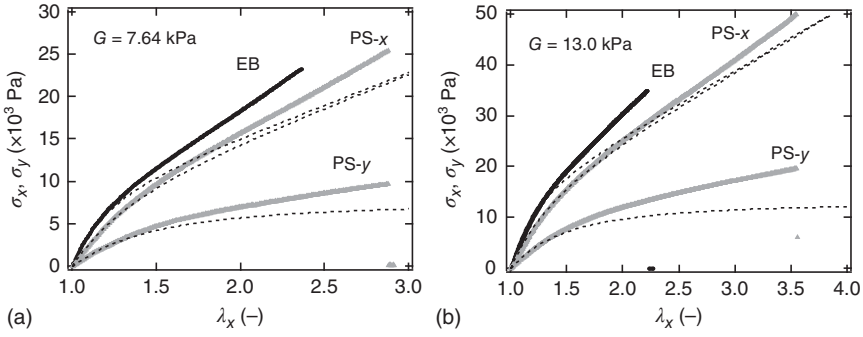

Figure 11.1 Nominal stress–elongation relationships for Tetra-PEG gels ((a) $\phi_0 = 0.0662$ and (b) $\phi_0 = 0.0961$) under EB stretching and PS. The dashed lines represent the stress–strain relationships of the NH model. Source: Reproduced with permission from Katashima et al. [4]. Copyright 2012, Royal Society of Chemistry.

Under PS, the samples were stretched in the x direction while maintaining the initial dimensions in the y direction ($\lambda_y = 1$). Under UB stretching, the samples were stretched in the x direction at a crosshead speed of 1.0 mm/s and in the y direction at a crosshead speed of 0.50 mm/s, which resulted in biaxial stretching satisfying the relationship $\lambda_y = (1 + \lambda_x)/2$. Under each type of deformation, the samples were elongated up to macroscopic rapture.

11.1.1 Applicability of Neo-Hookean Model

Figure 11.1 shows σ_{EB}, $\sigma_{PS\text{-}x}$, and $\sigma_{PS\text{-}y}$ as a function of λ_x. Under EB stretching, no appreciable difference was observed between $\sigma_{EB\text{-}x}$ and $\sigma_{EB\text{-}y}$, assuring the achievement of equal strains in the two directions. First, we examine the applicability of the neo-Hookean (NH) model [6–10] (see Section 5.3.1) to the biaxial data. The NH model, one of the simplest phenomenological W functions, is expressed as

$$W = \frac{G}{2}(\lambda_x^{\,2} + \lambda_y^{\,2} + \lambda_z^{\,2} - 3) = \frac{G}{2}(I_1 - 3) \tag{5.36}$$

This function includes only I_1, which is the first invariant of Green's deformation tensor, as a variable. The NH model has the same equation as the affine network model, which has been considered a model for ideal polymer networks with infinite extensibility and without structural defects. The stress–strain relationship for each deformation mode obtained by the NH model is given by

$$\sigma_{EB} = G(\lambda_x - \lambda_x^{\,-5}) \quad \text{(equi-biaxial)} \tag{11.1}$$

$$\sigma_{PS\text{-}x} = G(\lambda_x - \lambda_x^{\,-3}) \quad \text{(pure shear)} \tag{11.2}$$

$$\sigma_{PS\text{-}y} = G(1 - \lambda_x^{\,-2}) \quad \text{(pure shear)} \tag{11.3}$$

where the condition of isovolumetric deformation ($\lambda_x \lambda_y \lambda_z = 1$) is employed.

The dashed lines in Figure 11.1 represent the stress–strain relationships predicted by Eqs. (11.1)–(11.3). A satisfactory fit is observed in only the low-strain

region (approx. $\lambda_x < 1.3$), and the NH model evidently fails to describe the data even at a moderate deformation of $\lambda_x > 1.3$. Thus, the stress–elongation behaviors of the Tetra-PEG gels, which are assumed to be near-ideal networks, are far from those predicted by the NH model. This result indicates that the effects of finite extensibility and/or explicit strain coupling between different axes, such as $\lambda_i \lambda_j$, both of which are not considered in the NH model, exist in Tetra-PEG gels.

11.1.2 Finite Extensibility Effect

Conventionally, strain hardening at high deformation is modeled as the non-Gaussian statistics of strongly stretched chains [11, 12]. In this section, we adopt the Gent model [13], which describes the effect of finite extensibility by a minimal addition to the NH model. The elastic free energy of the Gent model is expressed as

$$W = -\frac{G}{2}(I_{\mathrm{m}} - 3)\ln\left(1 - \frac{I_1 - 3}{I_{\mathrm{m}} - 3}\right) \tag{5.24}$$

The quantity I_{m} is the maximum value of I_1 where the stress becomes infinite. Notably, Eq. (5.24) is reduced to the NH model in the low-strain region. The stress–strain relationship for each deformation mode is given by

$$\sigma_{\mathrm{EB}} = \frac{G(\lambda_x - {\lambda_x}^{-5})}{1 - (2{\lambda_x}^2 - {\lambda_x}^{-4} - 3)/(I_{\mathrm{m}} - 3)} \quad \text{(equi-biaxial)} \tag{11.4}$$

$$\sigma_{\mathrm{PS}\text{-}x} = \frac{G(\lambda_x - {\lambda_x}^{-3})}{1 - ({\lambda_x}^2 - {\lambda_x}^2 - 2)/(I_{\mathrm{m}} - 3)} \quad \text{(pure shear)} \tag{11.5}$$

$$\sigma_{\mathrm{PS}\text{-}y} = \frac{G(1 - {\lambda_x}^{-2})}{1 - ({\lambda_x}^2 - {\lambda_x}^{-2} - 2)/(I_{\mathrm{m}} - 3)} \quad \text{(pure shear)} \tag{11.6}$$

Although the fit for $\sigma_{\mathrm{PS}\text{-}x}$ using Eq. (11.5) works well, the theory fails to describe the data for $\sigma_{\mathrm{PS}\text{-}y}$ and σ_{EB} using the same fitting parameters (Figure 11.2). When

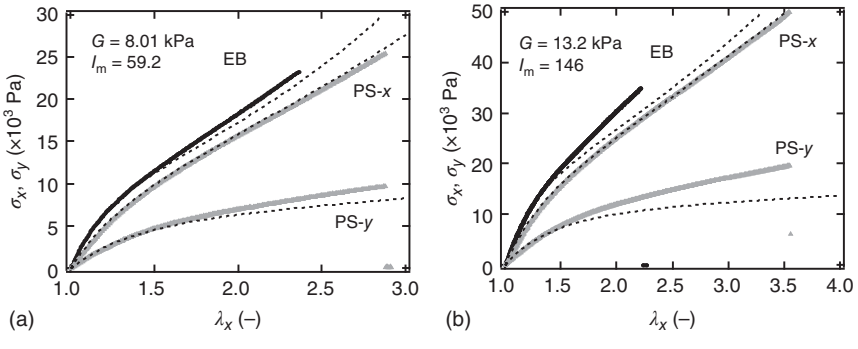

Figure 11.2 Nominal stress–elongation relationships for Tetra-PEG gels ((a) $\phi_0 = 0.0662$ and (b) $\phi_0 = 0.0961$) under EB stretching and PS. The dashed lines are the fitting results of the Gent model. Source: Reproduced with permission from Katashima et al. [4]. Copyright 2012, Royal Society of Chemistry.

we focus on $\sigma_{\text{PS-}y}$, the theoretical predictions shown are always lower than the experimental values; the effect of stretching in one direction on the stress in the other direction is stronger than the theoretically expected effect. In Section 11.1.3, we focus on this strain coupling between different axes.

11.1.3 Coupling Between Different Principal Axes

The NH model does not include explicit strain coupling, which is represented by the cross-terms $\lambda_i\lambda_j$ ($i, j = x, y, z$), except for the weak coupling as a result of volume conservation ($\lambda_x\lambda_y\lambda_z = 1$). The absence of the cross-term causes no significant difference in σ_x between the different types of deformation in the large λ_x region (Figure 11.1) and is most likely the reason for the failure of the NH model to represent experimental data.

The stress ratio under PS deformation ($\sigma_{\text{PS-}y}/\sigma_{\text{PS-}x}$) is known as a measure of the cross-effect of the strains in the x and y directions on stresses [14]. In general, the W function for incompressible materials ($\lambda_x\lambda_y\lambda_z = 1$) is expressed as a function of I_1 and I_2 as

$$W = W(I_1, I_2) \tag{11.7}$$

The stresses under biaxial deformation are given by [2]

$$\sigma_i = \frac{\partial W}{\partial \lambda_i} = \frac{2}{\lambda_i}\left(\lambda_i^2 - \frac{1}{\lambda_i^2\lambda_j^2}\right)(W_1 + \lambda_j^2 W_2) \quad (i, j = x, y) \tag{11.8}$$

where W_1 and W_2 are the derivatives of W with respect to I_1 and I_2, respectively. Equation (11.8) gives a general expression of the stress ratio under PS deformation as [14]

$$\frac{\sigma_y}{\sigma_x} = \frac{\lambda_x}{\lambda_x^2 + 1} + AW_2 \tag{11.9}$$

$$A = \frac{\lambda_x(\lambda_x^2 - 1)}{(\lambda_x^2 + 1)(W_1 + W_2)} \tag{11.10}$$

From Eq. (11.9), the stress ratio in the case of $W_2 = 0$, i.e. without an explicit cross-effect of strains, is expressed as

$$\frac{\sigma_y}{\sigma_x} = \frac{\lambda_x}{\lambda_x^2 + 1} \tag{11.11}$$

It should be noted that this is also the case with the Gent model, which does not include I_2 as a variable. The dashed line in Figure 11.3 is the prediction of Eq. (11.11). The values of the stress ratio for the Tetra-PEG gels in the moderate λ_x region were higher than the values predicted by the NH and Gent models. The stress ratio, i.e. the coupling strength, increases with an increase in ϕ_0. These results clearly show that the failure of the Gent model in Figure 11.2 is mainly attributable to the absence of explicit cross-effects.

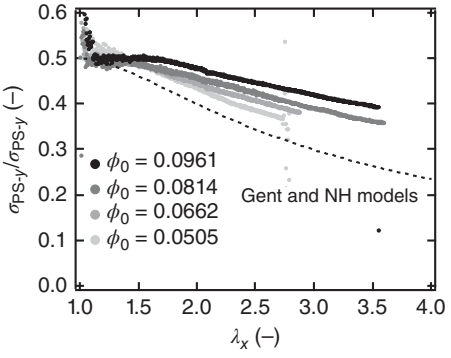

Figure 11.3 Stress ratio ($\sigma_{PS\text{-}y}/\sigma_{PS\text{-}x}$) as a function of λ_x under PS deformation for each sample. The dashed line shows the prediction of the Gent and NH models. Source: Reproduced with permission from Katashima et al. [4]. Copyright 2012, Royal Society of Chemistry.

11.1.4 Extended Gent Model

On the basis of the results in Section 11.1.3, we revealed that the W function of a Tetra-PEG gel required an explicit strain coupling term. Thus, to estimate how to introduce the I_2 term, we utilized the Rivlin–Saunders method, as introduced in Section 5.2.1. In this method, we can evaluate $\partial W/\partial I_1$, $\partial W/\partial I_2$ with respect to the experimental values σ_x and σ_y according to Eq. (5.26):

$$W_1 = \frac{\partial W}{\partial I_1} = \frac{1}{2({\lambda_x}^2 - {\lambda_y}^2)}\left[\frac{{\lambda_x}^3\sigma_x}{{\lambda_x}^2 - (\lambda_x\lambda_y)^2} - \frac{{\lambda_y}^3\sigma_y}{{\lambda_y}^2 - (\lambda_x\lambda_y)^2}\right]$$
$$W_2 = \frac{\partial W}{\partial I_2} = \frac{1}{2({\lambda_x}^2 - {\lambda_y}^2)}\left[\frac{\lambda_x\sigma_x}{{\lambda_x}^2 - (\lambda_x\lambda_y)^2} - \frac{\lambda_y\sigma_y}{{\lambda_y}^2 - (\lambda_x\lambda_y)^2}\right] \quad (5.26)$$

Figure 11.4 shows the normalized W_1 and W_2 values estimated from the PS data plotted against $I_1 - 3$ ($=I_2 - 3$). W_1 increased with increasing $I_1 - 3$, reflecting the finite extensibility effect. On the other hand, W_2 showed a finite positive value independent of the deformation ratio, suggesting that the "linear" I_2 term is necessary to reproduce the W function of the Tetra-PEG gel.

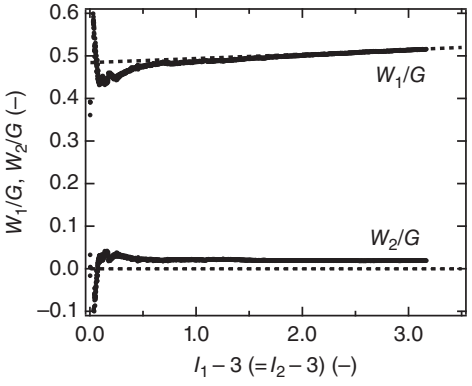

Figure 11.4 W_1 and W_2 estimated from the PS data plotted against $I_1 - 3$ ($=I_2 - 3$).

According to the Rivlin–Saunders plot, we proposed a new model (extended Gent model) that is expressed as a sum of the Gent model and a linear term of I_2:

$$W = \frac{G}{2}\left\{-(1-r)(I_{\mathrm{m}}-3)\ln\frac{I_1-3}{I_{\mathrm{m}}-3} + r(I_2-3)\right\} \tag{11.12}$$

Here, r determined the strength of the I_2 term in the modulus. The stress–strain relationship for each deformation mode in this model is given by

$$\sigma_{\mathrm{EB}} = G\left\{\frac{(1-r)(\lambda_x - {\lambda_x}^{-5})}{1-(2{\lambda_x}^2 - {\lambda_x}^{-4}-3)/(I_{\mathrm{m}}-3)} + r({\lambda_x}^2 - {\lambda_x}^{-3})\right\} \quad \text{(equi-biaxial)} \tag{11.13}$$

$$\sigma_{\mathrm{PS}\text{-}x} = G\left\{\frac{(1-r)(\lambda_x - {\lambda_x}^{-3})}{1-({\lambda_x}^2 - {\lambda_x}^{-2}-3)/(I_{\mathrm{m}}-3)} + r(\lambda_x - {\lambda_x}^{-3})\right\} \quad \text{(pure shear)} \tag{11.14}$$

$$\sigma_{\mathrm{PS}\text{-}x} = G\left\{\frac{(1-r)(1-{\lambda_x}^{-2})}{1-({\lambda_x}^2 - {\lambda_x}^{-2}-3)/(I_{\mathrm{m}}-3)} + r({\lambda_x}^2 - 1)\right\} \quad \text{(pure shear)} \tag{11.15}$$

The parameters r and I_{m} were independently determined by the following procedure. r was estimated from the fit of $\sigma_{\mathrm{PS}\text{-}y}/\sigma_{\mathrm{PS}\text{-}x}$ vs. λ_x because only the term I_2 governs the coupling strength between different axes (Figure 11.3). The I_{m} value was estimated from the fit to PS-x using the evaluated values of r. The theoretical predictions for EB and PS-y obtained with these parameters are shown by the dashed lines in Figure 11.5.

The data for all ϕ_0 values are in good agreement with Eqs. (11.13)–(11.15) over a wide range of λ_x values. Figure 11.5 also includes the data for UB stretching of $\lambda_y = (\lambda_x + 1)/2$. The stress–strain relationship for UB stretching in the extended

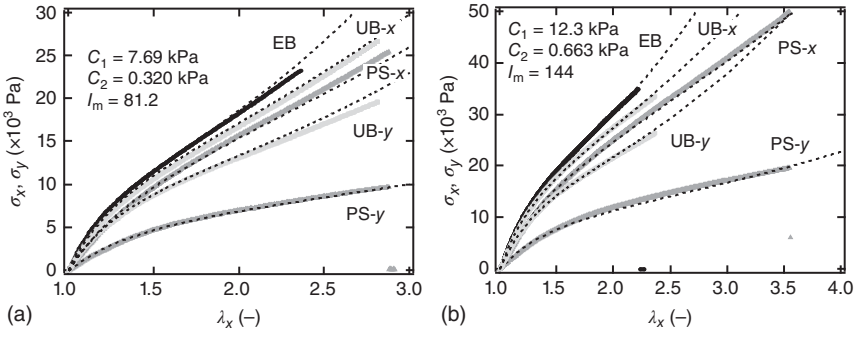

Figure 11.5 Nominal stress–elongation relationships for a Tetra-PEG gel ((a) $\phi_0 = 0.0662$ and (b) $\phi_0 = 0.0961$) under EB stretching, UB stretching, and PS. The dashed lines are fitting results for the extended Gent model. Source: Reproduced with permission from Katashima et al. [4]. Copyright 2012, Royal Society of Chemistry.

Gent model is given by

$$\sigma_{\text{UB-}x} = G\left\{\frac{(1-r)\left(\lambda_x - {\lambda_x}^{-3}\left(\frac{\lambda_x+1}{2}\right)^{-2}\right)}{1-\left({\lambda_x}^2 + \left(\frac{\lambda_x+1}{2}\right)^{-2} + {\lambda_x}^{-2}\left(\frac{\lambda_x+1}{2}\right)^{-2} - 3\right)\Big/(I_{\text{m}}-3)} + r\left(\lambda_x\left(\frac{\lambda_x+1}{2}\right)^{-2} - {\lambda_x}^{-3}\right)\right\} \quad \text{(unequi-biaxial)} \tag{11.16}$$

$$\sigma_{\text{UB-}y} = G\left\{\frac{(1-r)\left(\left(\frac{\lambda_x+1}{2}\right) - {\lambda_x}^{-2}\left(\frac{\lambda_x+1}{2}\right)^{-3}\right)}{1-\left({\lambda_x}^2 + \left(\frac{\lambda_x+1}{2}\right)^{-2} + {\lambda_x}^{-2}\left(\frac{\lambda_x+1}{2}\right)^{-2} - 3\right)/(I_{\text{m}}-3)} + r\left(\left(\frac{\lambda_x+1}{2}\right){\lambda_x}^2 - \left(\frac{\lambda_x+1}{2}\right)^{-3}\right)\right\} \quad \text{(unequi-biaxial)} \tag{11.17}$$

The data for UB stretching for all specimens is also well reproduced by Eqs. (11.16) and (11.17) with the parameters used in the other types of deformation. Thus, the extended Gent model successfully describes the stress–strain relationships for the Tetra-PEG gels with various ϕ_0 values under different types of deformation.

11.2 Cross-Coupling

In Section 11.1.4, we learned that the cross-coupling between the stresses in the stretching and perpendicular directions is represented by the I_2 term. The effect of cross-coupling was enhanced by an increase in the polymer volume fraction (ϕ_0). Previous studies attributed the cross-effect to the contribution of entanglements between network strands [2, 15–24]. However, this interpretation is most likely ruled out for the Tetra-PEG gels, which have no appreciable number of chain entanglements (see Chapters 10 and 12). Thus, the origin of the cross-coupling in the W function remains unclear. To elucidate the effect of the polymer volume fraction, we tuned three different polymer volume fractions: polymer volume fraction of elastically effective strands (ϕ_{elastic}), that of elastically ineffective strands ($\phi_{\text{inelastic}}$), and that of guest strands (ϕ_{guest}). We investigated the

relationship between the cross-coupling strength (r) in the extended Gent model and the structural parameters and discussed the molecular origin.

11.2.1 Effects of the Fraction of Elastically Effective and Ineffective Chains

To tune ϕ_{elastic} and $\phi_{\text{inelastic}}$, we tuned the fraction of connected arms, p, from 0.56 to 0.90. According to the Bethe approximation [25], the fractions of elastically ineffective and effective strands are estimated as (see Section 3.4.2)

$$\phi_{\text{elastic}} = \frac{(4P(X_4) + 3P(X_3) + 2P(X_2))}{4}\phi_0 \tag{11.18}$$

$$\phi_{\text{inelastic}} = \frac{(P(X_3) + 2P(X_2) + 4P(X_1))}{4}\phi_0 \tag{11.19}$$

The range of p values examined corresponds to a range of $0.11 < \phi_{\text{inelastic}}/\phi_{\text{elastic}} < 1.23$. Figure 11.6a,b illustrates the stress–elongation curves for the 20k Tetra-PEG gels of $\phi_0 = 0.066$ with various $\phi_{\text{inelastic}}/\phi_{\text{elastic}}$ values under PS deformation. The shear modulus (G) estimated from the initial slopes varied by approximately 1 order of magnitude from 7.30×10^3 to 1.01×10^3 Pa. The calculation based on the Bethe approximation [26] shows that even when p decreases to 0.56, the sol fraction ($\phi_{\text{sol}} = P(X_0)\phi_0$) remains at approximately $0.06\phi_0$, which suggests that the large variation in G is a direct consequence of a variation in $\phi_{\text{inelastic}}/\phi_{\text{elastic}}$.

Figure 11.7a shows the stress reduced by the shear modulus (G) as a function of λ_x. All the curves in each direction collapsed into a single curve. This result indicates that a change in $\phi_{\text{inelastic}}/\phi_{\text{elastic}}$ has a pronounced effect on the elastic modulus but has no appreciable influence on the form of the W function. This outcome does not contradict the finding that the ultimate elongation under uniaxial stretching was independent of p (see Section 11.3). Figure 11.7b shows σ_y/σ_x as a function of λ_x under PS deformation. The dashed line depicts the prediction of Eq. (11.11). Evidently, σ_y/σ_x was independent of $\phi_{\text{inelastic}}/\phi_{\text{elastic}}$

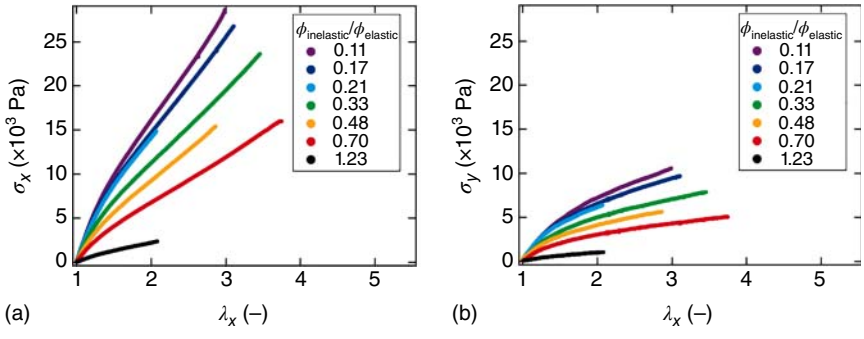

Figure 11.6 Results under PS deformation for the 20k Tetra-PEG gels of $\phi_0 = 0.066$ with various values of $\phi_{\text{inelastic}}/\phi_{\text{elastic}}$: (a) stress in the x direction and (b) stress in the y direction. Source: Reproduced with permission from Katashima et al. [5]. Copyright 2015, American Institute of Physics.

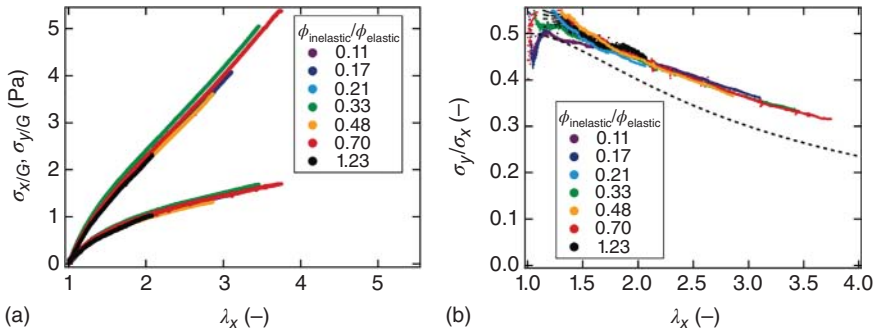

Figure 11.7 Results under PS deformation for the 20k Tetra-PEG gels of $\phi_0 = 0.066$ with various values of $\phi_{inelastic}/\phi_{elastic}$: (a) stress–elongation curves normalized by the shear modulus and (b) stress ratio (σ_y/σ_x) as a function of λ_x. Source: Reproduced with permission from Katashima et al. [5]. Copyright 2015, American Institute of Physics.

throughout the entire range of strain. This result indicates that the cross-effect of strains is influenced not only by the number of elastically effective strands but also by the number of elastically ineffective strands. Interestingly, the contribution of the elastically ineffective strands to the cross-effect is similar to that of the elastically effective network strands, although they have no contribution to the equilibrium stresses.

11.2.2 Effects of Polymer Volume Fraction and Network Strand Length

We performed PS measurements on Tetra-PEG gels with different ϕ_0 values and prepolymer molecular weights. Figure 11.8 shows the nominal stresses (σ_i: $i = x, y$) in the stretching (x) and constrained (y) directions as a function of λ_x under PS deformation for 10k and 40k Tetra-PEG gels with various polymer volume fractions in the preparation state (ϕ_0). The stress in Figure 11.8 is normalized by the initial shear modulus (G) of each specimen.

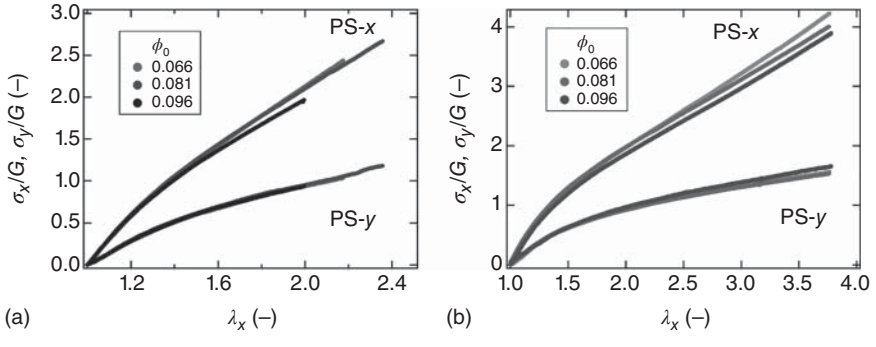

Figure 11.8 Normalized stress–elongation relationships under PS deformation for Tetra-PEG gels: (a) the 10k Tetra-PEG gels and (b) the 40k Tetra-PEG gels with various ϕ_0 values. Source: Reproduced with permission from Katashima et al. [5]. Copyright 2015, American Institute of Physics.

Figure 11.8 shows that the difference between σ_x/G and σ_y/G in the large deformation region decreased with an increase in ϕ_0. This tendency is obvious in Figure 11.9a,b, where the stress ratio (σ_y/σ_x) is plotted against λ_x using the data in Figure 11.8. The dashed lines are the prediction of Eq. (11.11). It is confirmed for the 10k and 40k Tetra-PEG gels that σ_y/σ_x at finite strain became larger as ϕ_0 increased. This tendency was also observed for the 20k Tetra-PEG gels in Figure 11.3 [4]. As we discussed in Section 11.1, the experimental data at finite strains for all specimens were located in the upper region of Eq. (11.11), which indicates that W_2 is finite and positive.

The ratio (σ_y/σ_x) at finite strain of each specimen tended to decrease with an increase in λ_x. The fluctuation in σ_y/σ_x in the small deformation region of $\lambda_x < 1.1$ is due to the sensitivity of the ratio to the experimental error involved in small strains and stresses. The stress ratio in the 0 strain limit provides the Poisson's ratio based on infinitesimal elasticity theory [27]. The λ_x-dependence of σ_y/σ_x for the Tetra-PEG gels with various N values but with the same value of ϕ_0 is compared at $\phi_0 = 0.096$, 0.081, and 0.066 in Figure 11.9c–e, respectively. No significant effect of N on the λ_x-dependence of σ_y/σ_x was observed at each ϕ_0. These results suggest that the λ_x-dependence of σ_y/σ_x is influenced by ϕ_0 but is not significantly sensitive to N.

The cross-effect of strains, which is similar to the C_2 term in the Mooney–Rivlin function [28], has been discussed from the viewpoints of trapped entanglements [16–18] and constraints on junction fluctuations [19–24]. However, Tetra-PEG gels are made in semidilute solutions of the precursor polymers ($\phi_0 < 0.1$) with modest molecular weights ($\approx 10^4$ g/mol). Considering that the entanglement molecular weight for polyethylene glycol melts (M_e) is 4.4×10^3 g/mol [48] and that the dilution effect on M_e obeys the scaling relationship $M_e \sim \phi^{-\alpha}$ ($\alpha = 7/3$ and 9/4 in θ and good solvents, respectively) [29], we can determine M_e in solutions of $\phi \approx 0.1$ to be $M_e \approx 1 \times 10^6$ g/mol, which is much larger than M_{pre}. This estimate indicates that trapped entanglements hardly influence the mechanical response of the gels. It was reported that the constraint junction model could account for the presence of the I_2 term in the W function for crosslinked rubber [30, 31]. However, the constraint junction model fails to quantitatively describe the data for the present specimens. In Section 11.1.4, we showed the applicability of the extended Gent model (Eq. (11.12)), which considers an explicit cross-effect of strains. The dashed lines in Figure 11.10 represent the results of the fitting of the extended Gent model to the stress–elongation data under PS deformation for the 10k and 40k Tetra-PEG gels with various ϕ_0 values. The extended Gent model well describes the biaxial data throughout the entire range of strain for all specimens.

The value of r ($0 < r < 1$) is a measure of the cross-effect of strains because r represents the contribution of the I_2 term to the total stress. Figure 11.11 shows the ϕ_0-dependence of r for the Tetra-PEG gels with various N values. The following two main features are observed: (i) r is mainly governed by ϕ_0, whereas N has no significant effect on r, and (ii) r tends to increase with an increase in ϕ_0, and the ϕ_0-dependence of r appears to be approximated by a linear relation passing through the origin. The latter feature indicates that no explicit cross-effect is expected exclusively in the 0 limit of ϕ_0. Classical rubber elasticity theory assumes that the entropy of the whole network is a simple sum of the entropy of each single

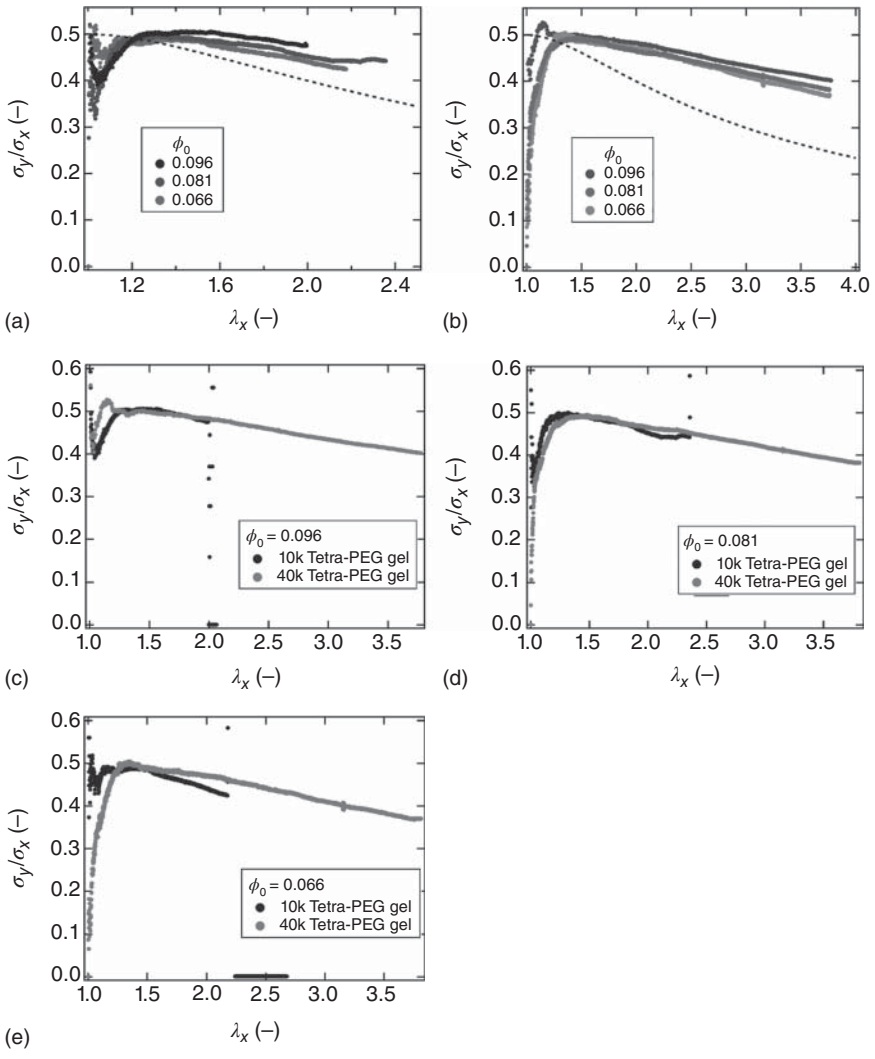

Figure 11.9 Stress ratio (σ_y/σ_x) as a function of λ_x under PS deformation for (a) the 10k Tetra-PEG gels and (b) the 40k Tetra-PEG gels with various ϕ_0 values. The dashed lines in (a) and (b) depict the results of Eq. (11.9) for every I_1-based model. The λ_x-dependence of σ_y/σ_x for the 10k and 40k Tetra-PEG gels is compared at (c) $\phi_0 = 0.096$, (d) $\phi_0 = 0.081$, and (e) $\phi_0 = 0.066$. Source: Reproduced with permission from Katashima et al. [5]. Copyright 2015, American Institute of Physics.

network strand and considers no interaction between the network strands. The finite cross-effect observed is expected to originate from some interaction (other than entanglement effects) between the polymer chains, which is not considered in the classical theory.

11.2.3 Effect of the Fraction of Guest Chains

In Sections 11.2.1 and 11.2.2, we revealed that the cross-effect is influenced by only the polymer volume fraction in the preparation state, ϕ_0, which encompasses

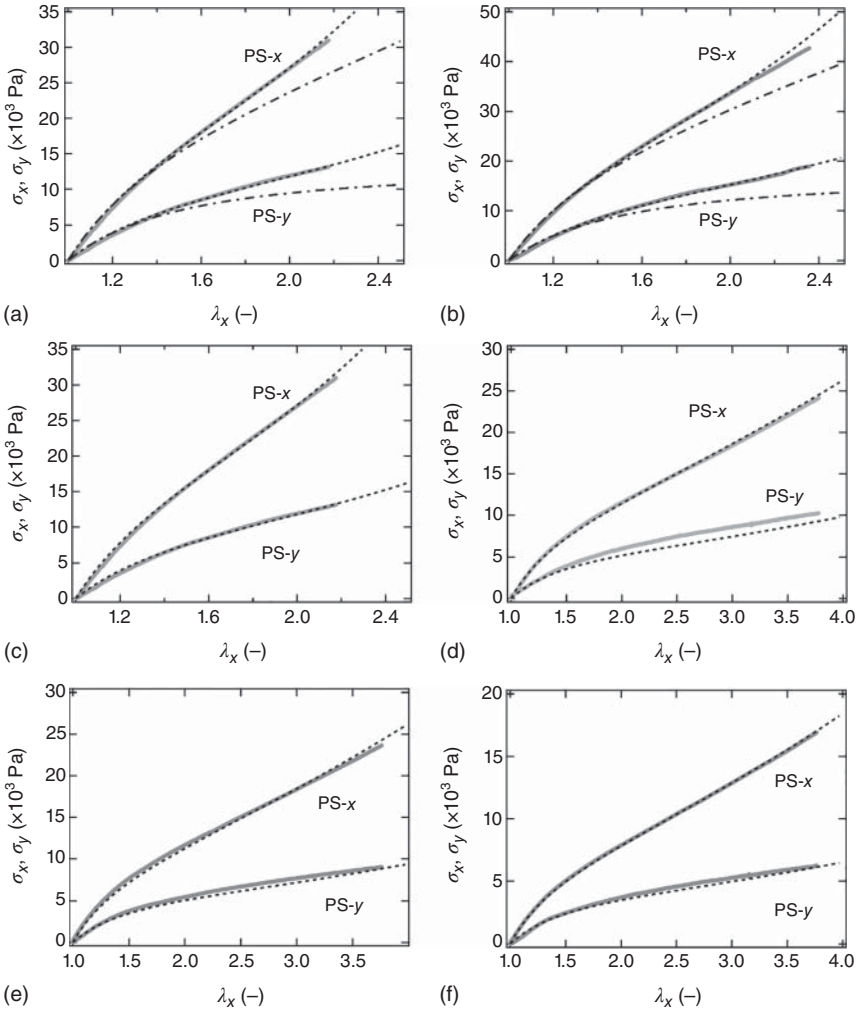

Figure 11.10 The results of the fitting of the extended Gent model to the stress–elongation data under PS deformation for the 10k Tetra-PEG gels of (a) $\phi_0 = 0.096$, (b) $\phi_0 = 0.081$, and (c) $\phi_0 = 0.066$ and for the 40k Tetra-PEG gels of (d) $\phi_0 = 0.096$, (e) $\phi_0 = 0.081$, and (f) $\phi_0 = 0.066$. The dashed lines depict the fitted curves of the extended Gent model. In (a) and (b), the dashed and dotted curves represent the fitted results of the eight-chain model (see Section 5.3). Source: Reproduced with permission from Katashima et al. [5]. Copyright 2015, American Institute of Physics.

the number of the chains connected to the whole network (elastically effective [ϕ_{elastic}] and ineffective strands [$\phi_{\text{inelastic}}$]) and the unconnected sol components (ϕ_{sol}). Notably, in the range tested, $\phi_{\text{sol}} \ll \phi_{\text{elastic}} + \phi_{\text{inelastic}} \approx 1$. Thus, we investigate only the case without sol components. In this section, we systematically introduce the unattached guest chains and elucidate their contribution to the cross-effect of strains.

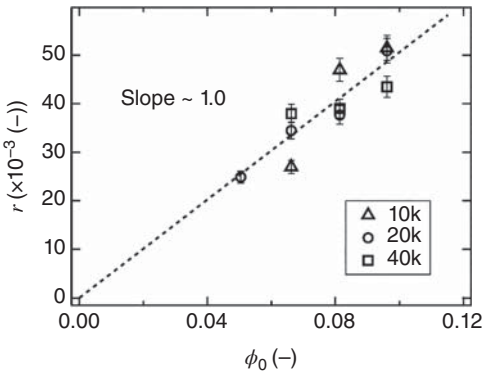

Figure 11.11 The ϕ_0-dependence of r. Triangle, circle, and square symbols represent the data for 10k, 20k, and 40k Tetra-PEG gels, respectively. The dotted line corresponds to the results of linear regression. Source: Reproduced with permission from Katashima et al. [5]. Copyright 2015, American Institute of Physics.

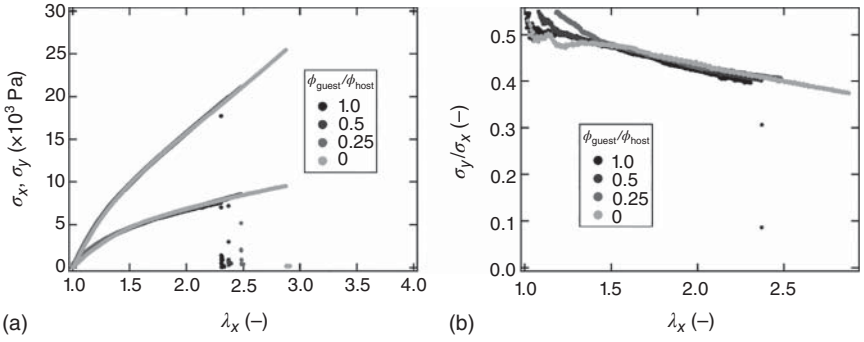

Figure 11.12 (a) Nominal stress and (b) stress ratio as a function of λ_x under PS deformation for the Tetra-PEG gels with various numbers of unattached guest chains ($\phi_{sol} = 0$, $0.25\phi_{host}$, $0.50\phi_{host}$, and $1.0\phi_{host}$). Source: Reproduced with permission from Katashima et al. [5]. Copyright 2015, American Institute of Physics.

Figure 11.12a,b shows the nominal stress and stress ratio as a function of λ_x for the 20k Tetra-PEG gels of ϕ_{host} ($=\phi_{elastic} + \phi_{inelastic}$) = 0.066 with various numbers of unattached guest chains ($\phi_{sol}/\phi_{host} = 0$, 0.25, 0.50, and 1.0) under PS deformation. In this study, we assumed that each ϕ_{host} equals the corresponding ϕ_0 because the sol fraction originating from the host network is negligibly small. The lack of an appreciable effect of ϕ_{guest} on the initial modulus shows that the presence of unattached chains during gelation has no significant influence on the content of elastically effective network strands in the resultant gels. Importantly, the presence of unattached chains had no appreciable effect on each stress and σ_y/σ_x throughout the entire range of strain. This result shows that the guest chains make no additional contribution to the stresses at finite biaxial strains. Evidently, non-network strands have no relation to the cross-effect of strains. It should be noted again that the stress–elongation data corresponded to the equilibrium data; the oscillatory measurements showed no significant viscoelastic relaxation in the frequency range from 0.1 to 10 Hz at room temperature. This result indicates that the viscoelastic relaxation of the guest chains employed is so fast that it cannot be detected in conventional tensile experiments.

11.2.4 Conjecture on Origin of Cross-Coupling

The results show the presence of an explicit cross-effect of strains even in the nearly regular networks without entanglement coupling of network strands. The cross-effect observed here most likely does not originate from the entanglement effect. In particular, the results in Figure 11.11 suggest that no cross-effect is expected exclusively in the 0 limit of network concentration in real polymer networks. The cross-effect originates from some interaction between network strands, which are not considered in the classical Gaussian models extended from the entropic elasticity of a single chain. Several types of interaction (other than entanglement effects) have been proposed to account for the deviation of the stress–elongation behavior of real crosslinked rubber from the classical theories. The existing attempts can be roughly classified into the three approaches. One is the anisotropic (nematic) interactions, which enhance the alignment of neighboring segments [32–37]. For instance, Bladon and Warner [34] theoretically discussed the nonlinear elasticity of a model nematic rubber composed of mesogenic moieties and assumed that conventional (non-mesogenic) rubber could be represented by nematic rubber with residual nematic interactions at temperatures much beyond the nematic–isotropic transition temperature. The second approach is the topological interactions between loop structures in polymer networks (see Section 3.5) [38–41]. The researchers assumed the ring-shaped structures or loops as structural elements of a crosslinked network and theoretically considered the elastic effects originating from the constraint that the topologies of the loop pairs remain unchanged under deformation. Hirayama and Tsurusaki showed that such a topological effect results in an explicit cross-effect of strains even for networks without entanglement loops [41]. The third approach considers the excluded volume effect as the source of interchain and intrachain interactions [42]. These interactions are pronounced in the high-concentration region and transmit tension among the chains, resulting in a finite cross-effect. Under tension, the force applied to a chain is no longer parallel to the chain vector. The force is the sum of the axial force and an applied moment, which produces a significant softening effect.

It is difficult to quantitatively assess the applicability of these approaches to the present biaxial data because most of the models do not provide the analytical form for the stress–elongation relations required for fitting these data. Furthermore, the physical meaning of most of the model parameters is qualitative, making it difficult to relate the parameters to the structural characteristics in the networks. These approaches are expected to actually reproduce the main features of the biaxial data for crosslinked rubber if some parameters are used as adjustable fitting parameters.

11.3 Stretchability in Uniaxial Stretching

In Section 11.1.4, we deduced the strain energy density function of the Tetra-PEG gels, which is well reproduced by extended Gent model. In this chapter, we attempt to reveal the molecular picture describing the stretchability in simple

uniaxial stretching. Here, we confirmed the inapplicability of the traditional Kuhn model and proposed a new molecular model for predicting the ultimate elongation ratio (λ_{max}) of a polymer gel.

11.3.1 Kuhn Model

λ_{max} is the indicator of how long a material can be deformed until breakage and is an important parameter. Among the models for predicting the ultimate elongation ratio (λ_{max}), the most popular is the Kuhn model (see Section 1.2.2) [43]. In the Kuhn model, λ_{max} is estimated as the ratio of the contour length (L) to the end-to-end distance (R_s) of the network strand. Assuming that the conformation of the network strand obeys a Gaussian distribution, λ_{max} is given by [44]

$$\lambda_{max} = \frac{L}{R_s} \sim \frac{aN}{aN^{1/2}} \sim N^{1/2} \tag{11.20}$$

where a is the monomer length and N is the polymerization degree of the network strands. The Kuhn model expects that λ_{max} is a function of N and that even the polymer concentration does not influence λ_{max}.

11.3.2 Effect of Connectivity

First, we investigated the effect of the fraction of connected arms (p) on the finite extensibility using a p-tuned Tetra-PEG gel. By tuning the hydrolysis time (t_{deg}), p is controlled from 0.92 to 0.55, and G is controlled from 11.2 to 2.4 kPa (Figure 11.13). Figure 11.14 shows the stress–elongation curves of the p-tuned Tetra-PEG gels. To focus on the difference in λ_{max}, the stress is normalized by G. The prediction of the NH model, as a prediction for an infinitely stretchable network, is also shown. The stress–elongation curves of p-tuned Tetra-PEG gels deviated upward from the NH model, reflecting the finite extensibility of real polymer gels. Apparent differences among the p-tuned Tetra-PEG gels were not observed except for G. The points where the upward deviation occurs seemed independent of p, and the normalized stress–elongation curves at various p

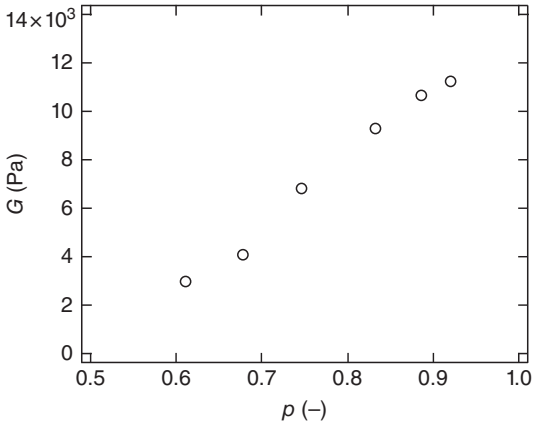

Figure 11.13 G as a function of p. Source: Akagi et al. 2013 [3]. Reproduced with permission of Royal Society of Chemistry.

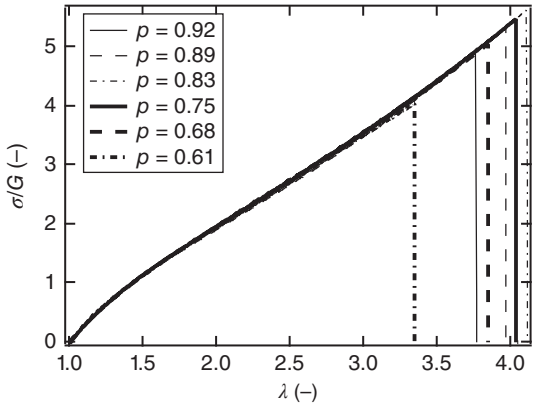

Figure 11.14 Reduced stress–elongation curves of the *p*-tuned Tetra-PEG gels. Source: Reproduced with permission from Akagi et al. [3]. Copyright 2013, Royal Society of Chemistry.

values fall on a single curve. These results indicate that p affects G but has little influence on the shape of the stress–elongation curves and λ_{max}.

This result can be explained by the heterogeneous distribution of connections in *p*-tuned Tetra-PEG gels discussed in Section 5.6. Let us start from a tetra-functional polymer network with complete connectivity. A scission of a network strand forms two dangling chains and transforms two tetra-functional junctions into two tri-functional junctions, which can still act as active crosslinks. This event causes only the decrease in an elastically effective chain, which decreases G, but does not change the number of crosslinks and the lengths of other network strands. Thus, the stretchability in the high p region is hardly influenced by the scissions. The Bethe approximation [45] and the percolated network model [46, 47] predict that this condition holds at $p > 0.7$, as almost all crosslinks are still crosslinks in the network.

11.3.3 Effect of Polymer Concentration and Network Strand Length

In Section 11.3.2, we have revealed that p does not influence N in the region $p > 0.7$ and thus also does not influence λ_{max}. To directly tune N, we fabricated Tetra-PEG gels from prepolymers with different molecular weights. Because the values of p for 5k, 10k, and 20k Tetra-PEG gels were higher than $p = 0.7$, N corresponds to the value predicted from the prepolymer molecular weight. In addition, we tuned another important parameter, ϕ_0, which did not appear in the Kuhn model.

Figure 11.15 shows the normalized stress–elongation curves of the 5k, 10k, and 20k Tetra-PEG gels. Upward deviation from the prediction of the NH model was observed in the high λ region. The onset λ of the upward deviation increased with increasing ϕ_0 and N. Thus, the stretchability was enhanced with an increase in N, which qualitatively agreed with the prediction of the Kuhn model. On the other hand, the enhancement in stretchability by an increase in ϕ_0 is not predicted by the Kuhn model.

To quantitatively discuss λ_{max}, the extended Gent model (Eq. (11.12)) was fit to the stress–elongation curves. Figure 11.16 shows λ_{max} as a function of N. λ_{max} increased with increasing N: $\lambda_{max} \sim N^{0.59}$, $N^{0.65}$, $N^{0.74}$, and $N^{0.61}$ for

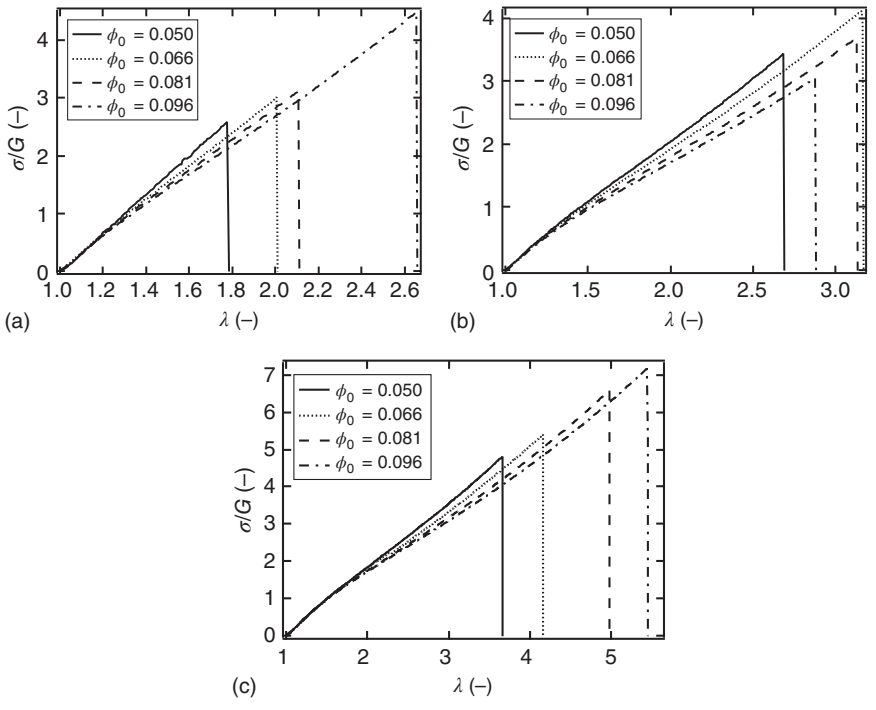

Figure 11.15 Reduced stress–elongation curves of the (a) 5k, (b) 10k, and (c) 20k Tetra-PEG gels. Source: Reproduced with permission from Akagi et al. [3]. Copyright 2013, Royal Society of Chemistry.

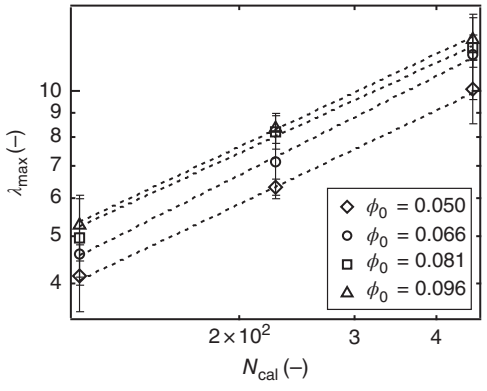

Figure 11.16 λ_{max} as a function of N_{cal} in Tetra-PEG gels ($\phi_0 = 0.050$, rhombus; $\phi_0 = 0.066$, circle; $\phi_0 = 0.081$, square; and $\phi_0 = 0.096$: triangle). The dashed lines show the results of fitting with a power function. Source: Reproduced with permission from Akagi et al. [3]. Copyright 2013, Royal Society of Chemistry.

$\phi_0 = 0.050$, 0.066, 0.081, and 0.096, respectively. On average, the λ_{max} scaled with N as $\lambda_{max} \sim N^{0.65}$, the power of which was slightly higher than that predicted by the Kuhn model. In addition, λ_{max} increased with increasing ϕ_0, showing the relationship $\lambda_{max} \sim {\phi_0}^{0.38}$ on average (Figure 11.17). Overall, the following relationship was experimentally observed:

$$\lambda_{max} \sim {\phi_0}^{0.38} {N_{cal}}^{0.65} \tag{11.21}$$

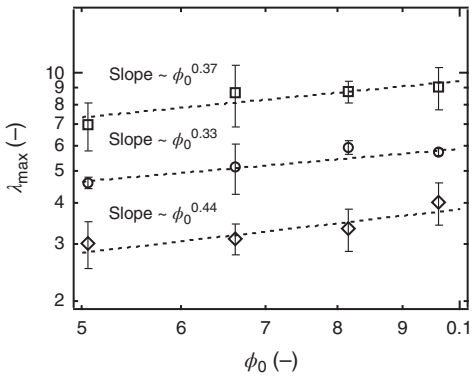

Figure 11.17 λ_{max} as a function of ϕ_0 in 5k, 10k, and 20k Tetra-PEG gels (5k, rhombus; 10k, circle; and 20k, square). The dotted lines show the fitting results. Source: Reproduced with permission from Akagi et al. [3]. Copyright 2013, Royal Society of Chemistry.

11.3.4 Semiempirical Model Based on Experiments

Here, we propose a molecular picture giving this empirical equation. In the Kuhn model, λ_{max} is estimated as the ratio of the contour length to the end-to-end distance of network strands. Because the contour length in the numerator has a distinct molecular picture associated with breakage, there is a problem with the denominator. Thus, we set the unknown, d, as a denominator and investigated the form of d in comparison with the experimental results.

$$\lambda_{max} = \frac{aN}{d} \sim {\phi_0}^{0.38} {N_{cal}}^{0.65} \tag{11.22}$$

By solving Eq. (11.22) for d, we obtained

$$d \sim {\phi_0}^{0.38} {N_{cal}}^{-0.35} \sim \left(\frac{\phi_0}{N_{cal}}\right)^{1/3} \sim \nu^{-1/3} \tag{11.23}$$

where ν scales with ϕ_0 and N as $\nu \sim \phi_0/N$. As a result, we obtain the semiempirical relationship $d \sim \nu^{-1/3}$; thus, $\lambda_{max} \sim N/\nu^{-1/3} \sim N^{2/3}{\phi_0}^{1/3}$. The power $-1/3$ suggests that d scales with the geometrical distance between the centers of neighboring prepolymers. We replotted all the data of λ_{max} against $N^{2/3}{\phi_0}^{1/3}$ in Figure 11.18, which shows the data collapse.

How can we draw a molecular picture from these results? Here, it should be noted that d has a strong ϕ_0-dependence compared with that of the

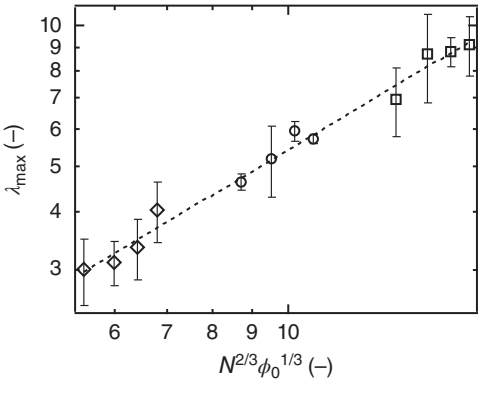

Figure 11.18 λ_{max} as a function of ${N_{cal}}^{2/3}{\phi_0}^{1/3}$ for the Tetra-PEG gels (5k, rhombus; 10k, circle; and 20k, square). The dashed line is the master curve showing $\lambda_{max} \sim {N_{cal}}^{2/3}{\phi_0}^{1/3}$. Source: Reproduced with permission from Akagi et al. [3]. Copyright 2013, Royal Society of Chemistry.

root-mean-square length of the free polymer chains in an athermal solution ($\langle {R_g}^2 \rangle^{1/2}$): $\langle {R_g}^2 \rangle^{1/2} \sim aN^{3/5}$ in the dilute regime, and $\langle {R_g}^2 \rangle^{1/2} \sim aN^{3/5}(\phi_0/\phi^*)^{-1/8}$in the semidilute regime. In contrast, $d \sim \nu^{-1/3} \sim (\phi_0/N)^{-1/3}$ in both regimes. The strong power law observed in our results ($\lambda_{max} \sim {\phi_0}^{0.38}$) cannot be explained by this weak ϕ_0-dependence in an athermal solution. Instead, our results suggest that d, the distance between the centers of neighboring prepolymers, should be set as the initial length of the network strand. This difference in the denominator is explained by the different mechanisms of the crosslinking reaction.

The Kuhn model assumes that the distance between crosslinks is maintained as the end-to-end distance of a free chain with a polymerization degree of N. To form a linkage under this condition, each arm of the prepolymer needs to find its reactive counterpart without changing the end-to-end distance. This situation seems to be realized in a condensed system because there are many reactive functional groups around the arm ends. This picture does not fit the dilute region, where only limited encounters of reactive ends are allowed.

On the other hand, our empirical model suggests that the distance between crosslinks is the distance between the centers of neighboring prepolymers, which changes with the concentration of prepolymers and does not depend on the initial arm length. This situation seems to be realized in a dilute system because there are few reactive counterparts around the arm ends. The prepolymers need to change the end-to-end distance of the arms to react with a counterpart. This idea is supported by the finding that the p of the Tetra-PEG gels formed below ϕ^* was not significantly smaller than that of the gels formed above ϕ^* and at approximately 0.9. If the molecular picture of the Kuhn model was valid, p would drastically decrease below ϕ^*.

References

1 Roland, C.M. (2011). *Viscoelastic Behavior of Rubbery Materials*. Oxford University Press.

2 Treloar, L.R.G. (1975). *The Physics of Rubber Elasticity*, 3e. Oxford: Clarendon Press.

3 Akagi, Y., Katashima, T., Sakurai, H. et al. (2013). Ultimate elongation of polymer gels with controlled network structure. *RSC Adv.* 3 (32): 13251–13258. https://doi.org/10.1039/c3ra41580e.

4 Katashima, T., Urayama, K., Chung, U.-i., and Sakai, T. (2012). Strain energy density function of a near-ideal polymer network estimated by biaxial deformation of tetra-PEG gel. *Soft Matter* 8 (31): 8217–8222. https://doi.org/10.1039/C2SM25340B.

5 Katashima, T., Urayama, K., Chung, U.-i., and Sakai, T. (2015). Probing the cross-effect of strains in non-linear elasticity of nearly regular polymer networks by pure shear deformation. *J. Chem. Phys.* 142 (17): 174908. https://doi.org/10.1063/1.4919653.

6 Flory, P.J. and Rehner, J. (1943). Statistical mechanics of cross-linked polymer networks I. Rubberlike elasticity. *J. Chem. Phys.* 11 (11): 512–520.

7 Treloar, L.R.G. (1943). The elasticity of a network of long-chain molecules. I. *Trans. Faraday Soc.* 39: 36–41. https://doi.org/10.1039/TF9433900036.

8 Treloar, L.R.G. (1943). The elasticity of a network of long-chain molecules. II. *Trans. Faraday Soc.* 39 (0): 241–246. https://doi.org/10.1039/TF9433900241.

9 Treloar, L.R.G. (1946). The elasticity of a network of long-chain molecules. III. *Trans. Faraday Soc.* 42 (1–2): 83–94.

10 Wall, F.T. (1942). Statistical thermodynamics of rubber II. *J. Chem. Phys.* 10 (7): 485–488. https://doi.org/10.1063/1.1723753.

11 Arruda, E.M. and Boyce, M.C. (1993). A 3-dimensional constitutive model for the large stretch behavior of rubber elastic-materials. *J. Mech. Phys. Solids* 41 (2): 389–412.

12 James, H.M. and Guth, E. (1943). Theory of the elastic properties of rubber. *J. Chem. Phys.* 11 (10): 455–481.

13 Gent, A.N. (1996). A new constitutive relation for rubber. *Rubber Chem. Technol.* 69 (1): 59–61.

14 Kondo, Y., Urayama, K., Kidowaki, M. et al. (2014). Applicability of a particularly simple model to nonlinear elasticity of slide-ring gels with movable cross-links as revealed by unequal biaxial deformation. *J. Chem. Phys.* 141 (13): 134906. https://doi.org/10.1063/1.4897134.

15 Ciferri, A. and Flory, P.J. (1959). Stress–strain isotherm for polymer networks. *J. Appl. Phys.* 30 (10): 1498–1507.

16 Ball, R.C., Doi, M., Edwards, S.F., and Warner, M. (1981). Elasticity of entangled networks. *Polymer* 22 (8): 1010–1018. https://doi.org/10.1016/0032-3861(81)90284-6.

17 Edwards, S.F. (1977). The theory of rubber elasticity. *Br. Polym. J.* 9 (2): 140–143. https://doi.org/10.1002/pi.4980090209.

18 Edwards, S.F. and Vilgis, T. (1986). The effect of entanglements in rubber elasticity. *Polymer* 27 (4): 483–492.

19 Flory, P.J. (1977). Theory of elasticity of polymer networks. The effect of local constraints on junctions. *J. Chem. Phys.* 66 (12): 5720–5729. https://doi.org/10.1063/1.433846.

20 Flory, P.J. and Erman, B. (1982). Theory of elasticity of polymer networks. 3. *Macromolecules* 15 (3): 800–806. https://doi.org/10.1021/ma00231a022.

21 Ronca, G. and Allegra, G. (1975). An approach to rubber elasticity with internal constraints. *J. Chem. Phys.* 63 (11): 4990–4997. https://doi.org/10.1063/1.431245.

22 Gaylord, R.J. and Douglas, J.F. (1990). The localization model of rubber elasticity. 2. *Polym. Bull.* 23 (5): 529–533.

23 Kaliske, M. and Heinrich, G. (1999). An extended tube-model for rubber elasticity: statistical–mechanical theory and finite element implementation. *Rubber Chem. Technol.* 72 (4): 602–632.

24 Rubinstein, M. and Panyukov, S. (1997). Nonaffine deformation and elasticity of polymer networks. *Macromolecules* 30 (25): 8036–8044.

25 Macosko, C.W. and Miller, D.R. (1976). A new derivation of average molecular weights of nonlinear polymers. *Macromolecules* 9 (2): 199–206. https://doi.org/10.1021/ma60050a003.

26 Miller, D.R. and Macosko, C.W. (1976). A new derivation of post gel properties of network polymers. *Macromolecules* 9 (2): 206–211. https://doi.org/10.1021/ma60050a004.

27 Landau, L.D., Lifshitz, E.M., Kosevich, A.M., and Pitaevskii, L.P. (1986). *Theory of Elasticity*, 3rd English ed. Oxford [Oxfordshire]/New York: Pergamon Press; viii, 187 p.

28 Mooney, M. (1940). A theory of large elastic deformation. *J. Appl. Phys.* 11 (9): 582–592.

29 Ferry, J.D. (1980). *Viscoelastic Properties of Polymers*. Wiley.

30 Erman, B. (1981). Effect of junction constraints on rubber elasticity in multiaxial states of stress. *J. Polym. Sci., Part B: Polym. Phys.* 19 (5): 829–835. https://doi.org/10.1002/pol.1981.180190510.

31 Treloar, L.R.G. (1982). Application of Flory–Erman theory to rubber in biaxial strain. *Br. Polym. J.* 14 (3): 121–125. https://doi.org/10.1002/pi.4980140308.

32 Deloche, B. and Samulski, E.T. (1981). Short-range nematic-like orientational order in strained elastomers: a deuterium magnetic resonance study. *Macromolecules* 14 (3): 575–581. https://doi.org/10.1021/ma50004a024.

33 Aoki, Y. and Tanaka, T. (1999). Viscoelastic properties of miscible poly(methyl methacrylate)/poly(styrene-*co*-acrylonitrile) blends in the molten state. *Macromolecules* 32 (25): 8560–8565. https://doi.org/10.1021/ma990281z.

34 Bladon, P. and Warner, M. (1993). Elasticity of nematic networks and nematic effects in conventional rubbers. *Macromolecules* 26 (5): 1078–1085. https://doi.org/10.1021/ma00057a031.

35 Di Marzio, E.A. (1994). Contribution to a liquid-like theory of rubber elasticity: 2. Existence of a $(\gamma_x\gamma_y+\gamma_y\gamma_z\ \gamma_z\gamma_x)$ term. *Polymer* 35 (9): 1819–1826. https://doi.org/10.1016/0032-3861(94)90970-9.

36 DiMarzio, E.A. (1962). Contribution to a liquid-like theory of rubber elasticity. *J. Chem. Phys.* 36 (6): 1563–1570. https://doi.org/10.1063/1.1732780.

37 Jarry, J.-P. and Monnerie, L. (1979). Effects of a nematic-like interaction in rubber elasticity theory. *Macromolecules* 12 (2): 316–320. https://doi.org/10.1021/ma60068a031.

38 Graessley, W.W. and Pearson, D.S. (1977). Stress–strain behavior in polymer networks containing nonlocalized junctions. *J. Chem. Phys.* 66 (8): 3363–3370. https://doi.org/10.1063/1.434421.

39 Iwata, K. and Edwards, S.F. (1989). New model of polymer entanglement: localized Gauss integral model. Plateau modulus G_N, topological second virial coefficient $A^{\theta}{}_2$ and physical foundation of the tube model. *J. Chem. Phys.* 90 (8): 4567–4581. https://doi.org/10.1063/1.456617.

40 Iwata, K. and Kimura, T. (1981). Topological distribution functions and the second virial coefficients of ring polymers. *J. Chem. Phys.* 74 (3): 2039–2048. https://doi.org/10.1063/1.441249.

41 Hirayama, N. and Tsurusaki, K. (2011). Topological interaction between loop structures in polymer networks and the nonlinear rubber elasticity. *Nihon Reoroji Gakk.* 39 (1–2): 65–73.

42 Gao, J. and Weiner, J.H. (1991). Chain force concept in systems of interacting chains. *Macromolecules* 24 (18): 5179–5191. https://doi.org/10.1021/ma00018a024.

43 Kuhn, W. (1946). Dependence of the average transversal on the longitudinal dimensions of statistical coils formed by chain molecules. *J. Polym. Sci.* 1 (5): 380–388. https://doi.org/10.1002/Pol.1946.120010505.
44 Kuhn, W. (1936). Beziehungen zwischen Molekülgröße, statistischer Molekülgestalt und elastischen Eigenschaften hochpolymerer Stoffe. *Kolloid Z.* 76 (3): 258–271. https://doi.org/10.1007/BF01451143.
45 Miller, D.R. and Macosko, C.W. (1976). New derivation of post gel properties of network polymers. *Macromolecules* 9 (2): 206–211.
46 Nishi, K., Chijiishi, M., Katsumoto, Y. et al. (2012). Rubber elasticity for incomplete polymer networks. *J. Chem. Phys.* 137 (22): 224903. https://doi.org/10.1063/1.4769829.
47 Nishi, K., Noguchi, H., Sakai, T., and Shibayama, M. (2015). Rubber elasticity for percolation network consisting of Gaussian chains. *J. Chem. Phys.* 143 (18): 184905. https://doi.org/10.1063/1.4935395.
48 Fetter, L., Lohse, D., Richter, D., et al. (1994). Connection between polymer molecular weight, density, chain dimensions, and melt viscoelastic properties. *Macromolecules* 27: 4639–4647.

12

Fracture

Takamasa Sakai and Takeshi Fujiyabu

Graduate School of Engineering, The University of Tokyo, Tokyo, Japan

The fracture energy (T_0) is the energy required to propagate a unit length of a crack and is known as a representative parameter indicating fracture. The fracture energy of elastomeric materials is known to be modeled by the Lake–Thomas model (see Section 5.5.2) [1]:

$$T_0 = \left(\frac{3}{8}\right)^{1/2} \nu L N U \tag{5.63}$$

where ν is the number density of network strands, L is the displacement length, N is the degree of polymerization of a network strand, and U is the total bond energy of the backbone of monomeric unit. Initially, L is related to the length of a network strand as $L \approx R_0 \approx aN^{1/2}$ (a: monomer length); however, there is ambiguity in L because there is no concrete experimental validation because of the practical absence of a model network. Instead, there were only semiquantitative experimental validations representatively performed by Gent [2, 3]. He confirmed the relationship between T_0 and G, $T_0 \sim G^{-1/2}$, which is given from Eq. (5.63), assuming that $\nu \sim G$ and $N \sim G^{-1}$. However, the direct contribution of each parameter to T_0, such as $T_0 \sim \nu$ or $T_0 \sim N^{3/2}$, has never been examined.

In the case of Tetra-PEG gel, one can tune ν and N independently and thus fully examine the Lake–Thomas model. Here, we prepared Tetra-PEG gels with systematically tuned degree of strand polymerization between crosslinks (N), the polymer volume fraction in the as-prepared state (ϕ_0), connectivity (p), and heterogeneous distribution in network strand length [4, 5]. To quantitatively examine Eq. (5.63), we directly substitute R_0 into Eq. (5.63) and introduce an enhancement factor (k) to accommodate the deviation of L from R_0 as [2, 6, 7].

$$T_0 = \left(\frac{3}{8}\right)^{1/2} k \nu R_0 N U \tag{12.1}$$

12.1 Estimation of Fracture Energy

To investigate the fracture energy (T_0), we performed tearing measurements on trouser-shaped specimens. The gel specimens were used in the as-prepared state,

Physics of Polymer Gels, First Edition. Edited by Takamasa Sakai.

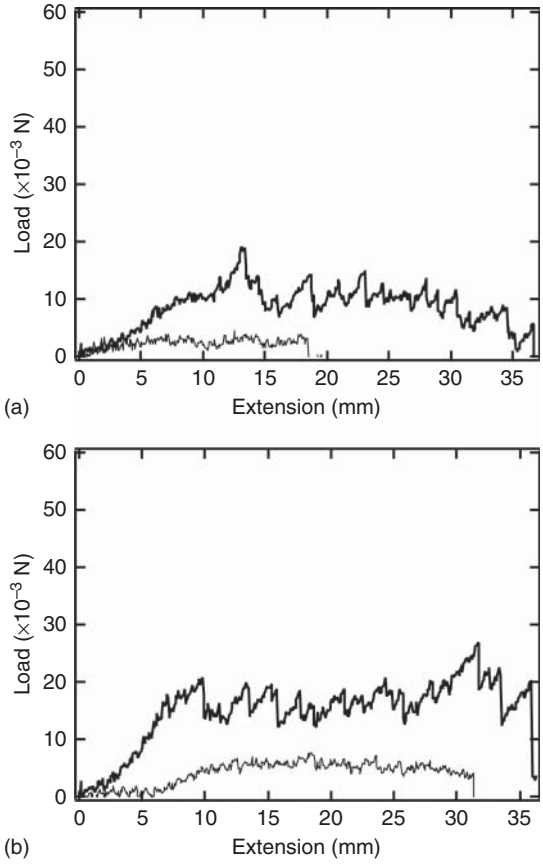

Figure 12.1 Tearing force–extension relationships in (a) 5k, (b) 10k, (c) 20k, and (d) 40k Tetra-PEG gels (fine line, $\phi_0 = 0.034$; bold line, $\phi_0 = 0.1$). Source: Reproduced with permission from Sakai et al. [5]. Copyright 2014, Royal Society of Chemistry.

not in the equilibrium-swollen state. One of the trouser legs was pulled upward at a constant velocity of 40 mm/min while keeping the other leg stationary, and the load (F) was recorded. We performed these tearing measurements at a different velocity of 500 mm/min and confirmed the rate-independent tearing behavior under this experimental condition. A similar rate-independent tearing behavior was observed for all Tetra-PEG gels, indicating the absence of a viscoelastic effect on tearing in the range tested.

Figure 12.1 shows the load–extension curves during tearing [5]. Initially, with extension, the load value monotonically increased, and the crack did not propagate. After crack propagation started, the load fluctuated with extension. The degree of fluctuation was smaller at lower concentrations and molecular weights, and vice versa. We estimated T_0 as the average of local minimum values of F as

$$T_0 = \frac{2F}{h} \tag{12.2}$$

where h is the thickness of the gel samples. Notably, the average of local minimum values of F were used in Eq. (12.2), because the elastic energy stored in the sample is almost released at the condition.

Figure 12.1 (*Continued*)

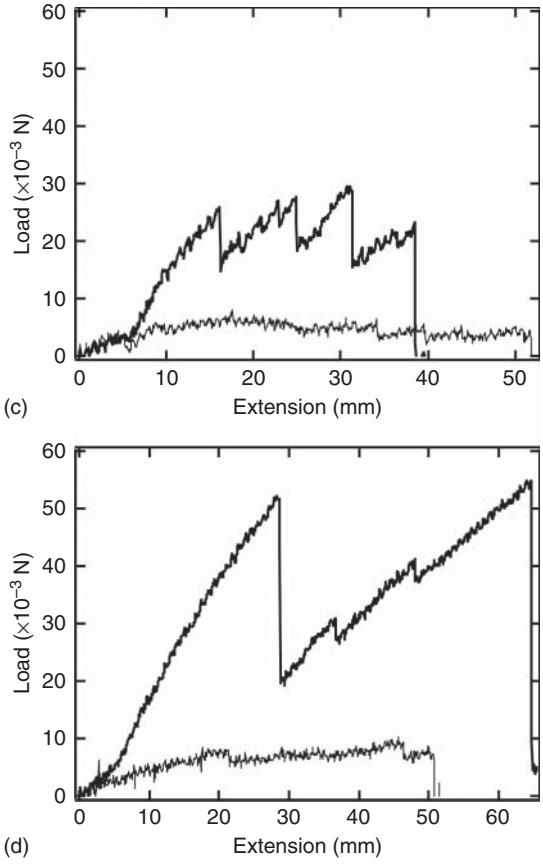

12.2 Conversion-Tuned Tetra-PEG Gels

First, we investigated and focused on the effect of connectivity (p) on T_0 by using conversion (p)-tuned Tetra-PEG gels and focused on the pure effect of p on T_0 while keeping ϕ_0 and N unchanged.

Figure 12.2 shows T_0 plotted against ν and the prediction of the Lake–Thomas model ($T_0 \sim \nu$) as the dashed line. As clearly shown in Figure 12.2, the experimental data obeyed the Lake–Thomas prediction in the region $\nu > 4.0$ ($p > 0.65$). The agreement in this region indicates that the Lake–Thomas model is valid and that the term LNU does not depend on p. Thus, it is strongly suggested that N is estimated as the half of that of the Tetra-PEGs and that U is estimated as the total bond energy of the backbone of monomeric unit of PEG with the degree of polymerization of N in the region $p > 0.65$. In addition, the region where the upward deviation is observed corresponds well with the region where the elastic modulus does not show linearity with $(\nu - \mu)$ in Chapter 10. A massive number of dangling chains may inhibit the mean-field treatment in this region and make it impossible to correctly estimate ν and μ. In addition, N can be increased in this region, because of the decrease in μ (see Section 3.6.2). In the following

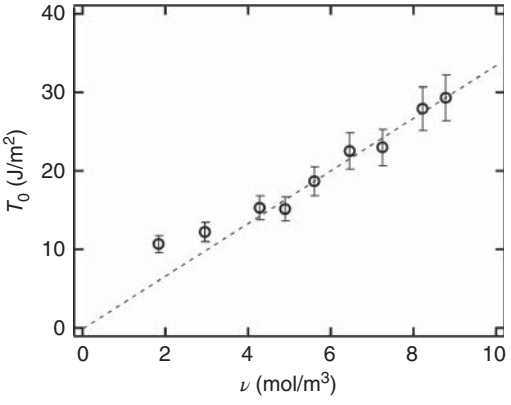

Figure 12.2 T_0 as a function of ν in p-tuned Tetra-PEG gels. Source: Reproduced with permission from Akagi et al. [4]. Copyright 2013, American Institute of Physics.

analyses, we focus on the almost complete reaction system ($p \approx 0.9$). Thus, we use the computed N and U values and focus on the effects of N and ϕ_0 on T_0.

12.3 Effects of Network Concentration and Strand Length

We then evaluated the T_0 of Tetra-PEG gels with different N and ϕ_0 values. Figure 12.3 shows the linear relationships between T_0 and ν; the T_0 values of samples with identical N values are on the same line proportional to ν, obeying the prediction of Lake–Thomas model. Because the difference in ν for Tetra-PEG gels with each N originated purely from ϕ_0, these data indicate that the slope (LNU) is independent of ϕ_0 but dependent of N. Based on the slopes, we estimated the values of L using the calculated values of N and U.

Figure 12.4 shows L of Tetra-PEG gels plotted against N. L increased from 13 to 34 nm with an increase in N. In the original Lake–Thomas model, L corresponds to R_0 ($\approx aN^{1/2}$) (dotted line). The values of L and R_0 have similar magnitudes and N-dependence but are still different. According to Eq. (12.1), we estimated k for each N and plotted it against N (Figure 12.5). The values of k were almost constant

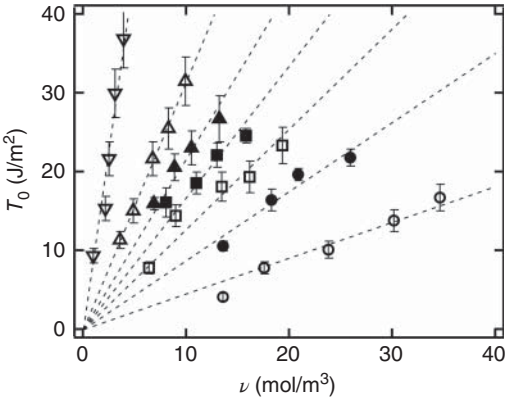

Figure 12.3 T_0 as a function of ν in conventional Tetra-PEG gels (open circles, 5k; open squares, 10k; open triangles, 20k; open lower triangles, 40k-Tetra-PEG gel) and hetero-Tetra-PEG gels (filled circles, 5k–10k; filled squares, 5k–20k; filled triangles, 10k–20k). Linear fits to the data are shown as the dotted lines. Source: Reproduced with permission from Sakai et al. [5]. Copyright 2014, Royal Society of Chemistry.

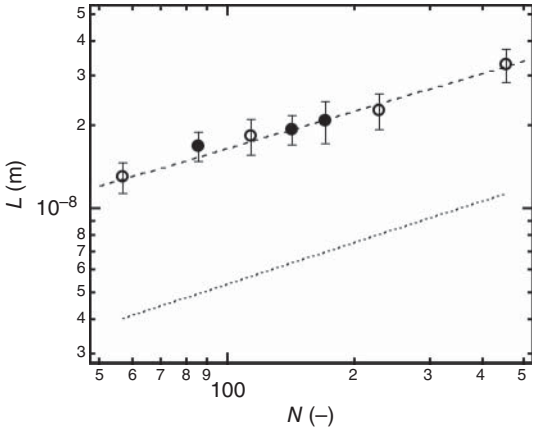

Figure 12.4 *L* as a function of *N* in Tetra-PEG gels (open circles) and hetero-Tetra-PEG gels (filled circles). The dotted line represents the guide of the calculated R_0. Source: Reproduced with permission from Sakai et al. [5]. Copyright 2014, Royal Society of Chemistry.

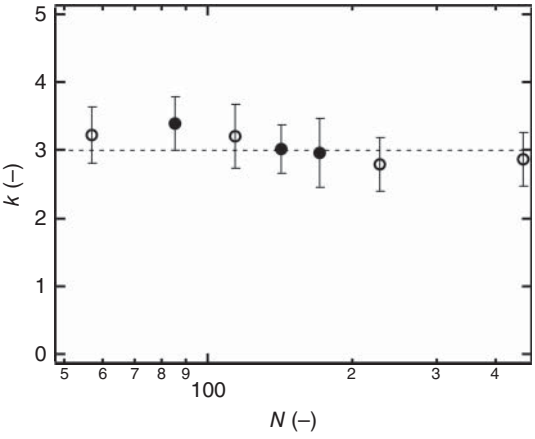

Figure 12.5 *k* as a function of *N* in Tetra-PEG gels (open circles) and hetero-Tetra-PEG gels (filled circles). Source: Reproduced with permission from Sakai et al. [5]. Copyright 2014, Royal Society of Chemistry.

and approximately 3 in the range examined. These data indicate that network strands within $3R_0$ from the crack tip are fully extended at the fracture and that the length is determined by only N, regardless of p and ϕ_0.

12.4 Bimodal Tetra-PEG Gels

In the fracture process, a breakage of the weakest link allows crack propagation. Because a shorter chain is weaker than a longer chain according to the Lake–Thomas model, it is expected that abnormal behavior can be observed in Tetra-PEG gels with a bimodal distribution in network strand lengths. We performed tearing experiments on bimodal Tetra-PEG gels and estimated L based on the Lake–Thomas model. Figure 12.6 shows the N_{ave}-dependence of L and R_0 calculated from N_{ave} (dotted line). Here, we assume that N_{ave} represent the number-average degree of polymerization of the prepolymers. The L and R_0 values have similar N_{ave}-dependence but are different from each other. We also estimated k and plotted it against N_{ave} in Figure 12.7. Although these k values were

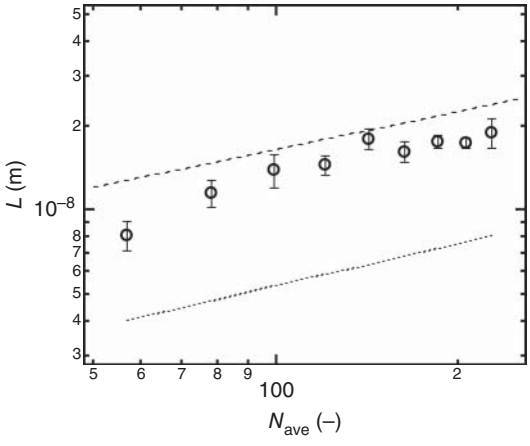

Figure 12.6 L as a function of N_{ave} in bimodal Tetra-PEG gels. The dotted line shows the guide of the calculated R_0. Source: Reproduced with permission from Sakai et al. [5]. Copyright 2014, Royal Society of Chemistry.

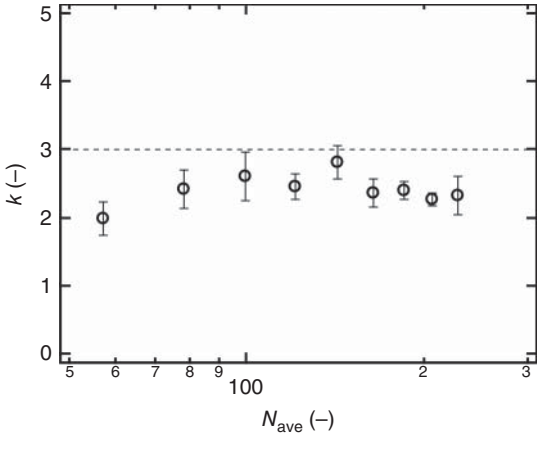

Figure 12.7 k as a function of N_{ave} in bimodal Tetra-PEG gels. The dashed line shows the guide of $k = 3$. Source: Reproduced with permission from Sakai et al. [5]. Copyright 2014, Royal Society of Chemistry.

slightly smaller than those for conventional and hetero Tetra-PEG gels, the values were still similar to each other. These data indicate that a heterogeneous distribution in network strand length does not significantly influence T_0 in the range considered in this study.

12.5 Summary

The fracture energies of Tetra-PEG gels with tuned structural parameters are fully explained by the Lake–Thomas model with $k \approx 3$. The k value is universal in the range considered in this study; not only changes in ϕ_0 and N but also the connective heterogeneity and heterogeneous distribution in strand length did not affect the value of k. These data suggest that the enhancement factor k estimated in this study can be applicable to conventional polymer gels with similar concentration ranges regardless of the degree of heterogeneity, although there is a possibility that macroscopic heterogeneity (∼μm), which was not observed in the Tetra-PEG gel system, affects the fracture toughness. The constant k near unity

suggests that it is difficult for conventional polymer gels to achieve enhanced fracture toughness. In other words, the network homogeneity does not strongly contribute to the enhancement in fracture toughness. Chain entanglements may play an important role in enhancing k, which is proposed by Gong and coworkers as a double-network gel or the concept of a "sacrificial bond" [8, 9].

References

1 Lake, G.J. and Thomas, A.G. (1967). The strength of highly elastic materials. *Proc. R. Soc. London, Ser. A* 300 (1460): 108–119. https://doi.org/10.1098/rspa.1967.0160.

2 Gent, A.N. and Tobias, R.H. (1982). Threshold tear strength of elastomers. *J. Polym. Sci., Part B: Polym. Phys.* 20 (11): 2051–2058. https://doi.org/10.1002/pol.1982.180201107.

3 Gent, A.N. (1996). Adhesion and strength of viscoelastic solids. Is there a relationship between adhesion and bulk properties? *Langmuir* 12 (19): 4492–4496. https://doi.org/10.1021/la950887q.

4 Akagi, Y., Sakurai, H., Gong, J.P. et al. (2013). Fracture energy of polymer gels with controlled network structures. *J. Chem. Phys.* 139 (14): 144905. https://doi.org/10.1063/1.4823834.

5 Sakai, T., Akagi, Y., Kondo, S., and Chung, U.-i. (2014). Experimental verification of fracture mechanism for polymer gels with controlled network structure. *Soft Matter* 10 (35): 6658–6665. https://doi.org/10.1039/c4sm00709c.

6 de Gennes, P.G. (1996). Soft adhesives. *Langmuir* 12 (19): 4497–4500. https://doi.org/10.1021/la950886y.

7 Okumura, K. (2004). Toughness of double elastic networks. *Europhys. Lett.* 67 (3): 470–476. https://doi.org/10.1209/epl/i2003-10292-x.

8 Nakajima, T., Fukuda, Y., Kurokawa, T. et al. (2013). Synthesis and fracture process analysis of double network hydrogels with a well-defined first network. *ACS Macro Lett.* 2 (6): 518–521. https://doi.org/10.1021/mz4002047.

9 Huang, M., Furukawa, H., Tanaka, Y. et al. (2007). Importance of entanglement between first and second components in high-strength double network gels. *Macromolecules* 40 (18): 6658–6664. https://doi.org/10.1021/ma062482q.

13

Mass Transport

Takamasa Sakai and Takeshi Fujiyabu

Graduate School of Engineering, The University of Tokyo, Tokyo, Japan

13.1 Diffusion of Water Molecules

Hydrogels are open systems that substances can diffuse into and out of. This unique property has attracted significant interest from academic and industrial viewpoints. As discussed in Section 6.3, there are three major theories describing the diffusion behavior of small particles in a polymer network: obstruction, hydrodynamic, and free-volume theories (Eqs. (6.16), (6.21), and (6.25)). Although there have been many attempts to examine these three theories, their applicability is still unclear due to ambiguity stemming from the heterogeneity of conventional hydrogels. To fundamentally understand the diffusion behavior of small particles in a polymer network, we investigated the diffusion coefficient of water molecules in Tetra-PEG gels (D) and tested the validity of the three major theories [1].

13.1.1 Estimation of Diffusion Coefficient of Water Molecules

We conducted a pulsed gradient spin echo (PGSE)-NMR experiment, which detects the NMR signal from the proton of diffusing particles, to estimate D. The NMR signal from the particles is related to D by the Stejskal–Tanner equation as [2]

$$\ln \frac{S}{S_0} = -G^2\gamma^2\delta^2 \left(\Delta - \frac{\delta}{3}\right) D \tag{13.1}$$

where S is the NMR echo signal intensity with the field gradient pulses, S_0 is the NMR echo signal intensity without the field gradient pulses, G is the strength of the magnetic field gradient, γ is the magnetogyric ratio of the probe molecule, δ is the gradient pulse length, Δ is the gradient pulse interval, and D is the diffusion coefficient of a particle. By plotting $\ln(S/S_0)$ against $G^2\gamma^2\delta^2(\Delta - \delta/3)$, we can assess D as the slope of the line. Tetra-PEG gels mainly contain two types of protons: protons in water molecules and those in poly(ethylene glycol) (PEG). In this type of system, D values are described by the sum of two terms with

Physics of Polymer Gels, First Edition. Edited by Takamasa Sakai.

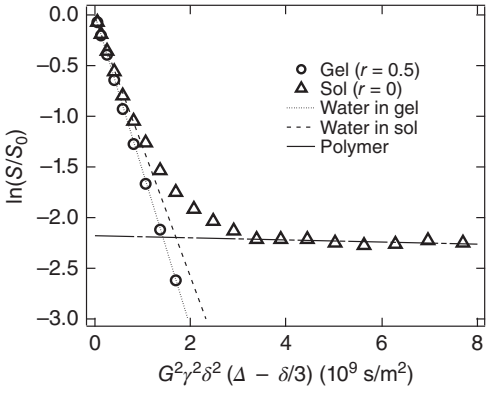

Figure 13.1 The relationship between $\ln(S/S_0)$ and $G^2\gamma^2\delta^2(\Delta - \delta/3)$ of Tetra-PEG gel (circles) and Tetra-PEG sol (triangles) with $M_w = 20$ kg/mol and $\phi_0 = 0.124$. Source: Reproduced with permission from Fujiyabu et al. [1]. Copyright 2019, American Chemical Society.

different D [3].

$$\ln = \ln \frac{S}{S_0} = f_A \exp\left(-G^2\gamma^2\delta^2\left(\Delta - \frac{\delta}{3}\right)D_A\right) + (1 - f_A)\exp\left(-G^2\gamma^2\delta^2\left(\Delta - \frac{\delta}{3}\right)D_B\right) \tag{13.2}$$

where f_A is the fraction of the NMR echo signal from particle A, D_A is the diffusion coefficient of particle A, and D_B is the diffusion coefficient of particle B. When D_A is much larger than D_B, D_A, and D_B are represented as slopes of the lines in the smaller and larger $G^2\gamma^2\delta^2(\Delta - \delta/3)$ regions, respectively.

To estimate D in Tetra-PEG gels, we decomposed D and the diffusion coefficient of PEG (D_{PEG}). In Figure 13.1, $\ln(S/S_0)$ of the Tetra-PEG gel and the Tetra-PEG sol are plotted against $G^2\gamma^2\delta^2(\Delta - \delta/3)$. In the gel state, only one slope was observed in most cases. This signal was assigned to that of water because the diffusion coefficient was close to that of pure water. All the lines passed through the origin, suggesting the applicability of Eq. (13.1) to the estimation of D. It was often difficult to observe any line in the large $G^2\gamma^2\delta^2(\Delta - \delta/3)$ region, suggesting that the diffusion of PEG was too small to be detected under our experimental conditions. On the other hand, we observed two slopes in the sol state; the diffusion of both water and PEG molecules was detected. Based on Eq. (13.2), the slopes in the small and large $G^2\gamma^2\delta^2(\Delta - \delta/3)$ regions were assigned to D ($\approx 10^9$ m^2/s) and D_{PEG} ($\approx 10^{11}$ m^2/s), respectively [4]. Because D was much larger than D_{PEG} and the slopes in the region $G^2\gamma^2\delta^2(\Delta - \delta/3) < 1.0 \times 10^9$ s/m^2 were constant for all samples, the influence of D_{PEG} on the estimation of D was almost negligible in this region. Therefore, we estimated D from the slope in the region $G^2\gamma^2\delta^2(\Delta - \delta/3) < 1.0 \times 10^9$ s/m^2.

13.1.2 Effect of Structural Parameters

We measured D by tuning three network structure parameters: the molecular weight of the prepolymers (M_w), the initial and equilibrium swollen polymer volume fractions (ϕ_0 and ϕ_e), and the imbalanced stoichiometries (r). r is related to the connectivity, p, as $p \approx 2r$ [5]. In this study, we tuned $r = 0$, 0.25, 0.375, 0.45, and 0.5, roughly corresponding to $p = 0$, 0.5, 0.75, 0.9, and 1.0, respectively. Only

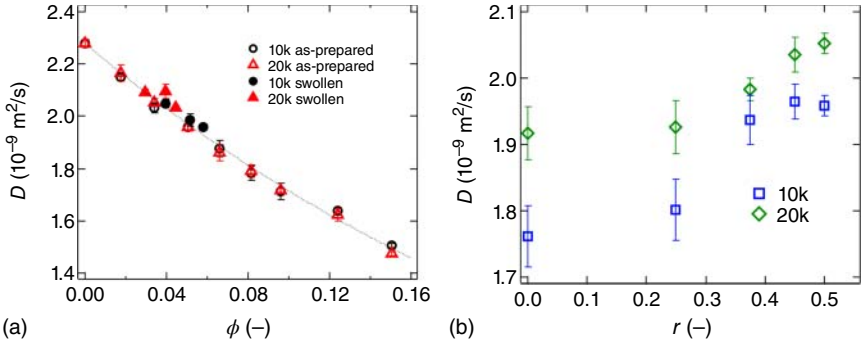

Figure 13.2 (a) The relationship between D and ϕ of Tetra-PEG gels with different M_w values (M_w: 10 kg/mol, circles; 20 kg/mol, triangles) in the as-prepared (open symbols) and equilibrium swollen states (full symbols). (b) The relationship between D and r of Tetra-PEG gels ($M_w = 10$ kg/mol and $\phi_0 = 0.050$, squares; $M_w = 20$ kg/mol and $\phi_0 = 0.034$, rhombuses). Source: Reproduced with permission from Fujiyabu et al. [1]. Copyright 2019, American Chemical Society.

the sample with $r = 0$ was in the sol state, while all the other samples were in the gel state. In Figure 13.2a, we plotted D against the polymer volume fraction (ϕ). In both the as-prepared and the equilibrium swollen Tetra-PEG gels, D decreased with an increase in ϕ, roughly obeying an exponential function. On the other hand, the effect of M_w on D was small. These results suggest that ϕ is the essential factor in controlling the diffusion behavior of water molecules in hydrogels; the presence of the polymer retards the diffusion of water molecules.

Figure 13.2b shows the relationship between D and r. D decreased with an increase in the deviation from stoichiometry (with a decrease in p), and no drastic change was observed at the gelation threshold. This results suggest that p is the second factor governing the diffusion of water molecules in hydrogels. Notably, this result is counterintuitive because the formation of a network leads to an increase in the mobility of water molecules. In other words, the pore size, characterized by p (see Section 5.6), is not an essential factor governing the diffusion of water molecules.

13.1.3 Applicability of Theoretical Models

We examined the applicability of three major theories: obstruction theory, hydrodynamic theory, and free-volume theory (see Section 6.3). For the examination of hydrodynamic theory, Eq. (6.21) is often transformed based on the combination of the scalings for the screening constant (κ) and the correlation length of a polymer network (ξ) with respect to ϕ [6].

$$\frac{D}{D_0} \approx \exp\left(-\frac{R}{\xi}\right) \approx \exp(-R\phi^{0.75}) \tag{13.3}$$

In Figure 13.3, the normalized diffusion coefficient of water molecules (D/D_0) is plotted against ϕ, where D_0 is the diffusion coefficient of pure water in the

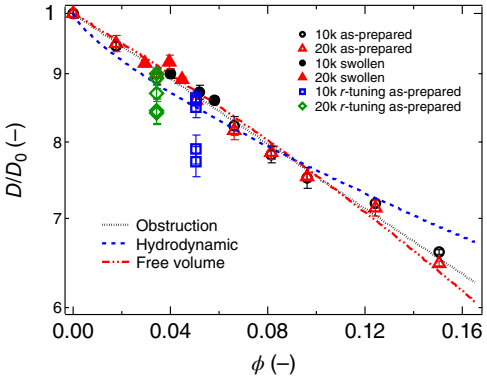

Figure 13.3 The relationship between D/D_0 and ϕ of Tetra-PEG gels with different M_w values (M_w: 10 kg/mol, circles; 20 kg/mol, triangles) in the as-prepared (open symbols) and equilibrium swollen states (full symbols) and of *r*-tuned Tetra-PEG gels ($M_w = 10$ kg/mol and $\phi_0 = 0.050$, squares; $M_w = 20$ kg/mol and $\phi_0 = 0.034$, rhombuses). Source: Reproduced with permission from Fujiyabu et al. [1]. Copyright 2019, American Chemical Society.

absence of polymers. The lines in Figure 13.3 show the fits by Eqs. (6.16), (13.3), and (6.25). All three models reproduced the ϕ- and M_w-dependences of D/D_0, and the difference among the models was negligible in this region. In the small ϕ region, the difference between Eqs. (6.16) and (6.25) is negligible because $(1 - \phi)$ is close to 1 and the effect of the difference in the exponents of ϕ in Eqs. (6.16) (1) and (13.3) (0.75) is also small. Therefore, it is impossible to test the applicability of the three major theories based on these experimental results.

On the other hand, the *r*-dependence of D/D_0 was not reproduced by any models (Figure 13.3). The reason for this deviation is clear: Eqs. (6.16), (13.3), and (6.25) only have ϕ as a variable and do not consider the effect of p. This deviation indicates that a model should include the effect of p. Notably, deviation from the three representative models was mainly observed in the low p region ($p < 0.5$). This deviation has not been observed in previous studies, most likely because the connectivity of the polymer network has not been changed intentionally.

13.1.4 Effect of Correlation Length on Diffusion

To explain the observed deviation in the *r*-dependence, we examined some representative plots and found a linear relationship between D/D_0 and $1/\xi$ (Figure 13.4). Here, ξ is the correlation length of a polymer network estimated from our previous small-angle neutron scattering (SANS) measurements (Chapter 9 and Column 2). All the data, including the *r*-dependence, fall onto the master relationship in this plot. The formula of the master relationship is the following:

$$\frac{D}{D_0} = 0.98 \exp\left(-\frac{2.9}{\xi}\right) \tag{13.4}$$

This formula is almost the same as the original equation of hydrodynamic theory (Eq. (13.3)). In addition, the front factor is almost unity, and 2.9 Å is close to the diameter of a water molecule (2.74–3.30 Å) [7]. Based on this correspondence, we propose a semiempirical equation:

$$\frac{D}{D_0} = \exp\left(-\frac{d}{\xi}\right) \tag{13.5}$$

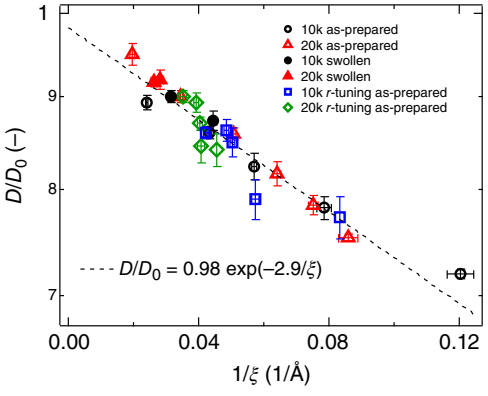

Figure 13.4 The relationship between D/D_0 and $1/\xi$ of Tetra-PEG gels with different M_w values (M_w: 10 kg/mol, circles; 20 kg/mol, triangles) in the as-prepared (open symbols) and equilibrium swollen states (full symbols) and of *r*-tuned Tetra-PEG gels ($M_w = 10$ kg/mol and $\phi_0 = 0.050$, squares; $M_w = 20$ kg/mol and $\phi_0 = 0.034$, rhombuses). Source: Reproduced with permission from Fujiyabu et al. [1]. Copyright 2019, American Chemical Society.

where d is the diameter of a particle. The importance of the term d/ξ, which is the ratio between the characteristic sizes of a particle and a polymer network, has been suggested by Tokita et al. as well [8]. Therefore, the diffusion behavior of small particles in hydrogels is considered to be determined by the ratio of the characteristic size of the particle to that of the polymer network based on the hydrodynamic theory.

13.2 Migration of Water Molecules in Hydrogels

In Section 13.1, we discussed the diffusion, which is the thermal fluctuation around the original position characterized by D. In this section, we discuss the directional motion driven by outer stimuli, i.e. migration. Here, we discuss the migration behavior of water molecules in hydrogels. Theoretically, the friction coefficient between the polymer network and water (f) governs the water migration in hydrogels. de Gennes predicted f based on the picture that water flows through the pores of concentration blobs [9, 10].

$$f \approx \frac{\eta}{\xi^2} \sim \xi^{-2} \tag{13.6}$$

where η is the solvent viscosity and ξ is the blob size. To understand the migration behavior of water molecules in hydrogels, we performed water permeation measurements on Tetra-PEG gels with different prepolymer molecular weights (M_w), polymer volume fractions (ϕ_0), and imbalanced stoichiometries (r) [11].

13.2.1 Water Permeation Through Hydrogel

The value of f is estimated by water permeation experiments; a hydrostatic pressure (P) is imposed from the top of a hydrogel membrane with a thickness of d, and the velocity of water permeating through the membrane (v) is measured.

$$f = \frac{P}{vd} \tag{13.7}$$

Notably, f differs from the dimensionless friction coefficient, although f is conventionally defined as the "friction coefficient" with units of $(\mathrm{N\,s})/\mathrm{m}^4$ in the

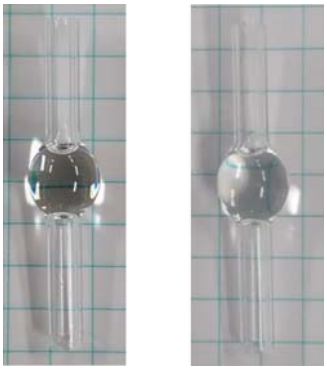

Figure 13.5 The gels were prepared in a glass tube rounded in the center. (a) As-prepared state and (b) equilibrium swollen state. Source: Reproduced with permission from Fujiyabu et al. [11]. Copyright 2017, American Chemical Society.

physics of polymer gels. In a water permeation experiment, a hydrogel always contacts water and is allowed to swell. Thus, a hydrogel in the as-prepared state swells during the experiments, preventing an accurate measurement of v. To solve this problem, we established a novel water permeation apparatus, which inhibited the swelling of the gel and enabled the water permeation experiment in a pseudo-as-prepared state (Figure 13.5).

First, we confirmed the inhibition of swelling in the apparatus. A glass tube containing a gel in its round part (Figure 13.5) was immersed in a water bath, and the gel was allowed to swell. After confirming that the gel reached its maximum change in weight, we measured the swelling ratio in the apparatus (Q, Figure 13.6). Most of the values of Q were lower than 1.05. Notably, the swelling ratio of these hydrogels without confinement was up to 3.1 [12]. Thus, this apparatus could prevent a gel from swelling and achieve a water permeation experiment in a pseudo-as-prepared condition.

Then, we checked the invariance of P and the absence of water leakage or gel deformation during the water permeation experiment. The amount of water loss caused by the permeation and evaporation was negligible, reflecting that P was almost constant during the experiments (Figure 13.7a). Figure 13.7b shows a typical result for meniscus movement. The meniscus position moved fast at the beginning of the experiment and then reached a steady velocity.

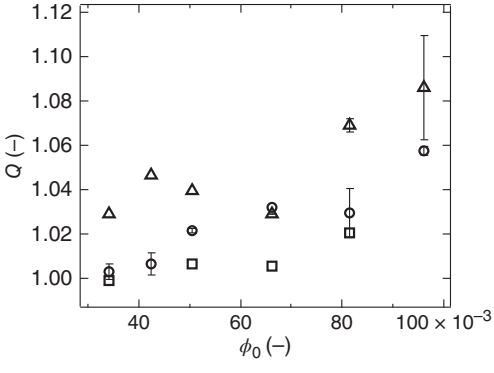

Figure 13.6 The ϕ_0-dependence of Q of Tetra-PEG gels with different M_w values (M_w: 5 kg/mol, squares; 10 kg/mol, circles; 20 kg/mol, triangles) in the round part of glass tubes. Source: Reproduced with permission from Fujiyabu et al. [11]. Copyright 2017, American Chemical Society.

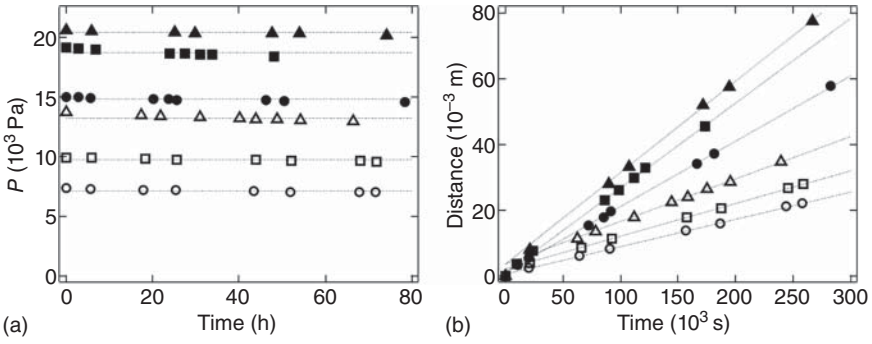

Figure 13.7 (a) The time course of P during the water permeation experiments for a Tetra-PEG gel (M_w: 10 kg/mol, ϕ_0: 0.034) at different pressures (P: 7100 Pa, circles; 9700 Pa, squares; 13 000 Pa, triangles; 15 000 Pa, full circles; 19 000 Pa, full squares; 20 000 Pa, full triangles). (b) The time course of the meniscus position during the water permeation experiments for a Tetra-PEG gel (M_w: 10 kg/mol, ϕ_0: 0.034) at different P values (P: 7100 Pa, circles; 9700 Pa, squares; 13 000 Pa, triangles; 15 000 Pa, full circles; 19 000 Pa, full squares; 20 000 Pa, full triangles). Source: Reproduced with permission from Fujiyabu et al. [11]. Copyright 2017, American Chemical Society.

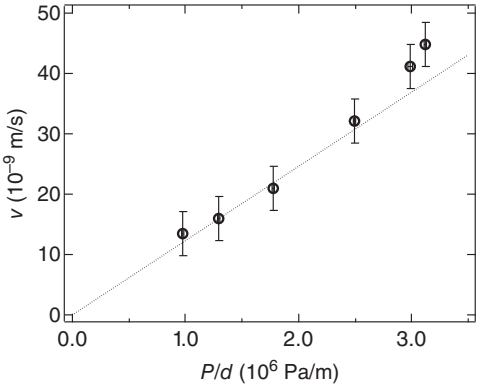

Figure 13.8 The P/d-dependence of v of a Tetra-PEG gel (M_w: 10 kg/mol, ϕ_0: 0.034). The dotted line shows the linear relationship between v and P/d in the small P/d region. Source: Reproduced with permission from Fujiyabu et al. [11]. Copyright 2017, American Chemical Society.

We plotted v as a function of P/d (Figure 13.8). The relationship between v and P/d was linear and agreed with Eq. (13.7) in the small P/d region. In contrast, slight upward deviations from the linear relationship were observed in the region above $P/d \approx 3.0 \times 10^6$ Pa/m. To minimize the nonlinear effect and the experimental error caused by the long experimental period, the water permeation experiments were conducted at approximately $P/d = 2.5 \times 10^6$ Pa/m.

13.2.2 Effect of Structural Parameters on Friction Coefficient

The friction coefficients (f) of 5k, 10k, and 20k Tetra-PEG gels are shown as a function of ϕ_0 in Figure 13.9. f increased with an increase in ϕ_0, suggesting that a denser polymer network more strongly retarded water permeation. When we focused on Tetra-PEG gels with the same ϕ_0 but different M_w values, Tetra-PEG gels with "higher" molecular weights between crosslinks retarded the water permeation more. Similar counterintuitive results were observed in Tetra-PEG gels

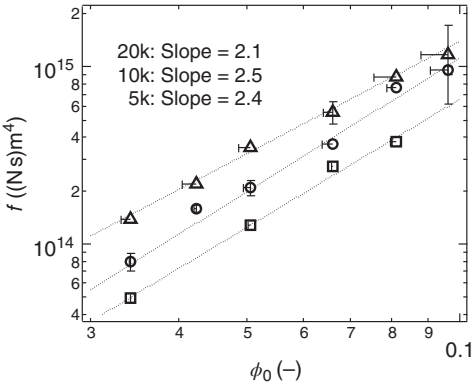

Figure 13.9 The ϕ_0-dependence of f of Tetra-PEG gel with different M_w (M_w: 5 kg/mol, squares; 10 kg/mol, circles; 20 kg/mol, triangles). Source: Reproduced with permission from Fujiyabu et al. [11]. Copyright 2017, American Chemical Society.

formed with a nonstoichiometric prepolymer ratio. f increased with an increase in the deviation from stoichiometry; loosely crosslinked polymer networks strongly retarded water permeation. When we focused on the power law relationships between f and ϕ_0 ($f \sim \phi_0{}^x$), the 5k, 10k, and 20k Tetra-PEG gels showed $x = 2.4$, 2.5, and 2.1, respectively. These scaling relationships were completely different from the theoretical prediction ($f \sim \phi^{1.5}$, Eqs. (2.15) and (13.6)).

13.2.3 Effect of Correlation Length on Friction Coefficient

To directly examine Eq. (13.6), we plotted f against the ξ estimated by SANS (Chapter 9) in Figure 13.10. Here, we assume that the correlation length of a polymer network estimated by SANS as the blob size (ξ). All the data fall onto a curve showing the scaling $f \sim \xi^{-2}$ (shown as a dotted line). This correspondence strongly suggests the validity of Eq. (13.6). In other words, water molecules permeate through a hydrogel by passing through a path with the size ξ. A slight deviation was observed in 5k Tetra-PEG gels, which may be due to local heterogeneity [13, 14].

Because the units of f and η/ξ^2 are the same, Eq. (13.6) becomes an identity formula with a dimensionless constant, a.

$$f = a\frac{\eta}{\xi^2} \tag{13.8}$$

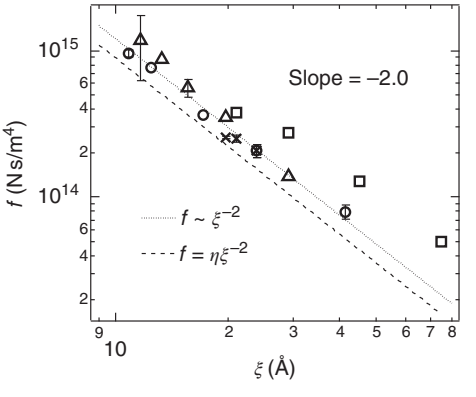

Figure 13.10 The ξ-dependence of f of Tetra-PEG gels with different M_w values and an r-tuned Tetra-PEG gel (M_w: 5 kg/mol, squares; 10 kg/mol, circles; 20 kg/mol, triangles; r-tuned, crosses). Source: Reproduced with permission from Fujiyabu et al. [11]. Copyright 2017, American Chemical Society.

We plotted the value of η/ξ^2 using the viscosity of water (η) at 25 °C (8.9×10^{-4} (N s)/m^2) as a dashed line in Figure 13.10. The calculated η/ξ^2 was close to f, indicating that a was on the order of unity ($a = 0.68$). Because ξ is strongly correlated with the osmotic pressure (see Section 2.3.5), the permeation of water molecules through hydrogels is, in other words, governed by the osmotic pressure, which indicates the water-retention ability of hydrogels.

13.3 Electro-Osmotic Flow in Electrically Charged Gels

Electro-osmosis is the bulk fluid flow that is stimulated when an electric field is applied to an electrolyte solution in a charged capillary. Counterions accumulating on a charged surface produce a net charge, producing a bulk flow called "electro-osmotic flow (EOF)" upon application of an electric field. A similar phenomenon occurs in polyelectrolyte gels; counterions accumulating in the polyelectrolyte network generate EOF.

In the case of the capillary electrophoresis of DNA molecules in agarose gels at an appropriate pH, EOF moves from the positive electrode toward the negative electrode because positive counterions in the vicinity of agarose chains move toward the negative electrode. The EOF decreases the observed electrophoretic mobility (μ_{obs}) of the oppositely migrating negatively charged DNA, resulting in an electrophoretic mobility (μ) of

$$\mu = \mu_{obs} - \mu_{EOF} \tag{13.9}$$

where μ_{EOF} is the mobility of EOF. Although Eq. (13.9) is known, systematic and qualitative investigation on polymer gels has never been performed. We investigated the EOF in various *r*-tuned and *p*-tuned Tetra-PEG gels and discussed the effects of fixed charges and polymer concentration. *r*-Tuned Tetra-PEG gels are formed from nonstoichiometric mixing of two Tetra-PEGs, resulting in the introduction of fixed charges (amine or carboxylic groups) into the polymer network. In addition, *p*-tuned Tetra-PEG gels were utilized as electrically neutral polymer networks that have equal amounts of positive and negative charges. In addition, to examine the validity of Eq. (13.9), the effect of EOF on the observed electrophoretic mobility of DNA was discussed.

13.3.1 Electro-Osmosis in an Electrically Balanced System

Our first question is how coexisting opposite charges influence electro-osmosis. The unreacted end groups (–NH_2 and –COOH) in *p*-tuned Tetra-PEG gels are positively (–NH_3^+) or negatively charged (–COO^-) in the buffers used in this study. Thus, the same amounts of positive and negative charges coexist in *p*-tuned Tetra-PEG gels. EOF was evaluated by measuring the electric field-mediated mobility of the uncharged low-molecular-weight fluorescent marker BODIPY FL hydrazide. Because of its low molecular weight, BODIPY FL hydrazide is expected to move at the same rate as EOF. After the injection of *p*-tuned Tetra-PEG gels into a custom-made capillary electrophoresis machine,

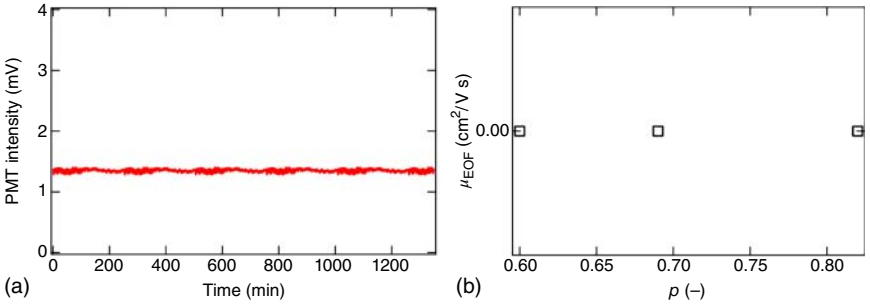

Figure 13.11 (a) Photomultiplier tube (PMT) intensity as a function of time in a *p*-tuned Tetra-PEG gel ($p = 0.6$) and (b) μ_{EOF} as a function of *p*. Source: Reproduced with permission from Khairulina et al. [17]. Copyright 2017, Royal Society of Chemistry.

the *p*-tuned Tetra-PEG gels were subjected to a constant electric field strength of 50 V/cm. The migration time of the neutral marker was measured 2.5 cm from the injection site. The electro-osmotic mobility values (μ_{EOF}) were calculated as follows:

$$\mu_{EOF} = \mu = \frac{\nu}{E} \tag{13.10}$$

where ν is the migration velocity and E is the electric field strength. As a result, we could not detect any fluorescence for 24 hours, indicating that $\mu_{EOF} \approx 0$ (Figure 13.11a). An increase in the amount of charged species did not change the results (Figure 13.11b). Notably, at this timescale, we could even detect the migration of DNA with 1000 bp, which has an extremely slow migration rate. These results strongly suggest that this absence of EOF is due to the electrically balanced nature of *p*-tuned Tetra-PEG gels and that net charge density is essential for electro-osmosis.

13.3.2 Electro-Osmosis in an Electrically Imbalanced System

Our second question is whether the same amount of opposite charges exactly induces the same magnitude of EOF in opposite directions. To fabricate polymer gels incorporating positive or negative charges, *r*-tuned Tetra-PEG gel system was utilized. We mixed buffered aqueous solutions of each prepolymer while tuning *r* at a fixed $C = 60$ g/l. The fixed charge molarity in the polymer network (ε) is given by

$$\varepsilon = (1 - 2r) \cdot \frac{C}{M_w} \cdot f \tag{13.11}$$

where M_w is the molecular weight of the prepolymer ($M_w = 20$ kg/mol) and f is the functionality of the prepolymers ($f = 4$). As a result, in the case $r < 0.5$, the polymer gel is positively charged, and in the case $r > 0.5$, the polymer gel is negatively charged.

The EOF of *r*-tuned Tetra-PEG gels was evaluated using the same method as that used for *p*-tuned Tetra-PEG gels. In contrast to *p*-tuned Tetra-PEG gels, *r*-tuned Tetra-PEG gels exhibited fluorescence from a neutral marker, indicating

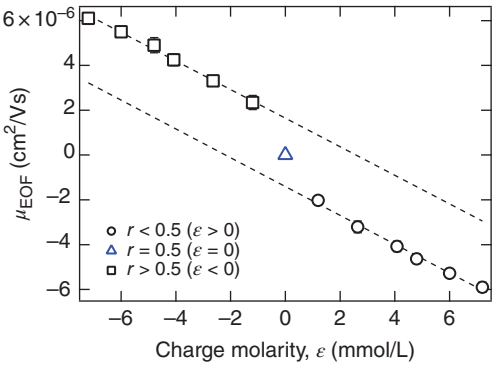

Figure 13.12 Correlation between EOF mobility measured in *r*-tuned and *p*-tuned Tetra-PEG gels ($C = 60$ g/l) and charge molarity (ε). Source: Reproduced with permission from Khairulina et al. [17]. Copyright 2017, Royal Society of Chemistry.

the generation of EOF. As shown in Figure 13.12, *r*-tuned gels with opposite charges generated EOF in opposite directions: from the cathode to the anode for negatively charged specimens ($r > 0.5$) and from the anode to the cathode for positively charged specimens ($r < 0.5$). The magnitude of EOF increased with an increase in $|\varepsilon|$, and the behaviors of positively and negatively charged specimens were completely symmetrical. These data strongly suggest that the same amounts of opposite charges induce the same magnitude of EOF in opposite directions. Another important point is that the extrapolation of ε to 0 does not go to $\mu_{EOF} = 0$, although an electrically neutral *p*-tuned system has $\mu_{EOF} = 0$. The origin of the offset may be due to nonspecific interactions between the neutral marker and the capillary wall, as discussed in the following text.

Next, we evaluated the effect of C on EOF. *r*-Tuned gels with various ε values were prepared with $C = 40$, 50, and 60 g/L. Figure 13.13 shows the ε-dependence

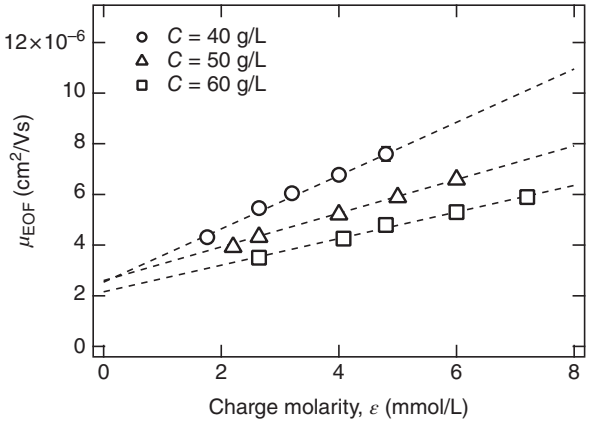

Figure 13.13 Correlation between EOF mobility (μ_{EOF}) measured in *r*-tuned Tetra-PEG gels with $C = 40$, 50, and 60 g/l and charge molarity (ε). Circles, triangles, and squares represent *r*-tuned Tetra-PEG gels with $C = 40$, 50, and 60 g/L, respectively. Also, the annotation in Figure 13.12 disappears; Circles, Triangle, and Squares represent $r < 0.5$ ($\varepsilon > 0$), $r = 0.5$ ($\varepsilon = 0$), and $r > 0.5$ ($\varepsilon < 0$), respectively. The label of the left axis is μ_{EOF} [cm^2/Vs], and that of the bottom axis is ε [mmol/L]. Source: Reproduced with permission from Khairulina et al. [17]. Copyright 2017, Royal Society of Chemistry.

of EOF for each concentration. Two main features can be observed from Figure 13.13. First, μ_{EOF} decreases with an increase in C, suggesting that the polymer network acts as an obstruction decelerating the EOF. Second, linear regression fitting of each data set in Figure 13.13 showed a constant offset regardless of C. This result indicates that the offset value is not related to any structural parameters of the polymer network but rather to the nonspecific interactions between the migrating neutral marker and the capillary wall. Overall, it is concluded that the charge molarity (ε) and polymer concentration (C) govern the electro-osmosis in weakly charged polyelectrolyte hydrogels. Notably, an increase in ε subsequently leads to a decrease in elastic modulus. Thus, this linear relationship implies that network architecture does not have an additional effect on the retardation of EOF.

13.3.3 Sum Rule of Electro-Osmotic Flow and Electrophoretic Motion

We then investigated how EOF contributes to the electrophoresis of negatively charged DNA molecules. To answer this question, the electrophoretic behavior of DNA markers in the size range of 20–1000 bp in p- and r-tuned Tetra-PEG gels was investigated. To examine the true effect of ε, gel specimens were set to have the same C and different values of ε ($-\varepsilon_0$, 0, and $+\varepsilon_0$).

Figure 13.14 shows the electrophoretic mobility values of DNA markers in the gel specimens. In general, the electrophoretic mobility of DNA decreases with an increase in the number of DNA base pairs (n) [15, 16]. Here, let us focus on the effect of charges on electrophoretic mobility. The observed mobility of DNA increased in networks with positive charges ($\varepsilon = \varepsilon_0$, $r < 0.5$) and decreased in networks with negative charges ($\varepsilon = -\varepsilon_0$, $r > 0.5$) compared with a neutral network ($\varepsilon = 0$, $r = 0.5$). This result is reasonable because the direction of EOF generated by fixed positive charges is the same as that of the electrophoretic mobility of DNA, and vice versa.

We then subtracted the influence of EOF from the data in Figure 13.14 based on Eq. (13.9). Notably, the EOF value applied to each DNA molecule is assumed to be constant regardless of n. As clearly shown in Figure 13.15, the subtracted data for the positively and negatively charged network converged with that of the

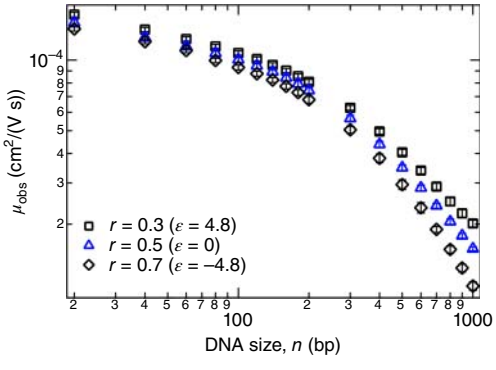

Figure 13.14 Double-logarithmic plot of observed DNA mobility (μ_{obs}) as a function of DNA base pairs (n) prior to EOF correction. Source: Reproduced with permission from Khairulina et al. [17]. Copyright 2017, Royal Society of Chemistry.

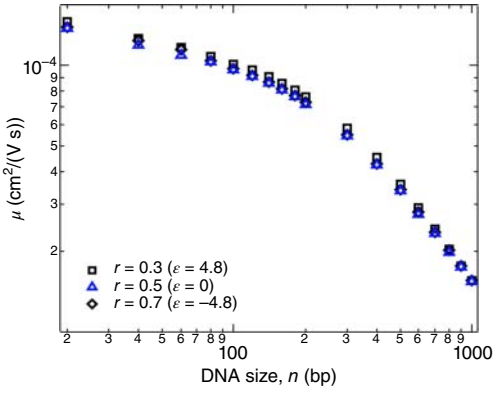

Figure 13.15 Double-logarithmic plot of the corrected mobility of DNA (μ) as a function of DNA base pairs (n) with EOF correction. Source: Reproduced with permission from Khairulina et al. [17]. Copyright 2017, Royal Society of Chemistry.

electrically neutral polymer network. These data strongly suggest the validity of Eq. (13.9); the fixed charges in a polymer network influence the electrophoretic mobility through only the EOF.

13.4 Migration of Small Double-Stranded DNAs

Next, we focused on the migration of double-stranded DNA (dsDNA), which is applied in gel electrophoresis. During electrophoresis, the interaction between the polymer network and the charged molecules is the key factor differentiating the electrophoretic mobility (μ) of the charged molecules according to length. When dsDNA is smaller than the persistence length of dsDNA (≈50 nm), it can be simply regarded as a stiff rod. In this case, the Ogston model (see Section 6.3.1) is often used to explain the migration behavior. In contrast, the reptation model (see Section 6.3.4) and the entropic trapping (ET) model (see Section 6.3.5) are used to explain the migration behavior of relatively large charged molecules. Although the validity of these models was experimentally confirmed to some extent, they are not fully understood.

In this section, we focus on the migration behavior of small dsDNA in neutral gels. To fundamentally understand the migration behavior of small dsDNA, we conducted electrophoresis on dsDNA in the range of 20–160 bp in Tetra-PEG gels with a series of precisely tuned ϕ and polymerization degree between crosslinks (N_s) values [15].

13.4.1 Electrophoresis of dsDNA in Tetra-PEG Gels and Solutions

We conducted capillary gel electrophoresis on dsDNA fragments with n from 20 to 160 bp in Tetra-PEG gels and PEG solutions by tuning ϕ and N_s. The electrophoretic mobility (μ) was calculated by the same method as in Section 13.3.1. The n-dependence of μ is displayed in Figure 13.16. Larger DNA had a lower μ. An increase in ϕ or a decrease in N_s also lowered μ. These results indicate that large DNA or a dense network leads to strong interactions and results in a decrease in μ.

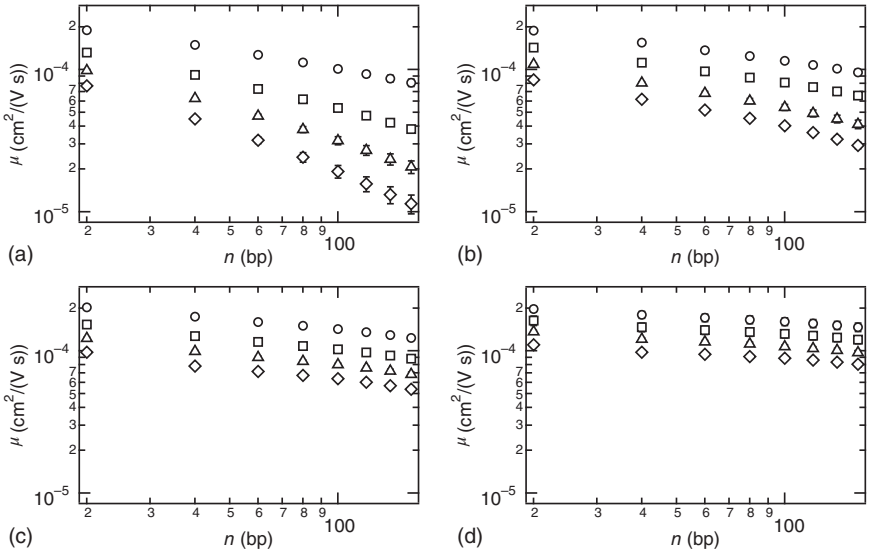

Figure 13.16 The n-dependence of μ in Tetra-PEG gels and PEG solutions with different ϕ (ϕ: 0.034, open circle; 0.050, square; 0.066, triangle; 0.081, rhombus). The error bars are hidden when the error bar is smaller than the symbol size. (a) $N_s = 113$, (b) $N_s = 227$, (c) $N_s = 454$, and (d) PEG solution. Source: Reproduced with permission from Li et al. [15]. Copyright 2013, American Chemical Society.

Figure 13.17 shows semilogarithmic plots of μ against ϕ for various N_s and n values. We assumed that the polymer volume fraction of the polymer gel was the same as that of the prepolymer solution because subsequent swelling or deswelling in the capillary tube with an extremely high aspect ratio hardly occurred. μ was an exponential function of ϕ for each N_s and n, which corresponds well to the Ogston model prediction (Eq. (6.16)). The deviation from the fitting curve in the low ϕ region is probably due to the imperfections of the network reported previously [12], which decrease the interaction of the network with dsDNA and increase the μ.

13.4.2 Semiempirical Model

According to the Ogston model, the extrapolation and slope in Figure 13.17 correspond to the free solution electrophoretic mobility (μ_0) and retardation coefficient (K_r), respectively. The K_r values estimated from the fit are plotted against n in Figure 13.18. The K_r values increased with an increase in n, and the increasing rate decreased with an increase in N_s. In contrast to the Ogston prediction (Eq. (6.17)), K_r was a simple power law function of n: $K_r = 6.4n^{0.34}$ ($N_s = 113$), $K_r = 8.1n^{0.22}$ ($N_s = 227$), $K_r = 10.5n^{0.11}$ ($N_s = 454$), and $K_r = 12.7n^0$ (PEG solution) (Figure 13.13). Thus, μ/μ_0 is semiempirically represented as follows:

$$\frac{\mu}{\mu_0} = \exp(-K_r\phi) \tag{13.12}$$

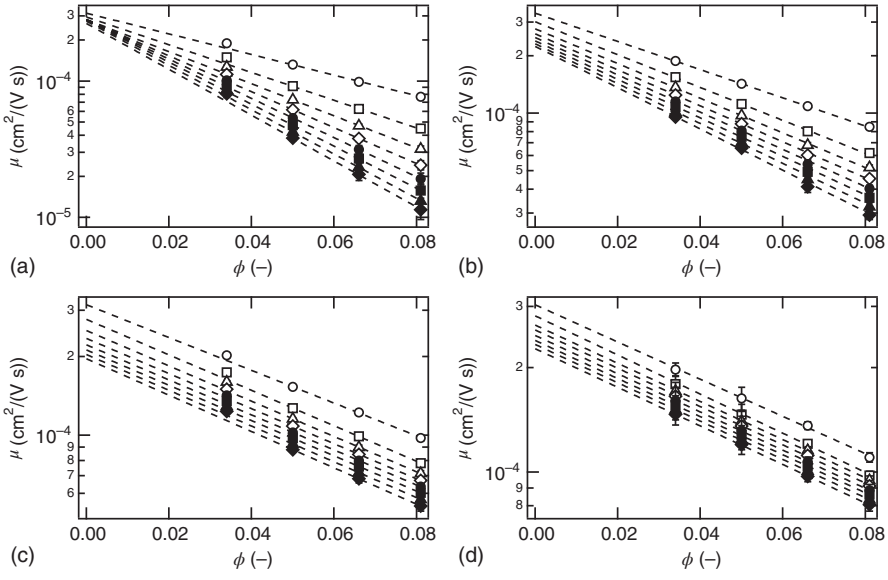

Figure 13.17 The ϕ-dependence of μ in Tetra-PEG gels and PEG solutions with dsDNA of size n (n: 20 bp, circle; 40 bp, square; 60 bp, triangle; 80 bp, rhombus; 100 bp, full circle; 120 bp, full square; 140 bp, full triangle; 160 bp, full rhombus). The error bars are hidden when they are smaller than the symbols. (a) $N_s = 113$, (b) $N_s = 227$, (c) $N_s = 454$, and (d) PEG solution. Source: Reproduced with permission from Li et al. [15]. Copyright 2013, American Chemical Society.

Figure 13.18 The n-dependence of K_r in Tetra-PEG gels and PEG solution with different N_s values (N_s: 113, open circle; 227, square; 454, triangle; PEG solution, rhombus). The dotted line is the fitting curve showing the relation $K_r = \alpha(N_s)n^{\beta(N_s)}$. Source: Reproduced with permission from Li et al. [15]. Copyright 2013, American Chemical Society.

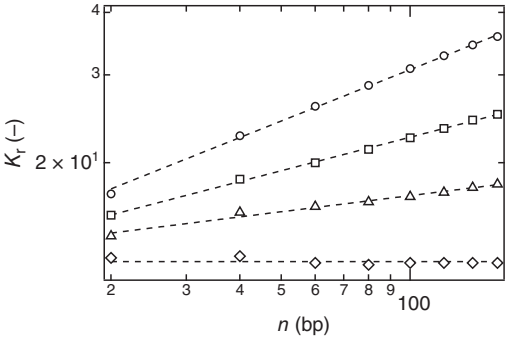

$$K_r = \alpha(N_s)n^{\beta(N_s)} \tag{13.13}$$

where $\alpha(N_s)$ and $\beta(N_s)$ are variables that depend on only N_s.

The N_s-dependence of $\alpha(N_s)$ and $\beta(N_s)$ is shown in Figure 13.19. The data for the PEG solution are shown as dotted lines. With increasing N_s, $\alpha(N_s)$ increased, and $\beta(N_s)$ decreased. Both $\alpha(N_s)$ and $\beta(N_s)$ asymptotically reached constants that correspond to those of the PEG solution ($\alpha = 12.7$ and $\beta = 0$). These data strongly suggest that the PEG solution can be practically treated as a polymer network with an infinite N_s and that the migration behavior is not critically influenced by the gelation threshold.

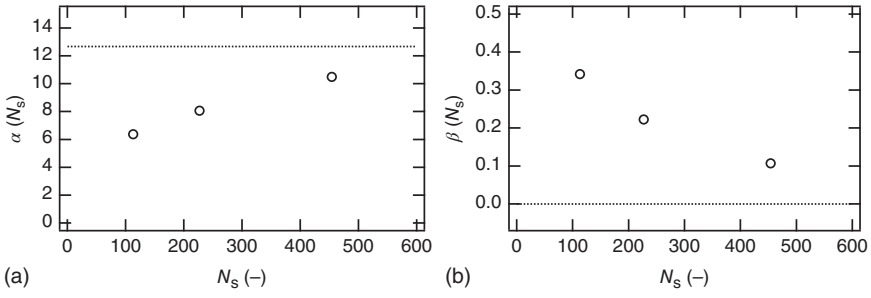

Figure 13.19 The N_s-dependence of $\alpha(N_s)$ (a) and $\beta(N_s)$ (b). The dotted line is the value for the PEG solution. Source: Reproduced with permission from Li et al. [15]. Copyright 2013, American Chemical Society.

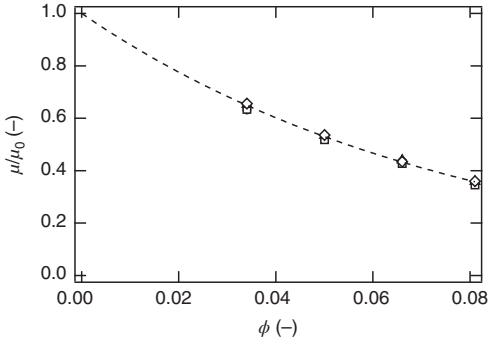

Figure 13.20 The ϕ-dependence of the reduced electrophoretic mobility (μ/μ_0) in PEG solution with dsDNA of size n (n: 20 bp, open circle; 40 bp, square; 80 bp, triangle; 160 bp, rhombus). The dotted curve is the guide of the relationship, $\mu/\mu_0 = \exp(-12.7\,\phi)$. Source: Reproduced with permission from Li et al. [15]. Copyright 2013, American Chemical Society.

13.4.3 Effect of Correlation Length on Electrophoretic Mobility

Let us focus on the μ/μ_0 of the PEG solution, which corresponds to a polymer gel with an infinite N_s. The 0 value of β in the PEG solution indicates that μ/μ_0 is defined by only ϕ and is represented as

$$\frac{\mu}{\mu_0} = \exp(-12.7\phi) \tag{13.14}$$

Figure 13.20 shows μ/μ_0 of the PEG solutions. In practice, the values of μ/μ_0 did not depend on n and were well predicted by Eq. (13.14). These data strongly suggest that the μ/μ_0 of polymer gels is defined by only ϕ, regardless of N_s and n, when N_s is large enough. Because K_r increases with a decrease in N_s (Figure 13.18), the value expected from Eq. (13.14) is the maximum μ/μ_0 at a specific ϕ, which is not influenced by N_s or n.

The ϕ-dependent and N_s-independent characteristics remind us of the molecular picture of a concentration blob (Chapter 9 and Column 2). Polymer solutions and polymer gels in semidilute solution are closely packed systems of concentration blobs. Because the concentration blob size (ξ, 0.5–3 nm) [14] is smaller than the the gyration radius (R_g) of dsDNA (7–54 nm), dsDNA may migrate in the packed concentration blobs, which cause friction against dsDNA. Because dsDNA may be treated as a free-draining rod-like structure, the friction against dsDNA from concentration blobs will be proportional to n. This n-dependence

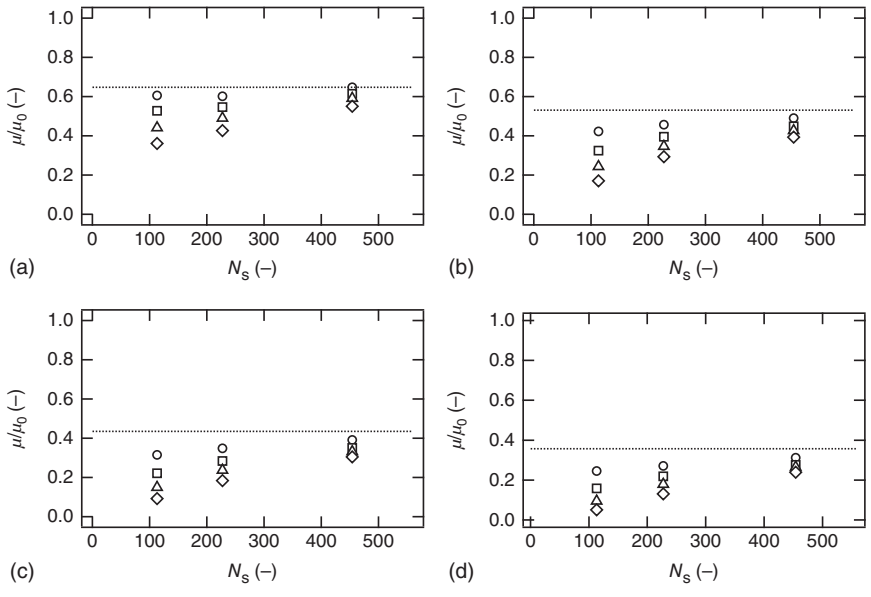

Figure 13.21 The N_s-dependence of μ/μ_0 in Tetra-PEG gels and PEG solution with dsDNA of size n (n: 20 bp, open circle; 40 bp, square; 80 bp, triangle; 160 bp, rhombus). The dotted line shows the average value of the PEG solution. (a) $\phi = 0.034$, (b) $\phi = 0.050$, (c) $\phi = 0.066$, and (d) $\phi = 0.081$. Source: Reproduced with permission from Li et al. [15]. Copyright 2013, American Chemical Society.

will be cancelled by the effect of electric force, which is also proportional to n, resulting in loss of the size-sieving effect. This expectation corresponds well to the experimental finding that n-dependence was not actually observed in the PEG solution ($\beta = 0$).

13.4.4 Interaction Between Elastic Blobs and Contour of dsDNA

Finally, we show the effects of N_s and n on μ/μ_0. The N_s-dependence of μ/μ_0 is displayed in Figure 13.21. With decreasing N_s, μ/μ_0 decreased from the value predicted by Eq. (13.14), and the decrease was remarkable in dsDNA with large n values. These data indicate that the N_s and n determine the degree of retardation from the maximum estimated by Eq. (13.14). Because the elastic blob is characterized by N_s, it is expected that the elastic blobs interact with the contour of dsDNA. The direct influence of N_s on the n-dependence of K_r seen in Eq. (13.13) also supports the strong interaction between the elastic blob and the contour of dsDNA.

13.5 Migration of Large Double-Stranded DNAs

To fully understand the dynamics in a polymer network, the migration of large molecules is as important as the diffusion and migration of small particles in

a polymer network discussed in Sections 13.1–13.4. Here, we also conducted a systematic study of the electrophoretic migration behavior of dsDNA with large n values (100–8000 bp) in polymer networks with controlled network structures [16].

13.5.1 Electrophoresis of Large dsDNA in Tetra-PEG Gels and Solutions

We performed capillary electrophoresis of dsDNA (n: 100–8000 bp) in Tetra-PEG gels and PEG solutions with different degrees of strand polymerization between crosslinks (N_s) and polymer volume fraction (ϕ) [16]. Figure 13.22 shows double-logarithmic plots of the n-dependence of μ. With increasing n, μ first decreased and then became independent of n; n-dependent and n-independent migration regions were observed. The boundary between these two regions was at approximately 1000 bp. The crossover from n-dependent to n-independent migration behavior qualitatively agrees with the biased reptation with fluctuations (BRF) model, signifying the former as reptation of unoriented

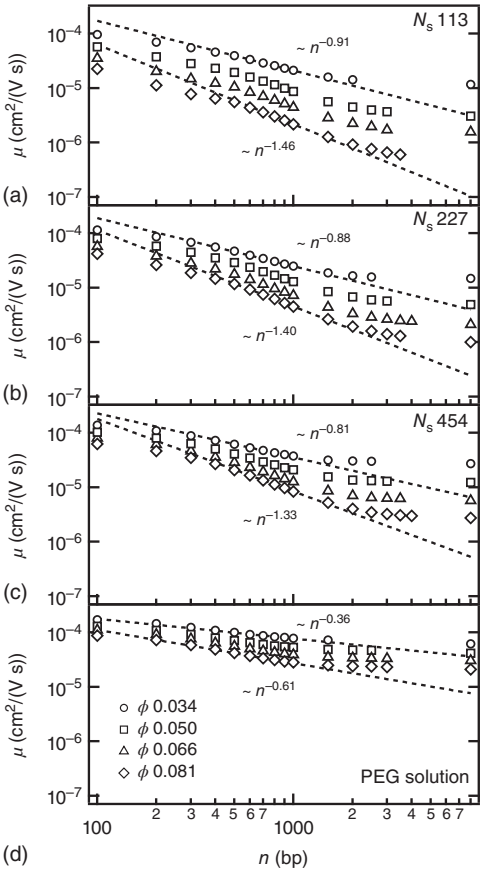

Figure 13.22 Double-logarithmic plots of μ as a function of n in Tetra-PEG gels with varied ϕ and N_s = (a) 113, (b) 227, and (c) 454 and (d) in PEG solutions with varied ϕ values. Source: Reproduced with permission from Li et al. [16]. Copyright 2014, American Chemical Society.

chains and the latter as reptation of oriented chains. In the following, we focus on and discuss only the n-dependent region, and we refer to the "reptation of unoriented chains" as "reptation" for simplicity.

All the existing models based on the reptation concept, including the BRF model, predict the power law relationship between μ and n for an ideal chain as $\mu \sim n^{-\gamma}$ with $\gamma = 1$. However, as shown in Figure 13.22 (dotted lines), γ varied from 0.36 to 1.46 depending on systems. This discrepancy with the reptation models indicates that the simple reptation concept cannot predict the migration behavior of dsDNA in polymer networks.

On the other hand, focusing on relatively large dsDNA ($n = 20$–1000), we can clearly observe linear relationships between $\log_{10} \mu$ and ϕ, similar to the observation in the small molecular dsDNA (Figure 13.17). This agreement indicates that Eqs. (13.12) and (13.13) may thus be applicable to larger dsDNA.

13.5.2 Transition of the Migration Mechanism

We estimated μ_0 and K from the fit in the same way as in Section 13.4.2. Figure 13.23 shows the double-logarithmic plot of μ_0 as a function of n. In general, μ_0 decreased with increasing n. A clear difference between the PEG solution and Tetra-PEG gels was observed: μ_0 scales as $\mu_0 \sim n^{-0.17}$ in the PEG solution, while the scaling relationship changed from $\mu_0 \sim n^{-0.17}$ to $\mu_0 \sim n^{-0.81}$ in the Tetra-PEG gels. A crossover was observed at approximately $n = 200$–300 regardless of N_s. These data indicate that although permanent crosslinks are vital for this crossover, the mesh size, which is defined by N_s, does not influence the crossover. Notably, the crossover is close to the number of base pairs n_p ($n_p \approx 150$ bp) that corresponds to the persistence length of dsDNA.

The other parameter obtained from the fit in the same way as in Section 13.4.2 is K. Figure 13.24 displays the double-logarithmic plot of K as a function of n. K increased with increasing n and decreasing N_s. For each N_s, two different power law relationships ($K = \alpha n^{\beta}$) with a crossover at approximately n_p were observed. Notably, K in the range $n < n_p$ increased with decreasing N_s, while K in the range $n > n_p$ was a universal value (~0.3) regardless of N_s. Through these analyses, we

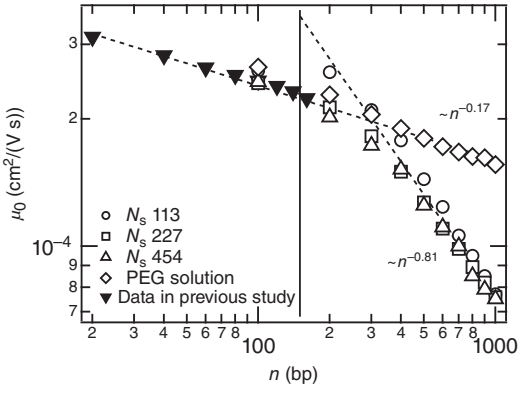

Figure 13.23 Double-logarithmic plot of μ_0 as a function of n. The dotted lines illustrate the fitting curves $\mu_0 \sim n^{-0.17}$ and $\mu_0 \sim n^{-0.81}$. The solid vertical line indicates the number of base pairs n_p ($n_p \approx 150$ bp) that corresponds to the persistence length of dsDNA. Source: Reproduced with permission from Li et al. [16]. Copyright 2014, American Chemical Society.

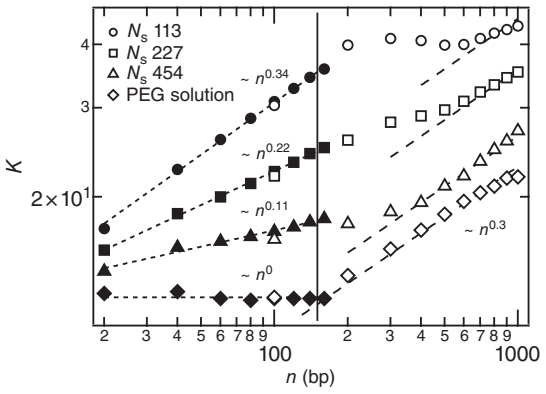

Figure 13.24 Double-logarithmic plot of K as a function of n. The dotted lines are the fitting curves $K = \alpha n^{\beta}$, where α and β are functions that depend on only N_s. The dashed lines indicate the guide $K = \alpha n^{0.3}$. The solid vertical line indicates n_p. The filled symbols are the data from a previous study [15]. Source: Reproduced with permission from Li et al. [16]. Copyright 2014, American Chemical Society.

obtained the following empirical equations for polymer solutions:

$$\mu = A_1 n^{-0.17} \exp(-12.7 n^0 \phi), \quad n < n_p \tag{13.15a}$$

$$\mu = A_1 n^{-0.17} \exp(-2.9 n^{0.3} \phi), \quad n > n_p \tag{13.15b}$$

and the following equations were obtained for gels:

$$\mu = A_1 n^{-0.17} \exp(-\alpha_1 n^{\beta_1} \phi), \quad n < n_p \tag{13.15c}$$

$$\mu = A_2 n^{-0.81} \exp(-\alpha_2 n^{0.3} \phi), \quad n > n_p \tag{13.15d}$$

where A_1 ($=5.4 \times 10^{-4}$) and A_2 ($=2.0 \times 10^{-2}$) are constants and α_1, α_2, and β_1 are functions that depend on only N_s.

Let us compare these empirical equations with the existing models for electrophoretic mobility. Considering the equation forms, we can roughly classify the existing models into two types based on either power law functions (the Rouse and reptation models; see Sections 6.2.2 and 6.3.4) or exponential functions (the Ogston and ET models; see Sections 6.3.1 and 6.3.5). Each of the empirical equations (Eqs. (13.15a)–(13.15d)) is neither a simple power law nor an exponential function but rather is a product of both. This observation strongly suggests that the migration of dsDNA in polymer networks involves the mechanisms of both types of models.

We will first focus on the power law terms in Eqs. (13.15a)–(13.15d). For migration in the gels, the power law term changed from $n^{-0.17}$ to $n^{-0.81}$ with a crossover at approximately n_p. The term $n^{-0.81}$ clearly corresponds to the reptation model ($\mu \sim n^{-0.8}$). In contrast, the term $n^{-0.17}$ is close to the prediction of the Rouse model ($\mu \sim n^0$). This similarity indicates that in gels, stiff chains ($n < n_p$) migrate via a Rouse-like manner, while semiflexible chains ($n < n_p$) migrate by reptation. Because the crossover is at approximately n_p, the flexibility of the chain is a key factor in reptation. Contrary to what was observed in the gels, in the polymer solutions, the power law term was always Rouse-like ($n^{-0.17}$) without a crossover. This result clearly indicates that reptation-type migration does not occur in polymer solutions under our experimental conditions. The presence of crosslinks is

another key factor for reptation; reptation may occur when crosslinks exist and the polymer chain is flexible enough to form the "reptation tubes."

Finally, we will focus on the exponential terms. The equations in the Ogston and ET models are derived by calculating the change in the number of states due to the geometric confinement of the network; both models are expressed as $\mu \sim \exp(\Delta S/k_B)$, where ΔS denotes the entropy loss and k_B represents the Boltzmann constant. Therefore, the exponential terms of Eqs. (13.15a)–(13.15d) may express entropy loss. In Eqs. (13.15a)–(13.15d), ΔS is proportional to ϕ regardless of n and N_s; the geometric confinement is proportional to the polymer volume fraction. However, the n-dependence of ΔS changed from $\Delta S \sim n^{\beta_1}$ to $\Delta S \sim n^{0.3}$ with a crossover at approximately n_p (Figure 13.24). This result indicates that the origin of the entropy loss changed drastically at approximately n_p.

For short and stiff dsDNA with $n < n_p$, the origin of the entropy loss may be an interaction of dsDNA with the mesh of the polymer network that is defined by N_s. As illustrated in Figure 13.24, the n-dependence of ΔS became weaker with increasing N_s and asymptotically approached the relationship of the PEG solution, for which $\Delta S \sim n^0$. In contrast, regarding the semiflexible dsDNA with $n > n_p$, ΔS had a constant scaling relationship with n ($\Delta S \sim n^{0.3}$) in both the gels and polymer solutions, indicating that the entropy loss does not originate from mesh–dsDNA interactions and might be due to the instantaneous conformational change of dsDNA that accompanies migration in polymer networks.

References

1 Fujiyabu, T., Li, X., Chung, U.I., and Sakai, T. (2019). Diffusion behavior of water molecules in hydrogels with controlled network structure. *Macromolecules* 52 (5): 1923–1929. https://doi.org/10.1021/acs.macromol.8b02488.

2 Stejskal, E.O. and Tanner, J.E. (1965). Spin diffusion measurements: spin echoes in the presence of a time-dependent field gradient. *J. Chem. Phys.* 42 (1): 288–292. https://doi.org/10.1063/1.1695690.

3 Tanner, J.E. and Stejskal, E.O. (1968). Restricted self-diffusion of protons in colloidal systems by the pulsed-gradient, spin-echo method. *J. Chem. Phys.* 49 (4): 1768–1777. https://doi.org/10.1063/1.1670306.

4 Le Feunteun, S. and Mariette, F. (2007). Impact of casein gel microstructure on self-diffusion coefficient of molecular probes measured by ^{1}H PFG-NMR. *J. Agric. Food. Chem.* 55 (26): 10764–10772. https://doi.org/10.1021/jf071982v.

5 Sakai, T., Katashima, T., Matsushita, T., and Chung, U.-i. (2016). Sol–gel transition behavior near critical concentration and connectivity. *Polym. J.* 48 (5): 629–634. https://doi.org/10.1038/pj.2015.124.

6 Amsden, B. (1998). Solute diffusion within hydrogels. Mechanisms and models. *Macromolecules* 31 (23): 8382–8395. https://doi.org/10.1021/ma980765f.

7 Zhang, Y. and Xu, Z. (1995). Atomic radii of noble gas elements in condensed phases. *Am. Mineral.* 80 (7–8): 670–675.

8 Tokita, M., Miyoshi, T., Takegoshi, K., and Hikichi, K. (1996). Probe diffusion in gels. *Phys. Rev. E* 53 (2): 1823–1827. https://doi.org/10.1103/PhysRevE.53.1823.

9 Brochard, F. and de Gennes, P.G. (1977). Dynamical scaling for polymers in theta solvents. *Macromolecules* 10 (5): 1157–1161. https://doi.org/10.1021/ma60059a048.

10 de Gennes, P.G. (1979). *Scaling Concepts in Polymer Physics*. Ithaca, NY: Cornell University Press.

11 Fujiyabu, T., Li, X., Shibayama, M. et al. (2017). Permeation of water through hydrogels with controlled network structure. *Macromolecules* 50 (23): 9411–9416. https://doi.org/10.1021/acs.macromol.7b01807.

12 Matsunaga, T., Sakai, T., Akagi, Y. et al. (2009). Structure characterization of tetra-PEG gel by small-angle neutron scattering. *Macromolecules* 42 (4): 1344–1351. https://doi.org/10.1021/ma802280n.

13 Nishi, K., Asai, H., Fujii, K. et al. (2014). Small-angle neutron scattering study on defect-controlled polymer networks. *Macromolecules* 47 (5): 1801–1809. https://doi.org/10.1021/ma402590n.

14 Matsunaga, T., Sakai, T., Akagi, Y. et al. (2009). SANS and SLS studies on tetra-arm PEG gels in as-prepared and swollen states. *Macromolecules* 42 (16): 6245–6252. https://doi.org/10.1021/ma901013q.

15 Li, X., Khairulina, K., Chung, U.-i., and Sakai, T. (2013). Migration behavior of rodlike dsDNA under electric field in homogeneous polymer networks. *Macromolecules* 46 (21): 8657–8663. https://doi.org/10.1021/ma401827g.

16 Li, X., Khairulina, K., Chung, U.-i., and Sakai, T. (2014). Electrophoretic mobility of double-stranded DNA in polymer solutions and gels with tuned structures. *Macromolecules* 47 (11): 3582–3586. https://doi.org/10.1021/ma500661r.

17 Khairulina, K., Chung, U.-i., and Sakai, T. (2017). New design of hydrogels with tuned electro-osmosis: a potential model system to understand electro-kinetic transport in biological tissues. *J. Mater. Chem. B* 5 (23): 4526–4534. https://doi.org/10.1039/c7tb00064b.

14

Osmotic Pressure

Takamasa Sakai

Graduate School of Engineering, The University of Tokyo, Tokyo, Japan

14.1 Osmotic Pressure of Gels and Prepolymer Solutions

Polymer gels have both solid-like and liquid-like nature, as demonstrated by the equation of state for polymer gels (Eq. (4.55)). The main factor representing their liquid-like nature is the osmotic pressure (Π_{os}) stemming from the enthalpy and entropy for configuration (Eq. (4.36)). We measured the osmotic pressure of the prepolymer solution and that of the gel by the deswelling method developed by Horkay et al. [1]. In this method, gels were equilibrated with aqueous poly(vinyl pyrrolidone) (PVP) solutions of known osmotic pressure. The swelling pressure ($\Pi_{sw} = \Pi_{os} - \Pi_{el}$) of the gel is estimated as the osmotic pressure of the outer PVP solution, in which the gel does not swell. Here, Π_{el} is elastic pressure. Figure 14.1 shows the osmotic pressure of the prepolymer solutions (open symbols) and gels (closed symbols) formed at different polymer concentrations (C) [2]. The prepolymer solution showed a crossover around c^*; the power-law relation changed from $\Pi_{os} \sim C^{1.3}$ to $\Pi_{os} \sim C^{2.0}$. These scalings correspond to those for the dilute and semidilute regions [3] (see Section 2.3.5), respectively. On the other hand, only a scaling $\Pi_{os} \sim C^{2.0}$ was observed in the gel regardless of C, suggesting that gel has a similarity with a semidilute solution. Notably, the Π_{os} of the gel is always lower than that of the prepolymer solution with the same C; i.e. Π_{os} decreases as the gelation reaction progresses.

14.2 Change in Osmotic Pressure During Gelation

To investigate the decrease in Π_{os} during the gelation process, we measured Π_{os} at different reaction conversions, i.e. connectivity (p) during the gelation process (Figure 14.2) [2]. At all C tested, Π_{os} showed a characteristic change with an increase in p; Π_{os} decreased with an increase in p in the sol region ($p < p_c$), while it became constant in the gel region ($p > p_c$). Here, p_c is the reaction conversion at the critical gelation point (gelation threshold). Given that the Π_{os} of the initial

Physics of Polymer Gels, First Edition. Edited by Takamasa Sakai.

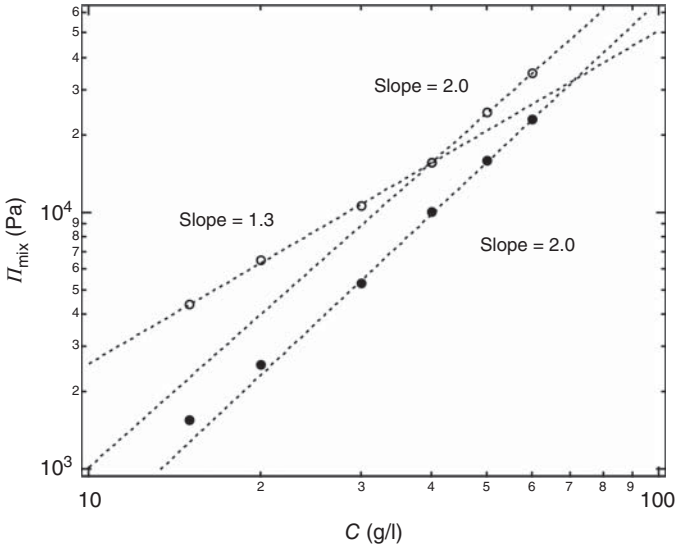

Figure 14.1 Polymer concentration (C)-dependence of the osmotic pressure (Π_{os}) in the prepolymer state (open circle) and the sol–gel critical state (filled circle). The dashed lines are the fitting curves based on the scaling rules.

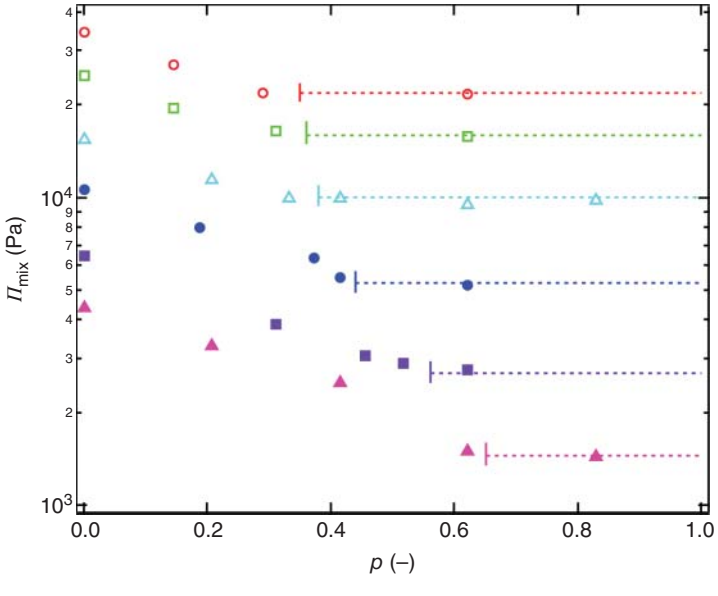

Figure 14.2 Connectivity (p)-dependence of the osmotic pressure (Π_{os}) for the Tetra-PEG gel with polymer concentrations of 60 g/l (open circle), 50 g/l (open square), 40 g/l (open triangle), 30 g/l (close circle), 20 g/l (close square), and 15 g/l (close triangle).

state obeys the van't Hoff's law at $C < c^*$, the decrease in Π_{os} is due to a decrease in the number of agglomerated polymers during gelation. Interestingly, no change in Π_{os} was observed at $p > p_c$; the gel has an identical osmotic pressure for each C obeying $\Pi_{os} \sim C^{2.0}$ (closed circles in Figure 14.1). The constant Π_{os} in the gel region suggests that crosslinking after the gelation threshold does not influence the concentration fluctuation of the polymer network (or blob size).

Here, it should be noted that Π_{os} reached the gel plateau at p_1 slightly below p_c; the Π_c of the gel is determined as the Π of a cluster solution at p_1. Here, we define the polymeric cluster at p_1 as the "critical cluster." To investigate the critical cluster, we apply the Bethe approximation from Flory [4] and Stockmayer [5] and estimate the average number of prepolymers included in a cluster (N). To apply this treatment, we convert the tetrafunctional gelation system to the equivalent virtual f-functional gelation system. In an f-functional system, N is represented as

$$N = \frac{1+p}{1-(f-1)p} \tag{14.1}$$

The gelation threshold ($p = p_c$) is defined as the point at which N diverges to infinity.

$$p_c = \frac{1}{(f-1)} \tag{14.2}$$

This equation predicted $p_c = 1/3$ for the tetrafunctional network, while the experimentally estimated p_c was higher than 1/3. This discrepancy suggests that the effective functionality (f_{eff}) in the real system is lower than 4. Thus, we estimate f_{eff} by substituting the experimentally estimated p_c into Eq. (14.2) and estimate N by substituting f_{eff} and p into Eq. (14.1). The estimated f_{eff} decreased with a decrease in C, reflecting the deviation from the ideal tetrafunctional system in the low C region (Figure 14.3).

Given that the osmotic pressure of the prepolymer solution ($C < c^*$) obeys the van't Hoff's law, the decrease in Π during gelation is most likely caused by the decrease in the number of clusters; thus, Π is expected to correlate with N. This expectation was validated by observing the master relationship between the normalized osmotic pressure (Π/Π_0) and N, $\Pi/\Pi_0 \sim N^{-0.25}$ [2]. This master relationship enables us to estimate the number of prepolymers included in the critical cluster N_c by the interpolation of $\Pi = \Pi_c$. The estimated (N_c) scaled with C/c^* as $N_c \sim (C/c^*)^{-2.0}$, indicating that the critical cluster grew more at lower C values. Because the osmotic pressure of the critical cluster solution obeys the scaling for a semidilute solution, the critical cluster is expected to fill the system even when the initial polymer concentration is lower than c^*. Indeed, the following simple discussion predicts the growth and subsequent space-filling by critical clusters.

14.3 *c** Theorem at the Gelation Threshold

Here, we consider an aggregation process in which particles (prepolymers) with a size (a) agglomerate with each other. Given that N particles agglomerate and form a cluster with a fractal dimension (D_f), the end-to-end distance of the cluster (R) is

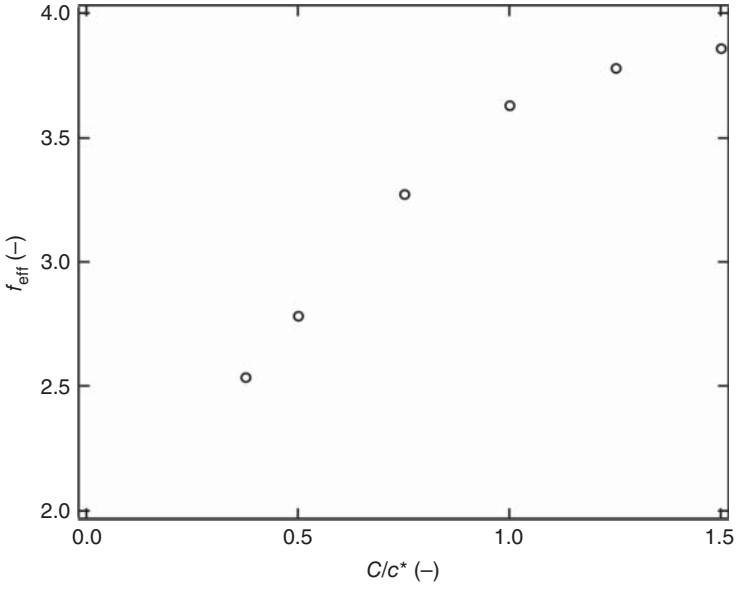

Figure 14.3 Effective functionality of the cluster (f_{eff}) as a function of normalized polymer concentration (C/c^*).

represented by $R \approx aN^{1/D_f}$ (see Section 1.2). Here, we define the expansion factor (ϵ) as the ratio of the volume of the cluster consisting of N particles to the sum of the volumes of the original N particles:

$$\epsilon = \frac{(aN^{1/D_f})^3}{a^3 N} = N^{(3-D_f)/D_f} \tag{14.3}$$

When one defines the volume fraction occupied by the original particles (Φ_0) and that occupied by the clusters formed by N particles (Φ_1), Eq. (14.3) is transformed to $\varepsilon = \Phi_1/\Phi_0$. Notably, Φ_0 is different from conventional polymer volume fraction, and indicates the occupancy by the envelope of the particles and clusters.The value of ε is larger than unity for $D_f < 3$ and increases with

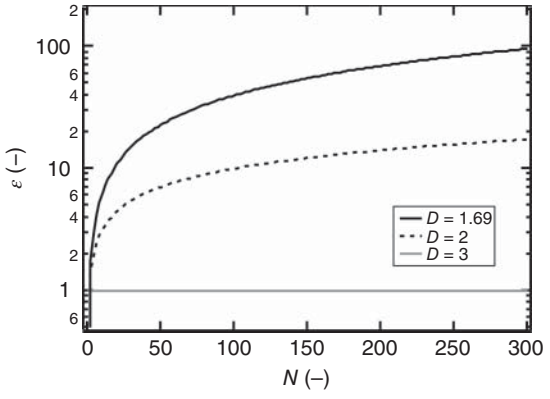

Figure 14.4 Relationship between the expansion factor and the number of particles in a cluster with different fractal dimensions.

an increase in N (Figure 14.4) [2]. Based on this equation, two clusters with volumes of V_1 and V_2 connect and form a cluster with $V_3 > V_1 + V_2$; the clusters anomalously grow during the aggregation process. When we accept this expansion, the cluster can fill the system during the gelation process, even if Φ_0 is not large enough to fill the system.

By substituting $D_f = 2.0$, which is measured in the small-angle neutron scattering (SANS) experiment [3], and $N_c \sim (C/c^*)^{-2.0}$ (estimated in Section 14.2) into Eq. (14.3), one obtains $\varepsilon = {N_c}^{1/2} = (C/c^*)^{-1.0}$. Given that the intramolecular polymer volume fraction inside the original prepolymer is ϕ^* (see Section 2.2.1), one obtains $\Phi_0 = C/c^*$. Finally, the following equation is achieved:

$$\Phi_1 \approx 1 \tag{14.4}$$

This equation indicates that the critical cluster just fills the system. This behavior was well reproduced by the molecular dynamics (MD) simulation [6–8].

Based on the results, the gelation process is transformed into a homogenization process. In the dilute region, monomer units constituting a prepolymer are localized inside the sparsely distributed prepolymer, and the local polymer concentration (c^*) is higher than the macroscopic polymer concentration (C). Each prepolymer behaves as a particle, showing the van't Hoff's law of osmotic pressure [9]. As the reaction proceeds, the agglomeration of the prepolymers decreases the number of particles, resulting in a decrease in the osmotic pressure. Subsequently, the volume occupied by clusters (Φ_1) increases. The clusters further grow, and below the gelation threshold, critical clusters fill the system ($\Phi_1 \approx 1$). Notably, further reaction did not change Π, suggesting the invariance in monomer distribution as the reaction proceeds; further reaction only connects the critical clusters and leads to percolation. This result can be rephrased as "*Polymer gels automatically maintain a concentration proportional to c* at the gelation threshold*." This statement is very similar to the popular c^* theorem proposed by de Gennes [10]. As discussed in Section 4.2.1, the original c^* theorem was proposed for predicting the equilibrium swelling, which was not correct. However, this statement is correct for the gelation threshold.

References

1 Horkay, F., Tasaki, I., and Basser, P.J. (2000). Osmotic swelling of polyacrylate hydrogels in physiological salt solutions. *Biomacromolecules* 1: 84–90.

2 Fujinaga, I., Yasuda, T., Asai, M. et al. (2019). Cluster growth from a dilute system in a percolation process. *Polym. J.*: https://doi.org/10.1038/s41428-019-0279-z.

3 Des Cloizeaux, J. and Noda, I. (1982). Osmotic pressure of long polymers in good solvents at moderate concentrations: a comparison between experiments and theory. *Macromolecules* 15: 1505–1507.

4 Flory, P.J. (1941). Molecular size distribution in three dimensional polymers. I. Gelation. *J. Am. Chem. Soc.* 63: 3083–3090.

5 Stockmayer, W.H. (1944). Theory of molecular size distribution and gel formation in branched polymers II. General cross linking. *J. Chem. Phys.* 12: 125–131.
6 Oh, C. and Sorensen, C.M. (1997). The effect of overlap between monomers on the determination of fractal cluster morphology. *J. Colloid Interface Sci.* 193: 17–25.
7 Sorensen, C.M. and Chakrabarti, A. (2011). The sol to gel transition in irreversible particulate systems. *Soft Matter* 7: 2284–2296.
8 Fry, D., Chakrabarti, A., Kim, W., and Sorensen, C.M. (2004). Structural crossover in dense irreversibly aggregating particulate systems. *Phys. Rev. E* 69: 061401.
9 Atkins, P. and de Paula, J. (2010). *Atkins' Physical Chemistry*. Oxford: OUP.
10 de Gennes, P.G. (1979). *Scaling Concepts in Polymer Physics*. Cornell University Press.

15

Swelling

Takamasa Sakai and Takeshi Fujiyabu

Graduate School of Engineering, The University of Tokyo, Tokyo, Japan

As discussed in Chapter 4, an as-prepared gel conventionally swells in the solvent that is used to prepare the gel. The pressure driving the swelling is the osmotic pressure, and the elastic pressure competes against the osmotic pressure, $\Pi_{sw} = \Pi_{mix} - \Pi_{el}$. As a result, after a certain degree of swelling, these pressures are balanced, achieving the equilibrium swollen state ($\Pi_{sw} = 0$ or $\Pi_{mix} = \Pi_{el}$, Eq. (4.28)). Here, we investigated the change in elastic modulus during the swelling and the condition for equilibrium swelling. Furthermore, we investigated the kinetics of swelling and discussed them based on the swelling equation (Eq. (4.78)).

15.1 Elastic Modulus of Swollen and Highly Deswollen Gels

As discussed in Section 4.1.2, a gel formed at an initial polymer volume fraction of ϕ_0 and swollen/deswollen to the polymer volume fraction of ϕ_m has a Young's modulus, E_m:

$$E_m \sim \frac{kT\phi_m}{N}\left(\frac{\lambda R_0}{R_{ref}}\right)^2 \tag{4.10′}$$

where k is the Boltzmann constant, T is the absolute temperature, N is the polymerization degree between crosslinks, λ is the uniaxial elongation ratio due to the volume change ($= (\phi_0/\phi_m)^{1/3}$), R_0 is the end-to-end distance of the network strand at ϕ_0, and R_{ref} is the end-to-end distance of the network strand at ϕ_m. To examine this model, we prepared Tetra-PEG gels at ϕ_0, partially swelled/deswelled them to ϕ_m, and measured E_m [1]. We focus on the normalized Young's modulus (E_m/E_0), where E_0 and E_m are the Young's moduli in the as-prepared and swollen/deswollen states, respectively. Given that $E_0 \sim kT\phi_0/N$

Physics of Polymer Gels, First Edition. Edited by Takamasa Sakai.

in the as-prepared state ($\phi_m = \phi_0$, $R_{ref} = R_0$, and $\lambda = 1$), the following equation is obtained [1–3]:

$$\frac{E_m}{E_0} = \frac{\phi_m}{\phi_0}\left(\frac{\lambda R_0}{R_{ref}}\right)^2 = \left(\frac{\phi_m}{\phi_0}\right)^{1/3}\left(\frac{R_0}{R_{ref}}\right)^2 \tag{15.1}$$

Assuming that R_0 and R_{ref} obey the scaling for the end-to-end distance of conventional polymers in solutions (Eqs. (4.12) and (4.13)), Eq. (15.1) predicts the following scalings: $E_m/E_0 \sim {\phi_m}^{0.33}$ below ϕ^* and $E_m/E_0 \sim {\phi_m}^{0.57}$ above ϕ^*.

On the other hand, highly deswollen gels, which are prepared around ϕ^* and deswollen to the concentrated region, show a different tendency from Eq. (15.1) due to their supercoiled structure (see Section 4.1.3). In the highly deswollen condition, pseudo-entanglements are formed, and the following relationship is obtained [4]:

$$\frac{E_m}{E_0} = \frac{\phi_m}{\phi_0}\left(\frac{\lambda R_0}{R_{ref}}\right)^2 = \left(\frac{\phi_m}{\phi_0}\right)^{1/3}\left(\frac{{\phi_0}^{(2\nu-1)/\{2\{1-3\nu\}\}}}{{\phi_m}^{\dfrac{(2\nu-1)}{\{2\{1-3\nu\}\}}+\dfrac{3}{7}\dfrac{1}{(2\nu-1)}}}\right)^2 \tag{15.2}$$

where ν is the exclusion volume index. Equation (15.2) is the generalized form of Eq. (4.27) and it predicts the scaling $E_m/E_0 \sim {\phi_m}^{1.1}$ above ϕ^{**} (see Section 4.1.2).

Figure 15.1 shows the E_m/E_0 of 20k Tetra-PEG gels ($\phi_0 = 0.034$ and 0.091) as a function of ϕ_m [1, 5, 6]. Triangles and circles denote the data of Tetra-PEG gels swollen in H_2O and 1-butyl-3-methylimidazolium tetrafluoroborate, respectively. All the ϕ_0 data are normalized by ϕ^* under each solvent condition. We fitted $\ln(E_m/E_0)$ vs. $\ln(\phi_m/\Phi_0)$ using two procedures: (i) fit with a power function for all data and (ii) fit with three power functions with slopes of 0.33, 0.57, and 1.1 for $\phi_m < \phi^*$, $\phi^* < \phi_m$, and $\phi^{**} < \phi_m$, respectively. Based on Pearson's correlation coefficients, the fits with the three power functions showed good correlation, suggesting that there were three regions with slopes of 0.33 (dotted-and-dashed line), 0.57 (solid line), and 1.1 (dashed line); i.e. crossovers around ϕ^* and ϕ^{**}

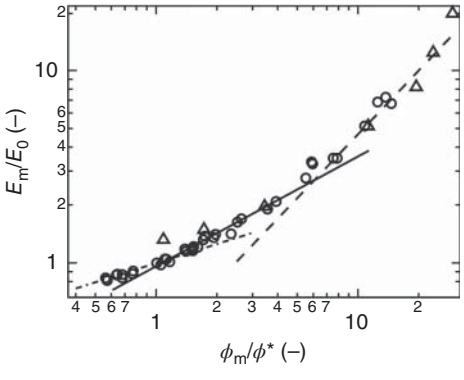

Figure 15.1 The ϕ_m-dependence of E_m/E_0 for Tetra-PEG gels prepared around the overlap concentration. Source: Reproduced with permission from Katashima et al. [5]. Copyright 2015, John Wiley and Sons.

were observed in Tetra-PEG gels. Notably, not only the data of swelling but also those of deswelling obey this relationship; crossover was observed at ϕ^* but was not observed between swelling and deswelling. Thus, we succeeded in examining the validity of these models from the dilute to the concentrated region.

15.2 Equilibrium Swelling

According to the criterion of Flory, the swelling equilibrium of polymer gels is achieved by minimization of the total free energy consisting of F_{mix} and F_{el} [7]:

$$\frac{\partial F_{\mathrm{el}}}{\partial \phi_{\mathrm{m}}} = \frac{\partial F_{\mathrm{mix}}}{\partial \phi_{\mathrm{m}}} \tag{4.28′}$$

In addition, in a semidilute good solvent system, F_{mix} scales with ϕ as

$$\frac{F_{\mathrm{mix}}}{k_{\mathrm{B}}T} \sim \phi^{\frac{3\nu}{3\nu-1}} \tag{2.63′}$$

Hence, one obtains the following relationship between the polymer fraction (ϕ_{s}) and the elastic modulus (E_{s}) in the equilibrium swollen state:

$$E_{\mathrm{s}} \sim \phi_{\mathrm{s}}^{\frac{3\nu}{3\nu-1}} \tag{4.32′}$$

Here, F_{mix} of polymer gels is assumed to obey the relationship for a semidilute solution, which has been confirmed in Chapter 14. In this section, we examined Eq. (4.32′) to validate Eq. (4.28′) and the form of F_{mix}.

Figure 15.2 shows E_{s} as a function of ϕ_{s} for 10k and 20k Tetra-PEG gels [1]. The data for the 10k and 20k Tetra-PEG gels fall onto a master curve showing $E_{\mathrm{s}} \sim \phi_{\mathrm{s}}^{2.3}$. By comparing the scaling exponent with Eq. (4.32′), we obtained $\nu = 0.59$. This value of ν was used to successfully reproduce the ϕ_{m}-dependence of

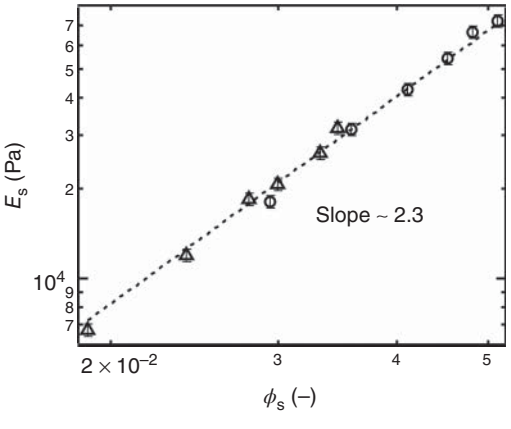

Figure 15.2 The ϕ_{s}-dependence of E_{s}. The circles and triangles represent the 10k Tetra-PEG gel and 20k Tetra-PEG gel, respectively. Source: Reproduced with permission from Sakai et al. [1]. Copyright 2012, Royal Society of Chemistry.

E_m/E_0 in Figure 15.1. In addition, this value is similar to that of a Flory chain (0.59) and that obtained for PEG by other researchers [8–10]. These results strongly suggest the validity of Eq. (4.28′) and the form of F_{mix}. It should be noted that $\phi_s^{2.3}$, which characterizes the equilibrium swelling condition, changes with the initial condition. This ϕ_0-dependence cannot be predicted by the popular c^* theorem of de Gennes; *the gel automatically maintains a concentration c proportional to* c^* [11]. The equilibrium swelling is predicted by Flory's criterion (Eq. (4.28)), not by the c^* theorem.

Here, we discussed the elastic and mixing part of free energy and achieved the equilibrium swelling by balancing these energies. The elastic part of free energy is governed by the elastically effective chains, which are characterized by the architecture, concentration at preparation, and concentration at measurement of the polymer network. On the other hand, the mixing part of free energy of polymer gel is determined only by the polymer concentration at measurement, not by any properties of the prepolymer (see Section 2.2.3 and Chapter 14).

15.3 Swelling Kinetics

15.3.1 Examination of Swelling Equation

As discussed in Section 4.4, the swelling kinetics of a gel are governed by the swelling equation (Eq. (4.66)) that describes the diffusion of a polymer network to the outer solution [12]. By applying the initial condition and the boundary condition to the swelling equation, we obtain an equation that describes the change in the volume of a gel (Eq. (4.94)) [13]. To examine the validity of the swelling equation, we conducted a swelling experiment [14]. The swelling behavior of Tetra-PEG gels with different ϕ_0 values is shown in Figure 15.3. The experimental results were well reproduced by Eq. (4.94) (dotted lines),

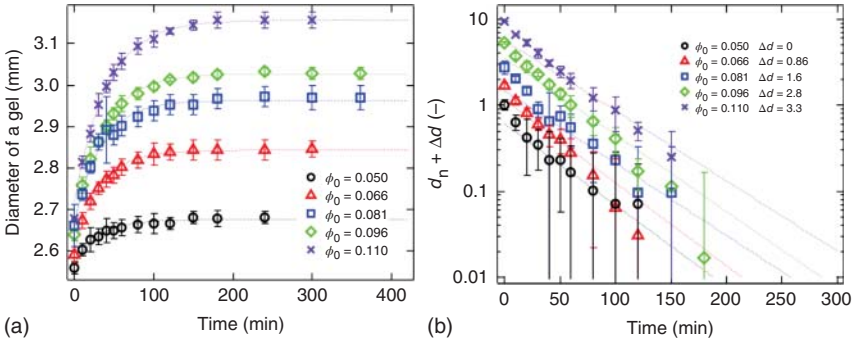

Figure 15.3 (a) Typical swelling curves of 10k Tetra-PEG gels with different ϕ_0 and (b) typical time courses of the normalized diameter of a gel (d_n) during the swelling experiments for 10k Tetra-PEG gels with different ϕ_0. Source: Reproduced with permission from Fujiyabu et al. [14]. Copyright 2018, Royal Society of Chemistry.

suggesting the validity of the swelling equation. This result corresponds to the results of a vast number of previous studies, thereby qualitatively confirming the validity of the swelling equation [13].

15.3.2 Cooperative Diffusion Coefficient

The swelling equation suggests that the dynamics of the polymer network are represented by the cooperative diffusion coefficient (D_c, Eq. (4.79)). The value of D_c can be estimated by three independent methods: the definition of D_c with K, G, and f (D_w, Eq. (4.79)), a swelling experiment with Eq. (4.92) (D_{sw}), and a dynamic light scattering (DLS) experiment (D_{DLS}) [15]. We estimated these three D_c values of Tetra-PEG gels with different molecular weights between crosslinks (M_w) and initial polymer volume fractions (ϕ_0) and compared them [14]. In Figure 15.4a, D_w, D_{sw}, and D_{DLS} are plotted against the initial polymer volume fraction (ϕ_0). These three diffusion coefficients were divided into two types: M_w-dependent D_w and ϕ_0-dependent D_{sw} and D_{DLS}. Theoretically, the cooperative diffusion of a polymer network is considered as the diffusion of blobs (Eq. (4.95)). Because the blob size (ξ) depends on only ϕ_0 (see Section 2.2.3), conceptually, D_c also depends on only ϕ_0. Therefore, the ϕ_0-dependence and M_w-independence of D_{sw} and D_{DLS} roughly agreed with the concept of D_c.

To further discuss the similarity between D_{sw} and D_{DLS}, we plotted D_{sw}/D_{DLS} against ϕ_0 in Figure 15.4b. As shown in Figure 15.4b, D_{sw}/D_{DLS} was nearly constant (≈0.64) over the whole experimental range, suggesting that D_{sw} corresponds to D_{DLS}. In other words, the macroscopic swelling behavior (represented by D_{sw}) is governed by the microscopic fluctuation of the polymer network (represented by D_{DLS}). The difference in absolute values between D_{sw} and D_{DLS} may stem from the following three points. The first is the difference in the motions described by

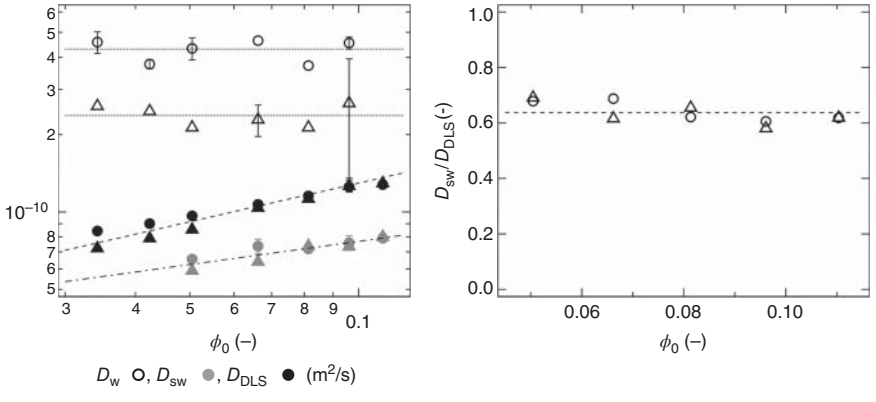

Figure 15.4 (a) The ϕ_0-dependences of D_w (white symbols), D_{DLS} (black symbols), and D_{sw} (gray symbols) of 10k (circles) and 20k (squares) Tetra-PEG gels. (b) The ϕ_0-dependence of D_{sw}/D_{DLS} of Tetra-PEG gels with different M_w values (M_w: 10 kg/mol, circle; 20 kg/mol, triangle). Source: Reproduced with permission from Fujiyabu et al. [14]. Copyright 2018, Royal Society of Chemistry.

D_{sw} and D_{DLS}; D_{sw} describes translational diffusion, while D_{DLS} describes thermal fluctuation. The second is the possible inapplicability of Eqs. (4.92) and (4.94) due to the larger swelling ratio (Q) of Tetra-PEG gels ($Q \approx 1.1–2.1$) than those of gels in previous studies ($Q \approx 1.2$) [13]. The third is the decrease in polymer volume fraction (ϕ) during the swelling. Based on Figure 15.4, one can expect that D_{sw} decreases with a decrease in ϕ and that the observed D_{sw} is smaller than the D_{sw} of the gel in the as-prepared state.

References

1 Sakai, T., Kurakazu, M., Akagi, Y. et al. (2012). Effect of swelling and deswelling on the elasticity of polymer networks in the dilute to semi-dilute region. *Soft Matter* 8 (9): 2730–2736.

2 Panyukov, S.V. (1990). Scaling theory of high elasticity. *Zh. Eksp. Teor. Fiz.* 98: 668–680.

3 James, H.M. and Guth, E. (1953). Statistical thermodynamics of rubber elasticity. *J. Chem. Phys.* 21 (6): 1039–1049.

4 Obukhov, S.P., Rubinstein, M., and Macromolecules, R.C. (1994). *Network Modulus and Superelasticity*. ACS Publications.

5 Katashima, T., Chung, U.-i., and Sakai, T. (2015). Effect of swelling and deswelling on mechanical properties of polymer gels. *Macromol. Symp.* 358 (1): 128–139.

6 Katashima, T., Asai, M., Urayama, K. et al. (2014). Mechanical properties of tetra-PEG gels with supercoiled network structure. *J. Chem. Phys.* 140 (7): 134906.

7 Flory, P.J. (1953). *Principles of Polymer Chemistry*. Ithaca, NY: Cornell University Press.

8 Gregory, P. and Huglin, M.B. (1986). Viscosity of aqueous and alkaline solutions of poly(ethylene oxide). *Makromol. Chem.* 187 (7): 1745–1755.

9 Hild, G., Okasha, R., Macret, M., and Gnanou, Y. (1986). Relationship between elastic modulus and volume swelling degree of polymer networks swollen to equilibrium in good diluents, 4. Interpretation of experimental results on the basis of scaling concepts. *Makromol. Chem.* 187 (9): 2271–2288.

10 Zrinyi, M. and Horkay, F. (1987). On the elastic modulus of swollen gels. *Polymer* 28 (7): 1139–1143.

11 de Gennes, P.G. (1979). *Scaling Concepts in Polymer Physics*. Ithaca, NY: Cornell University Press.

12 Tanaka, T., Hocker, L.O., and Benedek, G.B. (1973). Spectrum of light scattered from a viscoelastic gel. *J. Chem. Phys.* 59 (9): 5151–5159.

13 Tanaka, T. and Fillmore, D.J. (1979). Kinetics of swelling of gels. *J. Chem. Phys.* 70 (3): 1214–1218.
14 Fujiyabu, T., Toni, F., Li, X. et al. (2018). Three cooperative diffusion coefficients describing dynamics of polymer gels. *Chem. Commun.* 54 (50): 6784–6787.
15 Mitsuhiro, S. and Tomohisa, N. (2002). Gel formation analyses by dynamic light scattering. *Bull. Chem. Soc. Jpn.* 75 (4): 641–659.

16

Degradation

Takamasa Sakai and Takeshi Fujiyabu

Graduate School of Engineering, The University of Tokyo, Tokyo, Japan

Hydrogels inevitably degrade with time under practical conditions and in the environment. For example, a hydrogel implanted into a living organism suffers from oxidative stress, leading to degradation [1, 2]. In some bioapplications, such as scaffolds and carriers for drug delivery, implanted hydrogels should be disintegrated and released from the body after treatment. Therefore, controlling the degradation behavior of hydrogels is vital. In this chapter, we discuss two topics related to the degradation of polymer gels. One is the investigation of the degradation behavior of polymer gels caused by the cleavage of a specific unit in the network strand [3]. This investigation enables fine control and precise prediction of the disintegration time. The other is the investigation of the degradation behavior of polymer gels caused by nonspecific cleavage of monomeric units in network strands, which contributes to the understanding of the long-term stability of polymer gels [1]. A part of modeling has been discussed in Section 4.5, and this chapter is also strongly related to Chapters 15 and 17.

16.1 Cleavage of a Specific Site

Conventional Tetra-PEG gels consist of stable C–C, ether, amide, and maleimide–thiol linkages; thus, they are stable in physiological pH at 37 °C for more than two months and keep their shape more than one year in the eyes of rabbits [2, 3]. Here, in addition to the conventional two Tetra-PEG units (Tetra-PEG–OSu and Tetra-PEG–NH_2), we designed a cleavable Tetra-PEG unit containing a cleavable ester linkage upstream of each terminal activated ester group (Tetra-PEG-deg–OSu, Figure 16.1c) [3]. Tetra-PEG-deg–OSu reacts with Tetra-PEG–NH_2 to form an amide bond in the same manner as Tetra-PEG–OSu (Figure 16.1b); the only difference is the concurrent installation of one cleavable site in each network strand (Figure 16.1a). This design enabled us to control degradability by simply changing the ratio of Tetra-PEG–OSu to Tetra-PEG-deg–OSu.

We formed Tetra-PEG gels by mixing three kinds of Tetra-PEG units, i.e. Tetra-PEG–NH_2, Tetra-PEG-deg–OSu, and Tetra-PEG–OSu, at a 1 to r_{deg} to

Physics of Polymer Gels, First Edition. Edited by Takamasa Sakai.

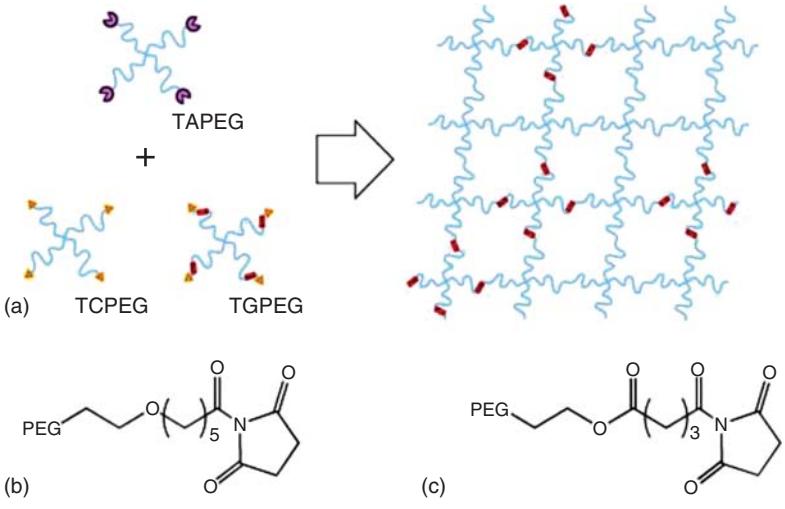

Figure 16.1 (a) Design of a degradability-tunable Tetra-PEG gel. The end-group structures of Tetra-PEG–OSu (b) and Tetra-PEG-deg–OSu (c). Tetra-PEG-deg–OSu introduced a cleavable carbonyl site (shown as a square) into the network structure. Source: Reproduced with permission from Li et al. [3]. Copyright 2011, American Chemical Society.

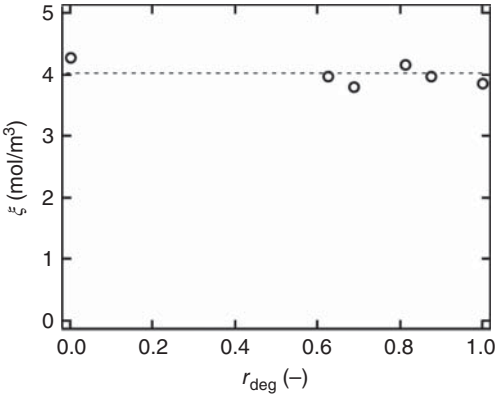

Figure 16.2 The cycle rank (ξ) of Tetra-PEG gels having different degradable unit fractions (r_{deg}). Source: Reproduced with permission from Li et al. [3]. Copyright 2011, American Chemical Society.

$(1 - r_{deg})$ ratio (Figure 16.1) [3]. To investigate the effect of r_{deg} on network formation, we measured the elastic moduli (G) of Tetra-PEG gels with different r_{deg} values. Here, we apply the phantom network model and estimate the mole density of cycle rank (ξ) from G based on Eq. (3.35). Figure 16.2 shows ξ as a function of r_{deg}. The values of ξ were almost constant, suggesting that r_{deg} does not affect network formation. In other words, Tetra-PEG–OSu and Tetra-PEG-deg–OSu have practically the same reactivity with Tetra-PEG–NH_2, and the obtained hydrogels have similar network architectures except for the presence of cleavable sites.

We investigated the degradation behavior of the hydrogels in phosphate buffer (pH 7.4) at 37 °C. The time evolution of the swelling ratio (Q), which is the ratio of the gel volume at time t to that in the as-prepared state, with various r_{deg} values

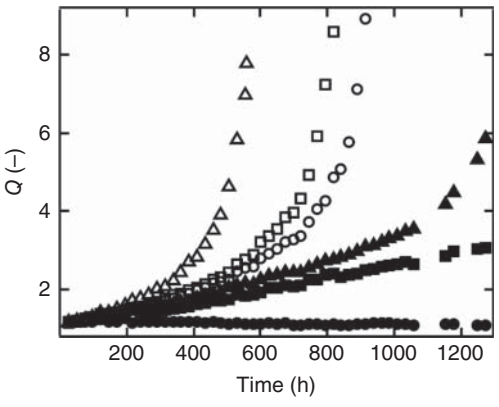

Figure 16.3 The time course of the swelling ratio (Q) of Tetra-PEG gels with different r_{deg} values. Closed circle, $r_{deg} = 0$; closed square, $r_{deg} = 0.63$; closed triangle, $r_{deg} = 0.69$; open circle, $r_{deg} = 0.81$; open square, $r_{deg} = 0.88$; and open triangle, $r_{deg} = 1.0$. Gels swelled with degradation, showing bulk degradation behavior. Source: Reproduced with permission from Li et al. [3]. Copyright 2011, American Chemical Society.

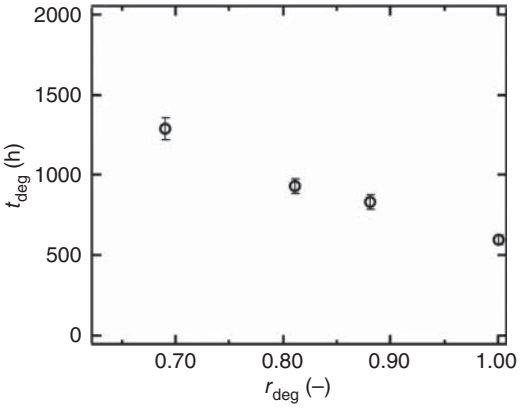

Figure 16.4 The degradation time (t_{deg}) as a function of r_{deg}. Degradation was accelerated by introducing a degradable Tetra-PEG unit. Source: Reproduced with permission from Li et al. [3]. Copyright 2011, American Chemical Society.

is shown in Figure 16.3. Notably, the size of the gel specimen is small enough to maintain the following condition: rate of degradation $\ll$ rate of swelling (see Section 4.4). Under this condition, we can consider the measured swelling ratio as the equilibrium swelling ratio at t. The gel samples ($r_{deg} \geq 0.69$) swelled with time and finally disintegrated, showing bulk degradation behavior. The disintegration time (t_{deg}) was determined as the point at which no gel could be observed. As shown in Figure 16.4, t_{deg} shortened with an increase in r_{deg}. The swelling ratio of a Tetra-PEG gel with no ester bond ($r_{deg} = 0$) was constant for more than 50 days, reflecting that neither Tetra-PEG–OSu nor Tetra-PEG–NH_2 has readily cleavable bonds.

The degradation process is quantitatively discussed based on the decrease in the number density of cycle rank ξ with time t. According to the Flory–Rehner equation with the phantom model [4], ξ is related to Q by

$$\xi = -\frac{\frac{\phi_0}{Q} + \ln\left(1 - \frac{\phi_0}{Q}\right) + \chi\left(\frac{\phi_0}{Q}\right)^2}{V_1 Q^{1/3}} \tag{4.98}$$

The value of χ was estimated to be 0.45 from the values of ξ and Q for the Tetra-PEG gel ($r_{deg} = 0$). This value corresponded well to the values estimated

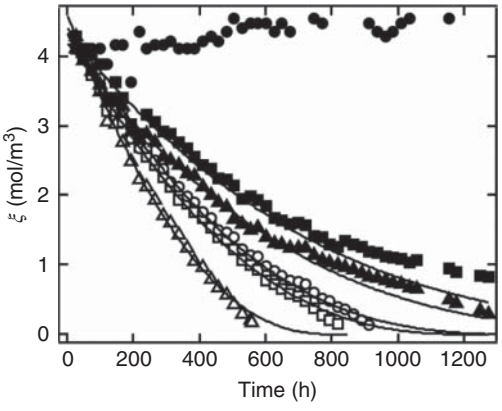

Figure 16.5 The variation in cycle rank (ξ) of Tetra-PEG gels having different degradable Tetra-PEG fractions (r_{deg}). The symbols correspond to the same samples as those in Figure 16.3. Source: Reproduced with permission from Li et al. [3]. Copyright 2011, American Chemical Society.

by other authors [5, 6]. Using Eq. (4.98), we can estimate the degradation of ξ (Figure 16.5) from the time course of Q. Importantly, the range of fit with Eq. (4.98) must be restricted in the high ξ region because the sol fraction dissociated from the gel decreases the osmotic pressure under the highly degraded condition (see Section 4.5.1).

We fit the results in Figure 16.5 with Eq. (4.98) and estimated k_{deg} by the least-squares method. Equation (4.98) successfully reproduced the results for all samples (solid lines); the slight upward deviation of the points was attributed to the dissociation of the sol mentioned earlier. As theoretically expected, the values of k_{deg} were almost constant ($\approx 9.76 \times 10^{-4}$ h^{-1}) regardless of r_{deg}, confirming the validity of our model. Because the degradation behavior of Tetra-PEG gels is successfully modeled with the parameter k_{deg}, we can now reproduce the time course of the connectivity (p). The time course of p was estimated using Eq. (4.96) for each r_{deg}. We then estimated the connectivity at degradation (p_c) by substituting the experimentally observed t_{deg} values into Eq. (4.96). As shown in Figure 16.6, all gel samples had identical values of p_c ($p_c = 0.46$); i.e. all gel samples sustained their 3D continuous structure above p_c and then immediately dissociated into soluble clusters below p_c. This value is slightly larger than the gelation threshold estimated in the gelation process (Chapter 8). This slight discrepancy is due to the limitation of the modeling based on the Flory–Rehner

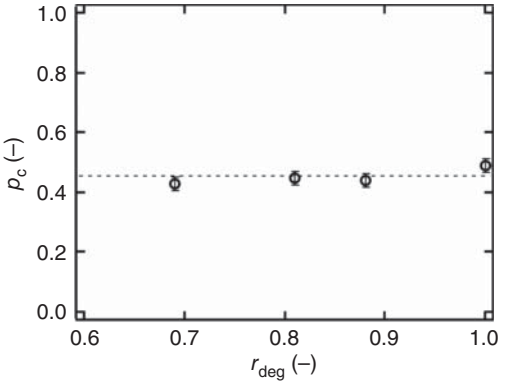

Figure 16.6 The fraction of connected bonds at degradation (p_c) as a function of r_{deg}. As theoretically predicted, p_c does not depend on r_{deg}. Source: Reproduced with permission from Li et al. [3]. Copyright 2011, American Chemical Society.

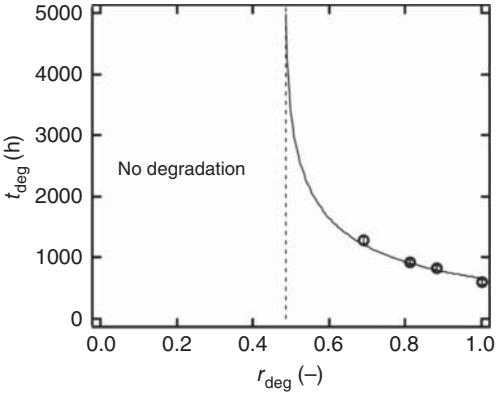

Figure 16.7 Experimental data (symbols) and prediction of Eq. (16.1) for disintegration time (t_{deg}) as a function of r_{deg}. The experimental results are well reproduced by the model. Source: Reproduced with permission from Li et al. [3]. Copyright 2011, American Chemical Society.

equation. In the other detailed measurements, we confirmed the identity of the gelation and reverse-gelation thresholds.

Although the value of p_c is different from the correct value in a strict sense, the value is useful for this modeling. By substituting $p = p_c$ into Eq. (4.96), we can derive the equation predicting the disintegration time of a degradable Tetra-PEG gel.

$$t_{deg} = \frac{1}{k_{deg}} \ln\left\{\frac{r_{deg}}{\frac{p_c}{p_0} - (1 - r_{deg})}\right\} \tag{16.1}$$

The prediction of Eq. (16.1) and experimental data for t_{deg} are shown in Figure 16.7. Our model succeeded in reproducing the degradation behavior of a Tetra-PEG gel. Notably, this modeling is based on simple assumptions: the phantom network model for elasticity, the Flory–Rehner model for equilibrium swelling, and first-order kinetics for bond cleavage [4, 7]. As discussed in Section 3.4.1, the elastic modulus has a roughly linear relationship with p (the percolation network model); thus, we can also use a linear assumption for elasticity. Because the other two assumptions are most likely valid for most systems, this modeling can also be applied to other degrading polymer gels.

16.2 Cleavage of Nonspecific Sites

Even when a polymer network does not have apparent cleavable bonds, the polymer gel inevitably degrades on a long-term basis because of "nonspecific cleavage" (see Section 4.5.2). Nonspecific cleavage of the polymer chain is caused by common stimuli in practical applications, such as oxidation *in vivo*, UV irradiation exposure, and mechanical stress [8–10]. Based on the model discussed in Section 4.5.2, the degradation process is accelerated with an increase in the network strand length. Here, we systematically investigated the degradation behavior of gels with tuned network strand lengths. To investigate the long-term stability, accelerated tests using H_2O_2 solution were performed

at different temperatures. The model well reproduced the experimental data [1], and the estimated degradation rate constants obeyed transition state theory, indicating the validity of our modeling [11].

16.2.1 Initial Swelling Equilibrium

The polymer volume fraction of gel specimens in the as-prepared state (ϕ_0) was set around the overlap polymer volume fraction, where the elastic moduli well obey the phantom network model [7]. The cycle rank density of gels in the as-prepared state (ξ_0) was estimated according to the phantom network model. We then measured the equilibrium-swelling ratio of the gel specimens (Q_e) in a 30 w/w% H_2O_2 aqueous solution at different temperature $T = 60$, 64, 70, and 80 °C (Figure 16.9). The H_2O_2 solution was used to accelerate the degradation rate. Here, the swelling ratio of gels is defined as the volume ratio of gels in the measurement state to that in the as-prepared state. Q_e values were calculated as the average values of the swelling ratio of the gel specimens in the period $t = 15$–30 minutes, where the temperature-induced volume change of the gel specimen was completed and the degradation-induced volume change was negligible. As expected from the lower critical solution temperature (LCST) behavior of PEG, Q_e decreased with increasing T [12]. According to the Flory–Rehner equation (Eq. (4.98)) [4], the Flory interaction parameter (χ) was estimated from the parameters ξ_0, ϕ_0, and ϕ_e, which is the polymer volume fraction of the gel in the equilibrium-swelling state. As shown in Figure 16.8, χ increased with increasing T and with decreasing N. The former trend reflects the decrease in Q_e with the increase in T. The latter trend qualitatively corresponds to the results of our previous study [13] and has been reported in another study as well [14]. The obtained values of χ were used as a fixed parameter for each experimental condition in the following analysis.

16.2.2 Degradation Behavior of Tetra-PEG Gels

Figure 16.9 shows the time course of the swelling ratio of Tetra-PEG gels during degradation ($Q(t)$) in H_2O_2 solution at different T. $Q(t)$ decreased slightly at the beginning ($t < 15$ minutes) and then increased over time. Ultimately, all specimens were disintegrated and dissolved into the solution. The initial decrease in

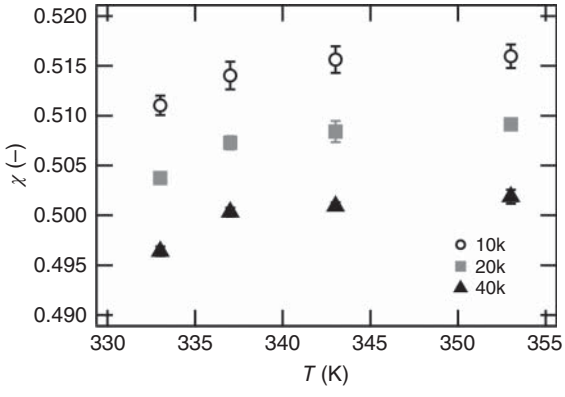

Figure 16.8 The Flory interaction parameter (χ) of different gel samples as a function of temperature (T). Error bars smaller than the symbols are hidden behind the symbols. Source: Reproduced with permission from Li et al. [1]. Copyright 2014, American Chemical Society.

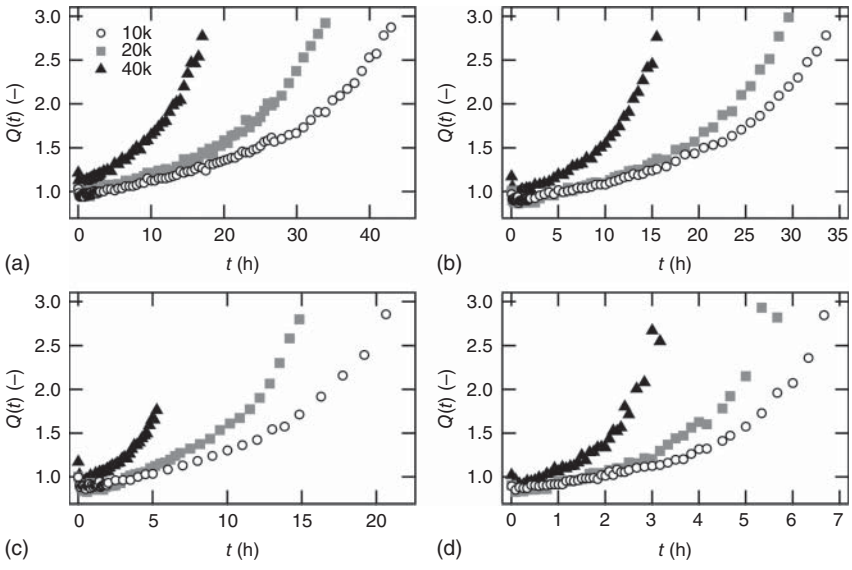

Figure 16.9 Time (t) course of the swelling ratio of Tetra-PEG gels during degradation ($Q(t)$) in H_2O_2 solution at predetermined T. (a) 60 °C, (b) 64 °C, (c) 70 °C, and (d) 80 °C. Source: Reproduced with permission from Li et al. [1]. Copyright 2014, American Chemical Society.

$Q(t)$ was caused by the volume change induced by the temperature change from room temperature to the predetermined temperatures (T: 60–80 °C), which was equilibrated within 15 minutes. We ignored these points in the following analyses because these points were irrelevant to the degradation behavior. The subsequent increase in $Q(t)$ indicates the progress of bulk degradation over time. We set the experimental conditions so that the swelling rate is much faster than the degradation rate. Under this condition, we can treat $Q(t)$ as the swelling ratio in the equilibrium-swelling state at a certain time t and estimate $\xi(t)$ from $Q(t)$, ϕ_0, and χ, according to Eq. (4.98). Figure 16.10 shows the estimated time course of $\xi(t)$. $\xi(t)$ decreased over time, reflecting the cleavage of the network strands.

16.2.3 A Model for Degradation

The network strands of the polymer network of Tetra-PEG gels consist of three different kinds of chemical units: carbon–carbon bonds, ether bonds, and amide bonds. Among these bonds, the ether bonds and amide bonds may be readily cleaved in H_2O_2 solution by oxidation and/or hydrolysis. Because the molar amount of H_2O_2 was much larger (10^5 times) than the total molar amount of ether and amide bonds, we can neglect the consumption of H_2O_2 accompanying the degradation of the gels and apply pseudo-first-order kinetics for the cleavage of the network strands. According to pseudo-first-order kinetics, the possibilities that an ether (p_{ether}) or an amide (p_{amide}) bond still exists after a time period can be expressed as

$$p_{\mathrm{ether}} = \exp(-k_{\mathrm{ether}}t) \tag{16.2}$$

$$p_{\mathrm{amide}} = \exp(-k_{\mathrm{amide}}t) \tag{16.3}$$

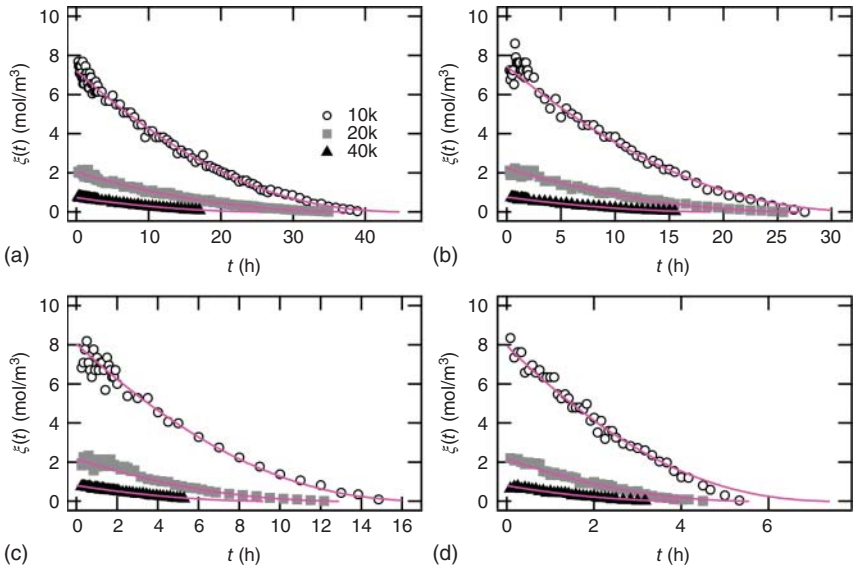

Figure 16.10 Time course of the cycle rank density of degrading gels ($\xi(t)$) in H_2O_2 solution at predetermined T. The solid curves show the fitting curves with Eq. (4.97′). (a) 60 °C, (b) 64 °C, (c) 70 °C, and (d) 80 °C. Source: Reproduced with permission from Li et al. [1]. Copyright 2014, American Chemical Society.

where k_{ether} and k_{amide} are the degradation rate constants of an ether and an amide, respectively. Because each network strand has one amide bonds and N ether bonds, the probability that a network strand still connects neighboring crosslinks after a time period ($p(t)$) is given by

$$p(t) = p_0(p_{\text{amide}}(t)(p_{ether}(t))^N) = p_0 \exp[-[k_{\text{amide}} + Nk_{\text{ether}}]t] \tag{16.4}$$

where p_0 is the fraction of connected arms (or reaction conversion) in the as-prepared state. p is related to $\xi(t)$ by the Bethe approximation as Eq. (4.97):

$$\xi(t) = U\left(\frac{1}{2} + \left(\frac{1}{p} - \frac{3}{4}\right)^{1/2}\right)\left(\frac{3}{2} - \left(\frac{1}{p} - \frac{3}{4}\right)^{1/2}\right)^3 \tag{4.97'}$$

where U is the molar concentration of tetra-arm prepolymers in the as-prepared state. According to Eqs. (16.4) and (4.97′) we finally obtain $\xi(t)$ as follows:

$$\xi(t) = U\left[\frac{1}{2} + \left[\frac{1}{p_0 \exp\left[-k_{app}t\right]} - \frac{3}{4}\right]^{1/2}\right]\left[\frac{3}{2} - \left[\frac{1}{p_0 \exp\left[-k_{app}t\right]} - \frac{3}{4}\right]^{1/2}\right]^3 \tag{16.5}$$

$$k_{\text{app}} = k_{\text{amide}} + Nk_{\text{ether}} \tag{16.6}$$

where k_{app} is the apparent degradation rate constant of a network strand.

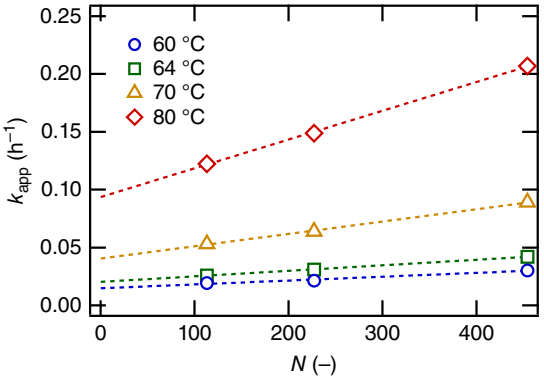

Figure 16.11 k_{app} as a function of N at different T. Source: Reproduced with permission from Li et al. [1]. Copyright 2014, American Chemical Society.

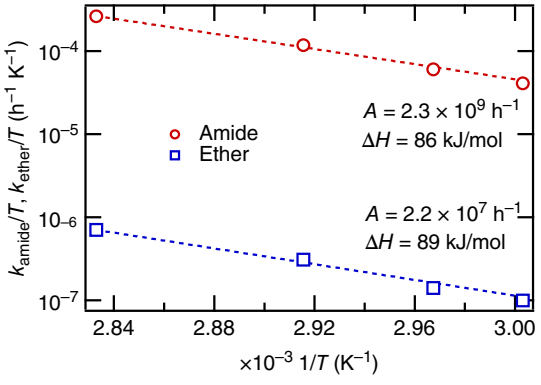

Figure 16.12 Semilogarithmic plots of k_{ether}/T and k_{amide}/T as a function of $1/T$. The dotted lines show the fitting curves of $k/T = A\exp(-\Delta H/RT)$. Source: Reproduced with permission from Li et al. [1]. Copyright 2014, American Chemical Society.

16.2.4 Estimation of Degradation Rate Constants

We fit the data in Figure 16.10 with Eq. (16.5) in the range where $\xi(t)$ is larger than half of $\xi(0)$. k_{app} and p_0 were set as the fitting parameters. The estimated p_0 values were in the range of ±2% error from the p_0 values that were directly measured by IR spectroscopy [15]. Figure 16.11 shows the estimated k_{app} plotted against N. k_{app} linearly increased with increasing N, which agrees well with Eq. (16.6). According to the equation, we estimated k_{amide} and k_{ether} from the intercepts and the slopes in Figure 16.11, respectively.

Figure 16.12 shows a semilogarithmic plot of k_{amide}/T and k_{ether}/T against $1/T$. A linear relationship was observed for both k_{amide} and k_{ether}, indicating that both follow transition state theory

$$k \sim \frac{1}{T}\exp\left(\frac{\Delta S^*}{R}\right)\exp\left(-\frac{\Delta H^*}{RT}\right) \tag{16.7}$$

where k is the reaction rate constant, ΔS^* is the activation entropy, ΔH^* is the activation enthalpy, and R is the gas constant [11]. The estimated ΔH^* values of an amide bond (~86 kJ/mol) and an ether bond (~89 kJ/mol) were comparable to the ΔH^* values estimated in previous studies [10, 16], supporting the validity of our analyses. Thus, we can also predict the time of disintegration caused by the nonspecific cleavage of strands, which is similar to that caused by the cleavage of a specific site (Eq. (16.1)).

References

1 Li, X., Kondo, S., Chung, U.-i., and Sakai, T. (2014). Degradation behavior of polymer gels caused by nonspecific cleavages of network strands. *Chem. Mater.* 26 (18): 5352–5357. https://doi.org/10.1021/cm502480f.

2 Hayashi, K., Okamoto, F., Hoshi, S. et al. (2017). Fast-forming hydrogel with ultralow polymeric content as an artificial vitreous body. *Nat. Biomed. Eng.* 1 (3): 1–7. https://doi.org/10.1038/s41551-017-0044.

3 Li, X., Tsutsui, Y., Matsunaga, T. et al. (2011). Precise control and prediction of hydrogel degradation behavior. *Macromolecules* 44 (9): 3567–3571. https://doi.org/10.1021/ma2004234.

4 Flory, P.J. (1953). *Principles of Polymer Chemistry*. Ithaca/London: Cornell University Press.

5 Metters, A. and Hubbell, J. (2005). Network formation and degradation behavior of hydrogels formed by Michael-type addition reactions. *Biomacromolecules* 6 (1): 290–301. https://doi.org/10.1021/bm049607o.

6 Mikos, A.G. and Peppas, N.A. (1988). Flory interaction parameter χ for hydrophilic copolymers with water. *Biomaterials* 9 (5): 419–423. https://doi.org/10.1016/0142-9612(88)90006-3.

7 James, H.M. and Guth, E. (1953). Statistical thermodynamics of rubber elasticity. *J. Chem. Phys.* 21 (6): 1039–1049. https://doi.org/10.1063/1.1699106.

8 Uchiyama, T., Kiritoshi, Y., Watanabe, J., and Ishihara, K. (2003). Degradation of phospholipid polymer hydrogel by hydrogen peroxide aiming at insulin release device. *Biomaterials* 24 (28): 5183–5190. https://doi.org/10.1016/S0142-9612(03)00441-1.

9 Gijsman, P., Meijers, G., and Vitarelli, G. (1999). Comparison of the UV-degradation chemistry of polypropylene, polyethylene, polyamide 6 and polybutylene terephthalate. *Polym. Degrad. Stab.* 65 (3): 433–441. https://doi.org/10.1016/S0141-3910(99)00033-6.

10 de Sainte Claire, P. (2009). Degradation of PEO in the solid state: a theoretical kinetic model. *Macromolecules* 42 (10): 3469–3482. https://doi.org/10.1021/ma802469u.

11 Laidler, K.J. and King, M.C. (1983). Development of transition-state theory. *J. Phys. Chem.* 87 (15): 2657–2664. https://doi.org/10.1021/j100238a002.

12 Ashbaugh, H.S. and Paulaitis, M.E. (2006). Monomer hydrophobicity as a mechanism for the LCST behavior of poly(ethylene oxide) in water. *Ind. Eng. Chem. Res.* 45 (16): 5531–5537. https://doi.org/10.1021/ie051131h.

13 Matsunaga, T., Sakai, T., Akagi, Y. et al. (2009). SANS and SLS studies on tetra-arm PEG gels in as-prepared and swollen states. *Macromolecules* 42 (16): 6245–6252. https://doi.org/10.1021/ma901013q.

14 Gnanou, Y., Hild, G., and Rempp, P. (1987). Molecular structure and elastic behavior of poly(ethylene oxide) networks swollen to equilibrium. *Macromolecules* 20 (7): 1662–1671. https://doi.org/10.1021/ma00173a037.

15 Akagi, Y., Gong, J.P., Chung, U.-i., and Sakai, T. (2013). Transition between phantom and affine network model observed in polymer gels with controlled network structure. *Macromolecules* 46 (3): 1035–1040. https://doi.org/10.1021/ma302270a.

16 Bender, M.L., Ginger, R.D., and Unik, J.P. (1958). Activation energies of the hydrolysis of esters and amides involving carbonyl oxygen exchange. *J. Am. Chem. Soc.* 80 (5): 1044–1048. https://doi.org/10.1021/ja01538a006.

17

Control Over Swelling of Injectable Gel

Takamasa Sakai and Takeshi Fujiyabu

Graduate School of Engineering, The University of Tokyo, Tokyo, Japan

Although a hydrogel can contain more than 90% water by weight, it behaves as a solid due to the crosslinked polymer network, which is a minor component. Due to the uniqueness derived from their "solid–liquid coexistence," hydrogels are promising for biomedical materials, such as drug delivery systems, scaffolds of tissue regeneration, and space-filling materials [1–4]. The formation process of hydrogels brings about another unique attribute: by connecting polymer chains in a polymer solution, the polymer solution turns into polymer gel, i.e. a liquid–solid transition occurs. By performing the gelation process *in vivo*, the pregel solution can be injected without any surgical procedures and can form a gel on site [5]. This minimally invasive "injectable gel" has an inherent superiority over other biomaterials.

However, injectable gels have a critical drawback, i.e. swelling. Swelling causes a drastic decrease in mechanical properties and can damage the surrounding tissues, especially when used as an infill material for a closed space. The swelling pressure $\Pi_{sw} = \Pi_{mix} - \Pi_{el}$ originates on the gel surface because Π_{mix} is much higher than Π_{el} in a good solvent [6]. Although the gel achieves equilibrium ($\Pi_{sw} = 0$) after a certain degree of swelling, as discussed in Section 4.2, this equilibrium is only transient because Π_{el} decreases with hydrogel degradation (Section 4.5 and Chapter 16). Thus, additional swelling is expected to occur *in vivo* on a long-term basis. Indeed, MIRA gel, which was developed as a buckle for treating retinal detachments and was clinically used for human patients, caused severe medical problems due to degradation-induced swelling approximately seven years after the implantation (Figure 17.1) [5]. This serious problem teaches us about the difficulties in keeping hydrogels stable on a long-term basis and in safely disintegrating hydrogels *in vivo*.

17.1 Nonswellable Gels

We developed a nonswellable gel based on the Tetra-PEG (TP) gel design [7]. This nonswellable gel is designed not to swell in the biological environment (37 °C) by introducing thermoresponsive segments into the network in a similar

Physics of Polymer Gels, First Edition. Edited by Takamasa Sakai.

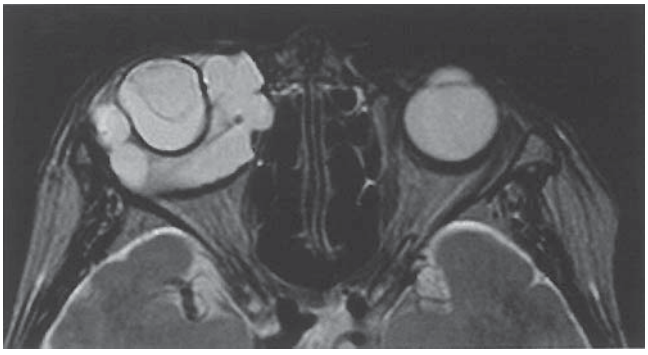

Figure 17.1 CT image of MIRA gel seven years after implantation. The swollen gel in the eye socket compressed and deformed the eye ball. Source: Reproduced from https://twinkle.repo.nii.ac.jp/?action=repository_uri&item_id=22367&file_id=22&file_no=1.

methodology to that used for controlling degradability (see Section 16.1). In addition to conventional mutually reactive TP units, we synthesized a third unit consisting of thermoresponsive polymer chains with four amine end groups (Figure 17.2). The thermoresponsive segments collapse above the lower critical solution temperature (T_c) and compete against the swelling behavior. The hydrogels are composed of TPs and thermoresponsive polymer units that align in an alternating fashion on the nanoscale. The fraction of thermoresponsive units can be modified by selecting the proper mixing ratio of polymer units without changing the network morphology. This feature allows the quantitative introduction of the thermoresponsive polymer unit, leading to precise control over the degree of swelling above T_c.

The swelling behavior of the hydrogels above T_c is regulated by the fraction of the thermoresponsive segment (r); for example, when $r = 0$, the hydrogel is a conventional TP gel without any thermoresponsiveness (Figure 17.2d, rightmost), whereas a perfect alternating structure is formed when $r = 0.5$ (Figure 17.2d, leftmost). Figure 17.3a shows the swelling ratio (Q) at different r values, where the hydrogels drastically changed their volume around their T_c (at approximately 25 °C, irrespective of r). This precise control of Q while maintaining T_c cannot be achieved with thermoresponsive hydrogels that are fabricated by random copolymerization of hydrophilic and thermoresponsive monomers. In that case, the T_c increases significantly with an increase in the amount of the hydrophilic monomer and finally exceeds 37 °C [8]. Notably, the Q of the hydrogel with $r = 0$ (a conventional TP gel) is greater than 100% over the whole temperature range, indicating that the hydrogel swells and alters its original shape under physiological conditions. In stark contrast, the Q of the hydrogel with $r = 0.4 \approx 100\%$ at approximately 37 °C, which indicates that the hydrogel is nonswellable under physiological conditions (Figure 17.3a). Unlike other conventional hydrogels with similar compositions, which often induce turbidity [9, 10], this hydrogel retained its transparency even after shrinking (Figure 17.3b). These data strongly suggest that hydrogels have an extremely homogeneous network structure and that the collapsed and swollen phases coexist on the nanoscale.

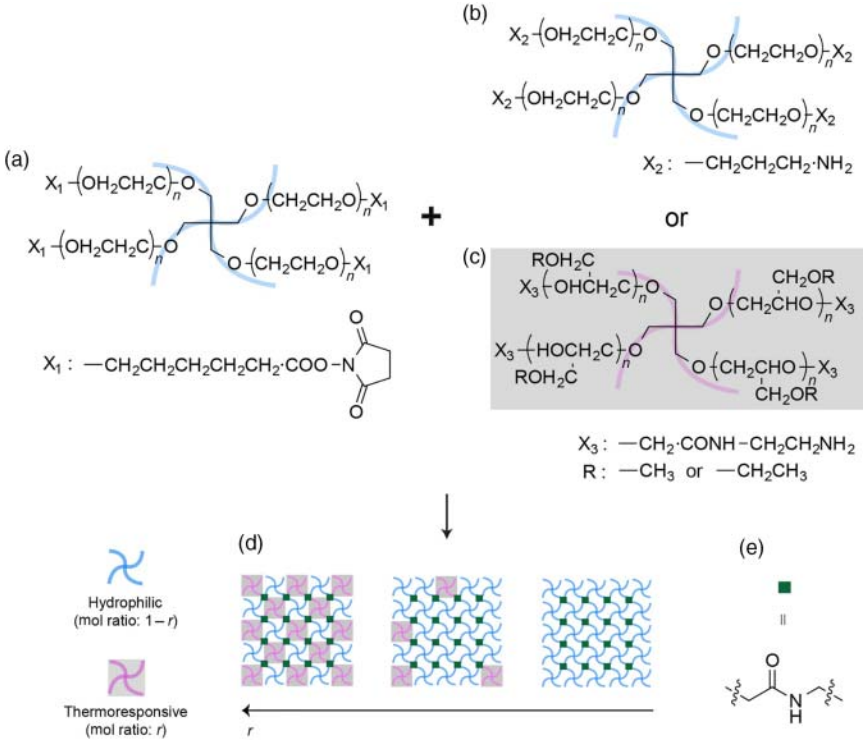

Figure 17.2 Schematic illustration of the thermoresponsive tetra-hydrogel system. (a) Tetra-arm poly(ethylene glycol) with active ester end groups. (b) Tetra-arm poly(ethylene glycol) with amino end groups. (c) Tetra-arm poly(ethyl glycidyl ether-*co*-methyl glycidyl ether) with amino end groups. (d) Polymer network composed of hydrophilic (white) and thermoresponsive (shadow) polymer units, where *r* represents the fraction of the thermoresponsive segment. Source: Reproduced with permission from Kamata et al. [7]. Copyright 2014, AAAS.

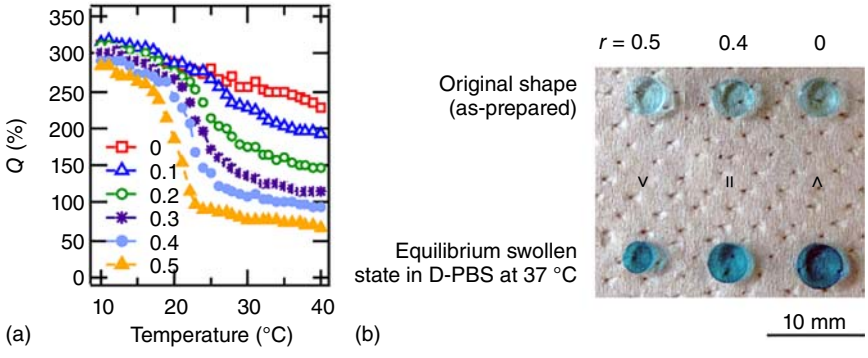

Figure 17.3 Swelling behavior of the hydrogels in Dulbecco's phosphate-buffered saline (D-PBS). *r* represents the fraction of the thermoresponsive segment. (a) The swelling ratio (*Q*) of the hydrogels as a function of temperature. $Q = (d/d_0)^3 \times 100$, where *d* is the diameter of the samples in the equilibrium-swollen state at each temperature and d_0 is the initial diameter of the samples (i.e. before swelling). (b) Photos of the hydrogels that exhibit different swelling degrees depending on *r*. The transparent hydrogels were colored only for visibility. Source: Reproduced with permission from Kamata et al. [7]. Copyright 2014, AAAS.

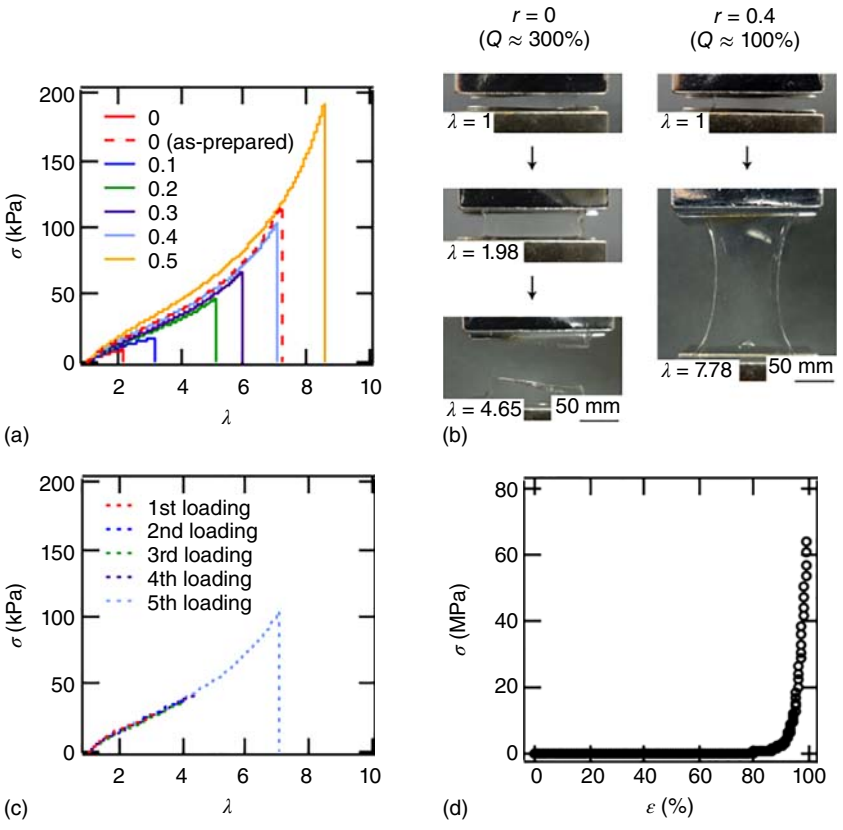

Figure 17.4 (a) Mechanical properties of the hydrogels fully swollen in D-PBS at 37 °C. The symbols represent the fraction of the thermoresponsive segment (*r*). (b) Photos of the hydrogels ($r = 0$ and 0.4) during elongation tests. (c) Stress–elongation ratio curves of the nonswellable hydrogel ($r = 0.4$). (d) The results of a compression test on the nonswellable hydrogel ($r = 0.4$). Source: Reproduced with permission from Kamata et al. [7]. Copyright 2014, AAAS.

The mechanical properties of the hydrogels are known to be strongly affected by their degree of swelling. To examine the general effect of swelling, we performed elongation tests on hydrogels with different *r* values in their equilibrium-swollen state. Representative stress–elongation curves of the hydrogels showed that the maximum elongation ratio (λ_{max}) diminished with a decrease in *r* (Figure 17.4a). This decrease in λ_{max} is explained by the following: the λ_{max} of polymer gels is defined as the ratio of two lengths of network strands – the fully stretched length and length in the initial state (see Sections 1.1 and 11.3). Because swelling prestretches the network strands in the initial state, λ_{max} inevitably decreases. Compared with the other hydrogels, the hydrogel with $r = 0.4$, in which the swelling is suppressed (hereafter referred to as a "nonswellable" hydrogel), showed improved mechanical properties. A conventional TP gel ($r = 0$) in the equilibrium-swollen state was easily torn off at approximately threefold stretching, while the nonswellable hydrogel did not rupture even after being

stretched more than sevenfold of its initial length (Figure 17.4b). The increased stretchability is mainly due to the unique alternating structure: prestretching of both the shrunken and swollen phases is inhibited. In addition, the nonswellable hydrogel showed practically no hysteresis, at least when stretched less than fourfold of its initial length, which indicates that the elongation did not break any covalent bonds in the polymer network (Figure 17.4c). Compared with the hysteresis exhibited by hydrogels during deformation, which essentially fail to tolerate a continual mechanical load, this completely reversible feature is prominent. In contrast to such hydrogels, nonswellable hydrogels showed no swelling or weakening in aqueous media even after repetitive mechanical overload. Notably, the nonswellable hydrogel endured a compressive stress of up to 60 MPa even in the equilibrium-swollen state (Figure 17.4d).

17.2 Nonosmotic Gel

Even the nonswellable gel that does not swell under physiological conditions swells when the network structure is degraded. As mentioned in Chapter 16, a polymer network degrades under physiological conditions on a long-term basis, resulting in swelling. Considering the swelling pressure $\Pi_{sw} = \Pi_{mix} - \Pi_{el}$, the maximum Π_{sw} is determined by only Π_{mix}. To suppress Π_{sw} even under degraded conditions ($\Pi_{el} \approx 0$), Π_{os} must be suppressed. When Π_{os} is small enough, the gel cannot swell or harm the surrounding tissues. The Π_{os} of gels is roughly determined by the polymer concentration and the interaction parameter between polymer and solvent as

$$\Pi_{mix} = -\frac{k_B T}{V_s}(\phi + \ln(1-\phi) + \chi\phi^2) \tag{17.1}$$

Notably, this equation is obtained by substituting $N = \infty$ into Eq. (2.49). This equation offers us two methods to suppress Π_{mix}: (i) decreasing ϕ_0 and (ii) setting $\chi = 0.5$ (θ condition). Method (i) has difficulty in forming a gel with a small ϕ_0 (Chapter 8). In addition, there are drawbacks such as poor mechanical properties and a long gelation time. In Section 17.3, we introduce a gel based on method (i): instantly formative gel with a super low polymeric component.

Here, we take method (ii), which provides nonswellability regardless of ϕ_0. To further analyze method (ii), we calculated the analytical solution of the Flory–Rehner model (Eq. (4.47)) for hydrogels with $\phi_0 = 0.10$ [11]. Figure 17.5a shows the equilibrium swelling ratio ($Q = \phi_0/\phi_e$) as a function of the elastic modulus (E) with different χ values. Swelling is induced by a decrease in E (i.e. degradation), and the swelling behavior is suppressed at high χ. In addition, Figure 17.5b focuses on the swelling ratio at the degradation point (Q at $E = 0$) as a function of χ. Although this parameter setting is representative, a unique behavior is predicted: a hydrogel with $\chi < 0.5$ swells to an infinite degree at the moment of disintegration, while that with $\chi > 0.5$ shows a finite degree of swelling. This analysis also suggests that a gel with $\chi \approx 0.53$ can maintain $Q = 1$ even during the degradation process. Given that conventional synthetic biocompatible polymers are hydrophilic ($\chi < 0.5$), conventional hydrogels swell

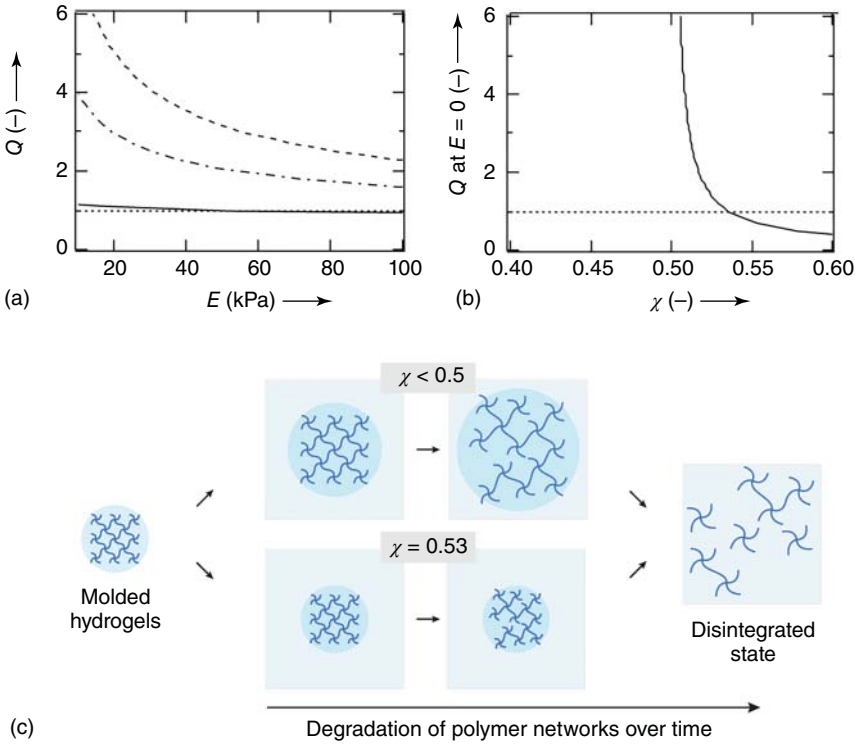

Figure 17.5 Theoretical prediction of the degradation behavior. (a) Q as a function of E calculated for hydrogels with $\phi_0 = 0.10$. Each line represents $\chi = 0.45$ (dashed line), 0.49 (dash–dot line), and 0.53 (solid line). The dotted line represents the state of non-swelling, $Q = 1$. (b) Q of hydrogels with $\phi_0 = 0.10$ at the disintegration point ($E = 0$) as a function of χ. (c) Conceptual illustration of different degradation routes depending on χ. Source: Reproduced with permission from Kamata et al. [11]. Copyright 2016, John Wiley and Sons.

during the degradation process. To achieve nonswellable behavior in degrading hydrogels, building a hydrogel from a polymer with $\chi \approx 0.53$ is theoretically required (Figure 17.5c). The fact that the χ value needed for realizing the "nonosmotic" condition is larger than 0.5 is due to the higher-order term that exists in Eq. (2.48) but is neglected in Eq. (2.49).

Our practical approach to realize such a "nonosmotic" condition is based on the synthetic control of χ by synthesizing copolymers from hydrophilic *N*,*N*-dimethylacrylamide (DMAAm) and hydrophobic *N*-*tert*-butylacrylamide (tBAAm) and subsequently forming hydrogels from the polymer units. We synthesized two types of four-arm polymers that are mutually reactive with their counterparts, and mixing aqueous solutions of the prepolymer units instantaneously produced hydrogels with controlled hydrophobicity (tetra-poly(DMAAm-*co*-tBAAm) hydrogels) (Figure 17.6) [11].

The swelling behavior of tetra-poly(DMAAm-*co*-tBAAm) hydrogels was tuned by controlling r_{tBAAm} (Figure 17.7a). At a constant temperature of 37 °C, the swelling ratio (Q) was a decreasing function of r_{tBAAm}, demonstrating the

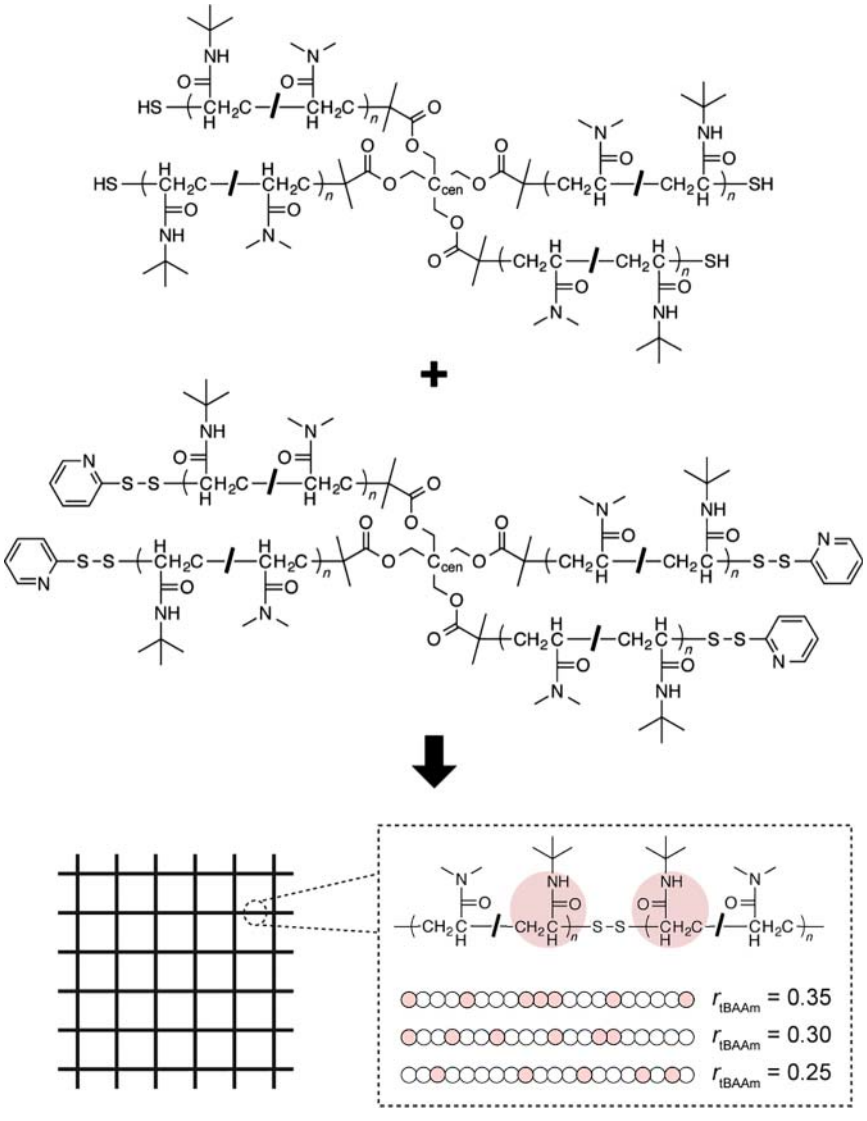

Figure 17.6 Chemical structures of polymer units and crosslinked polymer networks. Hydrophilic and hydrophobic monomers are depicted as white and shadow spheres, respectively. The hydrophobic monomer ratio is expressed as r_{tBAAm}. Source: Reproduced with permission from Kamata et al. [11]. Copyright 2016, John Wiley and Sons.

nonswelling property ($Q \approx 1$) at $r_{tBAAm} = 0.25$ (Figure 17.7b). Notably, pure poly(DMAAm) gels (hydrogels with $r_{tBAAm} = 0$) are known to swell ($Q \gg 1$) over the whole temperature range due to their hydrophilic nature. We fabricated gels from the prepolymers with $r_{tBAAm} = 0.25$ and different ϕ_0 values and confirmed that all the gels maintained the initial volume even when immersed in a physiological aqueous solution. Therefore, it is experimentally demonstrated that nonosmotic hydrogels exhibit unconditionally suppressed swelling properties.

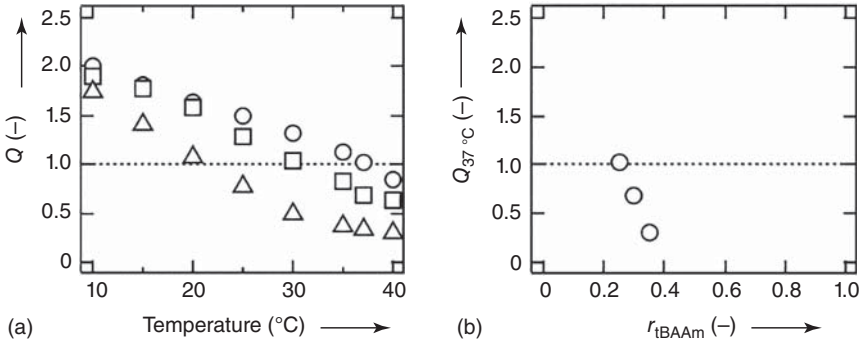

Figure 17.7 *Q* of tetra-poly(DMAAm-*co*-tBAAm) hydrogels. (a) *Q* as a function of temperature. ϕ_0 was fixed at 0.0965. The symbols represent $r_{tBAAm} = 0.25$ (circle), 0.30 (square), and 0.35 (triangle). (b) *Q* at 37 °C ($Q_{37\,°C}$) as a function of r_{tBAAm}. Source: Reproduced with permission from Kamata et al. [11]. Copyright 2016, John Wiley and Sons.

The degradation behavior of nonosmotic hydrogels was completely different from that of conventional hydrophilic hydrogels. To characterize the effect of the loss of elastic pressure, i.e. degradation, we intentionally cleaved the network strands and investigated the consequent swelling behavior. The time course of *Q* during the degradation process is shown in Figure 17.8a, left axis. The hydrogel volume was initially constant. From the middle stage, the boundary gradually became obscure over time, and the volume slightly increased. The swelling pressure ($\Pi_{37\,°C}$) of the degrading hydrogels ($Q \approx 2$) was estimated by the method shown in Chapter 14. The swelling pressure of the gel was always lower than 1 kPa (Figure 17.8a, right axis). Considering that the elastic modulus of biological soft tissues is conventional on the order of a few kilopascals [12], the swelling pressure generated by these nonosmotic hydrogels cannot harm

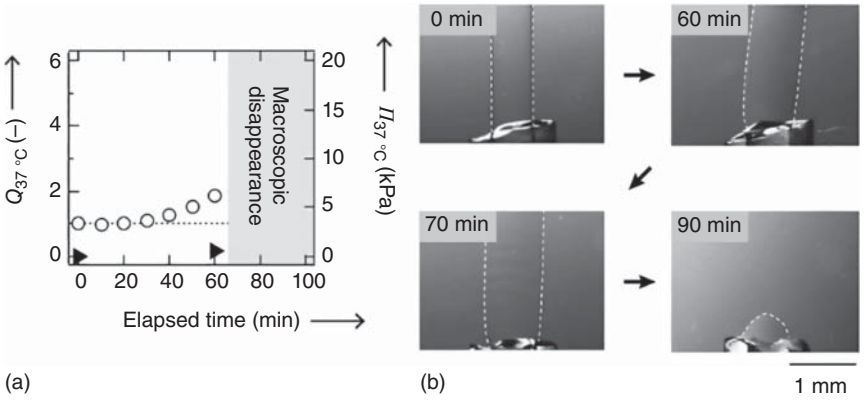

Figure 17.8 Degradation behavior of nonosmotic hydrogels. (a) Time course change in *Q* of a hydrogel with parameters $r_{tBAAm} = 0.25$ and $\phi_0 = 0.0965$ at 37 °C after the addition of dithiothreitol. (b) Representative photos of degrading hydrogels (outlined with dashed lines) taken at specified time points. Source: Reproduced with permission from Kamata et al. [11]. Copyright 2016, John Wiley and Sons.

the surrounding tissue even in confined *in vivo* spaces. After slight swelling, the hydrogels disintegrated without further obvious swelling (Figure 17.8b). This degradation behavior is noticeably different from that of conventional hydrogels, which significantly swell before reaching their disintegration points (Chapter 16). This behavior quantitatively agrees with the prediction in Figure 17.5c.

17.3 Oligo-Tetra-PEG Gel

According to Eq. (17.1), another methodology for reducing Π_{mix} is to decrease the polymer concentration. However, the inherent critical problem with this approach is the challenge of gel formation. Even in the case of TP gels with amine–OSu chemistry, the lowest gelation polymer concentration is 6.0 g/l, which requires seven hours for gelation (Figure 17.11a), far exceeding the time scale of surgery. To prepare an *in situ*-forming hydrogel with a low polymeric content within a reasonable time frame, the design and fabrication of polymeric modules with efficient gelation ability are essential.

During a conventional gelation process (Figure 17.9, top), polymer chains are connected to each other to form a highly branched polymeric structure

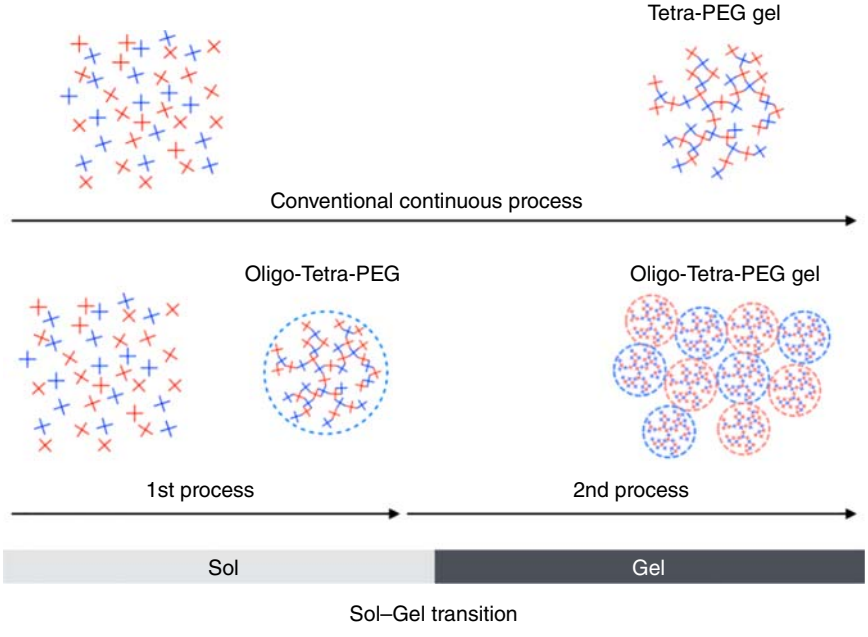

Figure 17.9 Schematic illustration of gelation processes of a conventional TP hydrogel and an Oligo-TP hydrogel. In the conventional TP hydrogel system, mutually reactive TPs are simply mixed and reacted with each other to form the hydrogel. In the case of the Oligo-TP hydrogel system, mutually reactive TPs were first mixed under excess TP–SH and excess TP–MA conditions to form highly branched polymeric clusters instead of hydrogels (Oligo-TPs). In the second *in vivo* process, mutually reactive Oligo-TPs were mixed to form an Oligo-TP hydrogel. Source: Reproduced with permission from Hayashi et al. [13]. Copyright 2017, Springer Nature.

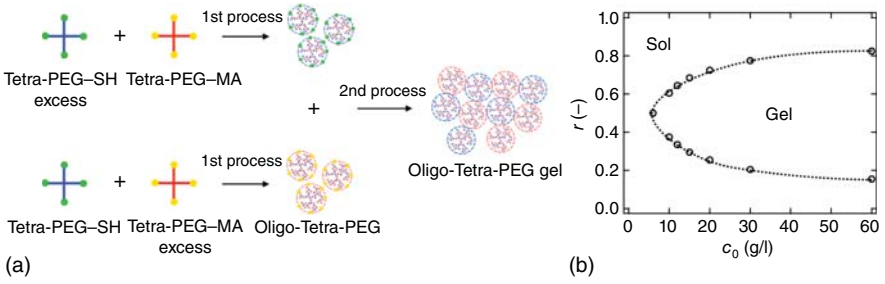

Figure 17.10 (a) Two-step fabrication process for Oligo-TP hydrogel. In the first step, TP–SH and TP–MA were mixed in nonstoichiometric conditions to form SH-excess and MA-excess Oligo-TPs. In the second process, these Oligo-TP solutions were equally diluted and mixed in equal amounts to form Oligo-TP hydrogel. (b) Sol–gel phase diagram: the relationship between the initial polymer concentration (c_0) and the mixing ratio of TP–SH to the total polymer concentration (r = [Tetra-PEG–SH]/([Tetra-PEG–SH] + [Tetra-PEG–MA])) at the sol–gel transition points. The conditions inside the dotted line produced gels, while the conditions outside did not. All the experiments were performed in triplicate and averaged. The lengths of error bars (SD) are smaller than the size of the symbols. Source: Reproduced with permission from Hayashi et al. [13]. Copyright 2017, Springer Nature.

(polymeric clusters). The polymeric clusters further grow and eventually form a macroscopic gel. Here, we separate the gelation at low polymer content into two processes (Figure 17.9, bottom) [13]. In the first process, the reaction is intentionally stopped immediately prior to the gelation point, at which stage polymeric clusters almost completely percolate throughout the system. The resulting polymeric cluster (Oligo-Tetra-PEG [Oligo-TP]) exhibited a unimodal size distribution of up to 90 nm, which was much larger than the size distributions of conventional hyperbranched polymers [14], suggesting that Oligo-TP had a highly branched structure. In the second process, the Oligo-TPs are co-crosslinked as individual modules to form a hydrogel (Oligo-TP hydrogels).

To systematically form Oligo-TPs, we utilized mutually reactive TPs with thiol terminal groups (TP–SH) and maleimide terminal groups (TP–MA) (Figure 17.10a). First, we investigated the critical ratio for forming hydrogels (r_c) by tuning the molar ratio of these prepolymers (r = [Tetra-PEG–SH]/([Tetra-PEG–SH] + [Tetra-PEG–MA])) for each initial polymer concentration (c_0). As shown in Figure 17.10b, the stoichiometric conditions ($r_c = 0.5$) produced hydrogels in the region $c_0 > 6.0$ g/l, and the r region that produced hydrogels decreased with a decrease in c_0. The Oligo-TPs are thus formed in the sol region close to the sol–gel transition line. In the case of $c_0 = 60$ g/l, MA-excess and SH-excess Oligo-TPs were formed at $r = 0.13$ and 0.87, respectively ($r_c = 0.16$ and 0.83). Based on the UV spectroscopy results, almost all minor species reacted with the excess species, indicating that only the excess functional group exists on each Oligo-TP.

In the second process, we co-crosslinked the mutually reactive Oligo-TPs (MA-excess and SH-excess Oligo-TPs) to form Oligo-TP hydrogels (Figure 17.10a). Each Oligo-TP solution was diluted to the same specific concentration (c) and mixed with each other in equal amounts. Figure 17.11a shows the gelation time (t_{gel}) as a function of c. For direct comparison, the

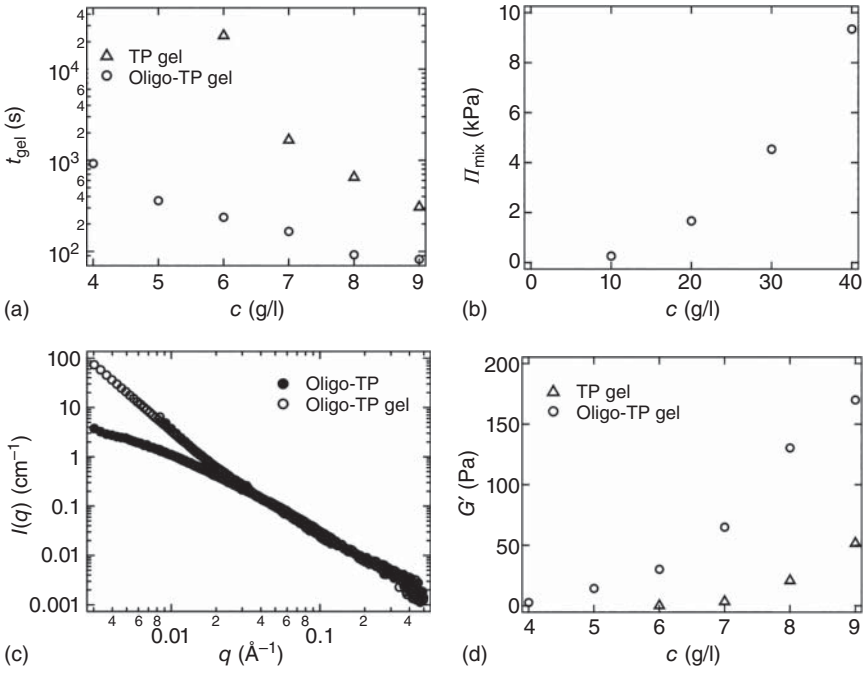

Figure 17.11 (a) Gelation time (t_{gel}) of Oligo-TP hydrogels (circles) and TP hydrogels (triangles) as a function of the polymer concentration (c). (b) Osmotic pressure (Π_{mix}) of Oligo-TP hydrogels as a function of c. (c) SANS measurements of an Oligo-TP solution and an Oligo-TP hydrogel. (d) Equilibrium storage modulus (G') of Oligo-TP hydrogels (circles) and TP hydrogels (triangles) as a function of c. All the experiments except for SANS measurements were performed in triplicate and averaged. The lengths of error bars (SD) are smaller than the size of the symbols. The error bars on the SANS profiles show the SD following complete data processing. Source: Reproduced with permission from Hayashi et al. [13]. Copyright 2017, Springer Nature.

results from the conventional one-step method, in which hydrogels were directly prepared using the first process with $r = 0.5$, i.e. TP hydrogels, are also presented. Compared with conventional TP gels, Oligo-TP hydrogels had shorter t_{gel} times that were nearly within the desired range, i.e. less than 10 minutes. In addition to the shortened t_{gel}, the lowest concentration for gelation and consequent hydrogel formation decreased to $c = 4.0$ g/l. Notably, it is difficult to properly accelerate gelation reactions by tuning the reactivity of the functional groups: if the reactivity is too great, the level of active species may result in sudden and heterogeneous gelation because gelation occurs prior to the homogeneous mixing of the prepolymers. In our methodology, we can continuously and easily control the "distance" to the gelation point by tuning r in the first process forming Oligo-TPs, resulting in a suitable approach to gelation. The Π_{mix} of the Oligo-TP hydrogels was a positive finite value and lower than typical eye pressure (~1 kPa) in the region $c < 10$ g/l (Figure 17.11b). Based on small-angle neutron scattering (SANS) measurements, the Oligo-TP hydrogel has a similar structure to the Oligo-TP in the high-q region ($0.03\,\text{Å}^{-1} < q$), as well as a

large structure with a wide and smooth size distribution in the low-q region ($q < 0.03$ Å^{-1}) (Figure 17.11c), where q is the magnitude of the scattering vector. The plateau moduli (G') of Oligo-TP hydrogels were always higher than those of the conventional hydrogels with the same c (Figure 17.11d), strongly suggesting efficient network formation.

We next evaluated the biocompatibility of the Oligo-TP hydrogel ($c = 7.0$ g/l, $G \approx 4$ Pa) *in vivo* by subcutaneously injecting it into mice. After four weeks, Oligo-TP hydrogels remained in the injected site without causing damage to adjacent tissues (Figure 17.12a). Histological analysis revealed mild infiltration of inflammatory cells in all tested materials. However, the expression of CD62L, a marker for inflammatory cells, and encapsulation of the material was detected only in the hydrogel formed from Oligo-TP crosslinked by small molecules (Figure 17.12a). Due to the similarity between gelation and reverse gelation (disintegration), Oligo-TPs are not only the raw materials but also the metabolites of Oligo-TP hydrogels. We thus examined the toxicity of the Oligo-TPs and confirmed the low toxicities of these specimens *in vitro* (Figure 17.12b) and *in vivo* (Figure 17.12c). The low toxicity of Oligo-TPs may stem from the low permeability of extremely large Oligo-TPs through the pores of surrounding tissues. These results strongly suggest the biosafety of Oligo-TP hydrogels throughout their full lifecycle from formation to disintegration.

The low cytotoxicity and extremely low swelling pressure of Oligo-TP hydrogels led us to examine the possibility of their application as an artificial vitreous body. The biocompatibility and effectiveness of Oligo-TP hydrogels ($c = 7.0$ g/l, $G \approx 4$ Pa) were evaluated using a normal Dutch pigmented rabbit model. The Oligo-TP pregel solution was compatible with the modality of current small-gauge incision vitreous surgeries and subsequently formed a hydrogel within the vitreous cavity. No significant difference in intraocular pressure was observed between the Oligo-TP hydrogel-injected and balanced salt solution-injected (control) groups throughout the observation period (up to 410 days, Figure 17.13a). Based on slit-lamp examinations (Figure 17.13b), images of eyes after dissection (Figure 17.13c), and H&E staining of histological sections (Figure 17.13g), neither significant inflammation nor toxic reaction was observed. The remaining Oligo-TP hydrogel in the vitreous cavity was detected by slit-lamp biomicroscopy with a 90-D fundus lens; however, it was not detected with histological analysis, probably because of technical limitations during histological sectioning. Electroretinography for assessing retinal function showed no significant difference in positive waveforms, implicit times, and amplitudes between the Oligo-TP hydrogel-injected and control groups (Figure 17.13d–f). Fundus photography revealed that the Oligo-TP hydrogel inside the vitreous cavity of the living rabbit eyes remained transparent throughout the follow-up period. Spectral-domain optical coherence tomography revealed neither retinal detachment nor edema, and the retinal microstructure was not morphologically damaged in either group. By contrast, lens opacity (Figure 17.13b), vitreous opacity (Figure 17.13c), and negative waveforms of electroretinography (Figure 17.13d) due to severe inflammation were observed in the high polymer concentration group ($c = 60$ g/l, $G \approx 9.5$ kPa), similar to previous artificial vitreous materials. The turbidity in the eyes prevented images

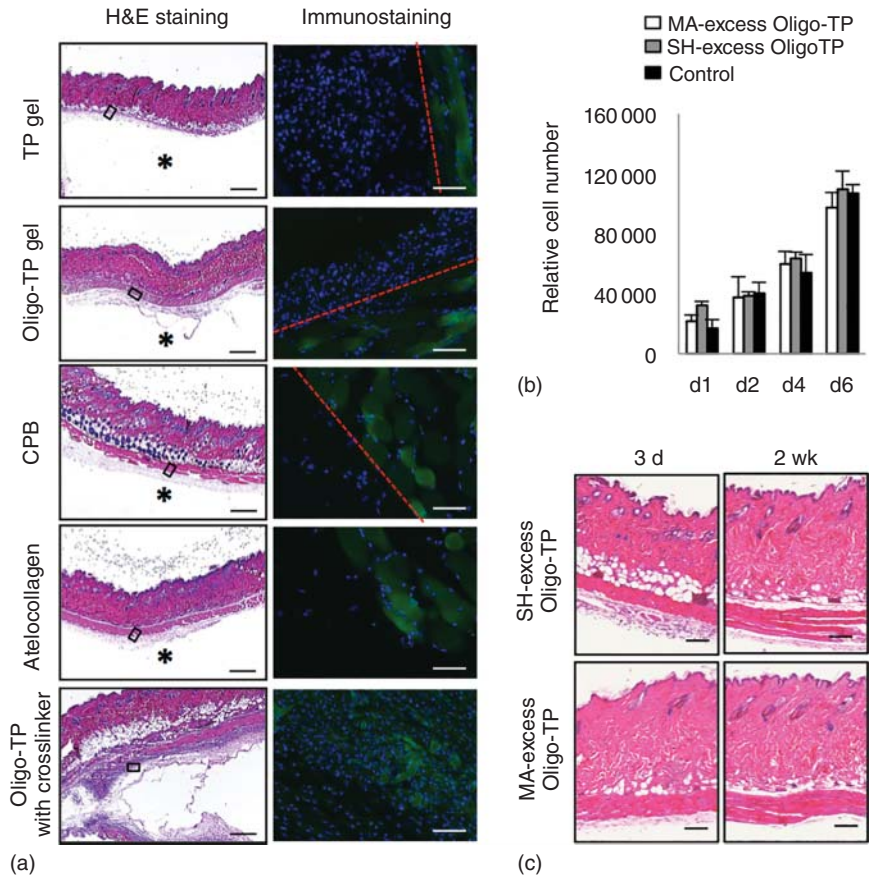

Figure 17.12 (a) Gel specimens and surrounding tissues and representative images of H&E staining and immunostaining for CD62L (GFP) in histological sections of mice at four weeks after subcutaneous injection of materials. Asterisks and rectangles denote, respectively, the hydrogel and the location of the immunostaining images. Nuclei were stained with DAPI. Nonspecific GFP signal was detected in muscles (dashed lines). Scale bars in the H&E staining and immunostaining images indicate 5 mm and 100 μm, respectively. (b) Proliferation of NIH3T3 cells cultured with or without Oligo-TPs. The data (relative cell number) are expressed as the mean ± SDs from four independent experiments. No statistically significant differences were found between MA-excess Oligo-TP and control, between SH-excess Oligo-TP and control, and between MA-excess and SH-excess Oligo-TPs via Student's *t*-test analysis. (c) Representative H&E staining images of histological sections in mice subcutaneously injected with MA-excess and SH-excess Oligo-TPs or PBS. Sections at three days and two weeks after the injection are shown. Scale bars, 200 μm. CPB, citrate-phosphate buffer; H&E, haematoxylin and eosin. Source: Reproduced with permission from Hayashi et al. [13]. Copyright 2017, Springer Nature.

of the retina from being obtained through the vitreous. Intraocular pressure also could not be measured correctly because of postoperative inflammatory corneal melting in this group. In addition, we developed an animal model of retinal detachment and injected an Oligo-TP hydrogel into the vitreous cavity as a vitreous tamponade material to evaluate whether pathological conditions

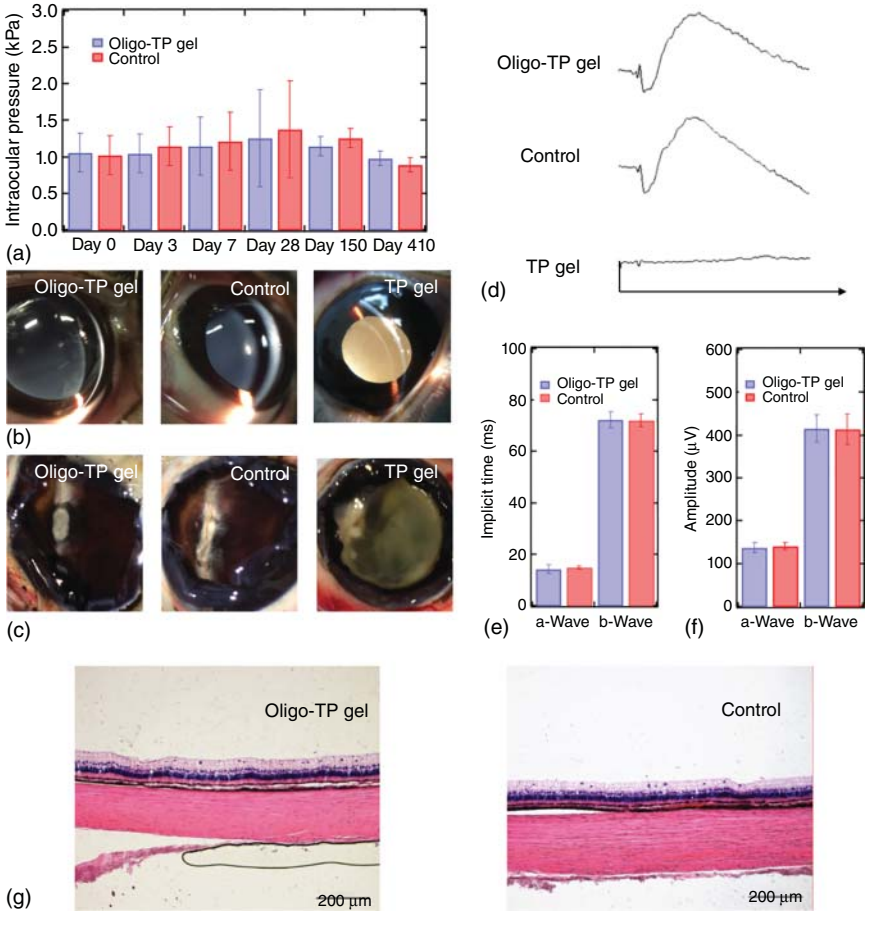

Figure 17.13 (a) Changes in the intraocular pressure in the Oligo-TP hydrogel-injected and balanced salt solution-injected (control) groups. No significant difference in intraocular pressure was observed between the Oligo-TP hydrogel-injected and control groups throughout the observation period (up to 410 days) via Student's *t*-test analysis. The data are expressed as the mean ± SD. (b) Anterior segments of rabbit eyes in the Oligo-TP hydrogel-injected, control, and TP hydrogel-injected groups on day 7 postoperation. (c) Images of eyes after dissection 90 days postoperation in the Oligo-TP hydrogel-injected, control, and TP hydrogel-injected groups. (d) Electroretinography waveforms of rabbit eyes in the Oligo-TP hydrogel-injected, control, and TP hydrogel-injected groups on day 90 postoperation. Bars: 100 μV and 25 ms. (e) Electroretinography data of a-wave and b-wave implicit times in the Oligo-TP hydrogel-injected and control groups on day 90 postoperation. The data are expressed as the mean ± SD. (f) Electroretinography data of a-wave and b-wave amplitudes in the Oligo-TP hydrogel-injected and control groups on day 90 postoperation. The data are expressed as the mean ± SD. No significant difference in implicit times and amplitudes was observed between the Oligo-TP hydrogel-injected and control groups. (g) Representative images of H&E staining in histological sections of rabbit eyes at 410 days postoperation. Scale bars indicate 200 μm. No apparent inflammation or alteration of the retinal microstructure was observed in either the Oligo-TP hydrogel-injected or control group. Source: Reproduced with permission from Hayashi et al. [13]. Copyright 2017, Springer Nature.

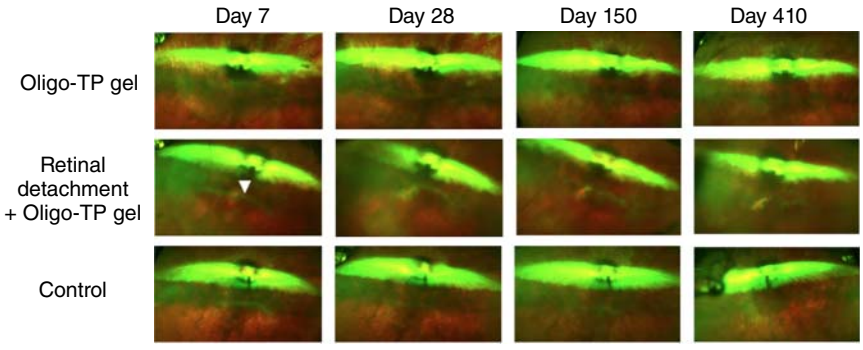

Figure 17.14 Fundus photography of rabbit eyes in the Oligo-TP hydrogel-injected, retinal detachment with the Oligo-TP hydrogel-injected, and control groups. Arrowhead = intentional retinal break. Source: Reproduced with permission from Hayashi et al. [13]. Copyright 2017, Springer Nature.

could be treated with the gel (Figure 17.14). As a result, retinal redetachment was inhibited for 410 days without any complications.

References

1 Kamata, H., Li, X., Chung, U.I., and Sakai, T. (2015). Design of hydrogels for biomedical applications. *Adv. Healthcare Mater.* 4 (16): 2360–2374. https://doi.org/10.1002/adhm.201500076.

2 Hoffman, A.S. (2002). Hydrogels for biomedical applications. *Adv. Drug Delivery Rev.* 54 (1): 3–12. https://doi.org/10.1016/S0169-409X(01)00239-3.

3 Nicodemus, G.D. and Bryant, S.J. (2008). Cell encapsulation in biodegradable hydrogels for tissue engineering applications. *Tissue Eng. Part B* 14 (2): 149–165. https://doi.org/10.1089/ten.teb.2007.0332.

4 Lee, K.Y. and Mooney, D.J. (2001). Hydrogels for tissue engineering. *Chem. Rev.* 101 (7): 1869–1880. https://doi.org/10.1021/cr000108x.

5 Marin, J.F. (1992). Long-term complications of the MAI hydrogel intrascleral buckling implant. *Arch. Ophthalmol.* 110 (1): 86. https://doi.org/10.1001/archopht.1992.01080130088031.

6 Flory, P.J. and Rehner, J. (1943). Statistical mechanics of cross-linked polymer networks II. Swelling. *J. Chem. Phys.* 11 (11): 521–526. https://doi.org/10.1063/1.1723792.

7 Kamata, H., Akagi, Y., Kayasuga-Kariya, Y. et al. (2014). "Nonswellable" hydrogel without mechanical hysteresis. *Science* 343 (6173): 873–875. https://doi.org/10.1126/science.1247811.

8 Cui, J., Lackey, M.A., Tew, G.N., and Crosby, A.J. (2012). Mechanical properties of end-linked PEG/PDMS hydrogels. *Macromolecules* 45 (15): 6104–6110. https://doi.org/10.1021/ma300593g.

9 Li, J., Li, X., Ni, X. et al. (2006). Self-assembled supramolecular hydrogels formed by biodegradable PEO–PHB–PEO triblock copolymers and

α-cyclodextrin for controlled drug delivery. *Biomaterials* 27 (22): 4132–4140. https://doi.org/10.1016/j.biomaterials.2006.03.025.

10 Reinicke, S., Schmelz, J., Lapp, A. et al. (2009). Smart hydrogels based on double responsive triblock terpolymers. *Soft Matter* https://doi.org/10.1039/b900539k.

11 Kamata, H., Kushiro, K., Takai, M. et al. (2016). Non-osmotic hydrogels: a rational strategy for safely degradable hydrogels. *Angew. Chem. Int. Ed.* 55 (32): 9282–9286. https://doi.org/10.1002/anie.201602610.

12 Pritchard, C.D., Crafoord, S., Andréasson, S. et al. (2011). Evaluation of viscoelastic poly(ethylene glycol) sols as vitreous substitutes in an experimental vitrectomy model in rabbits. *Acta Biomater.* 7 (3): 936–943. https://doi.org/10.1016/j.actbio.2010.11.013.

13 Hayashi, K., Okamoto, F., Hoshi, S. et al. (2017). Fast-forming hydrogel with ultralow polymeric content as an artificial vitreous body. *Nat. Biomed. Eng.* 1 (3): 1–7. https://doi.org/10.1038/s41551-017-0044.

14 Zheng, Y., Li, S., Weng, Z., and Gao, C. (2015). Hyperbranched polymers: advances from synthesis to applications. *Chem. Soc. Rev.* 44 (12): 4091–4130. https://doi.org/10.1039/C4CS00528G.

Index

Physics of Polymer Gels, First Edition. Edited by Takamasa Sakai.